Hydrodynamics of Alluvial Channel with Downward Seepage

Thesis submitted in partial fulfilment of the requirements for the award of the degree of

Doctor of Philosophy

in

Civil a Engineering

by

Vishal Deshpande

Department of Civil Engineering

Indian Institute of Technology Guwahati

Guwahati - 781039 Assam India

November 2014

Declaration of Authorship

I, Vishal Deshpande, declare that this thesis titled, 'Hydrodynamics of Alluvial Channel with Downward Seepage' and the work presented in it are my own. I confirm that:

- This work was done wholly or mainly while in candidature for a research degree at this Institute.
- Where any part of this thesis has previously been submitted for a degree or any other qualification at this Institute or any other institution, this has been clearly stated.
- Where I have consulted the published work of others, this is always clearly attributed.
- Where I have quoted from the work of others, the source is always given. With the exception of such quotations, this thesis is entirely my own work.
- I have acknowledged all main sources of help.
- Where the thesis is based on work done by myself jointly with others, I have made clear exactly what was done by others and what I have contributed myself.

Signed: _____

Date: _____

Department of Civil Engineering
Indian Institute of Technology Guwahati
Guwahati - 781039 Assam India

Dr. Bimlesh Kumar
Associate Professor
0361-2582420
bimk@iitg.ernet.in

Certificate

This is to certify that the thesis entitled **Hydrodynamics of Alluvial Channel with Downward Seepage** being submitted by **Vishal Deshpande** to the Department of Civil Engineering, Indian Institute of Technology Guwahati, is a record of bona fide research work under my supervision and is worthy of consideration for the award of the degree of Doctor of Philosophy of the Institute.

Date: 28^{th} November 2014
Place: Guwahati

Dr. Bimlesh Kumar

Journals

[1] Vishal Deshpande and Bimlesh Kumar. Advent of Sheet Flow in Suction Affected Alluvial Channels. *Environmental Fluid Mechanics*, pages 1 – 20, 2015.

[2] Vishal Deshpande and Bimlesh Kumar. Does Downward Seepage Initiate Lateral Channel Shift? *National Academy Science Letters*, 2015 (Accepted for Publication).

[3] Vishal Deshpande and Bimlesh Kumar. Review and Assessment of the Theories of Stable Alluvial Channel Design. *Water Resources*, 39(4): pages 481 – 487, 2012.

[4] Vishal Deshpande and Bimlesh Kumar. Analysing Turbulent Flow Structures in Alluvial Channels with Curved Cross-sections under Conditions of Downward Seepage. *Sedimentology*, 2014 (Under Review).

[5] Mahesh Patel, Vishal Deshpande, and Bimlesh Kumar. Turbulent Characteristics and Evolution of the Sheet Flow in Alluvial Channel with Downward Seepage. *Journal of Geophysical Research: Earth Surface (Revision Submitted)*, 2015.

[6] Vishal Deshpande and Bimlesh Kumar. Profile of Stable Channel with Seepage. *Journal of Hydraulic Engineering, ASCE*, 2013 (Under Review).

[7] Vishal Deshpande, Mahesh Patel and Bimlesh Kumar. Effect of Downward Seepage on the Velocity Power Spectra in Threshold Alluvial Channels. *Journal of Fluid Mechanics*, 2015 (Under Review)

Conferences

[1] Vishal Deshpande and Bimlesh Kumar. Spatio-temporal Quantification of Hydraulic Parameters at Stable Alluvial Channel. In *International Seminar on River, Society and Sustainable Development*, May 2011.

[2] Vishal Deshpande and Bimlesh Kumar. Generalized Downstream Hydraulic Geometry Relations. In *National Conference on Recent advancements in Civil Engineering and Infrastructure Development*, December 2011.

[3] Vishal Deshpande and Bimlesh Kumar. Downstream Hydraulic Geometry for a River in its Dynamic Equilibrium. In *Ensure*, Indian Institute of Technology Guwahati, India, February 2012.

[4] S. Talukdar, Vishal Deshpande, Bimlesh Kumar and S. Dutta. Explicit empirical prediction of Incipient motion for Alluvial River. In *Ensure*, Indian Institute of Technology Guwahati, India, 2012.

[5] Vishal Deshpande, Harish Patel, and Bimlesh Kumar. Evolution of Channel Shape with Seepage. In *Recent Advances in Civil Engineering (RACE)*, National Institute of Technology Patna, India, June 2013.

[6] Vishal Deshpande, Satish Patel and Bimlesh Kumar. Effect of Seepage on Mannings? Coefficient in Alluvial Channel. In *Recent Advances in Civil Engineering (RACE)*, National Institute of Technology Patna, India, June 2013.

[7] Vishal Deshpande, Mahesh Patel and Bimlesh Kumar. Spatio-Temporal variation of Critical Parameters in Threshold Channel. In *International Conference On Climate Change, Water Resources and Disasters in Mountainous Regions: Building Resilience to Changing Climate*, SOHAM-Nepal, November 27-29, 2013. Babarmahal, Kathmandu.

Dedicated to
Mother Nature

Mera mujh mein kuch nahi, jo kachu hai so toh
Tera tujhko saupate, kya lagat hai moh

मेरा मुझ में कुछ नहीं, जो कुछ है सो तोह |
तेरा तुझको सौपता, क्या लागे है मोह ||

Nothing mine belongs to me, all that is yours
To give all that to you, what's there for my remorse ?

EXPLANATION

Kabir affirms that all things of man belong to the Almighty Father as his grant of grace to man. As such, why should there be any hesitation on the part of man to give all that to the God, the giver ?

-Kabir

Acknowledgements

I have received help from numerous people in the course of this study and I would like to cordially thank them all. Without their help this study would not have been possible.

Particularly, I am greatly indebted to my supervisor, **Dr. Bimlesh Kumar** for his valuable advices on academics, life, and career. He was extremely helpful throughout the course of my work. He always pushed me hard and even harder because of which the study of this amount could be completed in relatively lesser period of time. He is the most famous person in the institute for his publications and I find myself very lucky for being his student. He always has contemporary and diverse ideas which nurtured my thoughts and reasoning. He was always very cooperative and caring during my tough times. He was very kind and was always available despite of his busy academic schedule whenever I needed help.

I am thankful to the Chairman of my Doctoral Committee **Prof. Arup Kumar Sarma** and other members **Prof. Subashisa Dutta**, and **Dr. Vinayak Kulkarni** (Dept. of Mechanical Engineering IIT Guwahati) for their valuable suggestions regarding the study.

I'm indebted to my parents **Aai** and **Papa** for their blessings and unconditional support for bringing me at such a level. Without their faith in me, I would not be able to carry out this study. I would like to thank my sister **Varsha**, her husband **Mr. Avinash Kardekar** and my sweet niece **Krutika** for their support, love and care which certainly helped me in the work.

I owe a great debt of gratitude to **Mr. Bajal Hoque** for being there to help me since I stepped into the study. He has always sweated with me whenever I was conducting the experiments. He has always advised me as like my elder brother. I am very thankful to him for lending a great hand of help whenever I needed without which the study wouldn't be possible. I am also thankful to his family for having fun and really very good times with me.

I cordially thank **Mr. Mahesh Patel** for all his supports since his presence in the institute and since the commencement of this study. With his presence I always felt that I was accompanied by my younger brother.

I'm indebted to my very good friend **Mr. Mayank Agarwal** (Dept. of Computer Science and Engineering IIT Guwahati) for his great help throughout the course of this study. My discussions and arguments with him were always fruitful. He indeed helped me in developing my personality, attitude and morals. I cannot forget that without the help of **Mr. Mayank Agarwal** and **Mr. Mahesh Patel** it would not be possible for me to perform this study and write the thesis.

I am grateful for the help given by **Ms. Smrati Jain** since her presence in the institute. She has always been very kind and supportive for me. She consistently helped me emotionally whenever I was down and whenever I was cheering.

I express sincere gratitude to my juniors Ms. Thokchom Bebina Devi, Mr. Satish Patel, Mr. Harish Patel, Mr. Anurag Sharma for the hard work they put while they were carrying out experiments for this study with me. I am indebted to the senior undergrad students Mr. Jaideep Sehrawat, Mr. Pankaj Meena and the junior undergrad students Mr. Sumit Kumar, Mr. Rishabh Daga, Mr. Rakesh Ranjan for the extreme help these boys provided me in my experiments and for all those funny moments in the lab. I am very thankful to the summer trainees Mr. D. Joardar and Mr. A. Krishnaprasad for helping me in my experiments during their training

I am very thankful to Mr. Sumit Talukdar for the great help he provided during the construction phase of the experimental set-up. I express my special thanks to Mr. Yousouf and his team for smooth construction of the experimental flume. I am grateful for the help provided by the people of Central Workshop IIT Guwahati: Mr. Upen Gohain and Mr. Dilip Chetri for making utility components which offered great ease during measurements. I am thankful to Mr. Ravishankar for providing sand every time when it was required in the experimental study.

I would like to thank one of my very good friends Mr. Bablu Kirar with whom I had long chats nearly about everything of life and for his great advices whenever I was in grief. We had wonder time during his stay in the institute and during my trips to his institute (IIT Roorkee).

I would like to cordially thank my colleagues: Mr. Arpit Chouksey and Mr. Amit Kumar Dubey for their support. We had fun filled parties and had great enjoyment which gave me incredible moments in my life in the institute.

I am very thankful to my juniors cum group friends: Ms. Isha Vishan, Ms. Jayshree Hazarika, Ms. Needhi Kotoki, Ms. Rutuja Chavan, Mr. Kuldeep Khare and Mr. Nilesh Jain for all those moments of joy we had in and outside the campus.

I specially thank Swapnali Bora ma'am who was very caring and loving throughout my stay in the institute.

I would like to thank Dr. Ashish Kumar Namdeo for having great discussions during lunch and dinner together with Mr. Mayank Agarwal at Barak Hostel Mess.

I would like to thank Dr. Vikas Sharma for nurturing my thoughts on almost every context of life. He was very supportive through out his stay in the institute.

I am thankful to Dr. Kumar Pallav who was very kind and supportive for me throughout his stay in the institute. I am also thankful to the scientific officers of the Dept. of Civil Engineering: Dr. Arun Borsaikia and Jonali Saikia ma'am for their support. I appreciate the staff members of various laboratories of the Dept. of Civil Engineering: Mr. Priyananda Saikia, Mr. Mrinal Sarma, Mr. Pranab Hazarika, Mr. Biswajit Debnath, Mr. P. Pathak, and Mr. Hariram Upadhyay for the help they provided whenever it was required.

I would like to thank Dr. Sanat Nalini Sahoo, Dr. Nirmalendu Debnath, Mr. Pranab Barman and Mr. Ravindra Patil for the discussions we had during my stay.

I would like to specially thank the members of my Badminton Gang: Dr. Aditya Panda, Dr. Anupam Saikia, Dr. Mohd. Qureshi, Dr. Arindam Dey for all those thrilling and exhausting games we played over the courts throughout my stay in the campus. They always had discussions with me during the play regarding my career and shared the experience of their lives which was really very helpful.

I gratefully acknowledge the advices provided by Prof. K. K. Punjabi (Dept. of Civil Engineering SATI Vidisha) and Mr. Hrishikesh Jain Sir (Sheetal Sagar Ji Maharaj) which were really very helpful in developing my morals.

I would like to express my sincere gratitude to Prof. Per-Åge Krogstad (Norwegian University of Science and Technology), Prof. Subhasish Dey (IIT Kharagpur),

Prof. V. P. Singh (Texas A&M University), Dr. Christopher D. Jetté (Seatek Instrumentation) for responding to my queries.

I owe a great debt of gratitude to the cloud storage websites: *Copy.com* & *Google Drive* for securing my valuable data which could have lost when my laptop stopped working in the final days of this study.

I would like to thank the workers of Barak hostel mess, Barak hostel canteens, Brahmaputra hostel mess, and Brahmaputra hostel canteens for providing food and being very kind to me. My special thanks to the owner of the utility store Mr. Haran Pathak and his boys Mr. Bimal and Mr. Mridul for being very kind to me.

I am very thankful to the Indian Institute of Technology Guwahati for providing magnificent facilities and beautiful atmosphere to carry out my research work. I thank my laptops Sony Vaio VGN CS24GH (resting in peace) and HP 15 R007 TX for working with me in very rough conditions. I also thank my bike Bajaj Pulsar DTSi 180 for always being up for me.

I gratefully acknowledge the financial support that was received from the Department of Science and Technology, Govt. of India (SERC-DST: SR/S3/MERC/005/2010) to carry out the research work presented in this thesis.

Finally, above all he is **Supreme Lord** who has ever been present with me irrespective of my ups and downs. I thank him for his endless blessings.

Abstract

Experimental investigation has been carried out in a 20 m long, 1 m wide, and 0.72 m deep flume on three sands of median diameter 1.1 mm, 0.418 mm, and 0.62 mm in two categories: no seepage experiments to check the stability of curvilinear cross-sectional channels with different top widths and when seepage is applied in the downward direction to these channels. Longitudinal and cross-sectional profiles of alluvial channels are altered by the presence of downward seepage. Available literature suggests that seepage affects the hydrodynamics of alluvial channels. In the present experimental study, downward seepage has been applied to the parabolic channels based on tractive force theory for finding its effect on the cross-sectional profiles of stable channels.

It has been observed that bed shear stress increased when downward seepage was applied to the channel. Cross-sectional parabolic shape does not hold when downward seepage is applied and channels take a new shape with flat-bed and two curved banks and achieve stability. An empirically derived exponential expression has also been suggested for the evaluation of bank profiles of threshold alluvial channels affected by the downward seepage which satisfactorily predicts the bank profiles at various cross-sections of the natural alluvial rivers. The relationship among hydraulic parameters for stable channel with downward seepage has also been developed on the basis of experimental observations.

At high bed shear stress in alluvial channels made of the non-cohesive material, sediment transport occurs as sheet flow layer of high sediment concentration. The sediment transport in the form of sheet flow has been observed in the present study when downward seepage was applied to the non-transporting channels designed on the basis of incipient motion condition of the bed particles. The erosion of the channel banks contributed to the sheet flow because of the increased channel bed shear stress. An empirical relation for the thickness of sheet flow layer has been developed which includes seepage in the downward direction as an independent parameter along with others. Regime relationships have been developed in the non-dimensional and dimensional form for the design of alluvial channels in the presence of downward seepage.

Turbulent structures of the flow have been analyzed in curved sand bed channels with and without the presence of downward seepage. Measures of turbulent

statistics such as time-averaged near-bed velocities, Reynolds stresses, thickness of roughness sublayer and shear velocities were found to increase with the application of downward seepage. Turbulent kinetic energy and Reynolds normal stresses were increased in the streamwise direction under the action of downward seepage, causing bed particles to move rapidly. Analysis of bursting events shows that the relative contributions of all events (ejections, sweeps and interactions) increased throughout the boundary layer, and the thickness of the zone of dominance of sweep events, which are responsible for the bed material movement, increased in the case of downward seepage. The increased sediment transport rate due to downward seepage deforms the cross-sectional geometry of the channel made of erodible boundaries. The deformation is caused by an increase in flow turbulence and an associated decrease in turbulent kinetic energy dissipation and turbulent diffusion.

Contents

List of Figures

List of Tables

Symbols

σ_g	Gradation coefficient
d_{50}	Median particle diameter
ϕ degree	Angle of repose (dry)
Q_0	Main channel discharge
C_d	Coefficient of discharge
Q	Discharge over the notch
L_n	Length of the notch
h	Height of water above the notch
E	Voltage generated in a conductor
u_c	Velocity of the conductor
B_s	Strength of the magnetic field
D	Length of the conductor
q_s	Seepage discharge
Ap	Area of the pipe in flow meter
U, V and W	Time-averaged velocities in the streamwise, lateral and vertical directions, respectively
U_i, V_i, and W_i	Instantaneous velocities in the streamwise, lateral and vertical directions
u', v' and w'	Fluctuating components of the instantaneous velocities in the streamwise, lateral and vertical directions, respectively
$F_{uu}(f)$	Velocity power spectra
f	Frequency
y	Flow depth of the channel
u	Mean flow velocity

B	Top width of the channel
S_0	Bed slope
S_{fs}	Friction slope of spatially varied flow
A	Cross-sectional area of channel
θ_c	Critical Shields parameter
R^*	Shear Reynolds number
S_w	Water surface slope
u_s	Average velocity of flow with seepage
Q_s	Average discharge with seepage
q_s	Seepage discharge over the reach length L
X	Distance from the tail gate
F_0 and F_s	Froude number with no seepage and seepage condition
R_{hs}	Hydraulic radius with seepage
p_s	Wetted perimeter with seepage
S_{ws}	Water surface slope with seepage
V_s	Seepage velocity through the sand bed of length L
τ_s	Shear stress for seepage experimental condition
τ_{bs}	Bed shear stress under seepage condition
S_{f0}	Friction slope under no seepage conditions
τ_0	Bed shear stress under no seepage conditions
R_{h0}	Hydraulic radius under no seepage conditions
A_0	Cross-sectional under no seepage conditions
p_0	Wetted perimeter under no seepage conditions
θ	Shields parameter
N	Seepage intensity parameter
M	Parameter in Equation (2.18)
τ_{c0} and τ_{cs}	Critical shear stress under no seepage and seepage condition
Ω_0 and Ω_S	Stream power under no seepage and seepage condition
u_0^* and u_s^*	Shear velocity under no seepage and seepage condition
y_0 and y_s	Depth of flow under no seepage and seepage condition
u_0 and u_s	Mean velocity under no seepage and Seepage condition

y_L	Lateral horizontal distance from the center of the channel
y_T	Lateral distance from the water margin
y_{local}	Local vertical channel depth
y_C	Centre line depth of the channel
K	Displacement thickness
μ	Submerged static coefficient of Coulomb friction
λ	Lagrange multiplier
h_{local}	Lateral distribution of the local depth
b	Half width of the channel
β	Channel shape parameter
x	Lateral horizontal distance from the center of the channel
Δ	Thickness of the sheet flow layer
ρ_s	Dry density of the sediments
ρ	Density of the fluid
Δ_S	Maximum sheet flow layer thickness
β_t and R_V	Wave shape indices
T_t	Half wave period of collinear waves and currents
$T_{t,w}$	Half wave period for pure waves
θ_{max}	Maximum Shields parameter
μ	Static friction coefficient
C_m	Mean sheet flow layer concentration
Ψ	Mobility number
s	Specific gravity
δ	Dimensionless sheet thickness
γ_s and γ	Specific weight of sediment particles and water
ν	Kinematic viscosity of water
$\delta_{Observed}$	Observed values of dimensionless sheet thickness
$\delta_{Predicted}$	Predicted values of dimensionless sheet thickness
$\overline{\delta_{\text{Observed}}}$	Mean of the observed values of dimensionless sheet thickness
U_{cr}	Critical velocity
m	Critical velocity ratio

f_l	Lacey's silt factor
N_a	Absolute rugosity
F_{bed}	Bed factor
F_{side}	Side factor
C	Suspended-sediment concentration
K_1, K_2, K_3 and K_4	Coefficients related to the canal type
m_e	Exponent of Simons and Albertson's study
b_p, f_p and m_p	Exponents of power function theory
a, c and k	Constants of power function theory
v_s	Fall velocity
Q_n and B_n	Discharge and width for the normalized channel
i, j, i_w, Z	Hydraulic gradient, friction gradient, hydraulic gradient of equivalent clear water flow, function of particle properties
Q_{sed}	Sediment discharge
W_p	Width control parameter
S_d	Slope of depth-width curve
Q_b	Total bed load discharge
P_n, P_B and P_y	Proportions of the adjustment of stream power by friction, channel width and depth of flow respectively
α, S_e and β_1	Roughness measure, energy slope and exponent
μ'	Relative bank strength
Q_f	Formative discharge
i_a	Average channel gradient
η	Maximum sediment transport efficiency
D_i	Discrepancy ratio based on logarithm ratio
D	Hydraulic mean depth
τ_{uw}	Reynolds shear stresses
τ_{turb} and τ_{visc}	Turbulent and viscous shear stresses
σ_u^+ and σ_w^+	Non-dimensional turbulence intensity in streamwise and vertical direction
z^+	Non-dimensional depth
D_u and C_u	Coefficients suggested by Nezu and Nakagawa (1993)

$Sk(u_i)$	Coefficient of skewness of a velocity time series
Δz	Depth of the virtual bed
z_0	Zero velocity level
k	von Karman's constant
U^*	Shear velocity evaluated by the linear projection of the RSS profile
σ_u	Streamwise turbulence intensities
σ_w	Vertical turbulence intensities
f_{TKEu} and f_{TKEw}	Flux of turbulent kinetic energy in the streamwise and vertical direction
T	Total sampling time of velocity pulse
$\delta_{i,H}$	Indicator function
H	Hyperbolic hole region
$S_{i,H}$	Fractional contribution of RSS
M_{30} and M_{03}	Flux of the Reynolds normal stress in the streamwise and vertical direction
M_{21} and M_{12}	Advection of RNS in the streamwise and vertical direction
TP, ED and TD	Non dimensional turbulence production, energy dissipation and turbulent diffusion
t_p, ε, and t_D	Turbulence production, energy dissipation and turbulent diffusion
l	Turbulent mixing length

Chapter 1

Introduction

All natural rivers are subjected to change, either through erosion or deposition. Flow of water in the river channel is altered normally by the river engineering works because of which the sediment movement in a channel is also altered and consequently the shape and plan form of the channel is affected. This alteration in the shape and plan form of a channel further affects the flow conditions in the channel, its conveyance and the composition of the bed sediments. Sediment characteristics of river channels have been approached from various directions in the past several decades.

It has long been observed in experimental channels and natural river channels that there is some threshold condition of flow below which sediment particles do not move. Shields (1936) in his pioneering study characterized this flow condition as the condition of incipient motion. These threshold flow conditions have since often been incorporated into the theories of sediment transport. Movement of sediment particles in a stream and the flow are closely related to each other. Although the sediment transport is determined by the flow, the movement of sediment particles determines the size and shape of bed features which in turn affects the hydraulic resistance and hence the flow.

On a broad scale the movement of sediments within river catchments is dependent upon many catchment characteristics which are strongly inter-related. These

characteristics may be physical such as topography, vegetation, geology and land use or hydrological in nature such as precipitation and temperature. For a long time the movement of sediment particles along the beds of the river channels has been one of the most complicated and challenging problems for the scientists and researchers around the globe who have tried to explain it.

Alluvial channels are the man-made channels constructed in alluvium which embodies deformable bed and banks. These alluvial channels are mostly used for irrigational and navigational purposes. Fluvial hydraulics is the branch of science which deals with the hydraulics of rivers flowing through loose non-cohesive material called alluvium. People in the different countries such as India, China, Mesopotamia, Egypt, Greece and Italy had built irrigation canals taking off from alluvial channels and faced problems due to sedimentation of canals.

In ancient India the developments of irrigation and rivers is given in religious scriptures which suggests that Indians were aware of ability of flowing water to carry gravels, sand, silt and clay. Further, this ability decreases as the velocity of flow is decreased. Indian literature suggests that in Vedic and post Vedic times Indians were aware of erosion caused by rivers and control of erosion (Garde, 1995).

Chinese engineers have contributed significantly to the present knowledge of fluvial hydraulics as they have dealt with sediment transporting rivers. China is the home of some of the most troublesome rivers such as the Yellow river which has very high sediment concentration in its flow. Some of the old irrigation projects constructed centuries ago in China are still functioning such as a diversion structure which was built on Minjiang river. A canal was dug which was used for irrigational and navigational purposes. This structure had been functioning till 1949 (Garde, 1995).

Work on the stable channels commenced in India by British engineer Kennedy (1895) late in the 19th century who worked on Upper Bari Doab canal network. In the first quarter of the 20th century Lindley (1919) worked on the Lower Chenab system and observed that stable channels have three degrees of freedom (i.e. width, depth and slope) which can adjust according to the given conditions. Gerald Lacey

made the most significant contribution towards the development of design procedure for regime channels. He analyzed the available data of the stable channels in India and gave relations for stable channel dimensions which are widely used in India.

Canals designed outside India on the basis of Lacey's equations were not successful to a greater extent because of the two major limitations (Garde, 1995). First, as pointed out by Lane (1937) that sediment load being an important parameter has not been incorporated as an independent parameter in Lacey's equations. Second, as observed by Blench and Simons and Albertson (1963) since Lacey worked on the data of the canals which had cohesive bank material, Lacey's design equations are applicable to those canals which are composed of sandy bed and cohesive bank material.

Alluvial channels often encounter permeable boundaries in natural environments such as porous boundaries consisting of sediment particles in natural rivers and in irrigation canals. Flow in natural channels is a complex interaction between surface and subsurface flow. Water is continuously seeping into or out of the channel bed and channel banks. Exchange of water (seepage) can occur in either way, flow from the channel (downward seepage) (Figure 1.1) or flow into the channel (upward seepage) (Figure 1.2) depending upon the difference of level between the water in the channel and surrounding ground water table.

With a difference between the water level in an alluvial channel and surrounding ground water table, seepage takes place through the porous boundary of the alluvial channels and substantial amount of water seep through the channel perimeter into the surrounding groundwater. Transfer of mass and momentum across the interface between the fluid and porous media takes place through the permeable boundaries. Condition of zero-velocity for the flow over impermeable boundary may be invalidated in the presence of seepage through the porous boundary. Additional hydrodynamic forces may be exerted on sediment particles on the channel boundary under the presence of seepage through it besides the forces which are normally considered. These additional forces can have significant effect on the

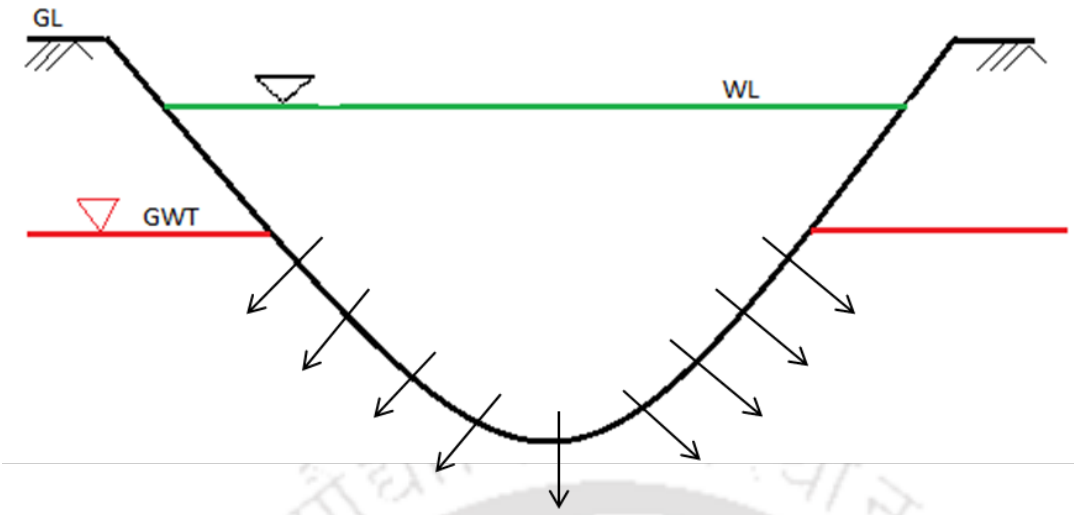

FIGURE 1.1: Flow from the channel (downward seepage)

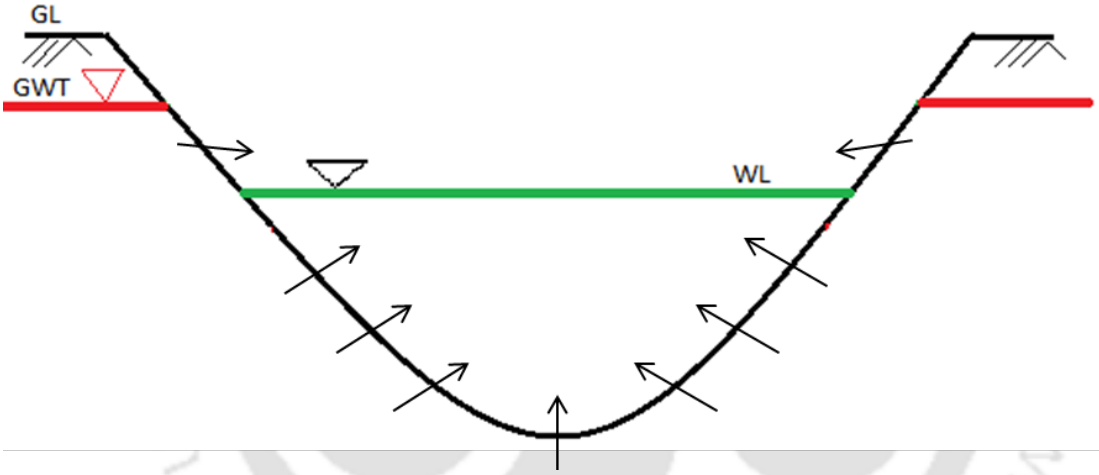

FIGURE 1.2: Flow into the channel (upnward seepage)

processes of sediment transport including the threshold of motion of the sediment particles and the flow resistance in alluvial streams which may lead to the change in their geometry.

Presence of seepage leads to a change in the bed deformation conditions and consequently the hydrodynamic characteristics of the channel. The study of the effect of seepage flows on the detachment of particles from the bed and further movement of the bed load is of great interest, since this study is related to the solution of important practical engineering problems. For instance, groundwater movement plays an exceptionally important role when constructing hydraulic structures, particularly dams; these challenges are urgent when solving problems concerned with

the stability of dams and canal slopes. Earthen irrigation channels in permeable soils lose considerable amounts of water through the bed and sides of the canals resulting in low conveyance efficiency. By the time the water reaches the field it has been estimated that depending upon the site specific condition, the seepage losses may be on the order of 45% of the water supplied at the head of the canal (Sharma and Chawla, 1975).

One of the early studies on canal losses using radioisotopes in the Ganga canal was done by Krishnamurthy and Rao (1969) and reported the seepage losses as 2.2 m^3 /day/m. Raja et al. (1983) estimated the seepage losses from an unlined channel by nuclear technique and reported that the seepage losses to vary from 1.3 to 4.3 m^3 /106 m^2 of the wetted surface area. Dukker (1994) measured the seepage losses from Lower Gugera Branch Canal using the inflow-outflow technique and found a wide range of variation in seepage rate due to errors and uncertainties in measurements. Their results vary from 3.54 to 62.04 cm per day. Weller and McAteer (1993) reviewed all seepage measurement techniques and discussed the statistical treatment of random errors in the inflow-outflow method. With fairly precise current metering the errors indicated in the inflow and outflow measurements are reported to be as high as ±110%.

An analysis of seepage from the New York Canal (NYC) estimates that cumulative seepage rates range between 12% and 20% at canal flows of 439 to 980 cubic feet per second (cfs) (Berenbrock, 1999; Carlson and Petrich, 1999). According to the estimation of Yussuff et al. (1994) and Tanji and Kielen (2002) in unlined canals of semi-arid regions seepage losses can account for 20-50% by volume of the total flow. Around 17% of the water that was conveyed for irrigation in 1985 was lost according to the report of Carr et al. (1990) in the United States due to evaporation or seepage to the groundwater. Conveyance efficiency from the point of diversion to the field in canals in the Lower Rio Grande Valley in Texas was found to be 69.7% (Fipps, 2005). Kinzli et al. (2010) used acoustic Doppler instrument to measure canal flow rates and found that more than 40% volume of the diverted water could be lost due to seepage in the Middle Rio Grande Valley of New Mexico.

Interactions between flow in the main stream and the ambient groundwater are important because of their role in controlling the transport of contaminants and maintaining a healthy stream ecosystem (Brunke and Gonser, 1997; Jones and Mulholland, 2000). The hydrodynamic process in such a physical system may result in changes to the structural features of the flow, implying modification to flow-resistance, sediment entrainment characteristics and morphology of the streambed, as compared to that with an impermeable boundary. For instance, a water intake, when drawing faster-moving flow towards the sediment bed, can increase the local bed shear stresses, resulting in bed erosion around the intake structure (Willetts and Drossos, 1975). More complex situations occur in the coastal environments, for example in swash zone, where seepage varies both temporally and spatially (Turner, 1995; Karambas, 2003).

Watters and Rao (1971) in their experimental study observed that lift forces should be considered in the stability criteria for bed particles as the lift and drag forces on a particle are of comparable magnitudes. When the drag forces on particles are considered; downward seepage increases particle motion, while upward seepage hinders it. When lift forces are considered; upward seepage prevents the motion of a plane bed particle but the motion of a particle above the general bed level is increased. Flow configuration near the bed is affected by the presence of seepage through the bed of an alluvial channel and seepage modifies the sub layer thickness of the channel bed.

Oldenziel and Brink (1974) found that a small increase in shear stress appreciably increases the rate of transport of sand particles. They concluded that the sediment transport rate is always decreased in case of downward seepage, while upward seepage increases the transport rate.

Willetts and Drossos (1975) through their experimental study in a narrow flume with small downward seepage zone observed that downward seepage produced a localized scour hole in the downward seepage zone and grains moved at a faster rate in the downward seepage zone than elsewhere in the flume.

Richardson et al. (1985) observed that upward seepage caused a very small increase in the stream power for flows near or in the upper regime. In low regime flows sediment transport was increased with upward seepage as compared to that when no seepage was present.

Maclean and Willetts (1986) measured the bed shear stress with and without downward seepage by observing the initiation of motion of the indicator grains. They observed that the shear stresses increased with the presence of downward seepage.

Maclean (1991a) carried out velocity measurements in two sets of experiments in an open channel and in a wind tunnel with high rates of downward seepage. He observed gradual decrease of shear velocity in the downstream direction over the seepage zone.

Maclean (1991b) concluded that downward seepage produced an increase in the bed shear stress which resulted in local scour. When the downward seepage velocity was 10% of the mean channel velocity, the increase in bed shear stress was approximately twice the uniform shear stress.

Prinos (1995) solved the Reynolds-averaged Navier-Stokes equations and studied the effect of downward seepage on the boundary shear stress. The bed shear stress increased with increasing downward seepage rate in the seepage zone. For downward seepage velocity 9% of the mean channel velocity, the increase in bed shear stress with downward seepage was about eight times to that of without downward seepage.

Cheng (1997) carried out experimental study to find out the effect of upward seepage on open channel flow. He observed increase in the root mean square values of velocity fluctuations and Reynolds shear stresses in the near-bed region.

Cheng and Chiew (1998b) derived an equation to evaluate the shear velocity by integrating the continuity and momentum equations. The derived equation for bed shear stress based on momentum integral equation compared well with the results obtained from the measured Reynolds shear stress distribution (Cheng,

1997). Cheng and Chiew (1998a) proposed another method for evaluating the bed shear stress by directly fitting the modified logarithmic law for upward seepage. Results indicated that the shear stress reduced noticeably at the beginning of the upward seepage zone and for the higher seepage intensity the reduction became more apparent. Nevertheless, gradual increase in the bed shear stress has been observed towards the downstream end of the upward seepage zone.

Cheng and Chiew (1999) considered an additional force due to upward seepage and performed a force analysis for the threshold condition of sediment movement. It has been observed that the critical shear velocity was reduced in the presence of upward seepage.

Rao and Sitaram (1999) through their experimental study observed that upward seepage increased the stability of bed particles, while under the application of downward seepage it reduced. They concluded qualitatively that turbulence intensities were higher for downward seepage than for upward seepage or without seepage. It has been argued by Rao and Sitaram (1999) that in case of upward seepage, the effective weight of bed particles reduces which causes the decrease in the resistance and because of the decrease in the near-bed velocity as well as turbulence intensity, hydrodynamic forces acting on the bed particles also reduce. Opposite results were observed for the case of downward seepage.

Krogstad and Kourakine (2000) investigated localized upward seepage effects on the turbulence structure in a boundary layer. It has been observed in their experimental results that as the incoming flow entered the upward seepage region, the bed shear stress was significantly reduced.

Chen and Chiew (2004) experimentally investigated the effect of downward seepage on bed shear stresses in open-channel flow. They observed that the conventional law of the wall is not applicable to open channel flow subjected to downward seepage. Velocity increased in the near-bed region and decreased near the water surface. This resulted in a more uniform velocity distribution. Further it has also been observed that the origin displacement, slip velocity and shear velocity increased with increase in relative downward seepage.

Lu and Chiew (2007b) in their experimental study over the fixed dune bed observed that the streamwise velocity profile became more uniform when compared to that without downward seepage. Sreenivasulu et al. (2010) observed higher velocities with seepage as compared to no-seepage in their experiments. Variation in the friction slope was small for no seepage as compared to that with downward seepage. Bed shear stress increased along the length of the flume for no seepage and a reverse trend was observed when downward seepage was applied. Overall bed shear stress was higher for downward seepage than that for no seepage.

Sreenivasulu et al. (2011) pointed out that in the presence of downward seepage stream power varied non-linearly in the channel and it decreased in the downstream direction. Higher stream power prevailed on the upstream end of the channel with downward seepage hence it got eroded. Deposition was observed at the downstream end of the flume. They recommended that the effects of downward seepage should be considered in channel design.

Cao and Chiew (2014) carried out experiments to observe the effects of downward seepage on sediment transport rate in closed-conduit flows. Their results indicate that the near-bed velocities are closely related to the sediment transport rate with downward seepage and bed load transport rate increased with rate of downward seepage. They also carried out numerical simulation of the closed-conduit flows and observed results similar to their experiments.

Lu and Chiew (2007a), Dey and Nath (2010) and Dey et al. (2012) carried out experiment to observe the effects of the presence of seepage on the turbulent characteristics of flow in open channels. Their findings among others on the effects of downward seepage and upward seepage on bed shear stress and sediment transport rate are summarized in Table 1.1.

Sediment transport dynamics can be viewed as one part of the field of two-phase flows i.e. flows of a fluid that contains discrete solid particles within it. This makes the system of an included phase and an including phase. Turbulent sediment-transporting flows represent one of the most challenging problems in all of hydraulics and fluid mechanics for two reasons. First, the presence of the included

phase can alter the turbulence structure of the including phase. Second, in many cases the flow boundary consists of the sediment particles, and then the flow can shape its own boundary but in turn may get affected by that shaped boundary.

TABLE 1.1: Effect of seepage on channel hydrodynamics

Authors	Flume dimensions			Seepage effects			
	Length (m)	Width (m)	Seepage zone (m)	Bed shear stress		Sediment transport rate	
				US	DS	US	DS
Watters and Rao (1971)	4.6	0.7	1.5	NA	NA	-	+
Oldenziel and Brink (1974)	15	0.5	4	NA	NA	+	-
Willetts and Drossos (1975)	3.6	0.076	0.125	NA	NA	NA	+
Richardson et al. (1985)	9.45	0.6	3	NA	NA	+	-
Maclean and Willetts (1986)	5	0.076	5	NA	+	NA	NA
Maclean (1991a)	12	0.3	0.28	NA	+	NA	NA
Maclean (1991b)	5	0.075	0.13	No	+	No	+
Prinos (1995)	Analytical model			NA	+	NA	NA
Cheng (1997)	7.6/30	0.21/0.7	0.5/2	-	NA	+	NA
Cheng and Chiew (1998b)	30	0.7	2	-	NA	NA	NA
Cheng and Chiew (1998a)	30	0.7	2	-	NA	NA	NA
Cheng and Chiew (1999)	7.6	0.21	0.5	-	NA	+	NA
Rao and Sitaram (1999)	3.6	0.158	2.4	+/-	+/-	-	+
Krogstad and Kourakine (2000)	3.5	0.46	0.12	-	NA	NA	NA
Chen and Chiew (2004)	30	0.7	2	NA	+	NA	NA
Lu and Chiew (2007a)	30	0.7	2	NA	NA	-	+
Dey and Nath (2010)	12	0.6	2	-	+	NA	NA
Sreenivasulu et al. (2010)	25	1.8	20	NA	+	NA	NA
Dey et al. (2011a)	15	0.6	2.1	-	+	NA	NA
Rao et al. (2011)	25	1.8	16	NA	NA	NA	+
Sreenivasulu et al. (2011)	25	1.8	20	NA	NA	NA	+
Cao and Chiew (2014)	9	0.3	0.5	NA	NA	NA	+

Changes in the essential nature of the flow, starting with turbulent flow in a closed-conduit and sediment-transporting flow over a loose sediment bed in the last have been depicted in Figure 1.3. The step from a circular pipe to a rectangular duct brings the presence of a weak but non-negligible secondary circulation, but there is no big difference in the structure of the shear-flow turbulence. In the next step from rectangular duct to an open rectangular channel, the turbulence structure is again only slightly different, as are the secondary circulations. But the presence of

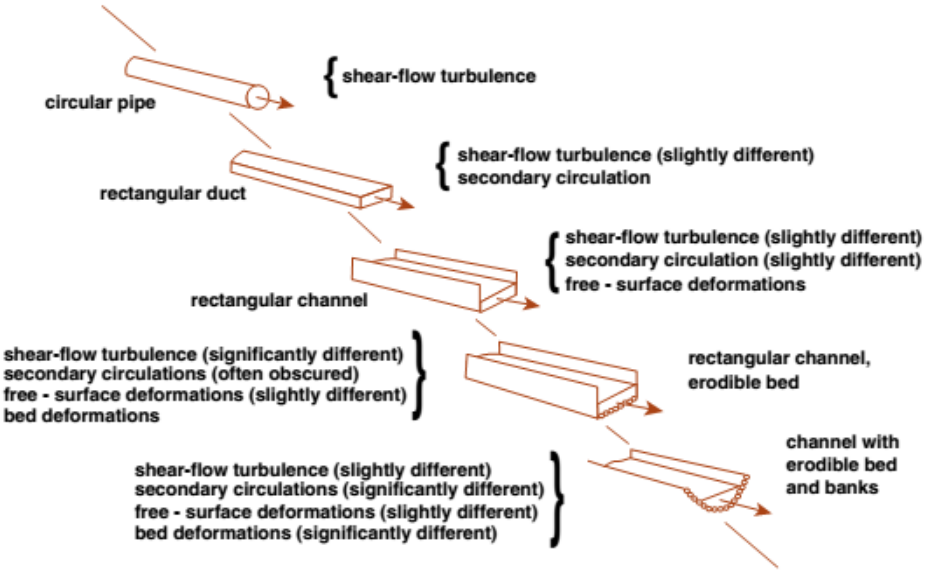

FIGURE 1.3: Complexity in sediment-transporting flows (Image source: MIT OpenCourseWare)

deformable free surface here in open rectangular channel makes for rather different effects in unsteady flows. In the next step to an open rectangular channel with a loose sediment bed, is the big one: because the flow here can mold the bed now, and the bed too has a strong effect on the flow, the turbulence structure and the free-surface geometry are significantly different in certain ranges of flow. The last step, to a channel with erodible boundaries, makes for greatly different bed geometry, at least in certain ranges of the flow.

Sediment transporting flows in the natural streams and canals are turbulent in nature. Elegant work has been carried out in the past to understand the characteristics of turbulent flows and its interaction with sediment transport. With recognition of bursting phenomenon (Kline et al., 1967), more insights into the coherent structure of turbulent flows were made possible.

Various researchers (Sutherland, 1967; Thorne et al., 1989; Clifford et al., 1991; Best, 1992; Cao, 1997; Dey and Raikar, 2007; Dwivedi et al., 2010; Dey et al., 2011b) studied the turbulent structure of flow over bed particles that were on the threshold of motion. Turbulent characteristics of flows over mobile beds have also been studied by Heathershaw and Thorne (1985), Drake et al. (1988), Song and

Graf (1994), Bennett and Bridge (1995), Nelson et al. (1995), Gallagher et al. (1999), Nikora and Goring (1999) and Nikora and Goring (2000), Sumer et al. (2003), Venditti et al. (2005) and Dey et al. (2012).

However, sediment transport in alluvial streams is highly influenced by the presence of seepage. Water in alluvial streams continuously seeps into or out of the channel bed and channel banks (Richardson et al., 1985). In previous studies, the effect of seepage through porous boundaries is clearly visible on the turbulent characteristics of flow. Nezu (1977) observed that the higher velocity region is attracted towards the wall in the case of downward seepage and it is lifted away from the wall in the case of upward seepage. Oldenziel and Brink (1974), Maclean (1991a) and Chen and Chiew (2004) have also observed increased velocity in the near-bed region in the case of downward seepage.

Similarly, Dey and Nath (2010) observed increased streamwise velocity towards the wall in the presence of downward seepage and decreased streamwise velocity in the presence of upward seepage. Antonia et al. (1988), Krogstad and Kourakine (2000) and Oyewola et al. (2004) observed increased anisotropy in the near-bed region in flows affected by downward seepage, while Dey and Nath's (2010) observation suggests strongly anisotropic turbulence. Watters and Rao (1971) observed increased hydrodynamic roughness and decreased levels of turbulence with lesser momentum exchange between fluid particles in the case of downward seepage. Nezu (1977), Antonia et al. (1988), Antonia et al. (1995), Lu and Chiew (2007b), Dey and Nath (2010) have observed that turbulent intensities decrease in case of downward seepage, while they increase in case of upward seepage (Nezu, 1977; Cheng and Chiew, 1998b; Krogstad and Kourakine, 2000; Dey and Nath, 2010).

From 1.1 it is clear that most of the researchers are of the view that downward seepage increases the bed shear stress, which initiate the sediment transport rate. Alluvial channels which are designed on the basis of the incipient motion condition of the particles resting on the bed and banks of the channel, do not transport sediment through them. Application of downward seepage to these channels causes deformation of the channel boundaries and channels may start transporting the

bed material. Most of the studies in the experimental flumes by previous researchers to observe turbulent characteristics of flow with downward seepage and upward seepage have been carried out on either plane or fixed bed. To understand the process of erosion of banks and deposition of eroded material on the channel bed after the application of seepage, study must be carried out on a channel which reflects similarity with the natural channels. Based on this, following are the objectives of the present research work:

1. Quantification of cross-sectional profile of stable alluvial channels with downward seepage.
2. Study on bank erosion and quantification of sheet flow layer in alluvial channels with downward seepage.
3. Development of the regime relationships for the design of stable channels.
4. Study of the turbulent characteristics of flow when downward seepage is applied to the channel.

The thesis contains five chapters. Brief review of each chapter is as follows:

Chapter 1: General sediment transport in alluvial channels is discussed. Review of the literature on the effects of seepage on the sediment transport and stability of the alluvial channels is carried out. Turbulent flow in channels and the studies carried out by previous researchers in the context are discussed. Further, the objectives of the present study are decided.

Chapter 2: This chapter presents the detailed description of the experimentations carried out in this study. Development of the flume is described. Bed material and various instrument used in the experimental study to collect data are presented. Detailed procedure of the data collection and its processing with the results is given.

Chapter 3: This chapter deals with the cross-sectional profile of stable channels considering the presence of downward seepage. Previous studies carried out regarding the cross-sectional profile of the alluvial channels are discussed in detail.

Changes in various profile parameters with seepage and channel shape parameter are discussed. Empirical equation has been developed for the prediction of the cross-sectional profile of stable channels affected by seepage. Bank profiles of some natural stable rivers are predicted with the generated empirical equation. Further, previous studies regarding the sheet flow layers in alluvial channels are discussed. Distortion of channel banks and bed material transport in the form of sheet flow layer with seepage are discussed. An empirical equation is generated for the prediction of the thickness of sheet flow layer of the sediment particles.

Chapter 4: In this chapter various empirical approaches, analytical methods, and extremal hypotheses available in the literature for the design of stable channels are discussed and a comparative analysis is carried out for the predictability of these theories using an independent set of data from natural stable channels. Further, regime relations are developed for the design of stable alluvial channels in dimensional and non-dimensional forms considering downward seepage.

Chapter 5: In this chapter the turbulent characteristics associated with the flow are presented and the comparison has been made between these characteristics with and without seepage. Mechanism of sediment transport is given when the seepage in the downward direction is applied to the channel which was non-transporting earlier when no seepage was present.

Chapter 6: In this chapter the conclusions of the study are made and the studies that should be carried out in future regarding the further understanding of the effects of downward seepage on the stability of alluvial channels are discussed.

Chapter 2

Methodology

One of the most important and interesting ways of studying sediment transport problems related to alluvial channels is by carrying out experiments in laboratory. Phenomena related to the design of alluvial channels are elucidated by hydraulic sediment transport experiments. For the design of a hydraulic phenomenon engineers have largely relied on empirical formulae and such formulae are often based on experimental measurement. Sound physical basis for an equation is important in that it may have far greater significance in solving problems. Various flow phenomena can be interpreted by experiments in laboratory with suitable dimensional analysis together with the process of reasoning. The chronological development in several fields of the sediment transport such as incipient motion and regime has been done through the experimental investigations.

As already mentioned in Chapter-1, the objective of the present work is to analyze the effect of downward seepage on various aspects of sand bed channels such as cross-sectional profile, channel bank distortion, sheet flow layer of high sediment concentration, regime theory of design and changes in the turbulent characteristics of flow. A flume can be used to simulate the channel behavior. The overall effects downward seepage on different hydraulic parameters can be observed in a flume by changing some parameters such as channel bed slope, discharge and seepage rate. The details of experimental set-up, measurement procedure and various

instrument used for measurements that were essential to achieve the objectives of the present work are also explained in this chapter.

2.1 Bed Material

Carefully sieved river sands of median sizes (d_{50}) 1.1 mm, 0.418 mm and 0.62 mm have been used for experiments. Particle size distribution for given sand can be said as uniform if the value of σ_g is less than 1.4 (Marsh et al., 2004). Table 2.1 enlists the physical characteristics of all three sands. Particle size analysis for all three sands is depicted in Figure 2.1.

TABLE 2.1: Physical characteristics of bed material

Serial No.	Bed Material	d_{50} (mm)	Gradation coefficient, σ_g	Angle of repose (dry), ϕ degree
1	River Sand	1.1	1.03	31.154
2	River Sand	0.418	1.17	32.55
3	River Sand	0.62	0.77	32.2

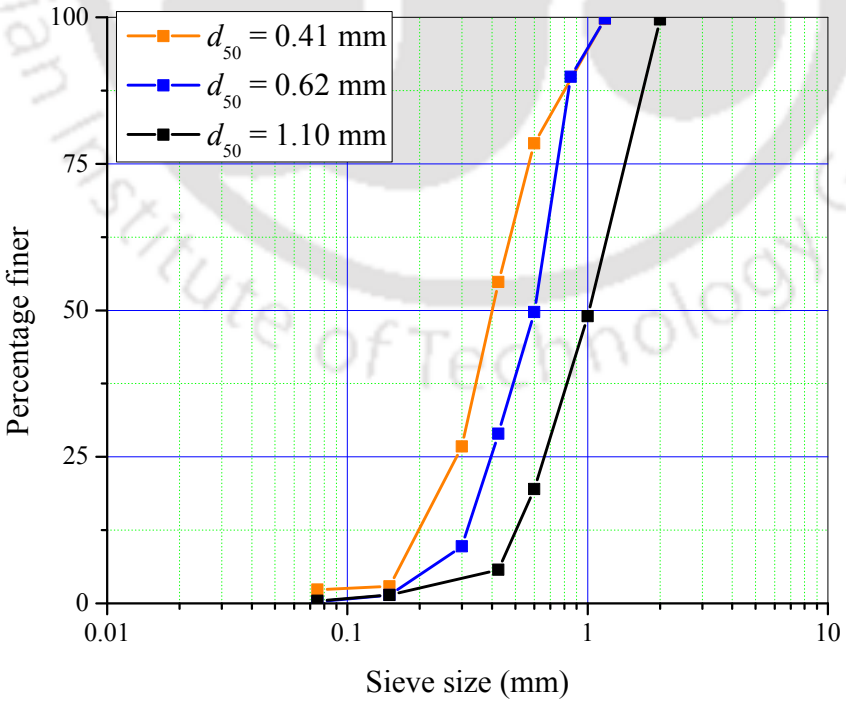

FIGURE 2.1: Sieve analysis

2.2 Tilting Flume

Experiments were carried out on a 20 m long, 1 m wide and 0.72 m deep glass-walled tilting flume (Figure 2.2). At the upstream end of the flume, a 2.8 m long, 1.5 m wide and 1.5 m deep collection tank was provided with a couple of wooden baffles installed in it to prevent highly turbulent flow from entering the channel. The entire length of the main channel bed, except a 2 m length at the upstream limit, was made porous by covering it with a fine mesh (0.1 mm) supported by a steel tube structure. This arrangement formed a basal pressure chamber 0.22 m high, 1 m wide and 15.20 m long between the bottom of the channel and the fine mesh. An adjustable tail gate was provided at the downstream end of the flume to maintain the required depth of flow in the channel during experiments.

Uniform river sand was used as bed material in the experiments, and was placed on the fine mesh in order to prevent its entrance into the basal pressure chamber. The basal pressure chamber was used to remove water from the main channel through the sand bed (uniformly) in the form of downward seepage. The amount of downward seepage was controlled by valves connected to the basal pressure chamber at the downstream end. A snapshot of the flume has been depicted in Figure 2.3.

2.3 Test Section

Flow in the test section of the flume is significantly affected by the entrance and exit conditions. Strong circulations are present in the flow if it is delivered to the flume directly by means of pipes. According to Nowell and Jumars (1987), "the problem can be viewed as getting the flow to 'forget' its recent history." In order to avoid the strong circulations present in the flow due to pipes, water was first collected into upstream collection tank of the flume. The level of water rose gradually in the upstream collection tank prior to its introduction into the channel.

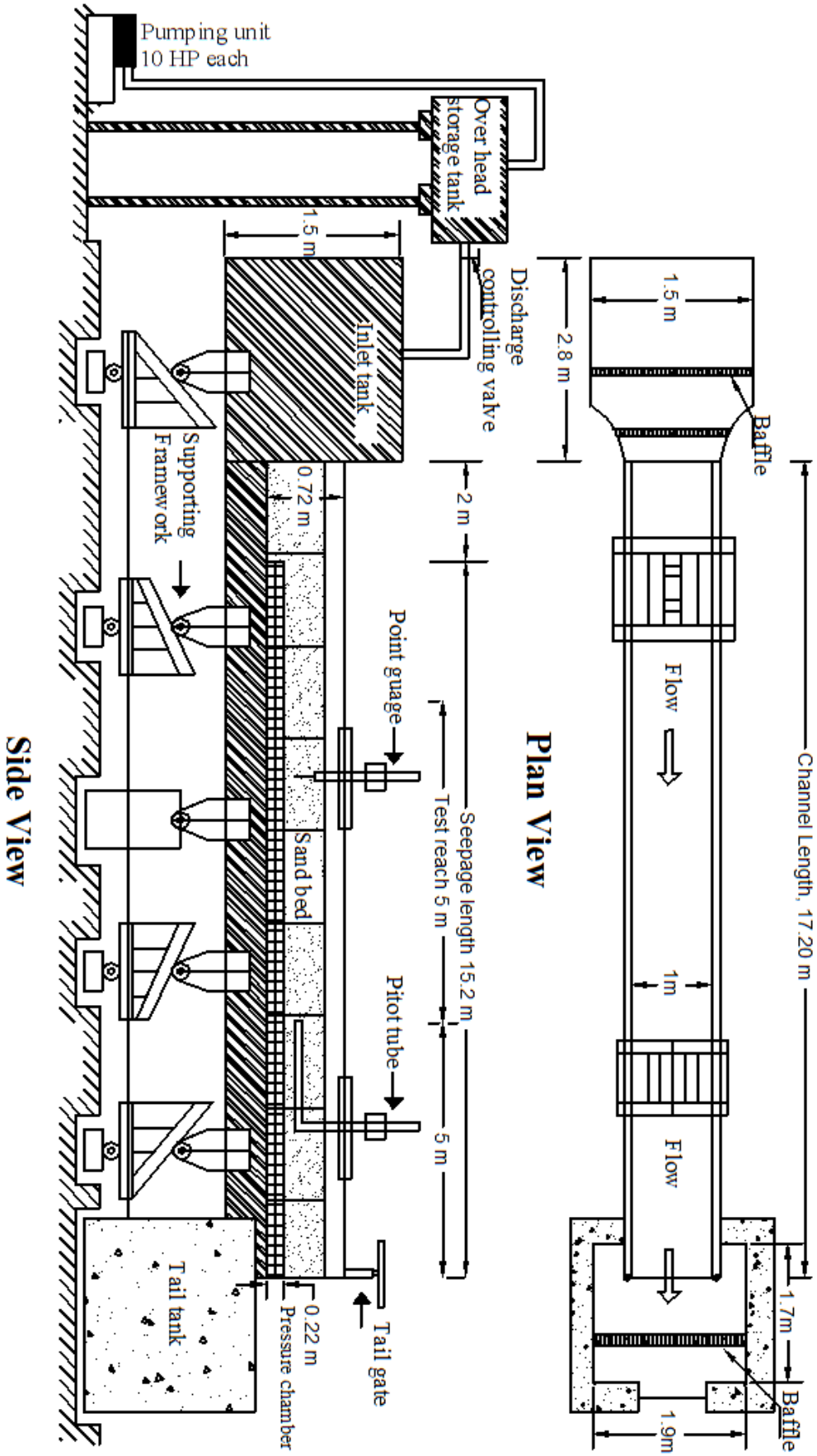

FIGURE 2.2: Schematic diagram of experimental flume

FIGURE 2.3: Snapshot of the tilting flume

To ensure the smooth entrance of flow into the channel, couple of baffles was installed in the upstream collection tank just upstream of the channel entrance. Nowell and Jumars (1987) further stated that "the exit problem can be viewed as not letting the flow know what is coming, i.e. of making a smooth exit without breaking cadence." Free overfall of flow from the tailgate causes acceleration of flow in the near-bed region just upstream of the tailgate. To minimize the effects of flow entrance and exit conditions in the channel, the test section in the present experiments was considered as a 5 m length in the middle of the flume (5m to 10 m from tail gate).

2.4 Main Channel Discharge

A rectangular notch has been provided at the downstream collection tank to measure the discharge coming out of the main channel (Q) volumetrically (Figure 2.4)

FIGURE 2.4: Rectangular notch for discharge measurement

Coefficient of discharge (C_d) for the rectangular notch has been shown in Figure 2.5 which was found to be 0.82, which can be calculated as:

$$Q = \frac{2}{3} C_d L_n \sqrt{2g} \left(h^{3/2}\right) \tag{2.1}$$

where Q is the discharge over the notch, L_n is the length of the notch ($L_n = 0.5$ m), g is the gravitational constant, and h is the height of water above the notch.

2.5 Seepage Discharge

The seepage flow from the seepage chamber (q_s) has been measured by a couple of electro-magnetic flow meters connected through the pipes to the seepage chamber as per the standards. The electro-magnetic flow meter is shown in Figure 2.6 The operation of an electro-magnetic flow meter is based upon Faraday's Law. According to the Faraday's Law the voltage induced across any conductor when it moves at right angles through a magnetic field is proportional to the velocity of

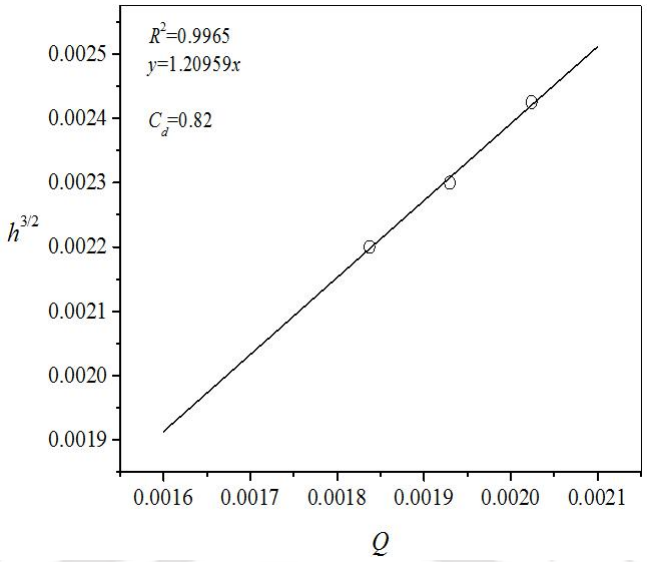

FIGURE 2.5: Coefficient of discharge for rectangular notch

that conductor.

$$E = f\left(u_c, B_s, D\right) \tag{2.2}$$

where E is the voltage generated in a conductor, u_c is the velocity of the conductor, B_s is the strength of the magnetic field, and D is the length of the conductor. The fluid being measured must be electrically conductive for the Faraday's law to apply. Faraday's Law indicates that signal voltage (E) is dependent on the average liquid velocity (u_c) the magnetic field strength (B_s) and the length of the conductor (D) (which in this instance is the distance between the electrodes). A magnetic field is established throughout the entire cross-section of the flow tube in the case of wafer-style magnetic flow meters. If this magnetic field is considered as the measuring element of the magnetic flow meter, it can be seen that the measuring element is exposed to the hydraulic conditions throughout the entire cross-section of the flow meter. The seepage discharge q_s can be calculated using the following relationship:

$$q_s = A_p u_c \tag{2.3}$$

where, q_s is the seepage discharge (m^3/s), A_p is the area of the pipe (m^2), and u_c is the fluid velocity passing through the flow meter (m/s).

FIGURE 2.6: Electro-magnetic flow meter

2.6 Flow Depth & Water Surface Elevation

Digital point gauge: The flow depth of water in to the channel is measured with the help of a digital point gauge attached to a moving trolley (Figure 2.7) This is a direct indicating gauge which eliminates observation errors due to vernier and scale reading. It can be set to zero anywhere in the operating range to permit easy relative level checking. The liquid crystal display is easy to read and has a resolution of ±0.01mm. A quick-release mechanism permits rapid changes of position. The depth of flow is defined as a difference between the water surface level and the bed level.

Pitot tube and digital manometer: Water surface slope in experiments is measured using a Pitot-static tube connected to a digital manometer which is

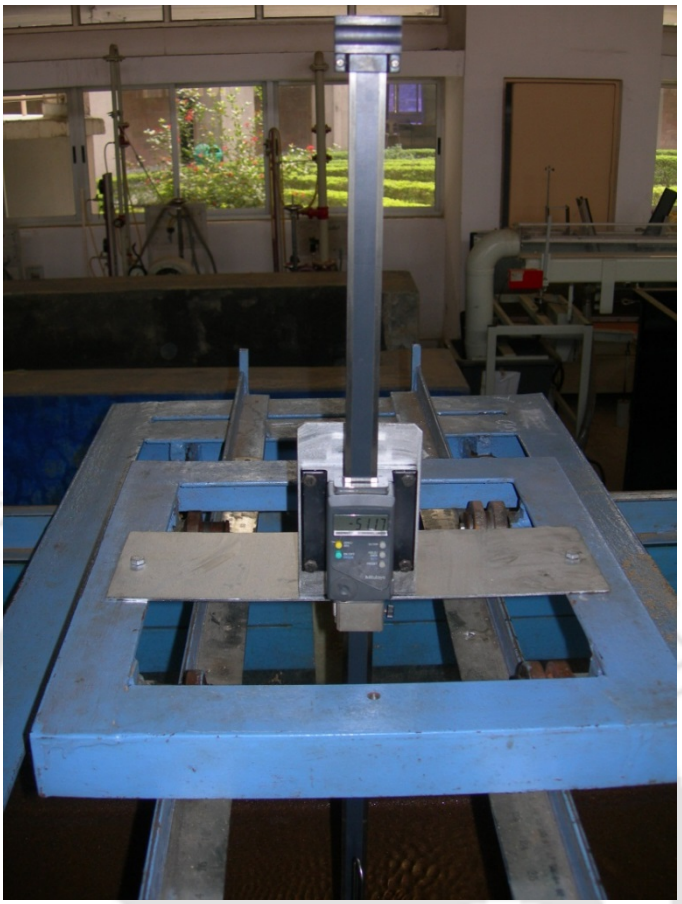

FIGURE 2.7: Digital point gauge

further attached to a moving trolley. The digital manometer is powered by two batteries of 12 Volts each connected in series. The outer tube consisting of static pressure holes when connected to digital manometer gives the piezometric height at that point. This way moving along the channel in the longitudinal direction, water surface slope is measured. Pitot-static tube and digital manometer arrangement are depicted in Figure 2.8.

2.7 Bed Slope (S_0)

Bed slope of the flume is measured by using Total Station (Figure 2.9). A Total Station is a modern electronic device that combines the ability to simultaneously measure a position horizontally and vertically. It has two components, a machine mounted on a static tripod, and a 'target' prism on a metal staff, which is moved

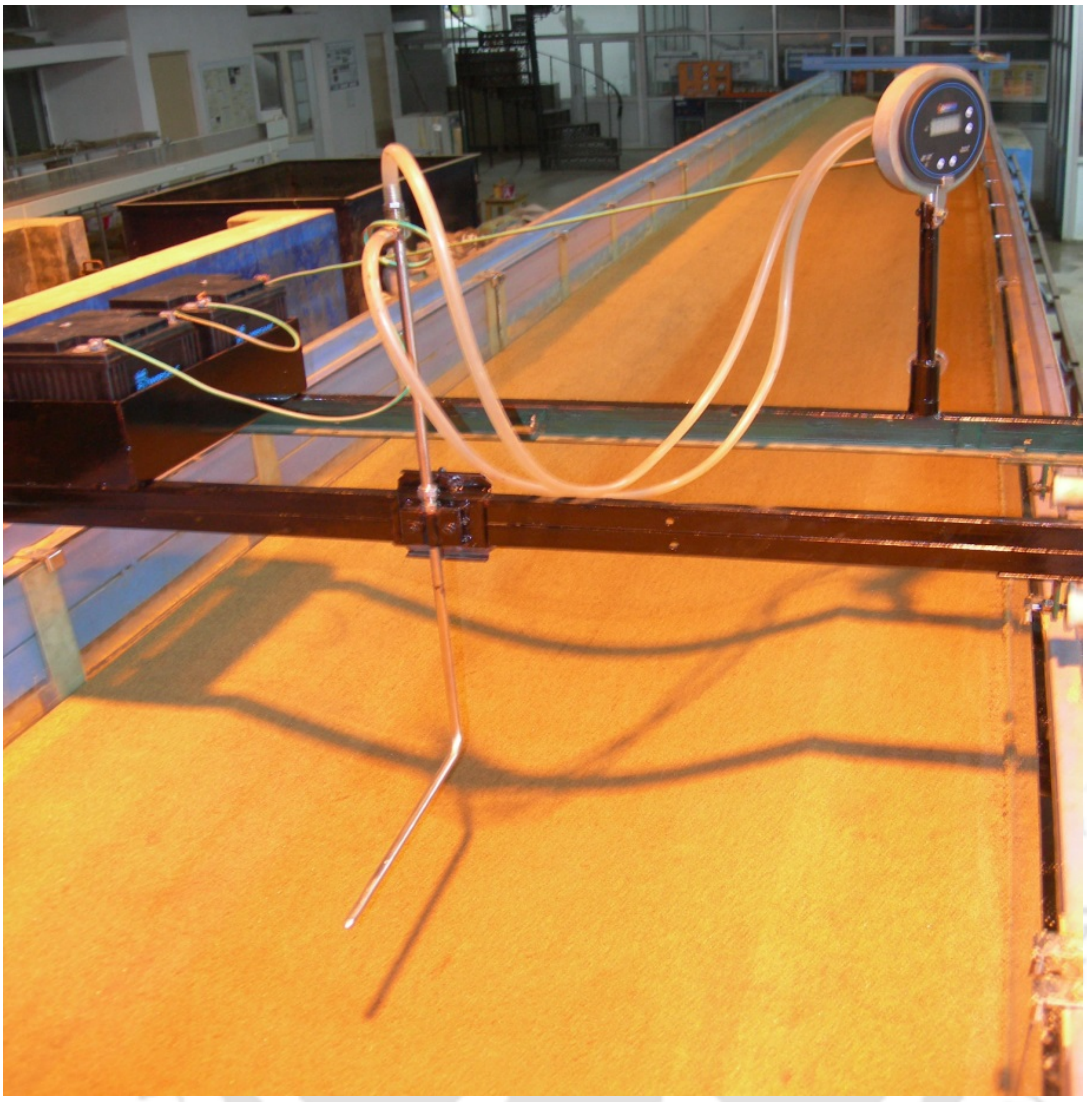

FIGURE 2.8: Pitot tube with digital manometer

around the site. The machine part of the Total Station has a lens somewhat like a telescopic rifle-sight with cross-hairs which are focused on the prism. The whole instrument revolves horizontally and the lens swivels vertically too. The Total Station is partly based on a principle used in traditional theodolites, where angles are calculated from vertical and horizontal 360-degree scales. It combines these with a device known as an Electronic Distance Measurer or EDM.

FIGURE 2.9: Measurement of bed slope by total station

2.8 Velocity and Turbulence Measurement

In order to understand the turbulent flow structure during no seepage and seepage experiments, instantaneous velocity readings along the vertical plane were taken using a four beam down looking Vectrino+ Acoustic Doppler Velocimeter (ADV) probe manufactured by Nortek (Figure 2.10) The instrument allowed data collection at a higher sampling rate up to 200 Hz. The Vectrino uses the Doppler effect to measure current velocity. The Doppler effect is the change in pitch that is heard when either the source of a sound or the observer is in motion. When

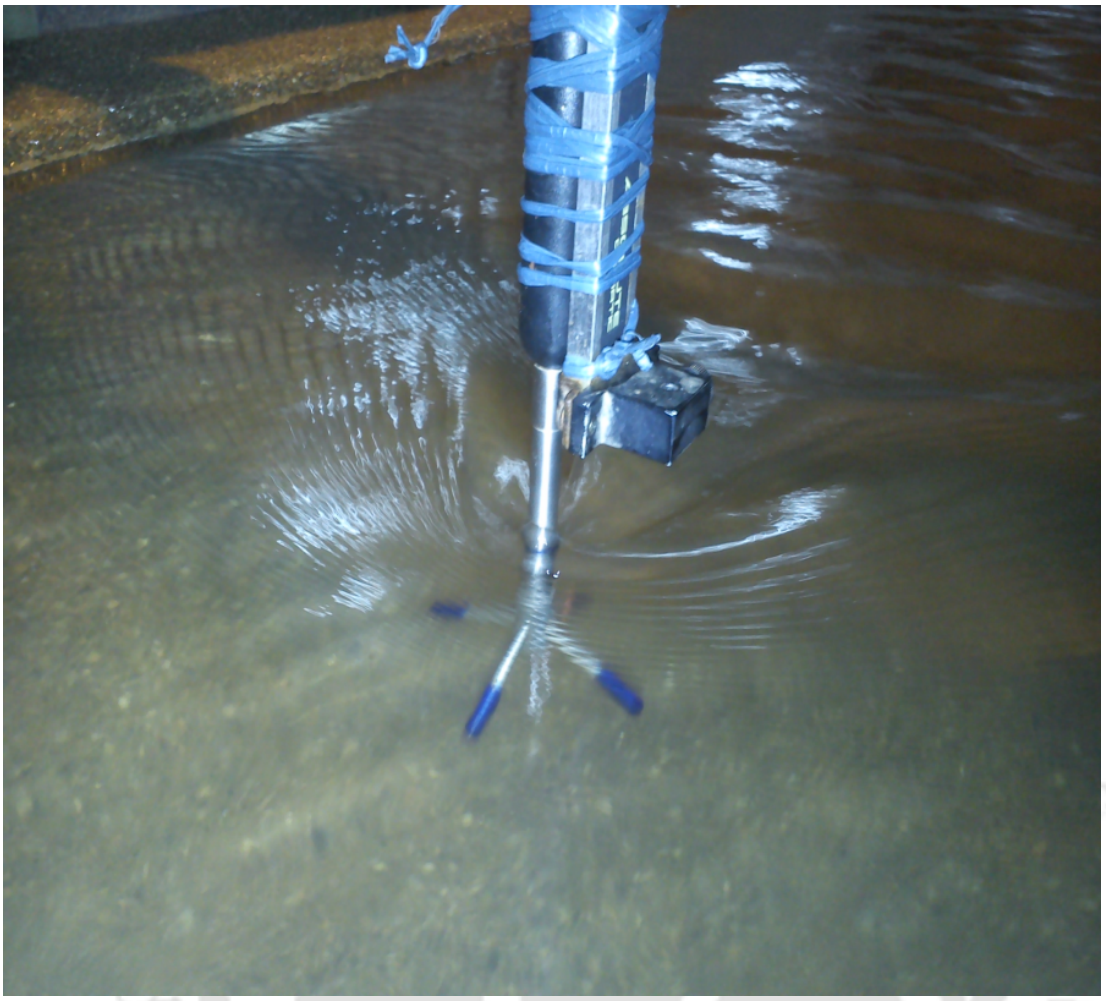

FIGURE 2.10: Vectrino+ Acoustic Doppler Velocimeter

an observer hears the horn of a vehicle, the pitch of the horn is higher when the vehicle is heading towards the observer, and the pitch is lower when the vehicle is moving away from the observer. This change in pitch tells us how fast the vehicle is moving. Vectrino transmits short pairs of acoustic pulses, listens to their echoes and ultimately measures the change in pitch or frequency of the returned sound.

This sound is not actually reflected from water. It is rather reflected from the suspended particles or the seeding particles present in water which move with same average speed as of water. Consequently, the measured velocity is the velocity of the water. In a separate echo sounder mode, the ADV also allowed the measurement of the distance of the central transmitter from the boundary. The instrument collects data in a cylindrical remote sampling volume of user adjustable height located 5 cm below the central transmitter (Figure 2.11).

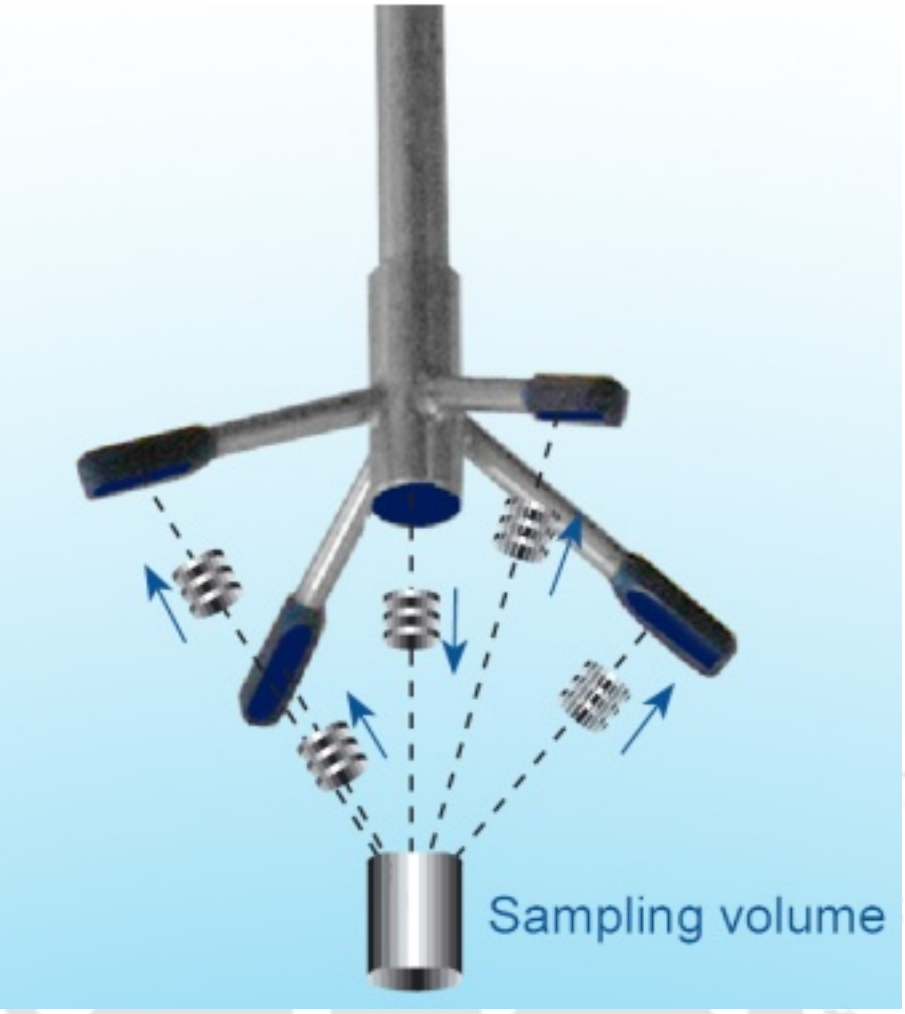

FIGURE 2.11: Vectrino ADV and the remote sampling volume (Image source: Vectrino user guide)

The velocity data is collected in the computer system using the software Vectrino+ developed by Nortek (Figure 2.12). In the present experiments, the height of the sampling volume was set at 1 mm when very near to the bed such that the sampling volume did not touch the particles on the bed surface, and at 4 mm when away from the bed. Data was collected at the centre line of the channel cross-section at a distance of 8 m from the downstream end of the flume. 30000 measurements were carried out on multiple heights for duration of 5 minutes.

Special care was taken to collect data with correlation >70% and signal to noise ratio (SNR) >15. Very near to the bed, slight deviation (± 5%) in the correlation was observed. In order to check the uncertainty associated with the ADV data,

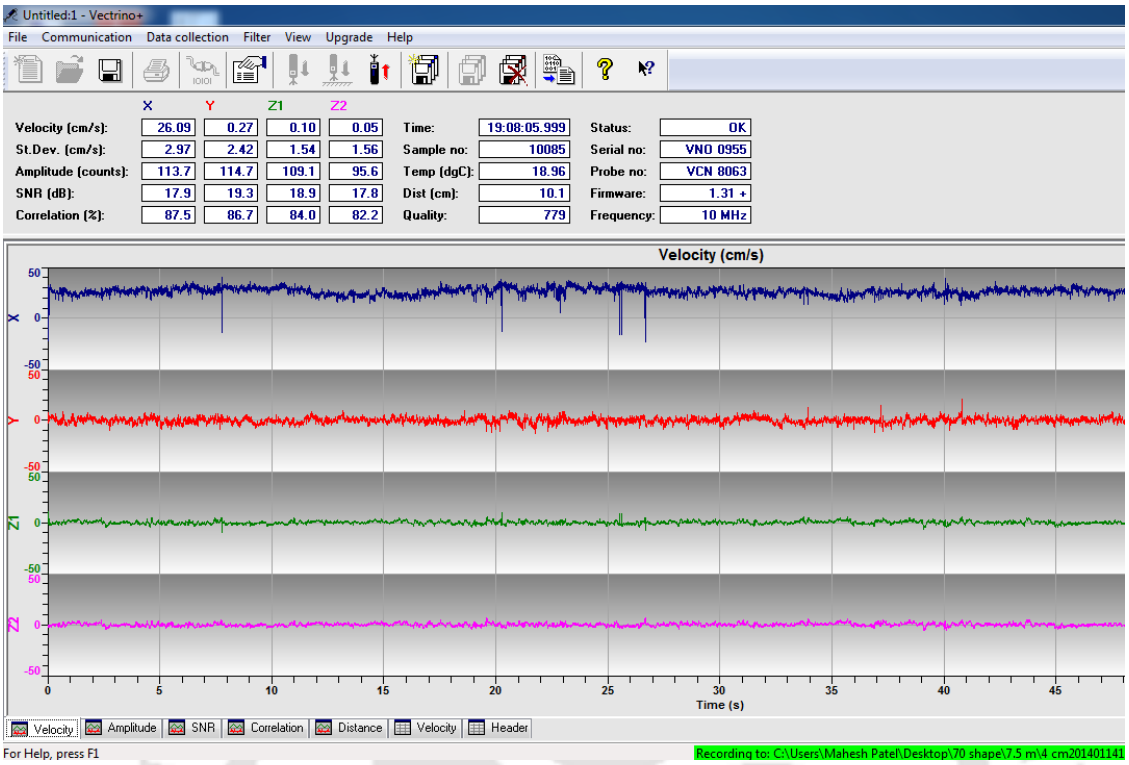

FIGURE 2.12: Vectrino+ software for velocity data collection

16 pulses of 30000 samples for duration of 5 minutes each have been collected at a location 3 mm above the bed level (Table 2.2).

In Table 2.2, U, V and W are the time-averaged velocities in the streamwise, lateral and vertical directions, respectively. u', v' and w' are the fluctuating components of the instantaneous velocities in the streamwise, lateral and vertical directions, respectively. $\left(\overline{u'u'}\right)^{0.5}$, $\left(\overline{v'v'}\right)^{0.5}$ and $\left(\overline{w'w'}\right)^{0.5}$ are the root mean square values of u', v' and w' respectively.

TABLE 2.2: Uncertainty associated with the ADV data

	U	V	W	$\left(\overline{u'u'}\right)^{0.5}$	$\left(\overline{v'v'}\right)^{0.5}$	$\left(\overline{w'w'}\right)^{0.5}$
Standard deviation	4.36×10^{-3}	9.66×10^{-4}	4.31×10^{-4}	1.06×10^{-3}	9.37×10^{-4}	3.43×10^{-4}
Uncertainty %	0.33	0.07	0.82	0.09	0.08	0.03

Post processing of the velocity data was carried out on ExploreV software developed by Nortek (Figure 2.13). Spikes in the velocity time series were filtered by using the acceleration threshold method (Goring and Nikora, 2002) with threshold

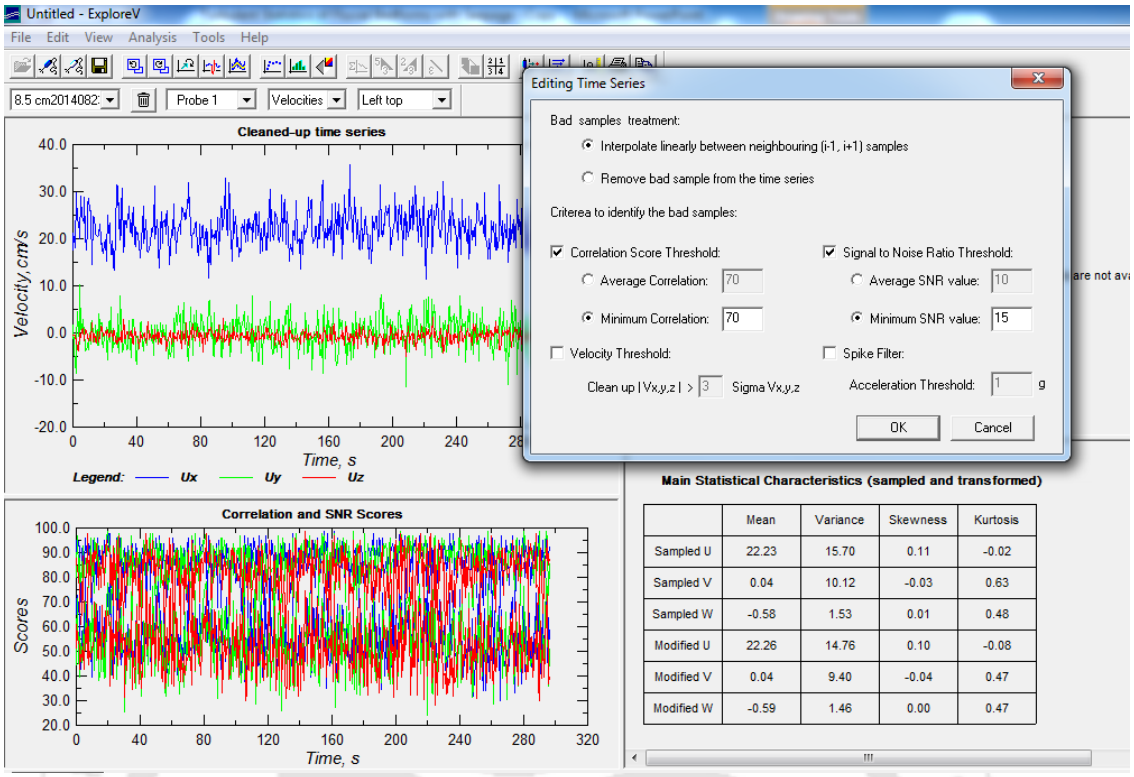

	Mean	Variance	Skewness	Kurtosis
Sampled U	22.23	15.70	0.11	-0.02
Sampled V	0.04	10.12	-0.03	0.63
Sampled W	-0.58	1.53	0.01	0.48
Modified U	22.26	14.76	0.10	-0.08
Modified V	0.04	9.40	-0.04	0.47
Modified W	-0.59	1.46	0.00	0.47

FIGURE 2.13: ExploreV software for post processing of the velocity data

values 1-1.5 based on trial and error (Dey et al., 2012) such that there was satisfactory fit in the velocity power spectra with Kolmogorov's $-5/3$ law in the inertial subrange. Velocity power spectra ($F_{uu}(f)$) for streamwise velocities of no seepage and seepage runs is shown in Figure 2.14. It can be observed from Figure 2.14(c) and (d) that power spectra for filtered velocity pulses is in good agreement with the Kolmogorov's $-5/3$ law in the inertial subrange. Further, it can also be observed that power spectra for both no seepage and seepage runs are similar which suggests that spectra are not adversely affected by the application of seepage.

2.9 Temperature and Kinematic Viscosity

Average temperature of water during an experiment is recorded by Vectrino+ ADV which has a temperature sensor (thermistor), located inside the probe head. The corresponding value of kinematic viscosity (cm^2/s) is determined from standard tables.

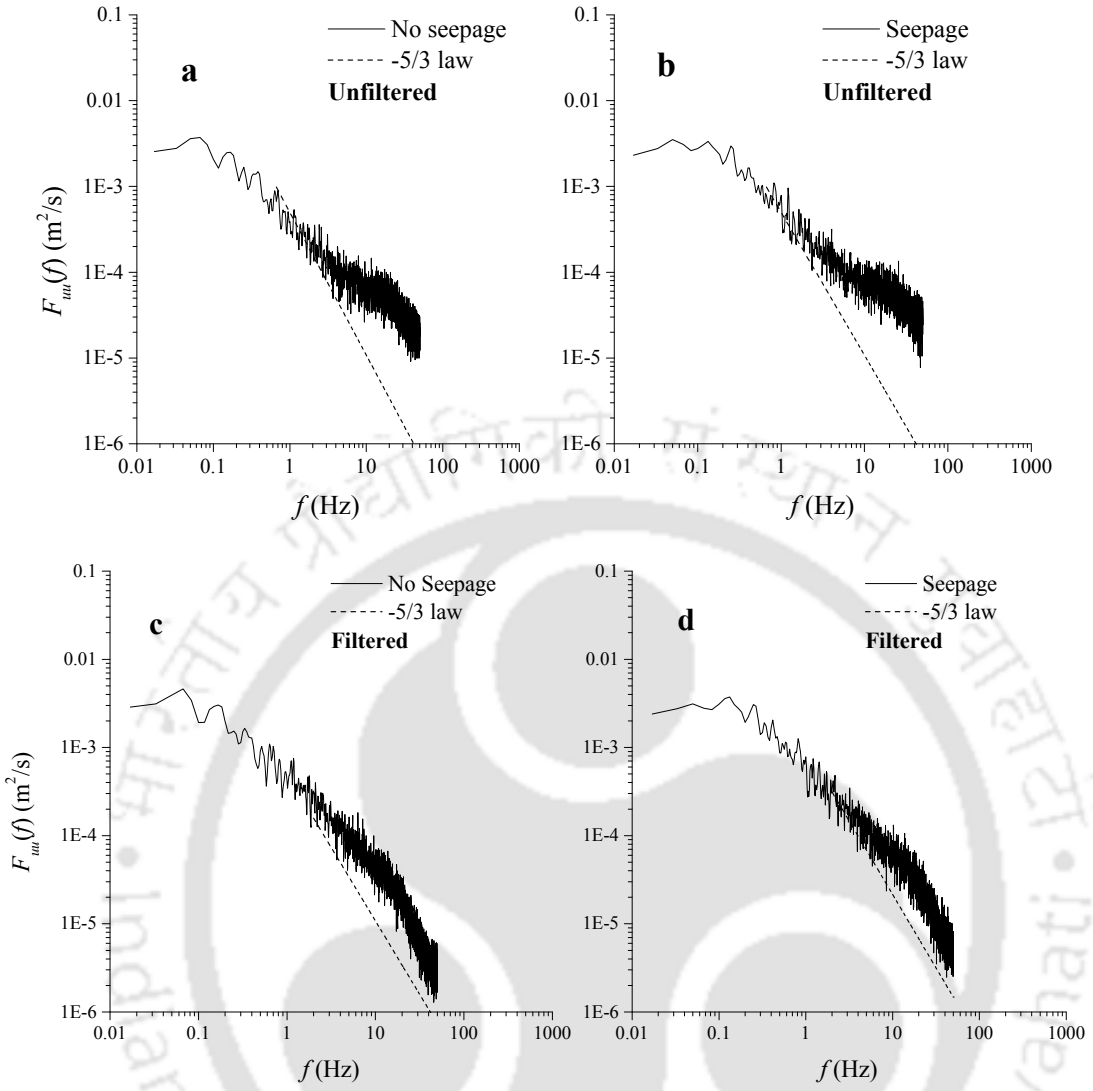

FIGURE 2.14: Velocity power spectra with Kolmogorov's -5/3 law at $z = 3$ mm ($z = +$ve when moving upwards away from the channel bed and at channel bed, $z = 0$)

2.10 Measurement of the Geometry

The geometry of the main channel was measured using a SeaTek 5 MHz Ultrasonic Ranging System that contains 4 transducers attached to an automated trolley (Figure 2.15), which moves on a rail at constant speed. The Seatek instrument uses 5 MHz ultrasound to measure the distance to a target. A transmit pulse of 10 microsecond duration is first sent from the transducer. The pulse travels through the water and is reflected off of a target. The reflected signal then travels back to the transducer. The transducer acts as both a transmitter and receiver.

FIGURE 2.15: SeaTek Ultrasonic Ranging System

This return signal is then detected by the electronics. Since the speed of sound in water is known, and the time it took for the pulse to travel from the transducer to the target and back is known, the distance to the target can be calculated. The wavelength of 5 MHz sound waves in water is 0.3 mm. The resolution of the system is 0.1 mm, the accuracy (if several pings are processed per return) is ± 0.2 mm.

2.11 Significance of Lane's (1953) Geometric Profile

Stability of a channel is defined as the ability of a stream, over time, to transport the flows and sediments of the watershed while neither aggrading nor degrading and while maintaining a consistent dimension, pattern and profile (Rosgen, 2006). The cross-sectional shape of a natural river channel controls the capacity of the system to carry water off a landscape, to convey sediment derived from upstream

and to erode its bed and banks (Wobus et al., 2008). Most of the stable channel shape predictors in terms of its width, depth and slope are empirical or semi-empirical in nature except the one proposed by Lane (1953). Empirical predictors are developed based on the experimentation and are usually valid within the ranges of parameters of the experiments.

Various researchers (Griffiths, 1983; Hey and Thorne, 1986; Millar and Quick, 1993) have argued that naturally stable stream channels are like curve shaped. Alluvial rivers need to spill over the banks regularly to maintain the dynamic equilibrium of sediment accumulation and erosion. The longitudinal profile of the river bottom has a convex shape since the bottom slope reduces along the river axis (Savenije, 2003). The theoretical regime equation developed by Lane (1953) fulfills this criteria contrary to others empirical predictors. Mahmood et al. (1988) has also stated that Lane's (1953) formulation of alluvial channel response is well suited for trend analysis.

Lane (1953) has derived the equation by solving various forces those can act on the sediment-water flow. Lane (1953) proposed the shape of a stable channel which is derived on the basis that the tendency to motion of a particle in the direction transverse to the flow is proportional to the slope of the stream bed, as measured by the tangent of the angle with the horizontal, and the direction of flow is proportional to the depth of the stream. In Lane's (1953) geometric profile, at and above the water surface, the maximum angle of the side slope approaches the angle of repose of the material, where the tractive stress provided by the flow vanishes. At points between the center and edge of the channel the particles are in a state of incipient motion, under the action of the resultant of the gravity component of the particles' submerged weight acting down the side slope and the tractive force exerted by the flowing water. Thus, as the shear stress increases towards the center of the channel, the inclination of the side slope declines. A concave-upwards cross-sectional profile of the main channel based on Lane's (1953) theory with 0.70 m top width is shown in Figure 2.16.

2.12 Experimental Measurements

Relations between flow depth (y) area (A), velocity (u) and top width (B) for a stable channel cross-section have been given by Lane (1953) as:

$$A = \frac{2y^2}{\tan\phi} \tag{2.4}$$

$$u = \frac{1}{n}\left[\frac{y\cos\phi}{E\left(\sin\phi\right)}\right]^{2/3} S_0^{1/2} \tag{2.5}$$

$$B = \frac{y\pi}{\tan\phi} \tag{2.6}$$

$$E\left(\sin\phi\right) \approx \left(\pi/2\right)\left(1 - 1/4\sin^2\phi\right) \tag{2.7}$$

$$y = y_c \cos\left\{\left(\frac{\tan\phi}{y_c}\right)x\right\} \tag{2.8}$$

Shape of the main channel has been given using Equation (2.8). Lane's (1953) geometric profiles with varying top widths i.e. 0.50 m (shape 50), 0.60 m (shape 60) and 0.70 m (shape 70) were used. For shape 70, maximum depth of flow can be calculated by rearranging Equation (2.6). Cross-sectional profile of the main channel is shown in Figure 2.16 for 1.1 mm median diameter sand.

Every single experiment in the present study has been carried out in two categories: No seepage experiment and Seepage experiment. Under the no seepage experimental conditions the stability of Lane's (1953) geometric profiles on incipient motion condition was checked. After the success of no seepage experiment, downward seepage, which was some percentage of Lane's (1953) discharge, was applied (seepage experiment). After running the experiment for several hours and when the channel adjusted itself measurements for water surface slope and flow depth were taken using pitot tube attached to digital manometer and digital point

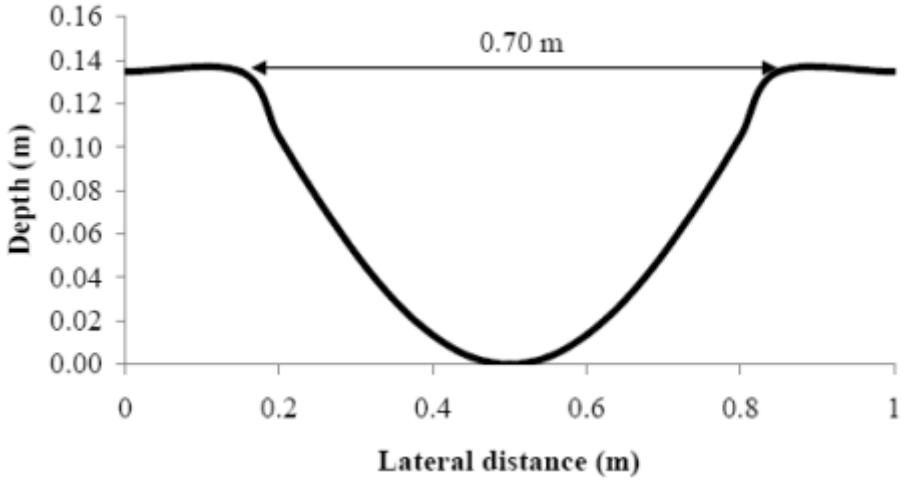

FIGURE 2.16: Lane's (1953) geometric profile

gauge, respectively during the experimental run. Flow discharge from the main channel has been measured by recording the depth of flow over the rectangular notch provided at the downstream collection tank. Seepage discharge from the main channel through the bottom pressure chamber has been measured by using electromagnetic flow meters connected to the seepage chamber. Ranges of various parameters for Lane's (1953) geometric profiles used in the experiments for all three sands are given in Table 2.3.

TABLE 2.3: Details of Lane's (1953) geometric profiles used in experiments

Sand size, d_{50} mm	Top width, B m	Bed slope S_0	Flow depth, y m	Cross-sectional Area, A m^2	Discharge, Q_0 m^3/s	Mean velocity, u m/s	Seepage discharge q_s (%Q_0)
1.1	0.5	0.00116-0.00249	0.0962	0.03062	0.010-0.015	0.33-0.49	50%
	0.6		0.1155	0.04414	0.017-0.024	0.38-0.54	40%
	0.7		0.1347	0.06003	0.025-0.037	0.42-0.62	30%
0.62	0.5		0.1002	0.031887	0.012-0.017	0.38-0.53	50%
	0.6		0.1203	0.045963	0.019-0.028	0.41-0.61	40%
	0.7		0.1403	0.062516	0.029-0.042	0.46-0.67	30%
0.418	0.5		0.1016	0.03234	0.013-0.019	0.40-0.58	50%
	0.6		0.1219	0.04656	0.021-0.031	0.45-0.66	40%
	0.7		0.1422	0.06338	0.032-0.046	0.50-0.73	30%

2.13 No Seepage Experiments

Lane's (1953) geometric profile was given initially to the sand bed with the help of a wooden shaper (Figure 2.17). Water was introduced to the channel gradually and after the bed was completely submerged, the tail gate was adjusted in such a way that the bankfull flow was maintained in the channel throughout the experiment and the upstream discharge was increased slowly in gradual manner so that the average value of the basal boundary shear stress increased gradually until a stage, when the hydro-dynamic forces of the flow exceeded the resistive forces of the bed particles and all fractions of bed particles (on the surface) initiated movement over a period of time.

At this state of incipient motion, the sediment particles were at critical condition, i.e. the bed shear stress (τ_{b0}) was equal to the critical bed shear stress (τ_{c0}). Yalin's (1976) criterion has been used as far as incipient motion is concerned with the value of ϵ has been chosen as 10^{-6} for practical purposes. Experiments were continued for several hours (around 12 to 24 hours) so that the channel geometry and longitudinal slope adjusted on its own such that the sediment particles remained in the state of incipient motion throughout the test reach in channel. Thus the stable conditions were achieved and measurements for water surface slope, flow discharge, flow depth and cross-sectional geometry were taken. The channels before no seepage experiment and after it are shown in Figure 2.18 and Figure 2.19, respectively.

2.14 Seepage Experiments

Without stopping the experiment some percentage of Lane's (1953) discharge for no seepage experiment was applied in the form of downward seepage and it was observed that the sediment bed maintained in incipient motion went on transporting condition. This experiment was continued for several hours (around 48 to 72 hour) until the channel geometry and longitudinal slope were adjusted on

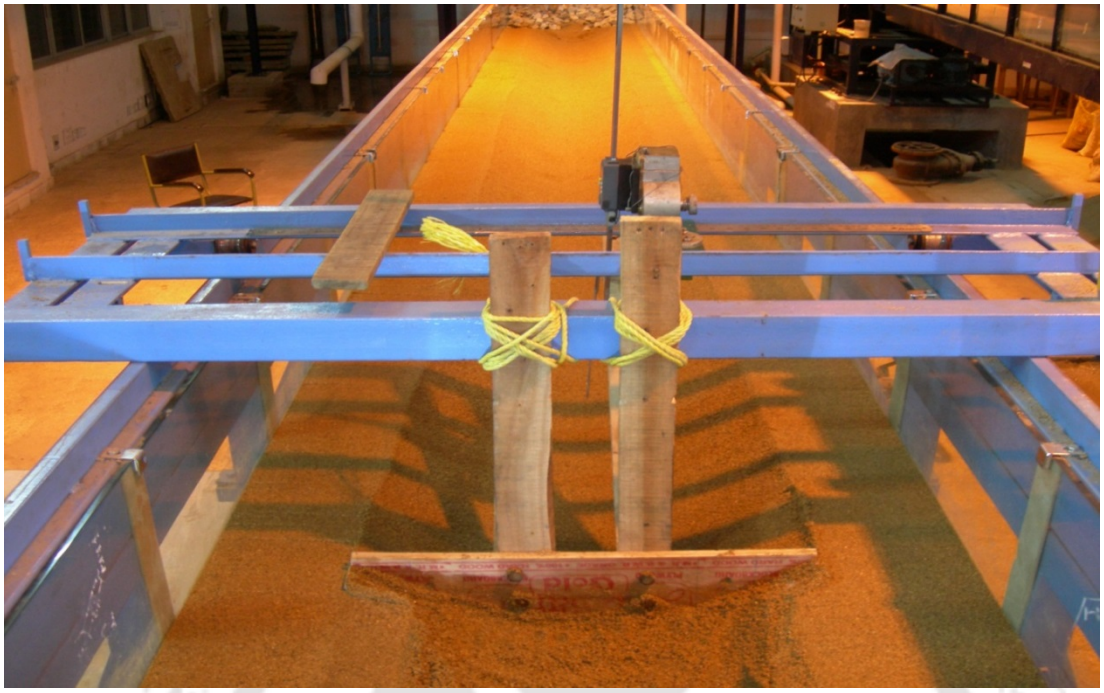

FIGURE 2.17: Wooden shaper

FIGURE 2.18: Channel before no seepage experiment

FIGURE 2.19: Channel after no seepage experiment

their own so that new state of incipient motion reached with seepage ($\tau_{bs} = \tau_{cs}$). No additional sediment input was allowed from the upstream of the channel. It has been observed that, on upstream side more erosion takes place. These eroded sediment particles from one section get deposited in the adjacent next section in the downstream direction and the process keeps on continuing.

The phenomenon of erosion and deposition alters the channel geometry everywhere throughout the length of the channel. During the process, the inflow and outflow discharges, the seepage discharge, depth of flow and water surface profiles were recorded at regular intervals. Velocity measurements through ADV were taken immediately after the application of seepage to understand the effects of downward seepage on the flow characteristics of the channel. Care was taken in velocity measurements that the complete vertical profile of velocity was obtained before the distortions reached the location of the velocity measurements i.e. section at 8 m from the downstream end of the channel. Finally, when the channel reached into a full equilibrium state, the experiment was stopped and the measurements for

FIGURE 2.20: Channel after seepage experiment on the sand of $d_{50} = 1.1$ mm

water surface slope, flow discharge, flow depth and cross-sectional geometry were recorded as like no seepage run. Channels obtained after the seepage experiments are shown in Figure 2.20 and Figure 2.21.

2.15 Results

In the present study, the incipient bed motion condition during no seepage runs has been validated by plotting the results on Shields curve, which gives a relationship between Shields parameter (θ) and shear Reynolds number (R^*) (Figure 2.22).

Seepage experiments are examples of spatially varied flow in nature. The friction slope of spatially varied flow can be given as (Rao et al., 2011):

$$S_{fs} = S_{ws}(1 - {F_s}^2) + S_0{F_s}^2 + 2\rho u_s V_s/(\gamma\gamma_s) \tag{2.9}$$

FIGURE 2.21: Channel after seepage experiment on the sand of $d_{50} = 0.62$ mm

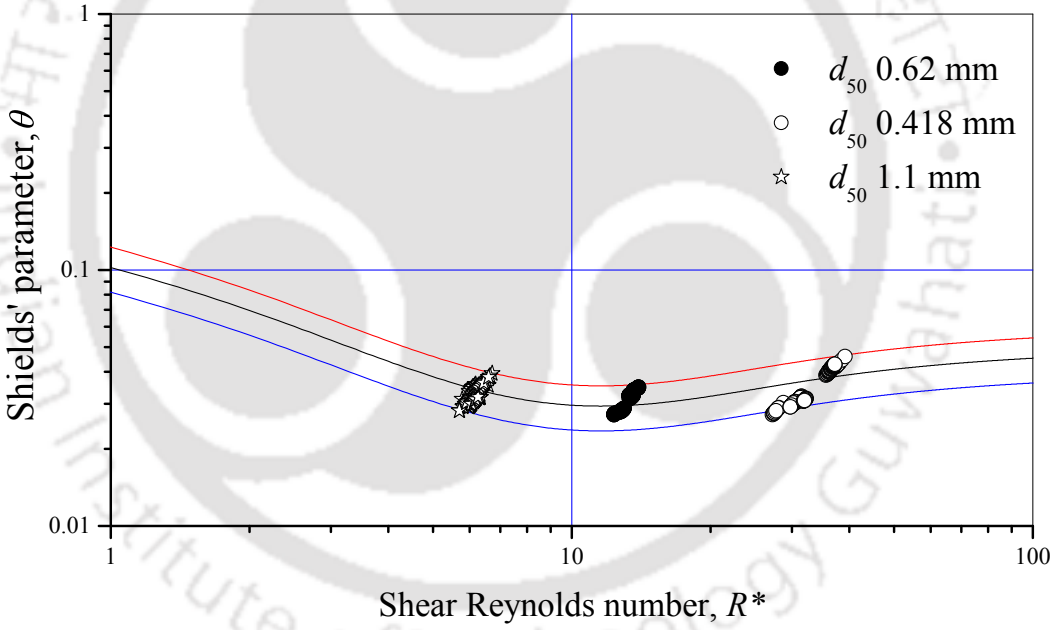

FIGURE 2.22: Shields diagram for the condition of incipient motion

Here, subscript 's' stands for seepage experiments and '0' represents no seepage experimental conditions. In Equation (2.9), S_w is water surface slope, and S_0 is bed slope, u_s is the average velocity of flow:

$$u_s = Q_s/A \tag{2.10}$$

A is the cross-sectional area, Q_s is average discharge:

$$Q_s = Q_0 - q_s \left(1 - {}^{X}/_{L}\right) \tag{2.11}$$

Q_0 is discharge for no seepage run, q_s is the seepage discharge over the reach length L of the channel, and X is the distance from the tail gate. F_s in Equation (2.9) is the Froude number:

$$F_s = u_s/(gR_{hs})^{1/2} \tag{2.12}$$

where, g is gravitational acceleration, R_{hs} is hydraulic radius, $R_{hs} = A_s/p_s$; p_s is wetted perimeter. The bed slope S_0 is considered to be the same in all of the runs in a given set, both under no seepage and seepage conditions; the water surface slope with seepage S_{ws} is found to be fairly linear in the test reach. In Equation (2.9), V_s is the seepage velocity through the sand bed of length L:

$$V_s = q_s/(p_s L) \tag{2.13}$$

Shear stress τ_s for seepage experimental conditions can be found as:

$$\tau_s = \gamma R_{hs} S_{fs} \tag{2.14}$$

The assumption of hydrostatic distribution such as taken in Equation (2.14) is reasonable in case of rectilinear, quasi-steady and quasi-uniform flows (Francalanci et al., 2008). Francalanci et al. (2008) also argued that by its very definition the Shields number assumes the pressure distribution of the water in which sediment grains are immersed to be hydrostatic. In a similar way, the friction slope S_{f0} and the channel shear stress τ_0 are under no seepage conditions and are arrived at by considering $V_s = 0$ in Equation (2.9) and by the following two equations:

$$S_{f0} = S_{w0}\left(1 - F_0^2\right) + S_0 F_0^2 \tag{2.15}$$

and

$$\tau_0 = \gamma R_{h0} S_{f0} \tag{2.16}$$

where, R_{h0} is the hydraulic radius, $R_{h0} = A_0/p_0$; A_0 and p_0 are the cross-sectional area and wetted perimeter, respectively for no seepage conditions. By dividing Equation (2.14) by Equation (2.16):

$$\frac{\tau_{cs}}{\tau_{c0}} = \frac{R_{hs}\left[S_0 {F_s}^2 + S_{ws}\left(1 - {F_s}^2\right)\right]}{R_{h0}\left[S_0 {F_0}^2 + S_{w0}\left(1 - {F_0}^2\right)\right]} + \frac{(2\rho u_s V_s)}{\tau_{c0}} \tag{2.17}$$

$$\frac{R_{hs}\left[S_0 {F_s}^2 + S_{ws}\left(1 - {F_s}^2\right)\right]}{R_{h0}\left[S_0 {F_0}^2 + S_{w0}\left(1 - {F_0}^2\right)\right]} = M \tag{2.18}$$

$$\frac{(2\rho u_s V_s)}{\tau_{c0}} = N \tag{2.19}$$

In Equation (2.19), N shows the relative intensity of seepage applied on sediment bed and has been termed as the seepage intensity parameter. Relationship between M and N from Equations (2.18) and (2.19), respectively, for the experimental data has been plotted in Figure 2.23.

For the no seepage experiments, flow in the channel is such that the bed shear stress is equal to critical bed shear stress ($\tau_0 = \tau_{c0}$) hence the bed particles are on the verge of motion. When downward seepage is applied to the no seepage experiments bed shear stress is increased and is higher than the critical bed shear stress ($\tau_s > \tau_{cs}$), consequently the erosion of bed particles takes place.

With the passage of time a condition of equilibrium is reached when bed shear stress becomes equal to critical bed shear stress ($\tau_0 = \tau_{c0}$) again and erosion of sediment particles reduces and finally when it comes to zero and the cross-sectional profile is changed to some different shape, the channel becomes stable with applied seepage but one can still observe the shaking of bed particles. Hence, the numerator and the denominator of Equation (2.18) become indistinguishable which results

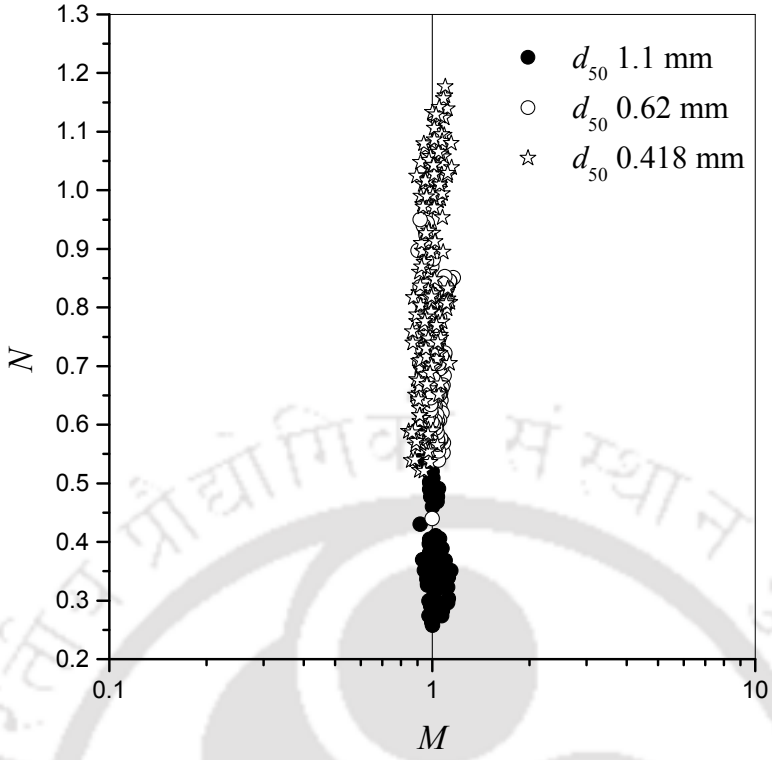

FIGURE 2.23: Relationship between M and N

in the value of parameter $M = 1$. Experimental data for no seepage and seepage runs on all three sands is given in Table 2.4 to Table 2.57. Stream power (Ω) has also been obtained which can be calculated for no seepage experiments as:

$$\Omega_0 = \gamma Q_0 S_{f0} \tag{2.20}$$

and for seepage experiments:

$$\Omega_s = \gamma Q_s S_{fs} \tag{2.21}$$

TABLE 2.4: Case: No seepage shape 50 (d_{50} = 1.1 mm, S_0 = 0.00116, Q_0 = 0.0104 m^3/s)

Section	y_0 (m)	Rh_0 (m)	u_0 (m/s)	F_0	Sf_0	τ_0 (N/m^2)	u_0^*	$R*$	Ω_s (N/s)
10	0.086	0.055	0.349	0.476	0.00092	0.495	0.022	27.383	0.094
9.5	0.089	0.054	0.356	0.488	0.00092	0.492	0.022	27.301	0.094
9	0.087	0.054	0.354	0.487	0.00092	0.490	0.022	27.239	0.094
8.5	0.085	0.057	0.336	0.451	0.00091	0.507	0.023	27.715	0.093
8	0.090	0.058	0.328	0.436	0.00091	0.515	0.023	27.943	0.093
7.5	0.089	0.056	0.341	0.458	0.00091	0.506	0.023	27.702	0.093
7	0.091	0.055	0.342	0.466	0.00092	0.495	0.022	27.395	0.094
6.5	0.095	0.055	0.348	0.475	0.00092	0.495	0.022	27.390	0.094
6	0.094	0.055	0.342	0.465	0.00092	0.497	0.022	27.438	0.094
5.5	0.094	0.058	0.326	0.434	0.00091	0.513	0.023	27.882	0.093
5	0.094	0.055	0.344	0.466	0.00092	0.499	0.022	27.508	0.094

TABLE 2.5: Case: Seepage shape 50 (d_{50} = 1.1 mm, S_0 = 0.00116, Q_0 = 0.0104 m^3/s)

Section	y_s (m)	Rh_s (m)	Q_s (m^3/s)	u_s (m/s)	V_s (m/s)	F_s	Sf_s	τ_s (N/m^2)	u_s^*	$R*$	Ω_s (N/s)
10	0.052	0.051	0.008	0.284	0.000559	0.400	0.00159	0.799	0.028	34.798	0.132
9.5	0.053	0.049	0.008	0.284	0.000547	0.410	0.00157	0.753	0.027	33.781	0.128
9	0.053	0.049	0.008	0.293	0.000568	0.424	0.00162	0.769	0.028	34.134	0.129
8.5	0.051	0.055	0.008	0.254	0.000568	0.346	0.00153	0.824	0.029	35.349	0.120
8	0.053	0.054	0.008	0.250	0.000560	0.345	0.00150	0.789	0.028	34.586	0.115
7.5	0.049	0.054	0.008	0.242	0.000562	0.331	0.00152	0.811	0.028	35.058	0.114
7	0.052	0.049	0.007	0.272	0.000579	0.393	0.00158	0.759	0.028	33.927	0.116
6.5	0.048	0.047	0.007	0.277	0.000580	0.407	0.00164	0.761	0.028	33.952	0.118
6	0.049	0.050	0.007	0.252	0.000567	0.361	0.00155	0.756	0.027	33.838	0.109
5.5	0.047	0.050	0.007	0.244	0.000565	0.350	0.00155	0.757	0.028	33.864	0.106
5	0.048	0.048	0.007	0.255	0.000580	0.372	0.00158	0.743	0.027	33.555	0.106

TABLE 2.6: Case: No seepage shape 60 (d_{50} = 1.1 mm, S_0 = 0.00116, Q_0 = 0.0165 m^3/s)

Section	y_0 (m)	Rh_0 (m)	u_0 (m/s)	F_0	Sf_0	τ_0 (N/m^2)	u_0^*	$R*$	Ω_s (N/s)
10	0.106	0.077	0.318	0.367	0.00076	0.572	0.024	31.372	0.123
9.5	0.104	0.078	0.312	0.358	0.00076	0.577	0.024	31.508	0.123
9	0.109	0.075	0.325	0.379	0.00077	0.563	0.024	31.117	0.124
8.5	0.106	0.076	0.321	0.372	0.00076	0.567	0.024	31.233	0.124
8	0.111	0.074	0.328	0.383	0.00077	0.561	0.024	31.057	0.124
7.5	0.113	0.076	0.318	0.367	0.00076	0.570	0.024	31.311	0.123
7	0.114	0.078	0.313	0.359	0.00076	0.577	0.024	31.512	0.123
6.5	0.117	0.077	0.313	0.360	0.00076	0.575	0.024	31.436	0.123
6	0.116	0.076	0.317	0.367	0.00076	0.571	0.024	31.337	0.123
5.5	0.113	0.075	0.322	0.375	0.00076	0.564	0.024	31.137	0.124
5	0.112	0.076	0.319	0.370	0.00076	0.569	0.024	31.294	0.123

TABLE 2.7: Case: Seepage shape 60 (d_{50} = 1.1 mm, S_0 = 0.00116, Q_0 = 0.0165 m^3/s)

Section	y_s (m)	Rh_s (m)	Q_s (m^3/s)	u_s (m/s)	V_s (m/s)	F_s	Sf_s	τ_s (N/m^2)	u_s^*	$R*$	Ω_s (N/s)
10	0.071	0.071	0.015	0.261	0.000394	0.312	0.00117	0.822	0.029	37.605	0.169
9.5	0.070	0.072	0.014	0.262	0.000400	0.313	0.00118	0.828	0.029	37.732	0.168
9	0.070	0.069	0.014	0.278	0.000411	0.338	0.00121	0.817	0.029	37.488	0.171
8.5	0.070	0.070	0.014	0.267	0.000406	0.324	0.00120	0.816	0.029	37.456	0.166
8	0.072	0.067	0.014	0.276	0.000407	0.341	0.00120	0.789	0.028	36.827	0.165
7.5	0.069	0.068	0.014	0.279	0.000420	0.342	0.00123	0.813	0.029	37.384	0.167
7	0.068	0.067	0.014	0.274	0.000414	0.339	0.00122	0.802	0.028	37.140	0.164
6.5	0.068	0.068	0.014	0.266	0.000415	0.325	0.00121	0.812	0.029	37.381	0.161
6	0.066	0.065	0.013	0.276	0.000413	0.347	0.00123	0.784	0.028	36.722	0.162
5.5	0.069	0.065	0.013	0.271	0.000412	0.338	0.00121	0.776	0.028	36.529	0.158
5	0.067	0.060	0.013	0.294	0.000416	0.384	0.00126	0.742	0.027	35.720	0.162

TABLE 2.8: Case: No seepage shape 70 (d_{50} = 1.1 mm, S_0 = 0.00116, Q_0 = 0.0196 m^3/s)

Section	y_0 (m)	Rh_0 (m)	u_0 (m/s)	F_0	Sf_0	τ_0 (N/m^2)	u_0^*	$R*$	Ω_s (N/s)
10	0.129	0.085	0.302	0.331	0.00066	0.550	0.023	30.470	0.127
9.5	0.130	0.085	0.302	0.332	0.00066	0.549	0.023	30.460	0.127
9	0.126	0.081	0.319	0.358	0.00067	0.533	0.023	30.014	0.129
8.5	0.127	0.083	0.311	0.344	0.00067	0.543	0.023	30.293	0.128
8	0.130	0.083	0.308	0.341	0.00067	0.544	0.023	30.297	0.128
7.5	0.130	0.083	0.309	0.342	0.00067	0.543	0.023	30.284	0.128
7	0.128	0.082	0.316	0.352	0.00067	0.537	0.023	30.107	0.129
6.5	0.130	0.082	0.312	0.348	0.00067	0.537	0.023	30.112	0.128
6	0.131	0.081	0.318	0.357	0.00067	0.532	0.023	29.962	0.129
5.5	0.129	0.080	0.322	0.364	0.00067	0.528	0.023	29.862	0.130
5	0.129	0.079	0.326	0.370	0.00068	0.525	0.023	29.773	0.130

TABLE 2.9: Case: Seepage shape 70 (d_{50} = 1.1 mm, S_0 = 0.00116, Q_0 = 0.0196 m^3/s)

Section	y_s (m)	Rh_s (m)	Q_s (m^3/s)	u_s (m/s)	V_s (m/s)	F_s	Sf_s	τ_s (N/m^2)	u_s^*	$R*$	Ω_s (N/s)
10	0.075	0.078	0.017	0.268	0.000613	0.306	0.00117	0.897	0.030	38.392	0.192
9.5	0.080	0.079	0.016	0.264	0.000621	0.300	0.00114	0.884	0.030	38.116	0.184
9	0.080	0.076	0.016	0.272	0.000629	0.314	0.00116	0.871	0.030	37.821	0.184
8.5	0.080	0.078	0.016	0.261	0.000624	0.299	0.00114	0.869	0.029	37.796	0.178
8	0.082	0.076	0.016	0.263	0.000625	0.305	0.00113	0.844	0.029	37.246	0.174
7.5	0.076	0.074	0.015	0.265	0.000624	0.310	0.00117	0.851	0.029	37.405	0.177
7	0.075	0.073	0.015	0.265	0.000624	0.312	0.00118	0.844	0.029	37.242	0.175
6.5	0.075	0.073	0.015	0.263	0.000628	0.312	0.00118	0.841	0.029	37.170	0.173
6	0.074	0.071	0.015	0.266	0.000626	0.320	0.00119	0.824	0.029	36.787	0.171
5.5	0.074	0.071	0.014	0.259	0.000625	0.310	0.00117	0.818	0.029	36.652	0.166
5	0.075	0.070	0.014	0.263	0.000631	0.319	0.00118	0.806	0.028	36.386	0.165

TABLE 2.10: Case: No seepage shape 50 (d_{50} = 1.1 mm, S_0 = 0.00176, Q_0 = 0.0116 m^3/s)

Section	y_0 (m)	Rh_0 (m)	u_0 (m/s)	F_0	Sf_0	τ_0 (N/m^2)	u_0^*	$R*$	Ω_s (N/s)
10.000	0.087	0.062	0.318	0.409	0.00129	0.779	0.028	36.529	0.146
9.000	0.090	0.059	0.339	0.447	0.00131	0.753	0.027	35.917	0.148
8.000	0.092	0.061	0.330	0.427	0.00130	0.776	0.028	36.440	0.147
7.000	0.096	0.060	0.333	0.433	0.00130	0.767	0.028	36.251	0.147
6.000	0.099	0.060	0.333	0.434	0.00130	0.767	0.028	36.234	0.147
5.000	0.097	0.064	0.312	0.395	0.00128	0.802	0.028	37.051	0.145

TABLE 2.11: Case: Seepage Shape 50 (d_{50} = 1.1 mm, S_0 = 0.00176, Q_0 = 0.0116 m^3/s)

Section	y_s (m)	Rh_s (m)	Q_s (m^3/s)	u_s (m/s)	V_s (m/s)	F_s	Sf_s	τ_s (N/m^2)	u_s^*	$R*$	Ω_s (N/s)
10.000	0.057	0.060	0.009	0.246	0.00057	0.32178	0.00193	1.134	0.034	44.066	0.178
9.000	0.056	0.060	0.009	0.234	0.00056	0.30594	0.00191	1.121	0.033	43.803	0.169
8.000	0.054	0.054	0.009	0.257	0.00058	0.35353	0.00200	1.057	0.033	42.543	0.170
7.000	0.053	0.056	0.008	0.235	0.00057	0.31708	0.00195	1.076	0.033	42.927	0.159
6.000	0.052	0.053	0.008	0.251	0.00061	0.34734	0.00204	1.062	0.033	42.650	0.159
5.000	0.050	0.053	0.008	0.242	0.00061	0.33492	0.00204	1.065	0.033	42.701	0.152

TABLE 2.12: Case: No seepage shape 60 (d_{50} = 1.1 mm, S_0 = 0.00176, Q_0 = 0.0156 m^3/s)

Section	y_0 (m)	Rh_0 (m)	u_0 (m/s)	F_0	Sf_0	τ_0 (N/m^2)	u_0^*	$R*$	Ω_s (N/s)
10	0.110	0.071	0.331	0.395	0.00080	0.562	0.024	31.022	0.123
9	0.108	0.071	0.329	0.393	0.00080	0.560	0.024	30.973	0.123
8	0.107	0.069	0.340	0.413	0.00082	0.557	0.024	30.889	0.125
7	0.110	0.068	0.342	0.418	0.00082	0.553	0.024	30.760	0.126
6	0.107	0.071	0.324	0.389	0.00080	0.556	0.024	30.856	0.122
5	0.108	0.070	0.332	0.401	0.00081	0.554	0.024	30.797	0.124

TABLE 2.13: Case: Seepage shape 60 (d_{50} = 1.1 mm, S_0 = 0.00176, Q_0 = 0.0156 m^3/s)

Section	y_s (m)	Rh_s (m)	Q_s (m^3/s)	u_s (m/s)	V_s (m/s)	F_s	Sf_s	τ_s (N/m^2)	u_s^*	$R*$	Ω_s (N/s)
10	0.069	0.069	0.014	0.253	0.00037	0.309	0.00117	0.785	0.028	36.658	0.159
9	0.069	0.065	0.014	0.264	0.00037	0.331	0.00120	0.762	0.028	36.120	0.159
8	0.067	0.065	0.013	0.253	0.00036	0.316	0.00118	0.756	0.027	35.972	0.154
7	0.067	0.064	0.013	0.255	0.00037	0.322	0.00119	0.745	0.027	35.722	0.151
6	0.066	0.064	0.013	0.247	0.00037	0.312	0.00118	0.738	0.027	35.550	0.146
5	0.065	0.062	0.012	0.258	0.00038	0.332	0.00121	0.733	0.027	35.437	0.147

TABLE 2.14: Case: No seepage shape 70 (d_{50} = 1.1 mm, S_0 = 0.00176, Q_0 = 0.0205 m^3/s)

Section	y_0 (m)	Rh_0 (m)	u_0 (m/s)	F_0	Sf_0	τ_0 (N/m^2)	u_0^*	$R*$	Ω_s (N/s)
10	0.124	0.083	0.318	0.353	0.00092	0.746	0.027	35.747	0.184
9	0.125	0.084	0.314	0.345	0.00091	0.752	0.027	35.893	0.183
8	0.126	0.083	0.318	0.352	0.00092	0.747	0.027	35.768	0.184
7	0.127	0.084	0.312	0.345	0.00091	0.748	0.027	35.794	0.183
6	0.129	0.086	0.305	0.331	0.00090	0.764	0.028	36.180	0.182
5	0.128	0.082	0.320	0.356	0.00092	0.742	0.027	35.649	0.185

TABLE 2.15: Case: Seepage shape 70 (d_{50} = 1.1 mm, S_0 = 0.00176, Q_0 = 0.0205 m^3/s)

Section	y_s (m)	Rh_s (m)	Q_s (m^3/s)	u_s (m/s)	V_s (m/s)	F_s	Sf_s	τ_s (N/m^2)	u_s^*	$R*$	Ω_s (N/s)
10	0.077	0.076	0.017	0.256	0.000573	0.296	0.00141	1.052	0.032	42.436	0.241
9	0.080	0.075	0.017	0.256	0.000583	0.299	0.00140	1.031	0.032	42.015	0.233
8	0.084	0.073	0.016	0.257	0.000587	0.304	0.00139	0.996	0.032	41.297	0.224
7	0.089	0.075	0.016	0.244	0.000587	0.285	0.00134	0.983	0.031	41.036	0.209
6	0.096	0.076	0.015	0.233	0.000592	0.269	0.00130	0.972	0.031	40.799	0.196
5	0.100	0.076	0.015	0.224	0.000588	0.259	0.00127	0.950	0.031	40.337	0.185

TABLE 2.16: Case: No seepage shape 50 (d_{50} = 1.1 mm, S_0 = 0.00249, Q_0 = 0.0104 m^3/s)

Section	y_0 (m)	Rh_0 (m)	u_0 (m/s)	F_0	Sf_0	τ_0 (N/m^2)	u_0^*	$R*$	Ω_s (N/s)
10	0.072	0.064	0.284	0.359	0.00114	0.711	0.027	34.889	0.117
9.5	0.071	0.064	0.282	0.356	0.00114	0.715	0.027	34.993	0.116
9	0.072	0.063	0.288	0.365	0.00115	0.711	0.027	34.898	0.117
8.5	0.079	0.064	0.284	0.358	0.00114	0.718	0.027	35.069	0.116
8	0.081	0.064	0.282	0.355	0.00114	0.718	0.027	35.054	0.116
7.5	0.084	0.065	0.277	0.347	0.00113	0.722	0.027	35.149	0.115
7	0.086	0.067	0.262	0.322	0.00110	0.728	0.027	35.309	0.113
6.5	0.091	0.066	0.264	0.328	0.00111	0.721	0.027	35.138	0.113
6	0.091	0.064	0.278	0.351	0.00113	0.710	0.027	34.868	0.116
5.5	0.092	0.065	0.271	0.338	0.00112	0.718	0.027	35.053	0.114
5	0.095	0.066	0.267	0.332	0.00111	0.718	0.027	35.058	0.114

TABLE 2.17: Case: Seepage shape 50 (d_{50} = 1.1 mm, S_0 = 0.00249, Q_0 = 0.0104 m^3/s)

Section	y_s (m)	Rh_s (m)	Q_s (m^3/s)	u_s (m/s)	V_s (m/s)	F_s	Sf_s	τ_s (N/m^2)	u_s^*	$R*$	Ω_s (N/s)
10	0.048	0.060	0.008	0.208	0.000483	0.270	0.00172	1.019	0.032	41.769	0.143
9.5	0.045	0.057	0.008	0.216	0.000485	0.289	0.00178	0.997	0.032	41.310	0.145
9	0.044	0.059	0.008	0.204	0.000484	0.268	0.00174	1.012	0.032	41.636	0.139
8.5	0.043	0.058	0.008	0.203	0.000484	0.268	0.00175	1.006	0.032	41.495	0.137
8	0.043	0.057	0.008	0.205	0.000485	0.276	0.00176	0.979	0.031	40.944	0.135
7.5	0.042	0.057	0.008	0.198	0.000480	0.264	0.00175	0.979	0.031	40.934	0.131
7	0.043	0.058	0.007	0.193	0.000487	0.255	0.00173	0.986	0.031	41.084	0.127
6.5	0.042	0.057	0.007	0.192	0.000491	0.256	0.00174	0.981	0.031	40.991	0.125
6	0.043	0.054	0.007	0.207	0.000512	0.283	0.00181	0.964	0.031	40.634	0.127
5.5	0.043	0.056	0.007	0.195	0.000504	0.264	0.00175	0.954	0.031	40.407	0.120
5	0.043	0.056	0.007	0.197	0.000528	0.266	0.00178	0.981	0.031	40.987	0.119

TABLE 2.18: Case: No seepage shape 60 (d_{50} = 1.1 mm, S_0 = 0.00249, Q_0 = 0.016 m^3/s)

Section	y_0 (m)	Rh_0 (m)	u_0 (m/s)	F_0	Sf_0	τ_0 (N/m^2)	u_0^*	$R*$	Ω_s (N/s)
10	0.085	0.067	0.347	0.427	0.00111	0.731	0.027	35.370	0.174
9.5	0.091	0.070	0.334	0.403	0.00107	0.740	0.027	35.594	0.169
9	0.092	0.069	0.341	0.414	0.00109	0.739	0.027	35.563	0.171
8.5	0.094	0.070	0.334	0.403	0.00107	0.740	0.027	35.594	0.169
8	0.100	0.069	0.350	0.426	0.00111	0.744	0.027	35.698	0.174
7.5	0.105	0.068	0.352	0.431	0.00111	0.744	0.027	35.686	0.175
7	0.103	0.069	0.348	0.423	0.00110	0.744	0.027	35.699	0.174
6.5	0.107	0.068	0.351	0.429	0.00111	0.744	0.027	35.686	0.175
6	0.107	0.068	0.357	0.438	0.00112	0.749	0.027	35.817	0.177
5.5	0.108	0.068	0.355	0.433	0.00112	0.750	0.027	35.831	0.176
5	0.110	0.069	0.345	0.419	0.00110	0.744	0.027	35.704	0.173

TABLE 2.19: Case: Seepage shape 60 (d_{50} = 1.1 mm, S_0 = 0.00249, Q_0 = 0.016 m^3/s)

Section	y_s (m)	Rh_s (m)	Q_s (m^3/s)	u_s (m/s)	V_s (m/s)	F_s	Sf_s	τ_s (N/m^2)	u_s^*	$R*$	Ω_s (N/s)
10	0.058	0.062	0.014	0.297	0.000392	0.380	0.00163	1.000	0.032	41.385	0.228
9.5	0.058	0.063	0.014	0.291	0.000389	0.371	0.00161	0.990	0.031	41.173	0.222
9	0.056	0.061	0.014	0.301	0.000398	0.388	0.00167	1.004	0.032	41.454	0.228
8.5	0.057	0.061	0.014	0.302	0.000400	0.391	0.00167	0.992	0.032	41.220	0.225
8	0.056	0.059	0.014	0.308	0.000398	0.406	0.00170	0.979	0.031	40.938	0.228
7.5	0.057	0.058	0.013	0.312	0.000401	0.415	0.00171	0.969	0.031	40.733	0.226
7	0.056	0.059	0.013	0.302	0.000402	0.397	0.00168	0.976	0.031	40.880	0.220
6.5	0.055	0.057	0.013	0.313	0.000411	0.417	0.00174	0.981	0.031	40.992	0.225
6	0.056	0.056	0.013	0.318	0.000414	0.428	0.00176	0.975	0.031	40.850	0.225
5.5	0.057	0.058	0.013	0.314	0.000424	0.418	0.00174	0.987	0.031	41.111	0.220
5	0.060	0.060	0.013	0.307	0.000434	0.401	0.00170	0.997	0.032	41.324	0.212

TABLE 2.20: Case: No seepage shape 70 (d_{50} = 1.1 mm, S_0 = 0.00249, Q_0 = 0.0196 m^3/s)

Section	y_0 (m)	Rh_0 (m)	u_0 (m/s)	F_0	Sf_0	τ_0 (N/m^2)	u_0^*	$R*$	Ω_s (N/s)
10	0.113	0.074	0.354	0.416	0.00105	0.763	0.028	36.152	0.202
9.5	0.114	0.075	0.348	0.404	0.00103	0.764	0.028	36.180	0.199
9	0.112	0.074	0.351	0.411	0.00104	0.760	0.028	36.085	0.201
8.5	0.118	0.074	0.354	0.416	0.00105	0.763	0.028	36.145	0.202
8	0.120	0.074	0.354	0.416	0.00105	0.760	0.028	36.081	0.202
7.5	0.121	0.074	0.355	0.417	0.00105	0.762	0.028	36.124	0.202
7	0.121	0.074	0.353	0.413	0.00105	0.763	0.028	36.144	0.201
6.5	0.125	0.076	0.340	0.394	0.00102	0.762	0.028	36.130	0.196
6	0.125	0.074	0.351	0.411	0.00104	0.760	0.028	36.077	0.201
5.5	0.133	0.077	0.332	0.381	0.00100	0.761	0.028	36.097	0.193
5	0.130	0.076	0.344	0.398	0.00103	0.764	0.028	36.164	0.197

TABLE 2.21: Case: Seepage shape 70 (d_{50} = 1.1 mm, S_0 = 0.00249, Q_0 = 0.0196 m^3/s)

Section	y_s (m)	Rh_s (m)	Q_s (m^3/s)	u_s (m/s)	V_s (m/s)	F_s	Sf_s	τ_s (N/m^2)	u_s^*	$R*$	Ω_s (N/s)
10	0.065	0.063	0.017	0.315	0.000582	0.402	0.00186	1.142	0.034	44.214	0.303
9.5	0.065	0.064	0.016	0.307	0.000584	0.388	0.00183	1.146	0.034	44.305	0.295
9	0.065	0.063	0.016	0.307	0.000586	0.391	0.00184	1.135	0.034	44.075	0.292
8.5	0.063	0.061	0.016	0.313	0.000590	0.404	0.00188	1.129	0.034	43.969	0.294
8	0.063	0.059	0.016	0.328	0.000603	0.433	0.00196	1.131	0.034	44.000	0.302
7.5	0.064	0.060	0.015	0.316	0.000597	0.413	0.00189	1.106	0.033	43.515	0.286
7	0.062	0.059	0.015	0.313	0.000597	0.411	0.00191	1.107	0.033	43.535	0.284
6.5	0.065	0.060	0.015	0.303	0.000600	0.394	0.00184	1.093	0.033	43.258	0.270
6	0.067	0.062	0.015	0.290	0.000602	0.371	0.00178	1.090	0.033	43.199	0.257
5.5	0.063	0.060	0.014	0.307	0.000620	0.401	0.00189	1.108	0.033	43.565	0.269
5	0.065	0.060	0.014	0.305	0.000629	0.398	0.00188	1.104	0.033	43.481	0.262

TABLE 2.22: Case: No seepage shape 50 (d_{50} = 0.418 mm, S_0 = 0.00116, Q_0 = 0.009 m^3/s)

Section	y_0 (m)	Rh_0 (m)	u_0 (m/s)	F_0	Sf_0	τ_0 (N/m^2)	u_0^*	$R*$	Ω_s (N/s)
10	0.094	0.057	0.284	0.379	0.00039	0.218	0.015	6.333	0.034
9.5	0.094	0.057	0.284	0.379	0.00039	0.218	0.015	6.333	0.034
9	0.101	0.058	0.276	0.366	0.00038	0.216	0.015	6.307	0.033
8.5	0.101	0.058	0.276	0.366	0.00038	0.216	0.015	6.307	0.033
8	0.097	0.058	0.279	0.371	0.00038	0.218	0.015	6.327	0.034
7.5	0.097	0.058	0.279	0.371	0.00038	0.218	0.015	6.327	0.034
7	0.098	0.057	0.282	0.376	0.00039	0.218	0.015	6.325	0.034
6.5	0.098	0.057	0.282	0.376	0.00039	0.218	0.015	6.325	0.034
6	0.098	0.057	0.283	0.379	0.00039	0.217	0.015	6.315	0.034
5.5	0.098	0.057	0.283	0.379	0.00039	0.217	0.015	6.315	0.034
5	0.098	0.058	0.279	0.370	0.00038	0.218	0.015	6.327	0.034

TABLE 2.23: Case: Seepage shape 50 (d_{50} = 0.418 mm, S_0 = 0.00116, Q_0 = 0.009 m^3/s)

Section	y_s (m)	Rh_s (m)	Q_s (m^3/s)	u_s (m/s)	V_s (m/s)	F_s	Sf_s	τ_s (N/m^2)	u_s^*	$R*$	Ω_s (N/s)
10	0.089	0.057	0.007	0.228	0.000503	0.303	0.00076	0.428	0.021	8.913	0.054
9.5	0.089	0.058	0.007	0.224	0.000499	0.298	0.00075	0.423	0.021	8.853	0.053
9	0.092	0.056	0.007	0.227	0.000496	0.307	0.00077	0.420	0.021	8.830	0.054
8.5	0.090	0.057	0.007	0.222	0.000500	0.297	0.00075	0.419	0.020	8.810	0.052
8	0.090	0.057	0.007	0.219	0.000504	0.292	0.00074	0.418	0.020	8.804	0.051
7.5	0.087	0.057	0.007	0.220	0.000505	0.294	0.00075	0.418	0.020	8.807	0.051
7	0.085	0.055	0.007	0.222	0.000502	0.302	0.00077	0.416	0.020	8.781	0.052
6.5	0.086	0.055	0.007	0.217	0.000496	0.295	0.00075	0.409	0.020	8.704	0.050
6	0.083	0.054	0.007	0.221	0.000500	0.303	0.00077	0.412	0.020	8.737	0.051
5.5	0.084	0.053	0.007	0.221	0.000496	0.305	0.00078	0.408	0.020	8.695	0.051
5	0.085	0.055	0.007	0.214	0.000499	0.291	0.00075	0.403	0.020	8.648	0.048

TABLE 2.24: Case: No seepage shape 60 (d_{50} = 0.418 mm, S_0 = 0.00116, Q_0 = 0.0127 m^3/s)

Section	y_0 (m)	Rh_0 (m)	u_0 (m/s)	F_0	Sf_0	τ_0 (N/m^2)	u_0^*	$R*$	Ω_s (N/s)
10	0.119	0.066	0.283	0.352	0.00031	0.201	0.014	5.994	0.039
9.5	0.120	0.065	0.285	0.357	0.00031	0.200	0.014	5.983	0.039
9	0.120	0.067	0.280	0.347	0.00031	0.200	0.014	5.986	0.038
8.5	0.118	0.067	0.282	0.349	0.00031	0.201	0.014	6.001	0.038
8	0.118	0.067	0.283	0.349	0.00031	0.202	0.014	6.017	0.038
7.5	0.118	0.067	0.279	0.344	0.00030	0.201	0.014	5.996	0.038
7	0.120	0.068	0.278	0.341	0.00030	0.201	0.014	6.004	0.038
6.5	0.117	0.066	0.287	0.356	0.00031	0.203	0.014	6.023	0.039
6	0.119	0.067	0.281	0.345	0.00031	0.202	0.014	6.008	0.038
5.5	0.118	0.067	0.282	0.349	0.00031	0.202	0.014	6.011	0.038
5	0.120	0.069	0.272	0.330	0.00030	0.201	0.014	5.995	0.037

TABLE 2.25: Case: Seepage shape 60 (d_{50} = 0.418 mm, S_0 = 0.00116, Q_0 = 0.0127 m^3/s)

Section	y_s (m)	Rh_s (m)	Q_s (m^3/s)	u_s (m/s)	V_s (m/s)	F_s	Sf_s	τ_s (N/m^2)	u_s^*	$R*$	Ω_s (N/s)
10	0.118	0.065	0.011	0.231	0.000442	0.289	0.00062	0.397	0.020	8.397	0.066
9.5	0.138	0.071	0.011	0.193	0.000408	0.232	0.00050	0.346	0.019	7.840	0.052
9	0.096	0.060	0.010	0.224	0.000408	0.291	0.00061	0.363	0.019	8.024	0.063
8.5	0.119	0.067	0.010	0.197	0.000405	0.244	0.00053	0.344	0.019	7.820	0.053
8	0.112	0.065	0.010	0.201	0.000407	0.252	0.00054	0.341	0.018	7.779	0.053
7.5	0.114	0.064	0.010	0.210	0.000427	0.265	0.00056	0.351	0.019	7.901	0.055
7	0.095	0.060	0.010	0.236	0.000460	0.307	0.00067	0.399	0.020	8.421	0.065
6.5	0.113	0.062	0.010	0.226	0.000456	0.291	0.00064	0.385	0.020	8.265	0.061
6	0.114	0.061	0.010	0.224	0.000457	0.289	0.00064	0.384	0.020	8.255	0.060
5.5	0.103	0.057	0.009	0.238	0.000456	0.319	0.00070	0.388	0.020	8.296	0.064
5	0.095	0.058	0.009	0.225	0.000453	0.297	0.00066	0.380	0.019	8.218	0.060

TABLE 2.26: Case: No seepage shape 70 (d_{50} = 0.418 mm, S_0 = 0.00116, Q_0 = 0.0178 m^3/s)

Section	y_0 (m)	Rh_0 (m)	u_0 (m/s)	F_0	Sf_0	τ_0 (N/m^2)	u_0^*	$R*$	Ω_s (N/s)
10	0.141	0.079	0.289	0.329	0.00029	0.221	0.015	6.187	0.050
9.5	0.139	0.079	0.290	0.330	0.00029	0.221	0.015	6.184	0.050
9	0.143	0.080	0.283	0.318	0.00028	0.220	0.015	6.172	0.049
8.5	0.139	0.078	0.293	0.335	0.00029	0.222	0.015	6.192	0.051
8	0.136	0.077	0.299	0.344	0.00030	0.224	0.015	6.220	0.052
7.5	0.139	0.077	0.295	0.339	0.00029	0.221	0.015	6.188	0.051
7	0.140	0.078	0.289	0.329	0.00029	0.220	0.015	6.173	0.050
6.5	0.139	0.080	0.285	0.321	0.00028	0.221	0.015	6.186	0.049
6	0.140	0.079	0.288	0.327	0.00028	0.221	0.015	6.184	0.050
5.5	0.140	0.080	0.280	0.316	0.00028	0.219	0.015	6.157	0.048
5	0.141	0.079	0.286	0.326	0.00028	0.219	0.015	6.154	0.050

TABLE 2.27: Case: Seepage shape 70 (d_{50} = 0.418 mm, S_0 = 0.00116, Q_0 = 0.0178 m^3/s)

Section	y_s (m)	Rh_s (m)	Q_s (m^3/s)	u_s (m/s)	V_s (m/s)	F_s	Sf_s	τ_s (N/m^2)	u_s^*	$R*$	Ω_s (N/s)
10	0.121	0.077	0.016	0.237	0.000385	0.273	0.00051	0.383	0.020	8.106	0.079
9.5	0.129	0.073	0.016	0.257	0.000398	0.305	0.00057	0.405	0.020	8.342	0.087
9	0.120	0.061	0.015	0.298	0.000391	0.386	0.00071	0.422	0.021	8.507	0.107
8.5	0.117	0.071	0.015	0.242	0.000374	0.290	0.00054	0.376	0.019	8.032	0.081
8	0.120	0.075	0.015	0.227	0.000375	0.265	0.00050	0.367	0.019	7.934	0.074
7.5	0.140	0.075	0.015	0.223	0.000374	0.260	0.00049	0.362	0.019	7.878	0.072
7	0.147	0.083	0.015	0.178	0.000335	0.198	0.00039	0.319	0.018	7.402	0.057
6.5	0.104	0.067	0.015	0.234	0.000355	0.289	0.00054	0.349	0.019	7.743	0.077
6	0.083	0.033	0.014	0.483	0.000363	0.856	0.00190	0.607	0.025	10.208	0.270
5.5	0.118	0.072	0.014	0.213	0.000358	0.254	0.00048	0.341	0.018	7.649	0.068
5	0.123	0.070	0.014	0.208	0.000343	0.251	0.00047	0.325	0.018	7.472	0.066

TABLE 2.28: Case: No seepage shape 50 (d_{50} = 0.418 mm, S_0 = 0.00176, Q_0 = 0.0086 m^3/s)

Section	y_0 (m)	Rh_0 (m)	u_0 (m/s)	F_0	Sf_0	τ_0 (N/m^2)	u_0^*	$R*$	Ω_s (N/s)
10	0.087	0.055	0.290	0.395	0.00044	0.239	0.015	6.113	0.037
9.5	0.092	0.055	0.291	0.398	0.00045	0.239	0.015	6.118	0.038
9	0.095	0.055	0.287	0.390	0.00044	0.237	0.015	6.091	0.037
8.5	0.094	0.055	0.288	0.391	0.00044	0.238	0.015	6.094	0.037
8	0.095	0.056	0.284	0.384	0.00043	0.235	0.015	6.065	0.036
7.5	0.111	0.066	0.234	0.291	0.00033	0.214	0.015	5.788	0.028
7	0.094	0.056	0.284	0.384	0.00043	0.235	0.015	6.067	0.036
6.5	0.097	0.057	0.275	0.366	0.00041	0.230	0.015	6.002	0.035
6	0.100	0.054	0.286	0.391	0.00044	0.234	0.015	6.053	0.037
5.5	0.097	0.056	0.276	0.372	0.00042	0.229	0.015	5.990	0.035
5	0.096	0.054	0.289	0.396	0.00045	0.237	0.015	6.092	0.038

TABLE 2.29: Case: Seepage shape 50 (d_{50} = 0.418 mm, S_0 = 0.00176, Q_0 = 0.0086 m^3/s)

Section	y_s (m)	Rh_s (m)	Q_s (m^3/s)	u_s (m/s)	V_s (m/s)	F_s	Sf_s	τ_s (N/m^2)	u_s^*	$R*$	Ω_s (N/s)
10	0.074	0.050	0.007	0.265	0.000508	0.379	0.00102	0.500	0.022	8.915	0.070
9.5	0.065	0.049	0.007	0.268	0.000510	0.388	0.00106	0.506	0.022	8.970	0.071
9	0.079	0.050	0.007	0.236	0.000468	0.339	0.00088	0.426	0.021	8.226	0.058
8.5	0.079	0.051	0.007	0.237	0.000488	0.336	0.00090	0.445	0.021	8.410	0.058
8	0.064	0.048	0.006	0.259	0.000513	0.379	0.00104	0.485	0.022	8.783	0.066
7.5	0.082	0.048	0.006	0.239	0.000490	0.348	0.00093	0.439	0.021	8.357	0.058
7	0.075	0.047	0.006	0.238	0.000489	0.349	0.00094	0.436	0.021	8.325	0.057
6.5	0.076	0.045	0.006	0.245	0.000494	0.367	0.00101	0.448	0.021	8.440	0.060
6	0.089	0.052	0.006	0.200	0.000471	0.280	0.00076	0.386	0.020	7.829	0.044
5.5	0.074	0.049	0.006	0.194	0.000440	0.280	0.00074	0.354	0.019	7.498	0.042
5	0.087	0.047	0.006	0.187	0.000423	0.275	0.00072	0.334	0.018	7.291	0.040

TABLE 2.30: Case: No seepage shape 60 (d_{50} = 0.418 mm, S_0 = 0.00176, Q_0 = 0.0131 m^3/s)

Section	y_0 (m)	Rh_0 (m)	u_0 (m/s)	F_0	Sf_0	τ_0 (N/m^2)	u_0^*	$R*$	Ω_s (N/s)
10	0.128	0.072	0.265	0.316	0.00031	0.218	0.015	6.017	0.040
9.5	0.122	0.067	0.287	0.353	0.00035	0.231	0.015	6.194	0.045
9	0.121	0.070	0.277	0.334	0.00033	0.227	0.015	6.135	0.042
8.5	0.122	0.069	0.282	0.343	0.00034	0.230	0.015	6.171	0.044
8	0.122	0.071	0.276	0.330	0.00033	0.228	0.015	6.145	0.042
7.5	0.125	0.071	0.276	0.331	0.00033	0.227	0.015	6.136	0.042
7	0.120	0.067	0.289	0.355	0.00035	0.234	0.015	6.226	0.045
6.5	0.121	0.070	0.284	0.343	0.00034	0.232	0.015	6.204	0.044
6	0.121	0.070	0.282	0.340	0.00034	0.231	0.015	6.191	0.043
5.5	0.119	0.070	0.287	0.346	0.00034	0.235	0.015	6.247	0.044
5	0.120	0.071	0.282	0.339	0.00033	0.232	0.015	6.209	0.043

TABLE 2.31: Case: Seepage shape 60 (d_{50} = 0.418 mm, S_0 = 0.00176, Q_0 = 0.0131 m^3/s)

Section	y_s (m)	Rh_s (m)	Q_s (m^3/s)	u_s (m/s)	V_s (m/s)	F_s	Sf_s	τ_s (N/m^2)	u_s^*	$R*$	Ω_s (N/s)
10	0.155	0.069	0.011	0.194	0.000396	0.235	0.00056	0.379	0.019	7.831	0.061
9.5	0.136	0.066	0.011	0.177	0.000349	0.221	0.00052	0.336	0.018	7.370	0.056
9	0.097	0.062	0.011	0.188	0.000352	0.242	0.00056	0.341	0.018	7.427	0.060
8.5	0.088	0.056	0.011	0.201	0.000348	0.271	0.00063	0.347	0.019	7.489	0.066
8	0.091	0.062	0.010	0.187	0.000361	0.239	0.00056	0.340	0.018	7.416	0.058
7.5	0.095	0.057	0.010	0.201	0.000361	0.270	0.00062	0.345	0.019	7.467	0.063
7	0.096	0.057	0.010	0.226	0.000419	0.301	0.00072	0.407	0.020	8.115	0.072
6.5	0.096	0.058	0.010	0.227	0.000433	0.300	0.00073	0.415	0.020	8.195	0.071
6	0.098	0.054	0.010	0.205	0.000368	0.281	0.00064	0.340	0.018	7.413	0.062
5.5	0.088	0.055	0.010	0.262	0.000486	0.358	0.00090	0.484	0.022	8.850	0.086
5	0.083	0.049	0.010	0.271	0.000456	0.392	0.00099	0.472	0.022	8.732	0.092

TABLE 2.32: Case: No seepage shape 70 (d_{50} = 0.418 mm, S_0 = 0.00176, Q_0 = 0.0178 m^3/s)

Section	y_0 (m)	Rh_0 (m)	u_0 (m/s)	F_0	Sf_0	τ_0 (N/m^2)	u_0^*	$R*$	Ω_s (N/s)
10	0.135	0.075	0.297	0.345	0.00032	0.240	0.015	6.362	0.057
9.5	0.134	0.075	0.297	0.346	0.00033	0.239	0.015	6.351	0.057
9	0.138	0.074	0.298	0.350	0.00033	0.240	0.015	6.358	0.058
8.5	0.133	0.072	0.307	0.366	0.00035	0.246	0.016	6.440	0.061
8	0.136	0.072	0.309	0.368	0.00035	0.248	0.016	6.466	0.061
7.5	0.138	0.075	0.305	0.357	0.00034	0.247	0.016	6.453	0.059
7	0.135	0.074	0.305	0.359	0.00034	0.246	0.016	6.449	0.059
6.5	0.136	0.077	0.296	0.341	0.00032	0.241	0.016	6.374	0.056
6	0.133	0.073	0.312	0.367	0.00035	0.252	0.016	6.525	0.061
5.5	0.137	0.076	0.294	0.340	0.00032	0.238	0.015	6.332	0.056
5	0.135	0.076	0.297	0.343	0.00032	0.241	0.016	6.372	0.056

TABLE 2.33: Case: Seepage shape 70 (d_{50} = 0.418 mm, S_0 = 0.00176, Q_0 = 0.0178 m^3/s)

Section	y_s (m)	Rh_s (m)	Q_s (m^3/s)	u_s (m/s)	V_s (m/s)	F_s	Sf_s	τ_s (N/m^2)	u_s^*	$R*$	Ω_s (N/s)
10	0.115	0.068	0.016	0.222	0.000319	0.271	0.00054	0.361	0.019	7.838	0.084
9.5	0.129	0.066	0.016	0.217	0.000305	0.269	0.00053	0.346	0.019	7.674	0.082
9	0.100	0.063	0.015	0.226	0.000309	0.287	0.00057	0.355	0.019	7.771	0.086
8.5	0.086	0.063	0.015	0.226	0.000309	0.289	0.00057	0.352	0.019	7.742	0.086
8	0.102	0.061	0.015	0.229	0.000308	0.295	0.00058	0.350	0.019	7.716	0.087
7.5	0.083	0.056	0.015	0.238	0.000299	0.319	0.00062	0.344	0.019	7.649	0.091
7	0.089	0.054	0.015	0.239	0.000292	0.327	0.00063	0.333	0.018	7.529	0.091
6.5	0.096	0.063	0.015	0.210	0.000299	0.268	0.00053	0.328	0.018	7.467	0.077
6	0.086	0.057	0.014	0.228	0.000298	0.306	0.00060	0.335	0.018	7.548	0.085
5.5	0.104	0.067	0.014	0.199	0.000312	0.244	0.00051	0.335	0.018	7.551	0.071
5	0.104	0.057	0.014	0.219	0.000296	0.292	0.00058	0.323	0.018	7.417	0.080

TABLE 2.34: Case: No seepage shape 50 (d_{50} = 0.418 mm, S_0 = 0.00249, Q_0 = 0.0086 m^3/s)

Section	y_0 (m)	Rh_0 (m)	u_0 (m/s)	F_0	Sf_0	τ_0 (N/m^2)	u_0^*	$R*$	Ω_s (N/s)
10	0.097	0.059	0.260	0.342	0.00034	0.194	0.014	5.719	0.028
9.5	0.096	0.057	0.273	0.363	0.00037	0.210	0.014	5.948	0.031
9	0.098	0.057	0.275	0.368	0.00038	0.213	0.015	5.990	0.032
8.5	0.096	0.057	0.280	0.375	0.00039	0.219	0.015	6.083	0.033
8	0.099	0.057	0.279	0.372	0.00039	0.218	0.015	6.061	0.033
7.5	0.098	0.057	0.277	0.370	0.00038	0.216	0.015	6.031	0.033
7	0.098	0.057	0.278	0.371	0.00039	0.216	0.015	6.036	0.033
6.5	0.098	0.058	0.273	0.363	0.00037	0.210	0.015	5.958	0.031
6	0.096	0.057	0.280	0.375	0.00039	0.219	0.015	6.075	0.033
5.5	0.096	0.057	0.281	0.377	0.00040	0.221	0.015	6.109	0.034
5	0.101	0.061	0.259	0.336	0.00032	0.193	0.014	5.708	0.027

TABLE 2.35: Case: Seepage shape 50 (d_{50} = 0.418 mm, S_0 = 0.00249, Q_0 = 0.0086 m^3/s)

Section	y_s (m)	Rh_s (m)	Q_s (m^3/s)	u_s (m/s)	V_s (m/s)	F_s	Sf_s	τ_s (N/m^2)	u_s^*	$R*$	Ω_s (N/s)
10	0.077	0.052	0.007	0.230	0.000456	0.323	0.00083	0.419	0.020	8.479	0.057
9.5	0.078	0.052	0.007	0.228	0.000464	0.319	0.00082	0.420	0.020	8.488	0.055
9	0.073	0.052	0.007	0.224	0.000461	0.314	0.00081	0.409	0.020	8.374	0.053
8.5	0.078	0.049	0.007	0.215	0.000427	0.311	0.00077	0.367	0.019	7.938	0.050
8	0.069	0.050	0.006	0.233	0.000481	0.333	0.00089	0.431	0.021	8.598	0.056
7.5	0.083	0.040	0.006	0.210	0.000357	0.335	0.00078	0.307	0.018	7.263	0.049
7	0.077	0.048	0.006	0.233	0.000483	0.340	0.00091	0.426	0.021	8.549	0.055
6.5	0.063	0.042	0.006	0.222	0.000411	0.348	0.00090	0.365	0.019	7.918	0.053
6	0.075	0.044	0.006	0.189	0.000380	0.286	0.00067	0.293	0.017	7.091	0.039
5.5	0.086	0.049	0.006	0.175	0.000396	0.254	0.00061	0.293	0.017	7.089	0.035
5	0.087	0.049	0.006	0.178	0.000412	0.257	0.00063	0.303	0.017	7.208	0.035

TABLE 2.36: Case: No seepage shape 60 (d_{50} = 0.418 mm, S_0 = 0.00249, Q_0 = 0.0108 m^3/s)

Section	y_0 (m)	Rh_0 (m)	u_0 (m/s)	F_0	Sf_0	τ_0 (N/m^2)	u_0^*	$R*$	Ω_s (N/s)
10	0.117	0.068	0.235	0.287	0.00031	0.211	0.015	6.150	0.033
9.5	0.118	0.066	0.242	0.301	0.00034	0.216	0.015	6.222	0.036
9	0.119	0.069	0.236	0.286	0.00031	0.213	0.015	6.181	0.033
8.5	0.109	0.061	0.268	0.347	0.00040	0.242	0.016	6.589	0.043
8	0.118	0.067	0.243	0.299	0.00033	0.219	0.015	6.259	0.035
7.5	0.117	0.068	0.244	0.299	0.00033	0.221	0.015	6.288	0.035
7	0.117	0.066	0.248	0.307	0.00034	0.223	0.015	6.326	0.036
6.5	0.119	0.069	0.237	0.289	0.00032	0.214	0.015	6.188	0.034
6	0.118	0.067	0.244	0.300	0.00033	0.220	0.015	6.279	0.035
5.5	0.118	0.067	0.245	0.302	0.00034	0.221	0.015	6.289	0.036
5	0.118	0.068	0.242	0.297	0.00033	0.219	0.015	6.258	0.035

TABLE 2.37: Case: Seepage shape 60 (d_{50} = 0.418 mm, S_0 = 0.00249, Q_0 = 0.0108 m^3/s)

Section	y_s (m)	Rh_s (m)	Q_s (m^3/s)	u_s (m/s)	V_s (m/s)	F_s	Sf_s	τ_s (N/m^2)	u_s^*	$R*$	Ω_s (N/s)
10	0.090	0.064	0.009	0.209	0.000391	0.265	0.00060	0.373	0.019	8.246	0.054
9.5	0.095	0.061	0.009	0.189	0.000345	0.245	0.00054	0.321	0.018	7.648	0.048
9	0.095	0.063	0.009	0.203	0.000388	0.259	0.00058	0.356	0.019	8.051	0.050
8.5	0.093	0.065	0.009	0.189	0.000377	0.237	0.00052	0.332	0.018	7.784	0.045
8	0.084	0.061	0.009	0.203	0.000386	0.263	0.00059	0.351	0.019	8.003	0.050
7.5	0.112	0.061	0.009	0.204	0.000394	0.264	0.00060	0.357	0.019	8.061	0.050
7	0.097	0.060	0.008	0.197	0.000383	0.256	0.00058	0.341	0.018	7.883	0.047
6.5	0.091	0.060	0.008	0.207	0.000409	0.270	0.00063	0.370	0.019	8.214	0.051
6	0.091	0.057	0.008	0.217	0.000413	0.291	0.00069	0.384	0.020	8.370	0.055
5.5	0.089	0.057	0.008	0.212	0.000409	0.283	0.00066	0.372	0.019	8.236	0.052
5	0.103	0.054	0.008	0.213	0.000395	0.292	0.00069	0.364	0.019	8.140	0.053

TABLE 2.38: Case: No seepage shape 70 (d_{50} = 0.418 mm, S_0 = 0.00249, Q_0 = 0.016 m^3/s)

Section	y_0 (m)	Rh_0 (m)	u_0 (m/s)	F_0	Sf_0	τ_0 (N/m^2)	u_0^*	$R*$	Ω_s (N/s)
10	0.136	0.074	0.271	0.318	0.00034	0.246	0.016	6.411	0.053
9.5	0.138	0.075	0.272	0.317	0.00034	0.246	0.016	6.421	0.053
9	0.133	0.072	0.280	0.334	0.00036	0.255	0.016	6.536	0.057
8.5	0.138	0.075	0.271	0.317	0.00034	0.246	0.016	6.411	0.053
8	0.137	0.078	0.267	0.306	0.00032	0.242	0.016	6.369	0.050
7.5	0.136	0.076	0.269	0.311	0.00033	0.244	0.016	6.385	0.051
7	0.138	0.080	0.260	0.294	0.00030	0.237	0.015	6.296	0.047
6.5	0.137	0.079	0.264	0.299	0.00031	0.241	0.016	6.350	0.049
6	0.134	0.078	0.273	0.312	0.00033	0.250	0.016	6.471	0.052
5.5	0.132	0.076	0.283	0.328	0.00035	0.263	0.016	6.629	0.055
5	0.135	0.078	0.273	0.312	0.00033	0.251	0.016	6.481	0.051

TABLE 2.39: Case: Seepage shape 70 (d_{50} = 0.418 mm, S_0 = 0.00249, Q_0 = 0.016 m^3/s)

Section	y_s (m)	Rh_s (m)	Q_s (m^3/s)	u_s (m/s)	V_s (m/s)	F_s	Sf_s	τ_s (N/m^2)	u_s^*	$R*$	Ω_s (N/s)
10	0.103	0.073	0.014	0.215	0.000333	0.254	0.00049	0.353	0.019	7.685	0.068
9.5	0.101	0.074	0.014	0.212	0.000333	0.249	0.00048	0.348	0.019	7.633	0.066
9	0.115	0.072	0.014	0.220	0.000343	0.261	0.00051	0.364	0.019	7.804	0.070
8.5	0.092	0.063	0.014	0.247	0.000342	0.313	0.00065	0.402	0.020	8.207	0.087
8	0.100	0.066	0.014	0.236	0.000343	0.295	0.00060	0.385	0.020	8.030	0.080
7.5	0.130	0.066	0.013	0.207	0.000306	0.257	0.00049	0.317	0.018	7.280	0.064
7	0.109	0.067	0.013	0.220	0.000332	0.271	0.00053	0.350	0.019	7.659	0.070
6.5	0.089	0.061	0.013	0.231	0.000321	0.299	0.00060	0.361	0.019	7.777	0.078
6	0.088	0.062	0.013	0.226	0.000324	0.290	0.00058	0.355	0.019	7.713	0.075
5.5	0.115	0.072	0.013	0.196	0.000332	0.233	0.00045	0.323	0.018	7.355	0.057
5	0.119	0.070	0.013	0.205	0.000338	0.249	0.00049	0.336	0.018	7.498	0.061

TABLE 2.40: Case: No seepage shape 50 (d_{50} = 0.62 mm, S_0 = 0.00116, Q_0 = 0.0097 m^3/s)

Section	y_0 (m)	Rh_0 (m)	u_0 (m/s)	F_0	Sf_0	τ_0 (N/m^2)	u_0^*	$R*$	Ω_s (N/s)
10	0.097	0.057	0.310	0.414	0.00057	0.321	0.018	13.370	0.054
9.5	0.097	0.057	0.314	0.422	0.00058	0.320	0.018	13.345	0.055
9	0.100	0.058	0.307	0.407	0.00057	0.322	0.018	13.386	0.054
8.5	0.101	0.059	0.302	0.398	0.00056	0.324	0.018	13.417	0.053
8	0.098	0.057	0.310	0.413	0.00057	0.321	0.018	13.368	0.054
7.5	0.099	0.057	0.308	0.410	0.00057	0.320	0.018	13.344	0.054
7	0.099	0.058	0.303	0.402	0.00056	0.321	0.018	13.371	0.054
6.5	0.100	0.058	0.300	0.396	0.00056	0.322	0.018	13.379	0.053
6	0.101	0.059	0.301	0.396	0.00056	0.324	0.018	13.422	0.053
5.5	0.101	0.058	0.302	0.400	0.00056	0.322	0.018	13.376	0.053
5	0.100	0.058	0.304	0.403	0.00057	0.323	0.018	13.399	0.054

TABLE 2.41: Case: Seepage shape 50 (d_{50} = 0.62 mm, S_0 = 0.00116, Q_0 = 0.0097 m^3/s)

Section	y_s (m)	Rh_s (m)	Q_s (m^3/s)	u_s (m/s)	V_s (m/s)	F_s	Sf_s	τ_s (N/m^2)	u_s^*	$R*$	Ω_s (N/s)
10	0.066	0.052	0.008	0.238	0.000471	0.335	0.00103	0.519	0.023	16.918	0.079
9.5	0.064	0.051	0.008	0.238	0.000480	0.336	0.00104	0.525	0.023	17.015	0.079
9	0.065	0.051	0.008	0.244	0.000494	0.347	0.00106	0.528	0.023	17.060	0.079
8.5	0.062	0.049	0.007	0.244	0.000489	0.352	0.00108	0.518	0.023	16.901	0.078
8	0.060	0.048	0.007	0.243	0.000490	0.352	0.00109	0.518	0.023	16.902	0.078
7.5	0.060	0.048	0.007	0.242	0.000491	0.355	0.00109	0.509	0.023	16.745	0.076
7	0.061	0.049	0.007	0.237	0.000500	0.343	0.00108	0.514	0.023	16.840	0.074
6.5	0.060	0.048	0.007	0.239	0.000506	0.349	0.00110	0.515	0.023	16.845	0.073
6	0.059	0.048	0.007	0.237	0.000518	0.346	0.00111	0.522	0.023	16.957	0.072
5.5	0.059	0.047	0.007	0.236	0.000518	0.347	0.00110	0.512	0.023	16.795	0.070
5	0.059	0.047	0.006	0.232	0.000524	0.341	0.00110	0.512	0.023	16.805	0.069

TABLE 2.42: Case: No seepage shape 60 (d_{50} = 0.62 mm, S_0 = 0.00116, Q_0 = 0.0169 m^3/s)

Section	y_0 (m)	Rh_0 (m)	u_0 (m/s)	F_0	Sf_0	τ_0 (N/m^2)	u_0^*	$R*$	Ω_s (N/s)
10	0.131	0.078	0.317	0.363	0.00045	0.346	0.019	13.686	0.075
9.5	0.130	0.077	0.320	0.368	0.00046	0.344	0.019	13.651	0.076
9	0.131	0.077	0.320	0.368	0.00046	0.344	0.019	13.646	0.075
8.5	0.130	0.077	0.321	0.369	0.00046	0.344	0.019	13.650	0.076
8	0.130	0.076	0.326	0.377	0.00046	0.345	0.019	13.656	0.076
7.5	0.130	0.077	0.318	0.365	0.00045	0.343	0.019	13.631	0.075
7	0.132	0.077	0.322	0.372	0.00046	0.344	0.019	13.640	0.076
6.5	0.132	0.077	0.323	0.371	0.00046	0.345	0.019	13.670	0.076
6	0.130	0.077	0.322	0.372	0.00046	0.344	0.019	13.643	0.076
5.5	0.131	0.077	0.323	0.372	0.00046	0.344	0.019	13.641	0.076
5	0.128	0.077	0.325	0.375	0.00046	0.345	0.019	13.665	0.076

TABLE 2.43: Case: Seepage shape 60 (d_{50} = 0.62 mm, S_0 = 0.00116, Q_0 = 0.0169 m^3/s)

Section	y_s (m)	Rh_s (m)	Q_s (m^3/s)	u_s (m/s)	V_s (m/s)	F_s	Sf_s	τ_s (N/m^2)	u_s^*	$R*$	Ω_s (N/s)
10	0.104	0.072	0.014	0.261	0.000553	0.310	0.00083	0.585	0.024	17.966	0.117
9.5	0.099	0.071	0.014	0.260	0.000553	0.311	0.00084	0.588	0.024	18.002	0.117
9	0.098	0.070	0.014	0.263	0.000558	0.317	0.00086	0.588	0.024	18.000	0.117
8.5	0.093	0.069	0.014	0.261	0.000554	0.317	0.00087	0.586	0.024	17.971	0.117
8	0.090	0.067	0.014	0.259	0.000544	0.318	0.00087	0.573	0.024	17.774	0.115
7.5	0.088	0.067	0.013	0.255	0.000540	0.316	0.00087	0.568	0.024	17.688	0.113
7	0.086	0.066	0.013	0.255	0.000541	0.318	0.00087	0.563	0.024	17.623	0.112
6.5	0.085	0.065	0.013	0.257	0.000548	0.323	0.00089	0.565	0.024	17.652	0.112
6	0.086	0.065	0.013	0.257	0.000559	0.321	0.00089	0.569	0.024	17.711	0.111
5.5	0.086	0.065	0.012	0.254	0.000555	0.319	0.00088	0.559	0.024	17.562	0.108
5	0.086	0.063	0.012	0.262	0.000572	0.333	0.00091	0.566	0.024	17.668	0.110

TABLE 2.44: Case: No seepage shape 70 (d_{50} = 0.62 mm, S_0 = 0.00116, Q_0 = 0.019 m^3/s)

Section	y_0 (m)	Rh_0 (m)	u_0 (m/s)	F_0	Sf_0	τ_0 (N/m^2)	u_0^*	$R*$	Ω_s (N/s)
10	0.137	0.081	0.307	0.345	0.00042	0.330	0.018	13.364	0.077
9.5	0.138	0.081	0.308	0.345	0.00042	0.330	0.018	13.363	0.077
9	0.136	0.081	0.309	0.347	0.00042	0.330	0.018	13.362	0.078
8.5	0.137	0.080	0.310	0.349	0.00042	0.330	0.018	13.356	0.078
8	0.138	0.081	0.306	0.344	0.00041	0.330	0.018	13.366	0.077
7.5	0.137	0.080	0.310	0.349	0.00042	0.329	0.018	13.355	0.078
7	0.137	0.081	0.307	0.344	0.00041	0.330	0.018	13.367	0.077
6.5	0.136	0.080	0.311	0.350	0.00042	0.329	0.018	13.352	0.078
6	0.137	0.080	0.310	0.348	0.00042	0.330	0.018	13.358	0.078
5.5	0.137	0.080	0.310	0.348	0.00042	0.329	0.018	13.355	0.078
5	0.137	0.081	0.309	0.348	0.00042	0.330	0.018	13.358	0.078

TABLE 2.45: Case: Seepage shape 70 (d_{50} = 0.62 mm, S_0 = 0.00116, Q_0 = 0.019 m^3/s)

Section	y_s (m)	Rh_s (m)	Q_s (m^3/s)	u_s (m/s)	V_s (m/s)	F_s	Sf_s	τ_s (N/m^2)	u_s^*	$R*$	Ω_s (N/s)
10	0.099	0.071	0.017	0.281	0.000421	0.337	0.00074	0.511	0.023	16.709	0.122
9.5	0.099	0.070	0.017	0.285	0.000428	0.342	0.00074	0.514	0.023	16.766	0.122
9	0.098	0.070	0.017	0.283	0.000430	0.341	0.00075	0.516	0.023	16.786	0.121
8.5	0.094	0.070	0.016	0.284	0.000434	0.343	0.00076	0.523	0.023	16.912	0.122
8	0.093	0.069	0.016	0.283	0.000432	0.343	0.00076	0.518	0.023	16.826	0.121
7.5	0.096	0.068	0.016	0.283	0.000430	0.347	0.00075	0.504	0.022	16.589	0.118
7	0.092	0.068	0.016	0.283	0.000436	0.345	0.00077	0.516	0.023	16.789	0.119
6.5	0.093	0.069	0.016	0.283	0.000447	0.344	0.00077	0.522	0.023	16.894	0.118
6	0.093	0.069	0.015	0.281	0.000448	0.341	0.00077	0.522	0.023	16.884	0.117
5.5	0.091	0.069	0.015	0.281	0.000449	0.342	0.00077	0.521	0.023	16.867	0.116
5	0.090	0.068	0.015	0.285	0.000454	0.350	0.00079	0.523	0.023	16.900	0.117

TABLE 2.46: Case: No seepage shape 50 (d_{50} = 0.62 mm, S_0 = 0.00176, Q_0 = 0.0097 m^3/s)

Section	y_0 (m)	Rh_0 (m)	u_0 (m/s)	F_0	Sf_0	τ_0 (N/m^2)	u_0^*	$R*$	Ω_s (N/s)
10	0.097	0.057	0.310	0.414	0.00058	0.328	0.018	13.568	0.055
9.5	0.097	0.057	0.314	0.422	0.00059	0.329	0.018	13.597	0.056
9	0.100	0.058	0.307	0.407	0.00058	0.326	0.018	13.539	0.055
8.5	0.101	0.059	0.302	0.398	0.00057	0.325	0.018	13.510	0.054
8	0.098	0.057	0.310	0.413	0.00058	0.328	0.018	13.563	0.055
7.5	0.099	0.057	0.308	0.410	0.00058	0.325	0.018	13.518	0.055
7	0.099	0.058	0.303	0.402	0.00057	0.324	0.018	13.488	0.054
6.5	0.100	0.058	0.300	0.396	0.00056	0.323	0.018	13.459	0.053
6	0.101	0.059	0.301	0.396	0.00056	0.324	0.018	13.498	0.053
5.5	0.101	0.058	0.302	0.400	0.00057	0.324	0.018	13.479	0.054
5	0.100	0.058	0.304	0.403	0.00057	0.326	0.018	13.525	0.054

TABLE 2.47: Case: Seepage shape 50 (d_{50} = 0.62 mm, S_0 = 0.00176, Q_0 = 0.0097 m^3/s)

Section	y_s (m)	Rh_s (m)	Q_s (m^3/s)	u_s (m/s)	V_s (m/s)	F_s	Sf_s	τ_s (N/m^2)	u_s^*	$R*$	Ω_s (N/s)
10	0.060	0.047	0.008	0.252	0.000458	0.371	0.00114	0.526	0.023	17.023	0.088
9.5	0.060	0.046	0.008	0.255	0.000461	0.379	0.00115	0.519	0.023	16.911	0.087
9	0.058	0.044	0.008	0.269	0.000469	0.411	0.00122	0.523	0.023	16.979	0.091
8.5	0.056	0.044	0.007	0.260	0.000467	0.396	0.00121	0.522	0.023	16.960	0.088
8	0.055	0.044	0.007	0.258	0.000469	0.395	0.00121	0.518	0.023	16.892	0.086
7.5	0.053	0.043	0.007	0.258	0.000474	0.396	0.00124	0.524	0.023	16.991	0.086
7	0.053	0.043	0.007	0.262	0.000486	0.406	0.00126	0.527	0.023	17.053	0.086
6.5	0.052	0.042	0.007	0.268	0.000495	0.420	0.00131	0.533	0.023	17.147	0.087
6	0.051	0.042	0.007	0.261	0.000493	0.409	0.00129	0.527	0.023	17.048	0.084
5.5	0.051	0.041	0.007	0.263	0.000495	0.417	0.00131	0.521	0.023	16.947	0.084
5	0.050	0.040	0.006	0.265	0.000504	0.424	0.00134	0.525	0.023	17.015	0.084

TABLE 2.48: Case: No seepage shape 60 (d_{50} = 0.62 mm, S_0 = 0.00176, Q_0 = 0.0135 m^3/s)

Section	y_0 (m)	Rh_0 (m)	u_0 (m/s)	F_0	Sf_0	τ_0 (N/m^2)	u_0^*	$R*$	Ω_s (N/s)
10	0.122	0.073	0.278	0.328	0.00049	0.351	0.019	13.902	0.065
9.5	0.126	0.075	0.273	0.318	0.00048	0.351	0.019	13.918	0.064
9	0.125	0.073	0.278	0.328	0.00049	0.350	0.019	13.894	0.065
8.5	0.125	0.074	0.275	0.324	0.00048	0.350	0.019	13.893	0.064
8	0.123	0.073	0.279	0.329	0.00049	0.352	0.019	13.931	0.065
7.5	0.123	0.072	0.281	0.333	0.00049	0.350	0.019	13.900	0.065
7	0.123	0.073	0.282	0.334	0.00049	0.352	0.019	13.935	0.066
6.5	0.123	0.073	0.282	0.334	0.00049	0.352	0.019	13.937	0.066
6	0.122	0.073	0.280	0.331	0.00049	0.352	0.019	13.934	0.065
5.5	0.125	0.072	0.281	0.334	0.00049	0.351	0.019	13.907	0.066
5	0.125	0.073	0.278	0.329	0.00049	0.351	0.019	13.902	0.065

TABLE 2.49: Case: Seepage shape 60 (d_{50} = 0.62 mm, S_0 = 0.00176, Q_0 = 0.0135 m^3/s)

Section	y_s (m)	Rh_s (m)	Q_s (m^3/s)	u_s (m/s)	V_s (m/s)	F_s	Sf_s	τ_s (N/m^2)	u_s^*	$R*$	Ω_s (N/s)
10	0.079	0.061	0.012	0.248	0.000444	0.322	0.00091	0.540	0.023	17.185	0.102
9.5	0.079	0.061	0.011	0.251	0.000457	0.325	0.00092	0.550	0.023	17.329	0.102
9	0.077	0.060	0.011	0.250	0.000458	0.325	0.00093	0.549	0.023	17.324	0.101
8.5	0.077	0.060	0.011	0.248	0.000460	0.322	0.00092	0.547	0.023	17.282	0.100
8	0.075	0.059	0.011	0.248	0.000460	0.325	0.00093	0.544	0.023	17.245	0.099
7.5	0.078	0.059	0.011	0.246	0.000464	0.322	0.00092	0.537	0.023	17.123	0.096
7	0.076	0.058	0.010	0.249	0.000467	0.330	0.00094	0.537	0.023	17.127	0.097
6.5	0.075	0.057	0.010	0.251	0.000471	0.335	0.00095	0.536	0.023	17.114	0.097
6	0.077	0.057	0.010	0.247	0.000472	0.330	0.00094	0.527	0.023	16.967	0.093
5.5	0.075	0.057	0.010	0.245	0.000470	0.328	0.00094	0.522	0.023	16.881	0.092
5	0.072	0.055	0.010	0.244	0.000466	0.332	0.00095	0.518	0.023	16.816	0.092

TABLE 2.50: Case: No seepage shape 70 (d_{50} = 0.62 mm, S_0 = 0.00176, Q_0 = 0.0173 m^3/s)

Section	y_0 (m)	Rh_0 (m)	u_0 (m/s)	F_0	Sf_0	τ_0 (N/m^2)	u_0^*	$R*$	Ω_s (N/s)
10	0.136	0.078	0.291	0.332	0.00044	0.337	0.018	13.576	0.075
9.5	0.136	0.079	0.288	0.327	0.00043	0.337	0.018	13.564	0.074
9	0.134	0.078	0.291	0.332	0.00044	0.337	0.018	13.575	0.075
8.5	0.134	0.078	0.291	0.332	0.00044	0.337	0.018	13.576	0.075
8	0.134	0.079	0.289	0.329	0.00044	0.337	0.018	13.569	0.074
7.5	0.134	0.079	0.290	0.331	0.00044	0.337	0.018	13.573	0.074
7	0.134	0.078	0.294	0.337	0.00044	0.338	0.018	13.591	0.075
6.5	0.133	0.077	0.298	0.343	0.00045	0.339	0.018	13.606	0.077
6	0.134	0.077	0.297	0.341	0.00045	0.339	0.018	13.601	0.076
5.5	0.134	0.077	0.297	0.342	0.00045	0.338	0.018	13.600	0.076
5	0.132	0.076	0.301	0.348	0.00046	0.340	0.018	13.624	0.077

TABLE 2.51: Case: Seepage shape 70 (d_{50} = 0.62 mm, S_0 = 0.00176, Q_0 = 0.0173 m^3/s)

Section	y_s (m)	Rh_s (m)	Q_s (m^3/s)	u_s (m/s)	V_s (m/s)	F_s	Sf_s	τ_s (N/m^2)	u_s^*	$R*$	Ω_s (N/s)
10	0.090	0.068	0.015	0.265	0.000381	0.323	0.00074	0.497	0.022	16.554	0.112
9.5	0.089	0.067	0.015	0.267	0.000381	0.330	0.00075	0.494	0.022	16.510	0.113
9	0.087	0.067	0.015	0.272	0.000391	0.337	0.00078	0.507	0.023	16.721	0.115
8.5	0.085	0.066	0.015	0.272	0.000391	0.339	0.00078	0.506	0.022	16.697	0.115
8	0.084	0.065	0.015	0.270	0.000389	0.337	0.00078	0.501	0.022	16.623	0.113
7.5	0.083	0.065	0.015	0.270	0.000392	0.338	0.00079	0.504	0.022	16.668	0.113
7	0.084	0.064	0.014	0.274	0.000396	0.345	0.00080	0.504	0.022	16.662	0.113
6.5	0.084	0.064	0.014	0.279	0.000405	0.352	0.00082	0.512	0.023	16.800	0.114
6	0.083	0.064	0.014	0.277	0.000405	0.350	0.00082	0.509	0.023	16.748	0.113
5.5	0.081	0.063	0.014	0.276	0.000405	0.351	0.00082	0.507	0.023	16.722	0.112
5	0.079	0.061	0.014	0.284	0.000408	0.368	0.00086	0.512	0.023	16.795	0.116

TABLE 2.52: Case: No seepage shape 50 (d_{50} = 0.62 mm, S_0 = 0.00249, Q_0 = 0.0079 m^3/s)

Section	y_0 (m)	Rh_0 (m)	u_0 (m/s)	F_0	Sf_0	τ_0 (N/m^2)	u_0^*	$R*$	Ω_s (N/s)
10	0.107	0.062	0.229	0.294	0.00046	0.278	0.017	12.380	0.036
9.5	0.108	0.063	0.227	0.289	0.00045	0.277	0.017	12.353	0.035
9	0.107	0.063	0.226	0.288	0.00045	0.277	0.017	12.347	0.035
8.5	0.107	0.063	0.227	0.289	0.00045	0.278	0.017	12.384	0.035
8	0.108	0.063	0.227	0.289	0.00045	0.278	0.017	12.388	0.035
7.5	0.107	0.063	0.226	0.288	0.00045	0.277	0.017	12.353	0.035
7	0.108	0.062	0.227	0.290	0.00045	0.277	0.017	12.364	0.035
6.5	0.108	0.063	0.227	0.289	0.00045	0.277	0.017	12.359	0.035
6	0.108	0.063	0.226	0.289	0.00045	0.277	0.017	12.356	0.035
5.5	0.109	0.063	0.226	0.288	0.00045	0.277	0.017	12.352	0.035
5	0.109	0.062	0.228	0.291	0.00045	0.277	0.017	12.363	0.035

TABLE 2.53: Case: Seepage shape 50 (d_{50} = 0.62 mm, S_0 = 0.00249, Q_0 = 0.0079 m^3/s)

Section	y_s (m)	Rh_s (m)	Q_s (m^3/s)	u_s (m/s)	V_s (m/s)	F_s	Sf_s	τ_s (N/m^2)	u_s^*	$R*$	Ω_s (N/s)
10	0.071	0.055	0.006	0.194	0.000411	0.263	0.00077	0.414	0.020	15.102	0.048
9.5	0.068	0.054	0.006	0.196	0.000412	0.271	0.00079	0.414	0.020	15.109	0.049
9	0.066	0.053	0.006	0.197	0.000414	0.274	0.00080	0.412	0.020	15.070	0.048
8.5	0.064	0.052	0.006	0.193	0.000406	0.271	0.00080	0.402	0.020	14.885	0.047
8	0.061	0.050	0.006	0.198	0.000412	0.282	0.00083	0.406	0.020	14.957	0.048
7.5	0.061	0.049	0.006	0.196	0.000412	0.281	0.00082	0.399	0.020	14.838	0.047
7	0.061	0.048	0.006	0.201	0.000422	0.292	0.00085	0.405	0.020	14.942	0.048
6.5	0.059	0.047	0.006	0.201	0.000422	0.296	0.00087	0.401	0.020	14.874	0.047
6	0.058	0.047	0.005	0.205	0.000434	0.304	0.00090	0.409	0.020	15.009	0.048
5.5	0.058	0.045	0.005	0.206	0.000433	0.309	0.00091	0.402	0.020	14.887	0.047
5	0.054	0.043	0.005	0.209	0.000429	0.321	0.00095	0.400	0.020	14.846	0.048

TABLE 2.54: Case: No seepage shape 60 (d_{50} = 0.62 mm, S_0 = 0.00249, Q_0 = 0.0104 m^3/s)

Section	y_0 (m)	Rh_0 (m)	u_0 (m/s)	F_0	Sf_0	τ_0 (N/m^2)	u_0^*	$R*$	Ω_s (N/s)
10	0.121	0.070	0.225	0.271	0.00041	0.285	0.017	12.764	0.042
9.5	0.122	0.071	0.221	0.265	0.00041	0.284	0.017	12.736	0.042
9	0.121	0.070	0.226	0.273	0.00042	0.286	0.017	12.799	0.042
8.5	0.123	0.072	0.219	0.261	0.00040	0.283	0.017	12.724	0.041
8	0.123	0.071	0.222	0.266	0.00041	0.284	0.017	12.742	0.042
7.5	0.121	0.071	0.223	0.267	0.00041	0.285	0.017	12.773	0.042
7	0.123	0.072	0.220	0.261	0.00040	0.284	0.017	12.752	0.041
6.5	0.122	0.071	0.222	0.265	0.00041	0.285	0.017	12.768	0.042
6	0.119	0.068	0.231	0.282	0.00043	0.287	0.017	12.815	0.044
5.5	0.123	0.071	0.221	0.265	0.00041	0.284	0.017	12.738	0.042
5	0.122	0.071	0.222	0.266	0.00041	0.285	0.017	12.772	0.042

TABLE 2.55: Case: Seepage shape 60 (d_{50} = 0.62 mm, S_0 = 0.00249, Q_0 = 0.0104 m^3/s)

Section	y_s (m)	Rh_s (m)	Q_s (m^3/s)	u_s (m/s)	V_s (m/s)	F_s	Sf_s	τ_s (N/m^2)	u_s^*	$R*$	Ω_s (N/s)
10	0.082	0.061	0.009	0.214	0.000383	0.277	0.00070	0.418	0.020	15.541	0.061
9.5	0.083	0.059	0.009	0.217	0.000384	0.284	0.00071	0.413	0.020	15.436	0.061
9	0.078	0.059	0.009	0.219	0.000389	0.288	0.00073	0.422	0.021	15.615	0.062
8.5	0.079	0.058	0.008	0.222	0.000393	0.296	0.00074	0.420	0.020	15.575	0.062
8	0.078	0.057	0.008	0.219	0.000393	0.292	0.00074	0.417	0.020	15.513	0.060
7.5	0.076	0.057	0.008	0.217	0.000395	0.289	0.00074	0.416	0.020	15.506	0.059
7	0.074	0.056	0.008	0.218	0.000393	0.295	0.00076	0.414	0.020	15.462	0.060
6.5	0.070	0.054	0.008	0.223	0.000397	0.305	0.00079	0.419	0.020	15.561	0.061
6	0.070	0.053	0.008	0.222	0.000396	0.307	0.00079	0.414	0.020	15.455	0.060
5.5	0.068	0.052	0.008	0.221	0.000389	0.310	0.00080	0.406	0.020	15.304	0.060
5	0.063	0.050	0.008	0.233	0.000404	0.332	0.00087	0.429	0.021	15.745	0.064

TABLE 2.56: Case: No seepage shape 70 (d_{50} = 0.62 mm, S_0 = 0.00249, Q_0 = 0.0165 m^3/s)

Section	y_0 (m)	Rh_0 (m)	u_0 (m/s)	F_0	Sf_0	τ_0 (N/m^2)	u_0^*	$R*$	Ω_s (N/s)
10	0.142	0.083	0.258	0.285	0.00035	0.290	0.017	12.932	0.057
9.5	0.142	0.083	0.260	0.288	0.00036	0.291	0.017	12.962	0.058
9	0.142	0.082	0.260	0.289	0.00036	0.290	0.017	12.943	0.058
8.5	0.140	0.082	0.262	0.291	0.00036	0.292	0.017	12.992	0.059
8	0.141	0.083	0.260	0.289	0.00036	0.291	0.017	12.969	0.058
7.5	0.141	0.082	0.261	0.290	0.00036	0.292	0.017	12.981	0.058
7	0.141	0.081	0.260	0.292	0.00036	0.288	0.017	12.897	0.059
6.5	0.141	0.084	0.257	0.283	0.00035	0.289	0.017	12.908	0.057
6	0.140	0.082	0.262	0.291	0.00036	0.292	0.017	12.993	0.059
5.5	0.140	0.082	0.260	0.289	0.00036	0.290	0.017	12.943	0.058
5	0.142	0.084	0.255	0.282	0.00035	0.287	0.017	12.866	0.057

TABLE 2.57: Case: Seepage shape 70 (d_{50} = 0.62 mm, S_0 = 0.00249, Q_0 = 0.0165 m^3/s)

Section	y_s (m)	Rh_s (m)	Q_s (m^3/s)	u_s (m/s)	V_s (m/s)	F_s	Sf_s	τ_s (N/m^2)	u_s^*	$R*$	Ω_s (N/s)
10	0.112	0.075	0.015	0.254	0.000403	0.296	0.00059	0.433	0.021	15.820	0.084
9.5	0.107	0.073	0.014	0.261	0.000407	0.309	0.00062	0.445	0.021	16.028	0.088
9	0.101	0.071	0.014	0.260	0.000400	0.312	0.00063	0.442	0.021	15.978	0.089
8.5	0.096	0.070	0.014	0.267	0.000407	0.323	0.00067	0.460	0.021	16.293	0.093
8	0.093	0.068	0.014	0.269	0.000404	0.329	0.00069	0.459	0.021	16.279	0.094
7.5	0.091	0.067	0.014	0.274	0.000411	0.338	0.00072	0.472	0.022	16.505	0.097
7	0.088	0.065	0.014	0.276	0.000408	0.345	0.00073	0.472	0.022	16.505	0.099
6.5	0.090	0.064	0.014	0.274	0.000399	0.346	0.00072	0.453	0.021	16.167	0.096
6	0.096	0.063	0.013	0.280	0.000407	0.357	0.00074	0.454	0.021	16.192	0.097
5.5	0.094	0.062	0.013	0.272	0.000394	0.348	0.00071	0.434	0.021	15.820	0.092
5	0.141	0.084	0.013	0.200	0.000395	0.220	0.00043	0.350	0.019	14.224	0.055

Chapter 3

Cross-Sectional Profile of Stable Alluvial Channels With Seepage

The accurate determination of the geometry of an alluvial channel whose boundary is composed of particles that are all on the verge of motion is very important in the design of unlined irrigation canals and canalization schemes. The approach of Glover and Florey (1951) is one of the first methods employed to obtain the shape of this stable channel. Their resulting channel had a continuously curving boundary, which they described with a cosine function, however does not provide satisfactory results in field condition (Diplas, 1990). Parker (1978) resolution of "stable channel paradox" by considering a cross-section with a flat-bed region with two curving banks. For this shape, over the flat-bed region, fluid stresses can be above its critical value and below critical over the bank region. Thus, allowing the sediment transport over the flat-bed region and maintaining the banks stable. Parker (1978) derived the geometry of threshold channel taking into account the effect of lateral momentum-diffusion from the center of the channel towards the banks and the derived profile was different from the cosine shape. Diplas and Vigilar (1992) described the cross-sectional profile of a channel by a fifth order polynomial by numerically solving the momentum-diffusion equation in combination with the force balance equation proposed by Ikeda (1982). According to them, fluid shear stresses are higher than its critical value over the bed for a stable

channel. The fifth order polynomial proposed by Diplas and Vigilar (1992):

$$D^* = C_5 y^{*5} + C_4 y^{*4} + C_2 y^{*2} + 1 \tag{3.1}$$

where $D^* = y_{local}/y_c$, $y^* = y_L/y_c$ and expressions for C_2, C_4, and C_5 were given numerically.

It has been observed (Kellerhals, 1967; Parker, 1978) that sediment is transported in natural channels along the bed as well as in suspension. It can be considered that most of the natural rivers and channels cannot be represented satisfactorily by the concept of threshold channels because according to the concept of threshold channels, the particles on the entire perimeter are on the verge of motion, not actually in the state of motion. So, the continuously curving shape of threshold channel is incompatible with the sediment transport as has been observed among others by Wolman and Brush Jr (1961) and Stebbings (1963) that in laboratory flumes, stable channels are capable of transporting sediment. Ikeda (1981) suggested an exponential function to describe the bank profile:

$$\frac{y_{local}}{y_C} = 1 - \exp\left(-\frac{y_T}{K}\right) \tag{3.2}$$

$$K = y_C \left[1 - \exp\left(-B/2y_C\right)\right] \tag{3.3}$$

$$y_T = B/2 - y_L \tag{3.4}$$

where:

y_L : is the lateral horizontal distance from the center of the channel.

y_T : is the lateral distance from the water margin.

y_{local} : is the local vertical channel depth.

y_C : is the centre line depth of the channel.

K : is displacement thickness.

B : is the channel width.

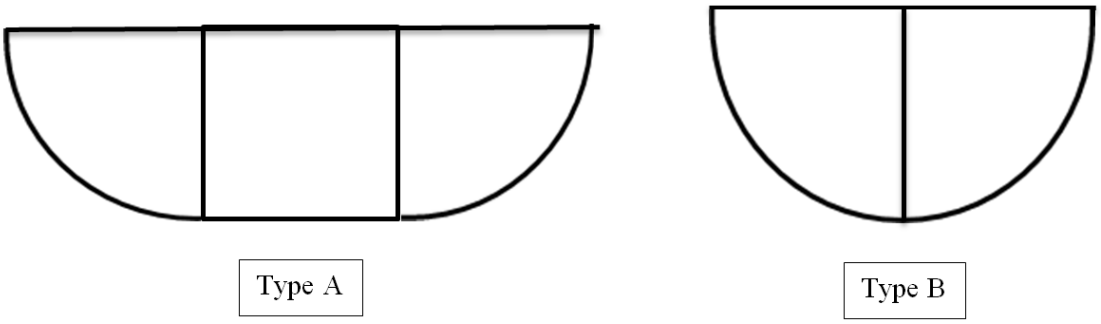

FIGURE 3.1: Two different shapes for stable channels Cao and Knight (1997)

Diplas (1990) employed a normal-depth method for the approximation of the bank profile. The whole bank profile has been described by an exponential function similar to the one proposed by Ikeda (1981):

$$\frac{y_{local}}{y_C} = 1 - \exp\left(-\frac{y_T}{y_C}\right) \tag{3.5}$$

Diplas (1990) further argued that the exponential function proposed by Ikeda (1981) cannot be used as a design tool because calculation of K requires prior knowledge of bank profile. Cao and Knight (1997) in their work considered two different shapes for stable channels: One with curved banks and flat-bed with constant depth (Type-A) and the other with two curved banks only (Type-B) (Figure 3.1).

Type-B cross-section has been considered as a threshold channel where all the particles on the bank profile are at a state of threshold of motion and by using the entropy-maximization principle and the calculus of variations, a general formula for the lateral distribution of transverse slopes has been derived for threshold channels. The bank profile equation proposed by Cao and Knight (1997):

$$z = \frac{1}{\lambda}\left(\frac{1 + 2\beta y_L/B}{2\beta/B}\ln\left(1 + 2\beta y_L/B\right) - y_L\right) \tag{3.6}$$

where $\beta = \exp(\lambda\mu) - 1$, z is channel boundary elevation, $B/2$ is semi-width, μ is the submerged static coefficient of Coulomb friction, y_L is the lateral distance, and λ is Lagrange multiplier. Lateral distribution of the local depth h_{local} was given

as:

$$h_{local} = \frac{1}{\beta\lambda}\left(\lambda\mu B e^{\lambda\mu}/2 \; + \frac{B}{2}\left(1 + 2\beta y_L/B\;\right) - \beta\left(\frac{B - y_L}{2}\right)\right) \tag{3.7}$$

The equations for bank profile and local depth proposed by Cao and Knight (1997) are dependent on the behavior of the Lagrange multiplier λ. Another solution for the stable channel paradox has been proposed by Cao and Knight (1998) which is based on the analytical solution of the depth-mean-averaged momentum equation (Shiono and Knight, 1991) by considering the contribution of secondary currents in lateral transfer of stream-wise momentum. Cao and Knight (1998) considered the channel cross-section similar to Type A cross-section of Cao and Knight (1997) and proposed a geometric model by coupling entropy based bank profile and center bed depth equations. Dimensionless equations for the bank hydraulic geometry were:

$$z_b^* = \left\{\left[\mu(y_L - b/2\;)^*\right]^2\right\}/4 \tag{3.8}$$

$$H_b^* = 1 - \left\{\left[\mu(y_L - b/2\;)^*\right]^2\right\}/4 \tag{3.9}$$

where: $z_b^* = z_b/y_C$, $H_b^* = y_{local}\,(y_L)/y_C$, $(y_L - b/2\;)^* = (y_L - b/2\;)/y_C$, b is the width of the flat-bed region, y_{local} is the depth of the bank zone, y_C is the centreline depth the channel, and y_L is the lateral coordinate.

3.1 Changes in Profile Parameters with Downward Seepage

During the no seepage experiments various parameters like channel perimeter, hydraulic radius and top width were fairly constant along the channel reach, but variation in these parameters has been observed for the channel when seepage in the downward direction was applied to the channel. Figure 3.2, Figure 3.3,

and Figure 3.4 show the variation in channel perimeter, hydraulic radius and top width respectively, along the length of the channel after no seepage and seepage experiments for shape 50.

It can be observed that there is no variation in channel perimeter and top width for no seepage experiment and as the entire channel is at the condition of incipient motion, no erosion takes place during the experiment. But for seepage experiment, bed shear stress becomes higher than its critical value which causes more erosion at the upstream side and hence the channel perimeter and top width become higher as compared to the no seepage experiment. As the water loses its kinetic energy along the length of channel towards downstream, the rate of erosion falls down and as a result of this, the channel perimeter and top width also decrease towards downstream.

It can be noticed that the hydraulic radius is fairly constant along the length of the channel for no seepage experiment and it decreases towards downstream in the case of seepage experiment. The decrease in hydraulic radius along the length of the channel in the downstream direction for seepage experiment can be explained as the bed material that was eroded from upstream was carried along and finally deposited by the flow as the available stream power decreased. Figure 3.5, Figure 3.6, and Figure 3.7 show the similar trend of variation in channel perimeter, hydraulic radius and top width for shape 70. It is interesting to observe that the similar trend of variation in the profile parameters has been witnessed when the experiments were carried out on the sand of median diameter 0.62 mm and have been depicted in Figure 3.8 to Figure 3.13 for shape 50 and 70, respectively.

3.2 Channel Shape Parameter

Deng et al. (2001) proposed a relation for the variation of dimensionless depth in a channel cross-section:

$$\frac{y_{local}}{y_C} = 1 - \left(\frac{y_L}{b}\right)^{\beta} \tag{3.10}$$

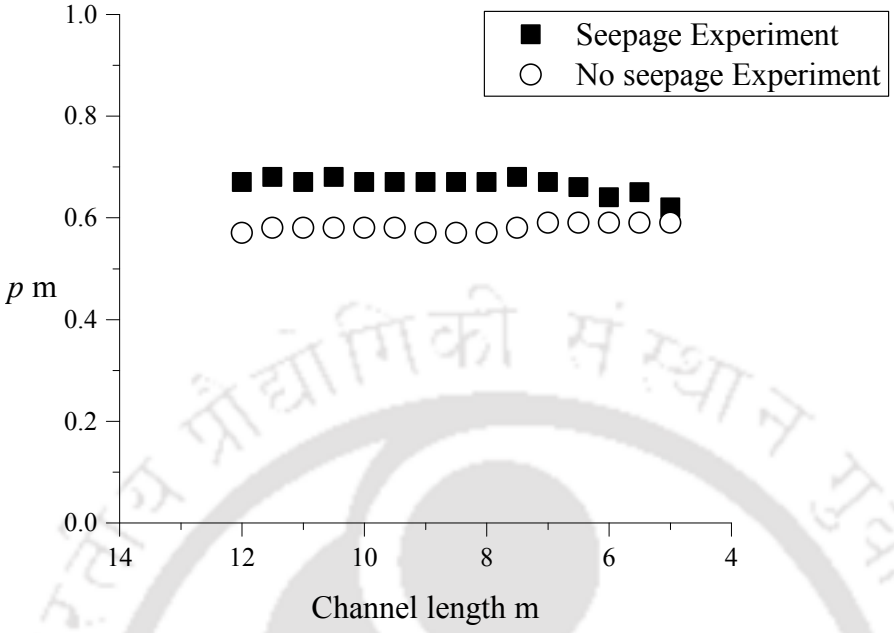

FIGURE 3.2: Variation in perimeter for shape 50 (d_{50} = 1.1 mm)

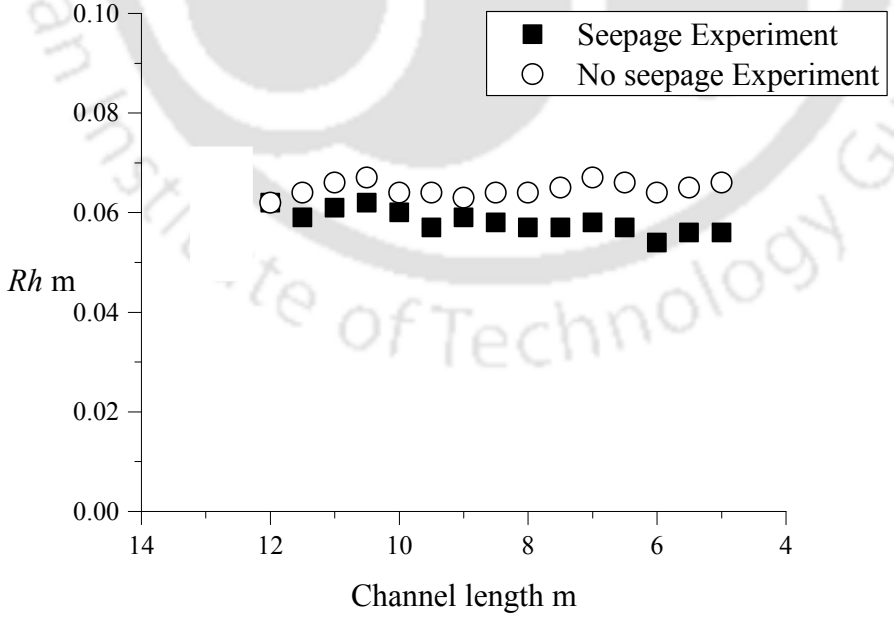

FIGURE 3.3: Variation in hydraulic radius for shape 50 (d_{50} = 1.1 mm)

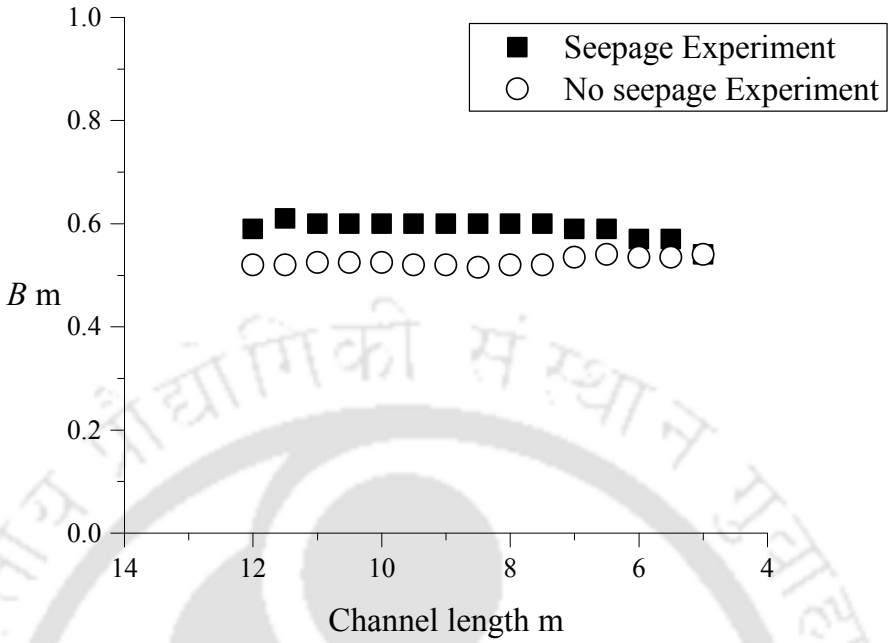

FIGURE 3.4: Variation in top width for shape 50 (d_{50} = 1.1 mm)

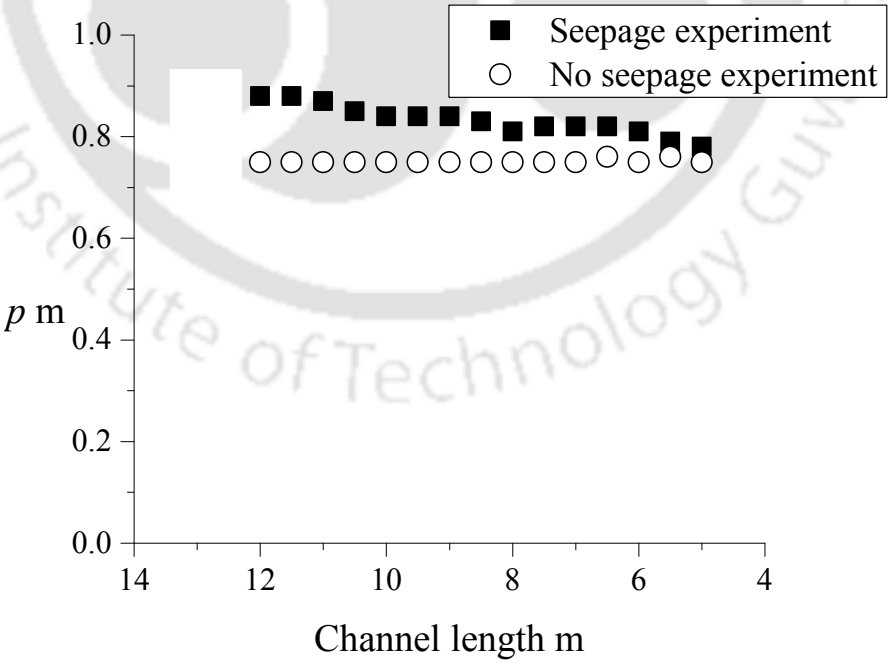

FIGURE 3.5: Variation in perimeter for shape 70 (d_{50} = 1.1 mm)

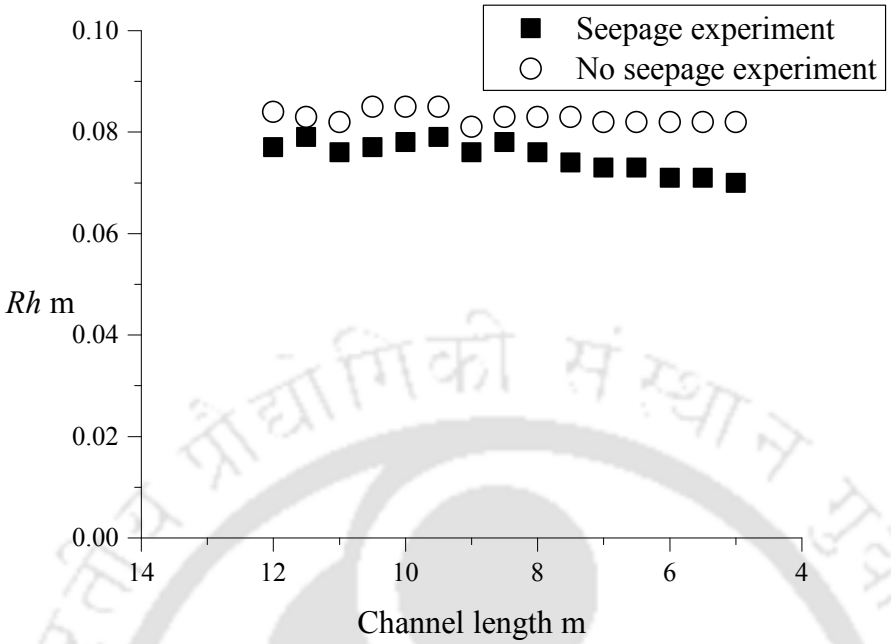

FIGURE 3.6: Variation in hydraulic radius for shape 70 (d_{50} = 1.1 mm)

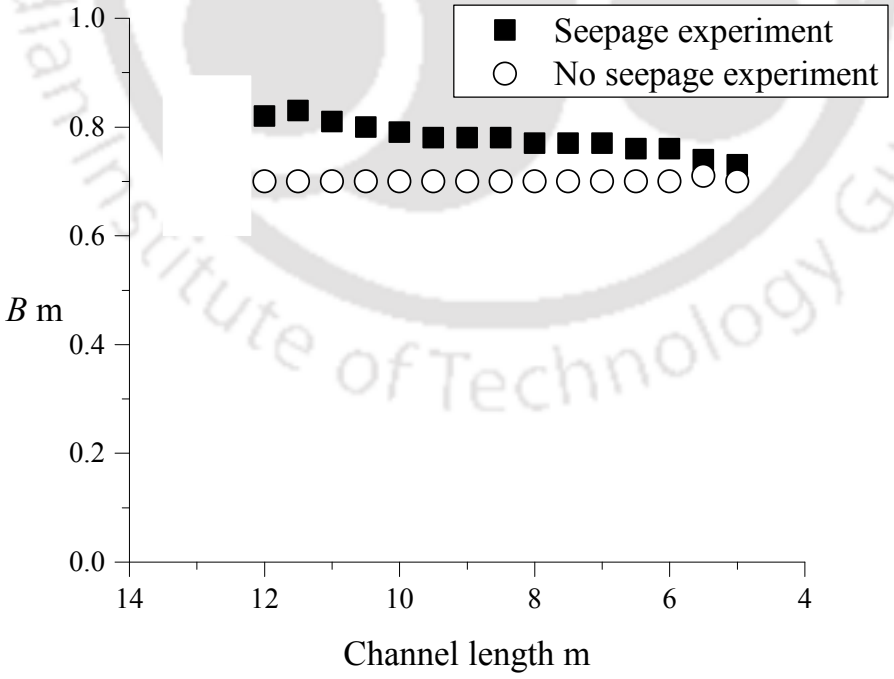

FIGURE 3.7: Variation in top width for shape 70 (d_{50} = 1.1 mm)

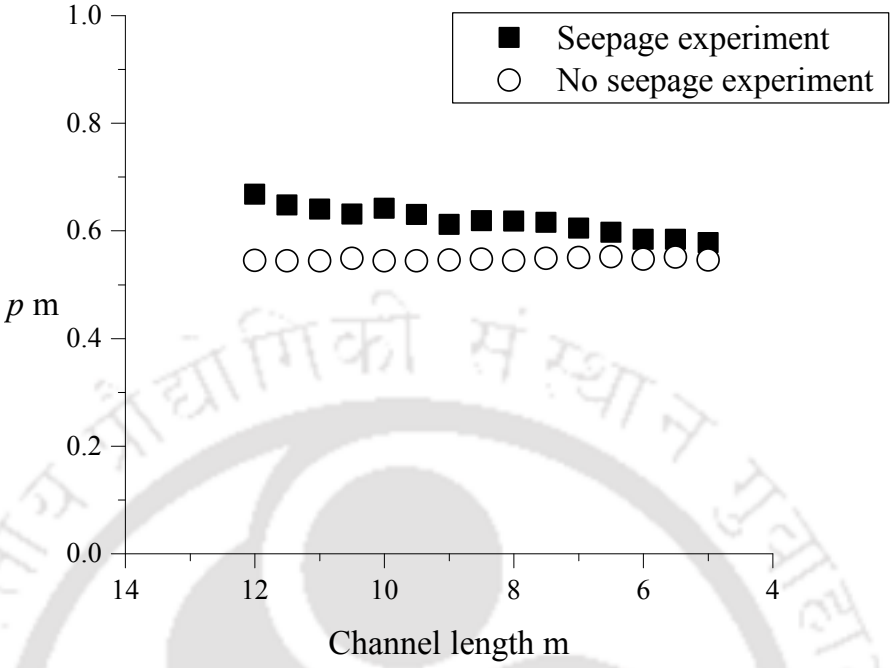

FIGURE 3.8: Variation in perimeter for shape 50 ($d_{50} = 0.62$ mm)

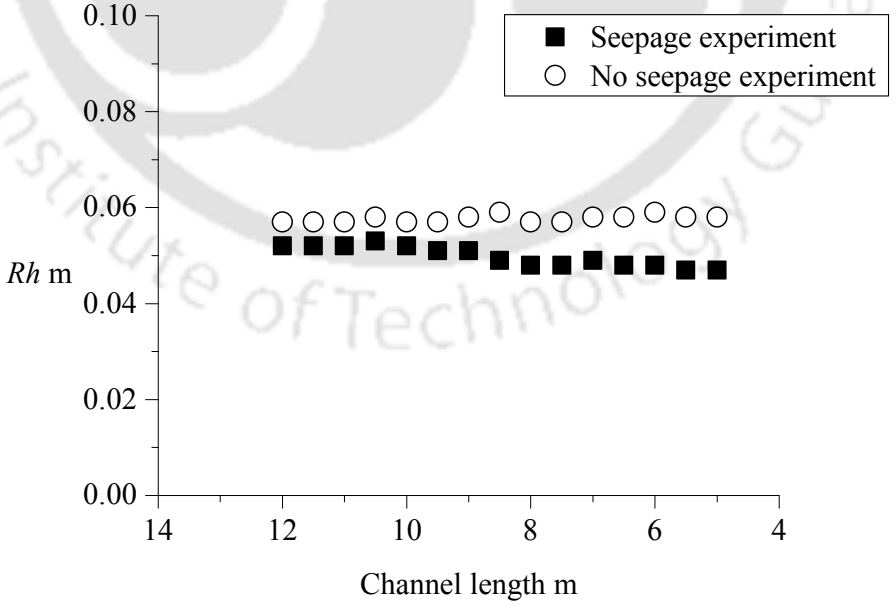

FIGURE 3.9: Variation in hydraulic radius for shape 50 ($d_{50} = 0.62$ mm)

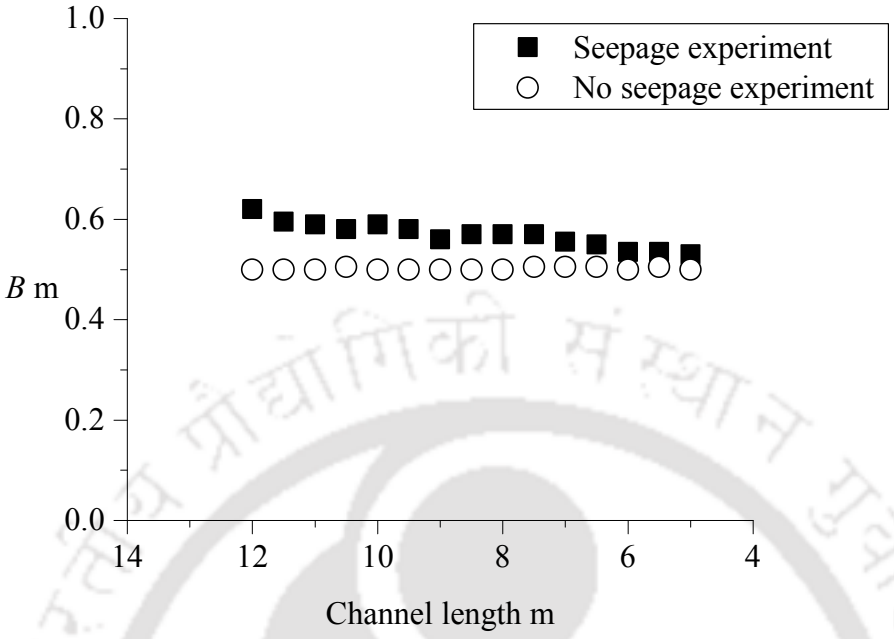

FIGURE 3.10: Variation in top width for shape 50 ($d_{50} = 0.62$ mm)

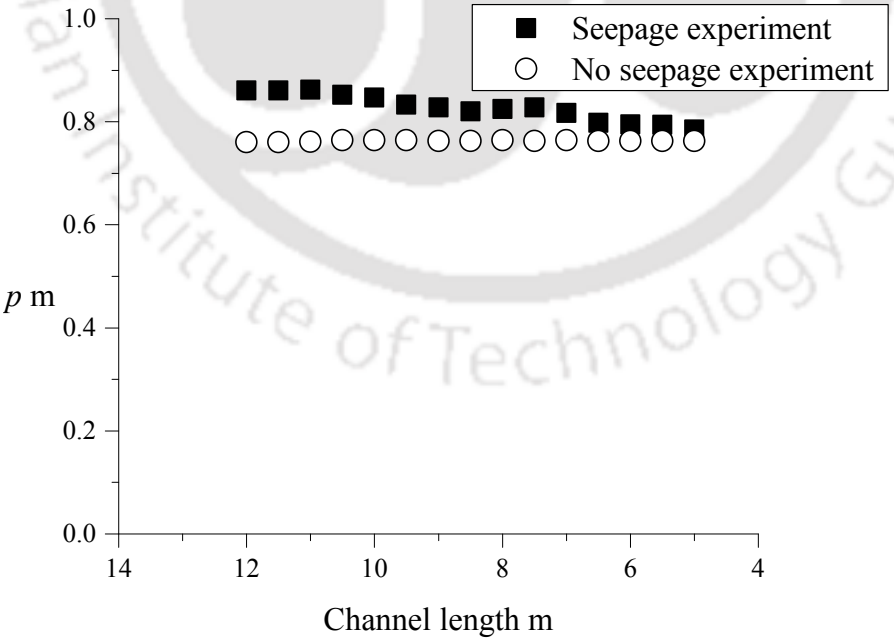

FIGURE 3.11: Variation in perimeter for shape 70 ($d_{50} = 0.62$ mm)

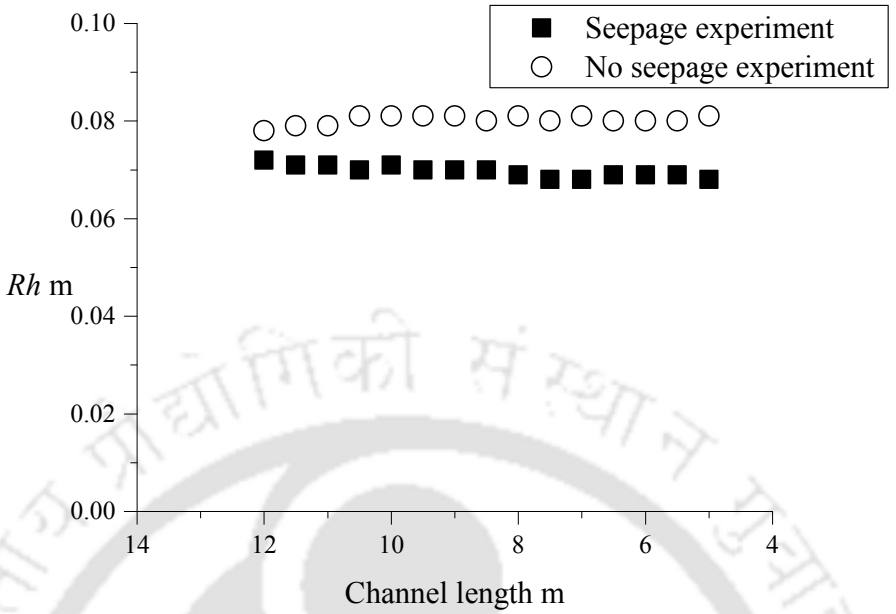

FIGURE 3.12: Variation in hydraulic radius for shape 70 (d_{50} = 0.62 mm)

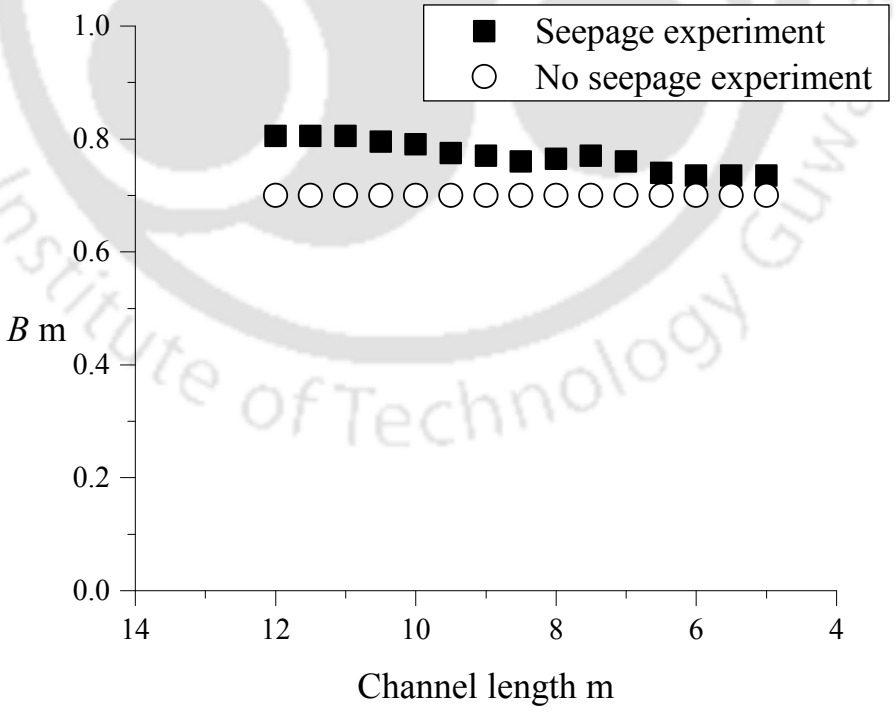

FIGURE 3.13: Variation in top width for shape 70 (d_{50} = 0.62 mm)

where, y_L is the lateral distance with $y = 0$ at the channel center, y_{local} is the local depth, b is the half width of the channel, β is the channel shape parameter, and y_C is the depth at channel centerline. Deng et al. (2001) argued that for straight stable rivers β is generally greater than 2. It has been established by Deng et al. (2001) that a mathematical relation exists between the channel shape parameter and width to depth ratio of the channel which can be expressed as:

$$\beta = \ln\left(\frac{B}{y}\right) \tag{3.11}$$

It can be observed that Equation (3.11) together with Equation (3.10) provide useful information regarding the cross-sectional shape of the channel. Equation (3.10) represents triangular shaped channel for $\beta = 1$, parabolic shaped channel for $\beta = 2$, an approximately natural channel shape with flat bed and curved banks for $\beta > 2$, and rectangular shape for $\beta = \infty$. Schematic diagram for Equation (3.10) is presented in Figure 3.14. For the present study, the values of β have been computed (Table 3.1) for the channel cross-sections which have been obtained after seepage experiments.

It is interesting to observe that the value of β is greater than 2 for all the shapes on both the sands that have been used in the present experiments which suggest that the channel profile obtained after each and every seepage experiment renders an approximately natural channel shape with flat bed and curved banks.

TABLE 3.1: Average values of β for various shapes and bed slopes

Sand size d_{50} mm	Slope	β		
		Shape 50	Shape 60	Shape 70
1.1	0.00116	2.31	2.31	2.21
	0.00176	2.32	2.36	2.25
	0.00249	2.57	2.49	2.49
0.62	0.00116	2.2	2.02	2.09
	0.00176	2.4	2.2	2.2
	0.00249	2.41	2.41	2.3

Further, it can also be observed that the average value of β, along the test reach for all shapes used in the experiments, increases with the increase in bed slope. Snapshot of experimental channel after no seepage and seepage experiments has been shown in Figure 3.15. Channel cross-sectional profiles obtained after no seepage and seepage experiments are shown in Figure 3.16 and Figure 3.17 for various shapes on both the sands used in this study.

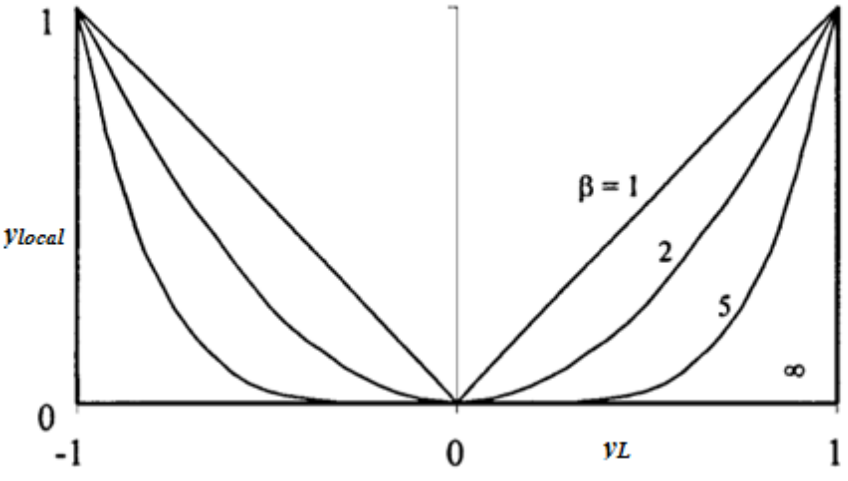

FIGURE 3.14: Cross-sectional shapes for different values of β (Deng et al., 2001)

FIGURE 3.15: Snapshot of the channel after (A) no seepage experiment and (B) seepage experiment

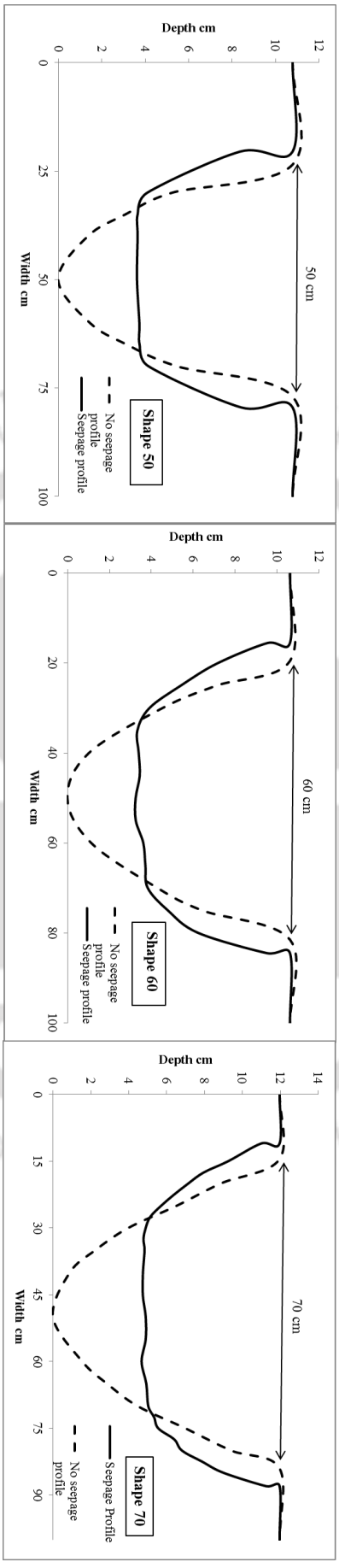

FIGURE 3.16: Cross-sectional profiles for various shapes after no seepage and seepage experiments at 7 m from downstream end (d_{50} = 1.1 mm)

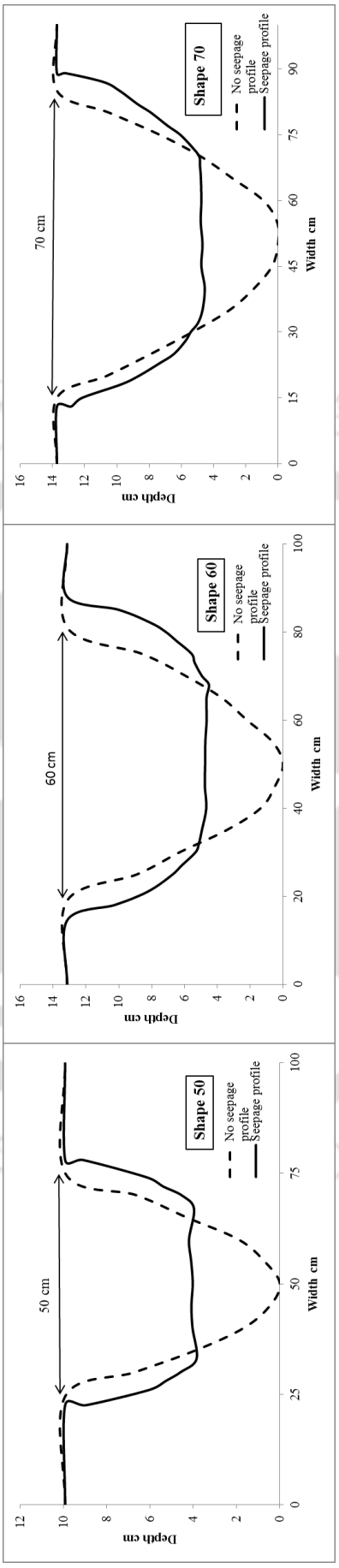

FIGURE 3.17: Cross-sectional profiles for various shapes after no seepage and seepage experiments at 7 m from downstream end (d_{50} = 0.62 mm)

3.3 Cross-sectional Profile of the Channel Bank with Downward Seepage

It has also been observed that the value of shape factor β came out to be greater than 2 for entire seepage experiments, indicating the shape of natural channels with flat-bed and two curving banks. The variation of the present profiles from existing predictors (Parker, 1978; Diplas, 1990; Pizzuto, 1990; Diplas and Vigilar, 1992; Cao and Knight, 1998) can be attributed to the seepage applied in the experiments. Based on experimentations on the sand of median diameter 1.1, an empirical equation has been developed for a stable alluvial channel affected by seepage as follows:

$$y* = 1 - \exp(a\mu x*^{b}) \tag{3.12}$$

where,$y^* = y_{local}/y_C$; y is vertical channel depth, y_C is central depth, $x^* = (\frac{B}{2}x)/y_C$; B is channel top width, x is lateral horizontal distance from the center of the channel, $\mu = tan\phi$. Value of μ for the present study, is in good agreement of the empirical relationship proposed by Yu et al. (1998). Definition sketch of channel cross-section for Equation (3.12) has been shown in Figure 3.18. Non-dimensional bank profiles obtained after the seepage experiments for shape 70, shape 60, and shape 50 on the sand of median diameter 0.62 mm have been predicted using Equation (3.12) which has been found to be in a very good agreement of the experimental data. Experimental bank profiles for shape 70, shape 60, and shape 50 for the sand of median diameter 0.62 mm and empirically generated bank profiles using Equation (3.12) have been shown in Figure 3.19, Figure 3.20, and Figure 3.21, respectively, for the sections at 8 m, 9 m, and 10 m from the downstream end. Comparison among the bank profile from Equation (3.12) for shape 70 and profiles given by Parker (1978), Diplas (1990) ,Pizzuto (1990) and Cao and Knight (1998) has been shown in Figure 3.22 and Figure 3.23 for both the sands (median diameter 0.62 mm and 1.1 mm), from which it is evident that present model takes

better care of the curvature and simulates the experimental bank profile significantly well. In Figure 3.19 to Figure 3.23, only the region of curving banks of stable channel cross-section has been shown and the flat bed region has not been shown. If we look at the Equation (3.12), it can be observed that it is in a close resemblance of the exponential bank profiles suggested by Diplas (1990) and Pizzuto (1990) in which turbulent-diffusion model has been considered.

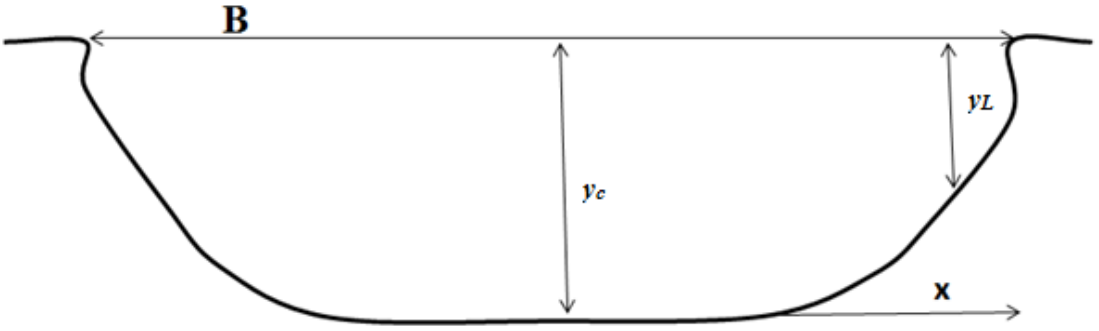

FIGURE 3.18: Definition sketch

However, these exponential bank profiles (Diplas, 1990; Pizzuto, 1990) do not agree with the experimental data from the present study where seepage is applied to the

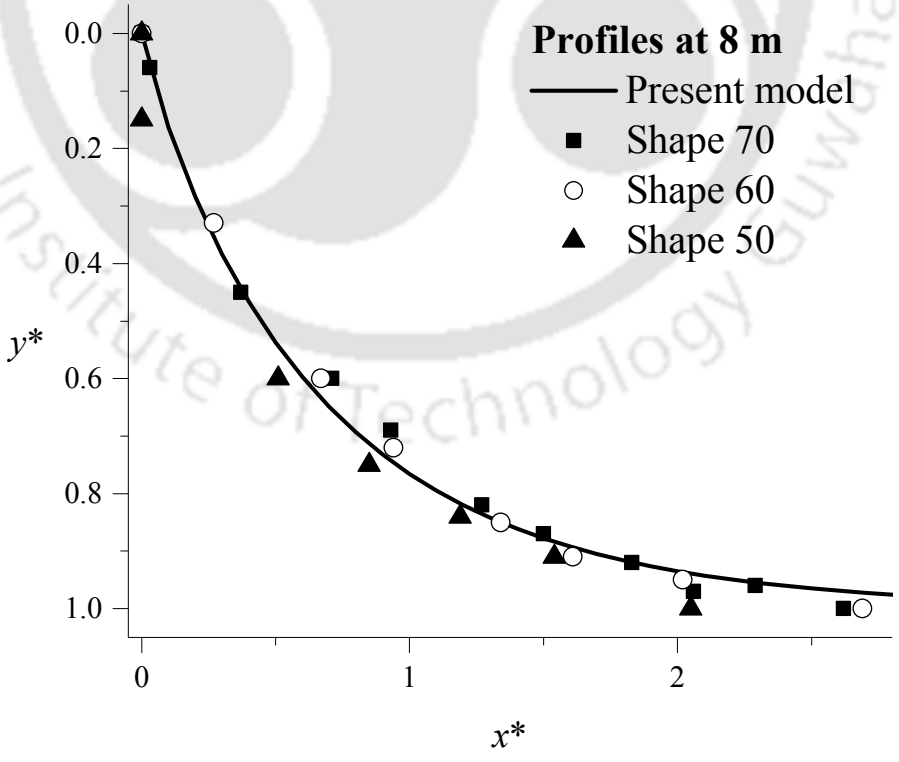

FIGURE 3.19: Non-dimensional bank profiles for section at 8 m

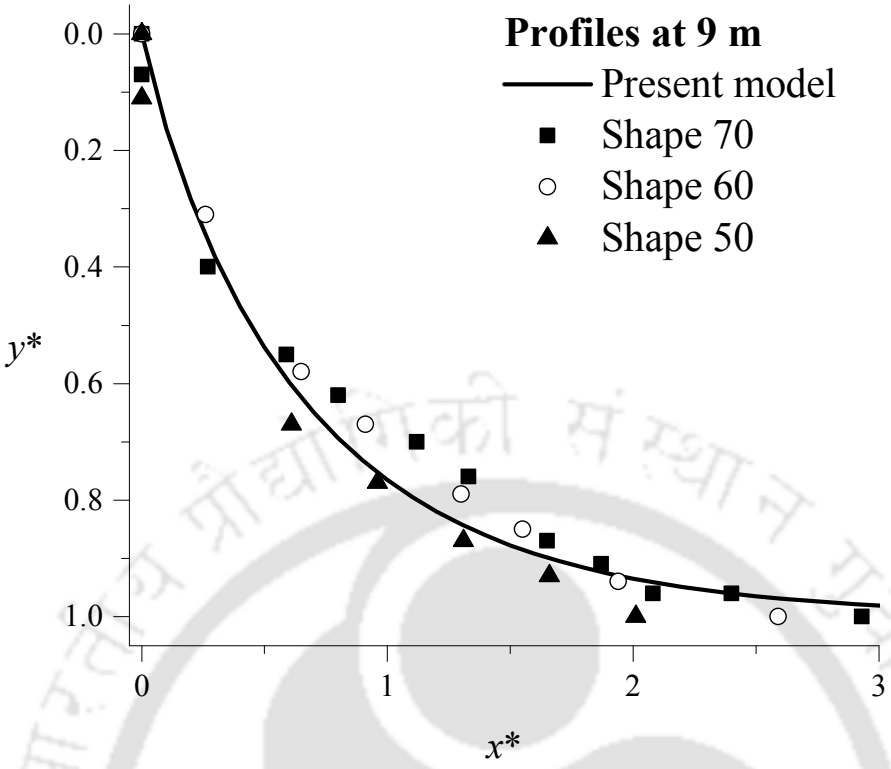

FIGURE 3.20: Non-dimensional bank profiles for section at 9 m

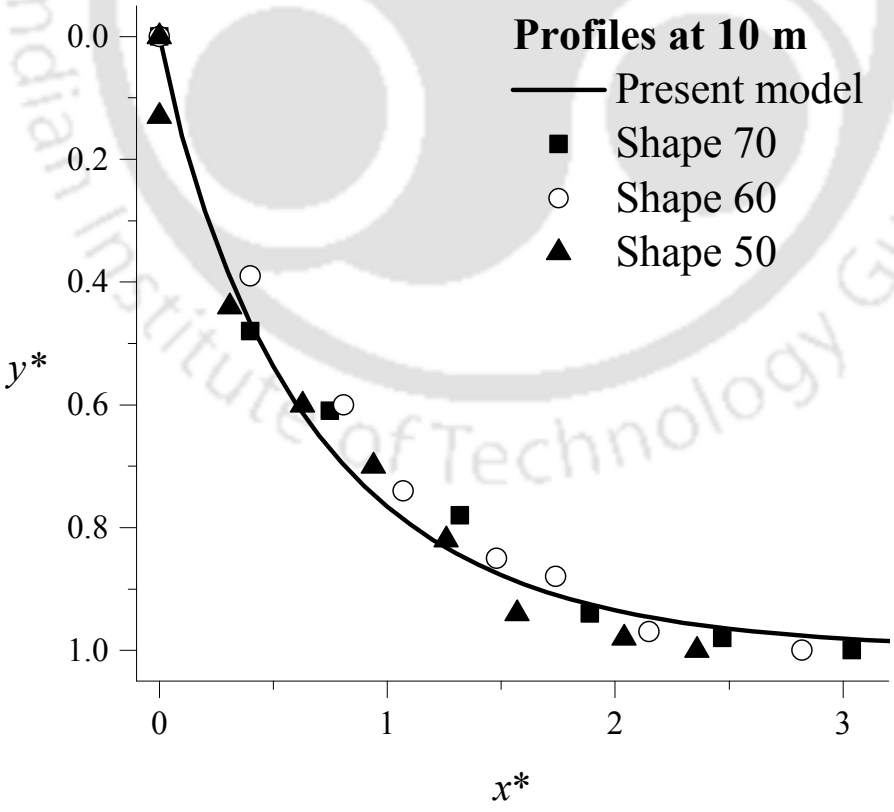

FIGURE 3.21: Non-dimensional bank profiles for section at 10 m

alluvial channel. It is an established fact that seepage affects the hydrodynamics of the alluvial channel and in the present experimental study it has been observed that the bed shear stress and sediment transport rate increased when downward seepage was applied to the alluvial channel which is in agreement of the findings by several researchers (Table 1.1). This necessitates a more realistic model that could represent the seepage affected stable channel bank profile in a good degree of agreement. An empirically generated exponential bank profile given in Equation (3.12) seems to fulfill this requirement as shown in Figure 3.19 - Figure 3.21.

It should be observed that the value of coefficient 'a' and exponent 'b' in Equation (3.12) is unity in the equations for bank profiles given by various authors (Parker, 1978; Diplas, 1990; Pizzuto, 1990; Cao and Knight, 1998). In the present study, where the effect of seepage has been considered on the alluvial channel banks, the values of coefficient and exponent come out to be -2.306 and 0.912 respectively. Standard error associated with the values of 'a' and 'b' is 2.10E-2 and 1.54E-2, respectively. Coefficient of multiple determination (R^2) for Equation (3.12) has been found to be 0.92, which makes the Equation (3.12) a good approximation of cross-sectional bank profiles of stable alluvial channels affected by seepage.

Equation (3.12) has been tested at bank profiles at different cross-sections of the Kankakee River in Momence Wetlands reach, Illinois (Terrio and Nazimek, 1997), bank profile of the Kootenai River at the Tribal Hatchery near Bonners Ferry, ID (Hanson and Lin, 2008) and bank profiles of the River Brahmaputra near Guwahati, and comparison has been made with the bank profiles given by Parker (1978), Diplas (1990), Pizzuto (1990) and Cao and Knight (1998).

Bed material is predominantly fine to medium sand, measuring 0.1 to 0.4 mm in diameter and has less than 5 percent silt and clay. It is evident from Figure 3.24 to Figure 3.30 that Equation (3.12) generated from present study predicts the bank profiles of natural rivers significantly well. The value of μ for predicting bank profiles of natural alluvial river has been taken as suggested by Cao and Knight (1998).

Although it has been observed that the prediction of bank profiles of natural rivers at some locations using the model of Cao and Knight (1998) was within acceptable limits but in the model of Cao and Knight (1998), flat bed region at the center has been eliminated and the horizontal coordinate in the lateral direction (x-coordinate) starts from the junction point of flat-bed region and curved bank region.

Thus, the model given by Cao and Knight (1998) does not take into consideration the top width of natural stream. Whereas in the present model (Equation 3.12), horizontal coordinate in the lateral direction (x-coordinate) starts from the center of the cross-section thus, takes into account the central flat-bed region along with top width of the natural stream.

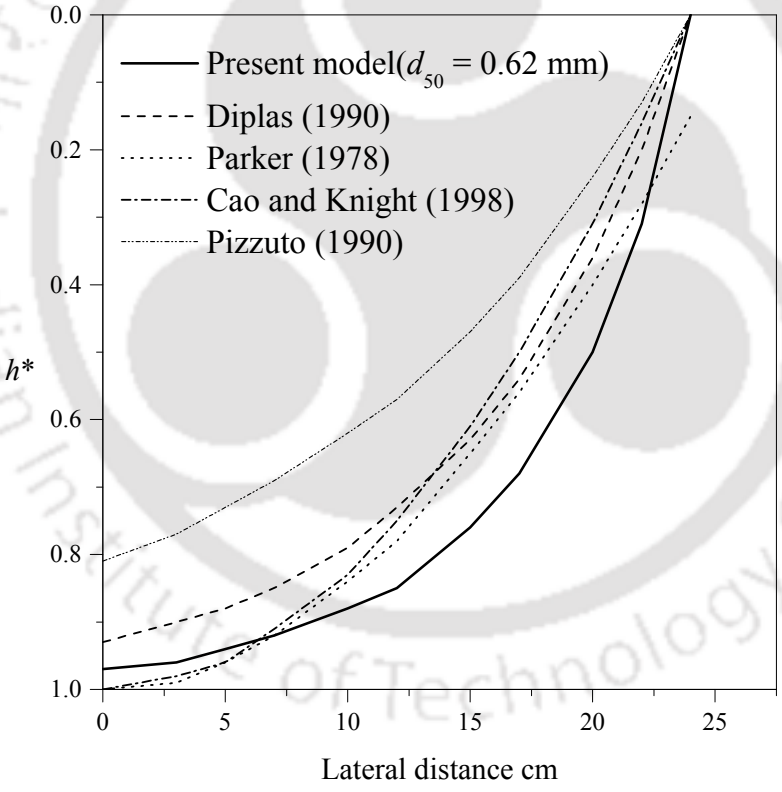

FIGURE 3.22: Comparison among bank profiles for the sand of $d_{50} = 0.62$ mm

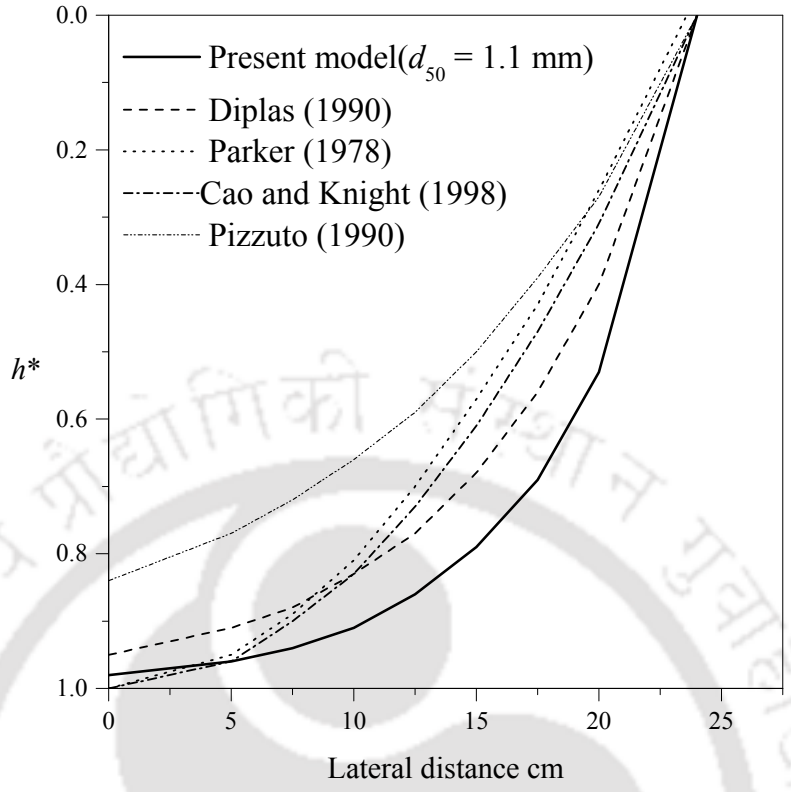

FIGURE 3.23: Comparison among bank profiles for the sand of d_{50} = 1.1 mm

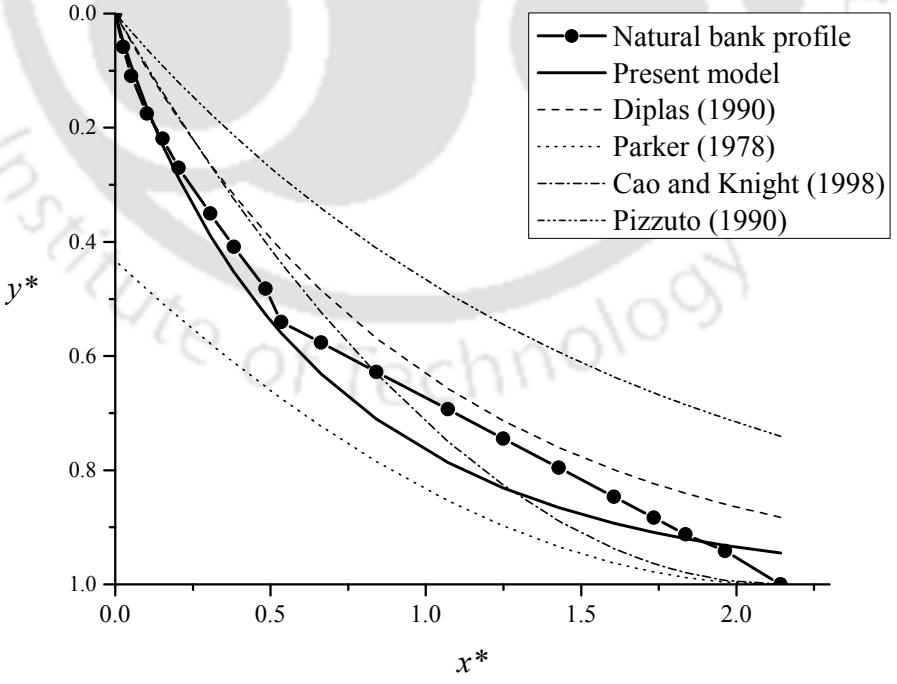

FIGURE 3.24: Bank profile in 1980 at section 9 in the Momence Wetlands reach of the Kankakee River in Illinois (Terrio and Nazimek, 1997)

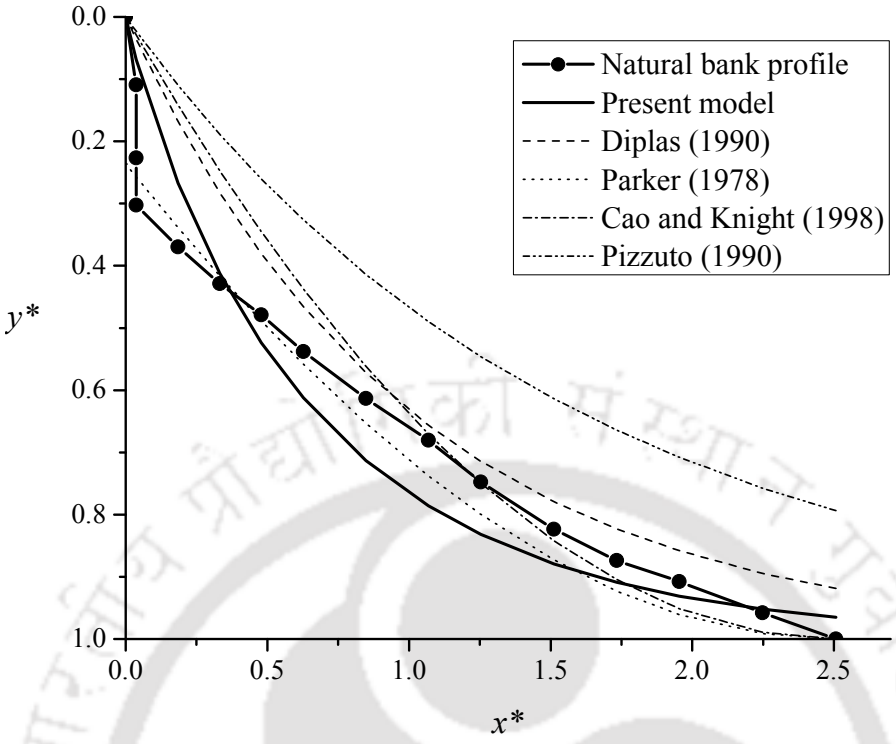

FIGURE 3.25: Bank profile in 1980 at section 39 in the Momence Wetlands reach of the Kankakee River in Illinois (Terrio and Nazimek, 1997)

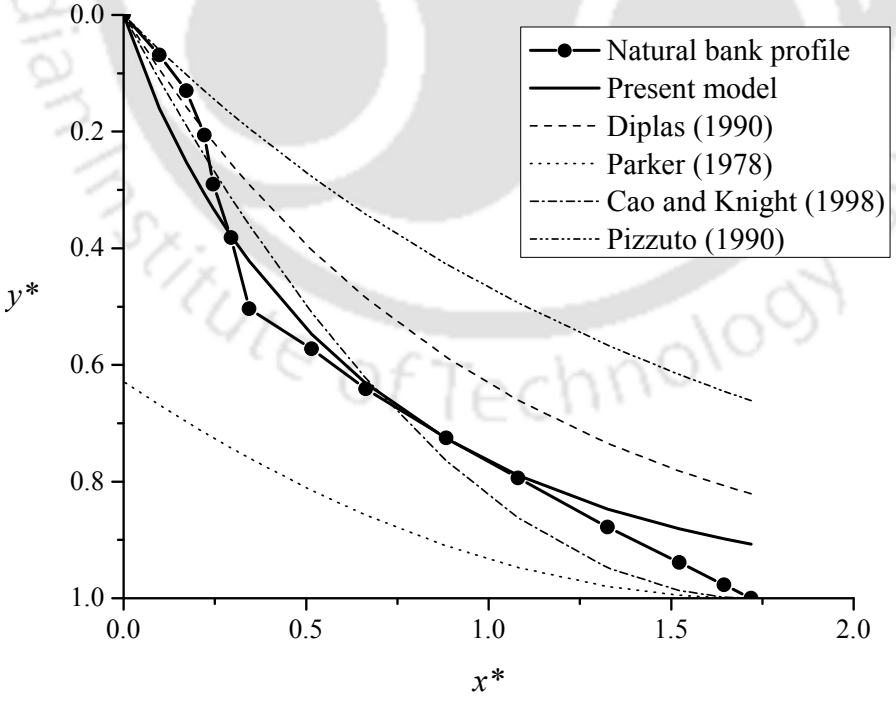

FIGURE 3.26: Bank profile in 1980 at section 53 in the Momence Wetlands reach of the Kankakee River in Illinois (Terrio and Nazimek, 1997)

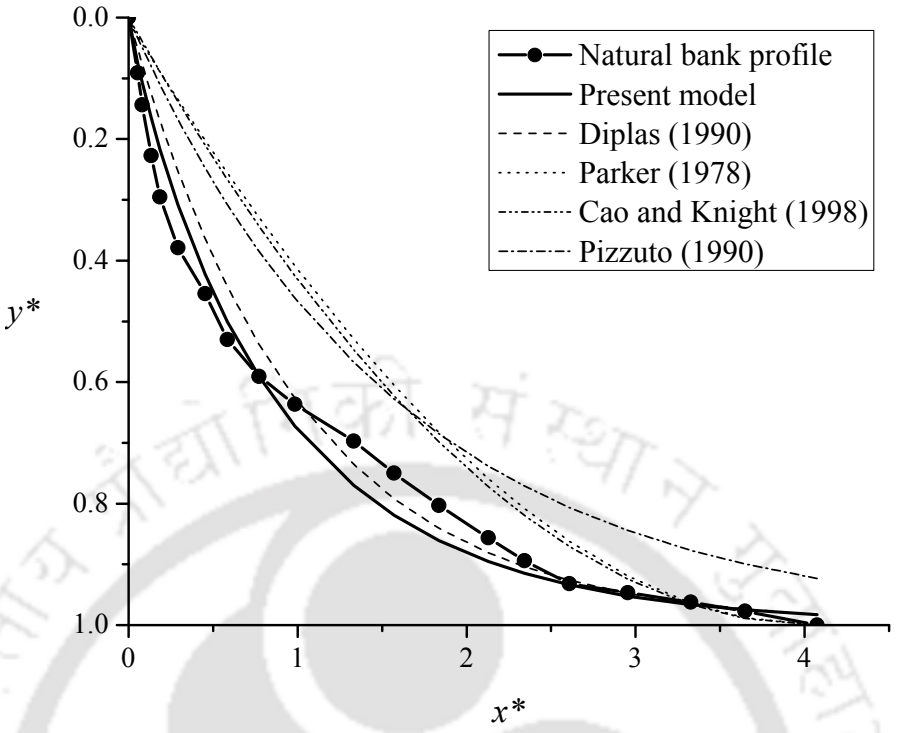

FIGURE 3.27: Bank profile in 1980 at section 65 in the Momence Wetlands reach of the Kankakee River in Illinois (Terrio and Nazimek, 1997)

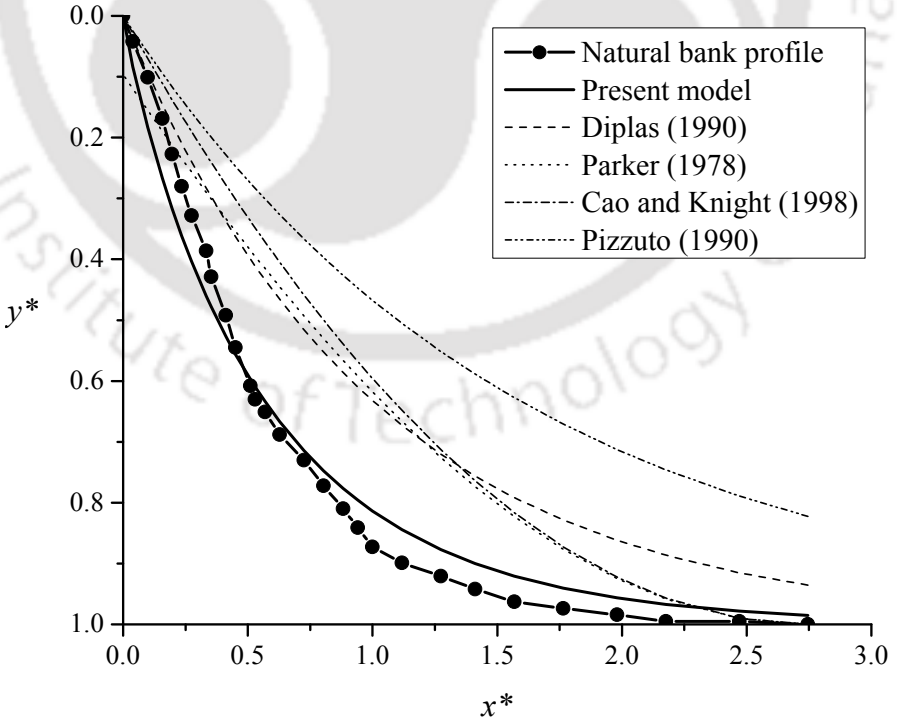

FIGURE 3.28: Bank profile of the Kootenai River at the Tribal Hatchery near Bonners Ferry, ID (Hanson and Lin, 2008)

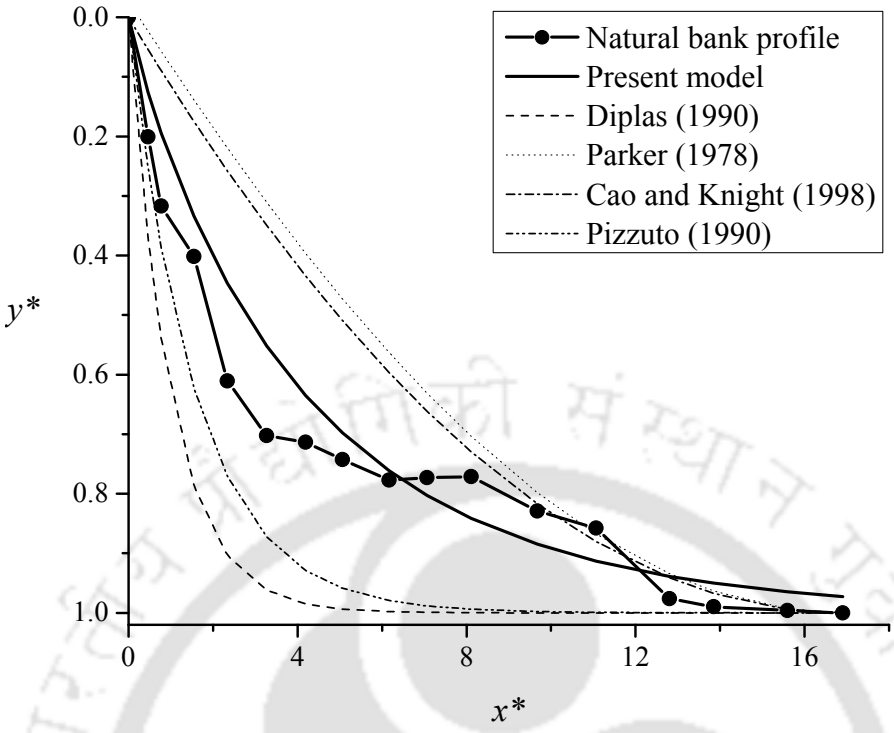

FIGURE 3.29: Bank profile of the Brahmaputra river at chainage 250 m u/s from Saraighat bridge center near Guwahati, India

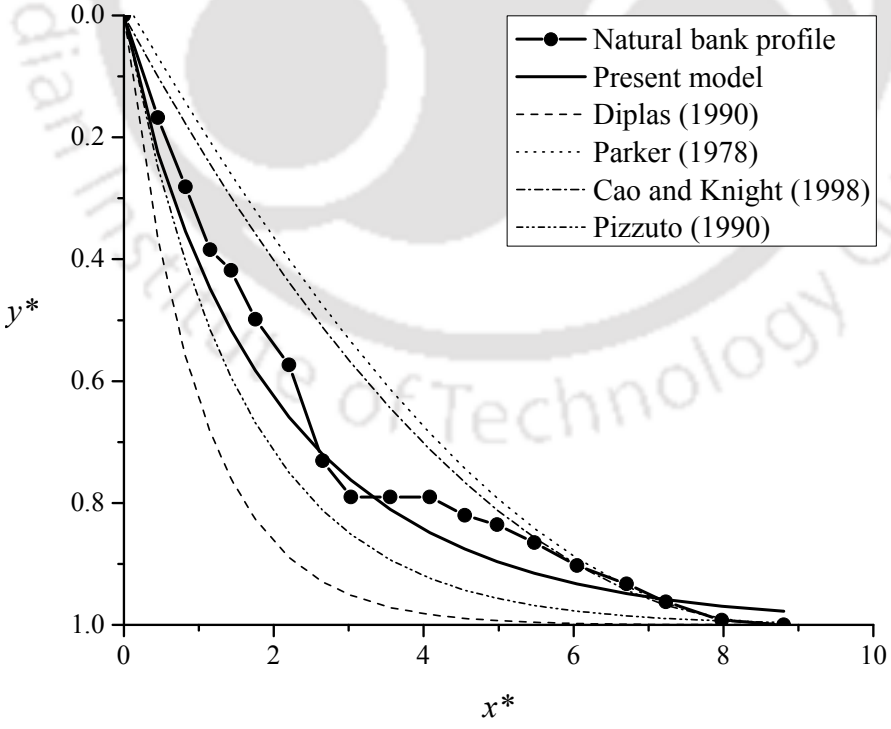

FIGURE 3.30: Bank profile of the Brahmaputra river at chainage 100 m d/s from Saraighat bridge center near Guwahati, India

3.4 Advent of Sheet Flow in Alluvial Channels with Downward Seepage

Flow in an alluvial channel is significantly affected by the presence of the sheet flow layer of high sediment concentration which corresponds to the upper flow regime. In the upper flow regime where the bed topography features such as ripples and dunes disappear, the roughness height is significantly affected by the sediment transport in the form of sheet flow. According to Wilson (1966) and Sumer et al. (1996) the roughness height may be much larger under the sheet flow conditions. The increase in roughness can be attributed to the increased energy dissipation in the sheet flow layer caused by interaction between individual sediment particles and by the interaction between the sediment particles and water (Camenen et al., 2006). Experimental observations of Wilson (1987) and the study carried out by Van Rijn (1993) suggest that the roughness height is about the thickness of the sheet flow layer.

Thickness of the sheet flow layer being an interesting topic has been studied by several researchers with Asano (1992) implemented the video observation technique and proposed the thickness of the sheet flow layer as a function of the Shields parameter:

$$\frac{\Delta}{d_{50}} = 5.0\theta \tag{3.13}$$

where Δ is the thickness of the sheet flow layer, d_{50} is the particle diameter, and θ is the Shields parameter.

Ahmed and Sato (2003) developed an image analysis technique. Distance between the relatively maximum brightness at unmoved beds up to level of 5% of maximum brightness values was defined as the time dependent sheet flow layer thickness. Dohmen-Janssen et al. (2002) and O'Donoghue and Wright (2004) utilized conductivity concentration meter (CCM) probes to measure the sheet flow

layer thickness. Maximum thickness of sheet flow layer has been related to the flow intensity through Shields parameter (Wilson, 1989; Dohmen-Janssen, 1999).

Linear relationship between the normalized thickness sheet flow layer and the maximum wave-related Shields parameter has been proposed for the maximum sheet flow layer thickness (Wilson, 1987; Sumer et al., 1996; Dohmen-Janssen et al., 2001). Flores and Sleath (1998) also carried out experimental study and proposed relations for the sheet flow layer thickness with Shields parameter and median particle diameter:

$$\frac{\Delta}{d_{50}} = 3\frac{\tau_0}{(\rho_s - \rho)\, g d_{50}} \tag{3.14}$$

where ρ_s is the dry density of the sediments, ρ is the density of the fluid, g is the acceleration due to gravity, and τ_0 is the amplitude of the shear stress acting on the upper surface of the mobile layer. O'Donoghue and Wright (2004) proposed relation between time-varying thickness of sheet flow layer and time-varying Shields parameter and observed that the thickness of the sheet flow layer is greatest for the fine sand and smallest for the coarse sand and grading plays a substantial role in sheet flow layer thickness.

Myrhaug and Holmedal (2007) developed analytical relations for characteristic statistical values of the sheet flow layer thickness by considering a stationary Gaussian narrow-band random process. Dong and Sato (2011) carried out experiments to investigate sediment transport of uniform sand in sheet flow condition under asymmetric oscillatory flows in combination with relatively strong opposite currents. Image analysis technique was performed to study the influence of wave shape and current by observing the instantaneous sheet flow layer thickness. Maximum thickness of the sheet flow layer was expressed as:

$$\frac{\Delta_S}{d_{50}} = 24 R_V k_{Tt} \frac{\theta_{\max}}{\sqrt{2\beta_t}} \tag{3.15}$$

where Δ_S is the maximum sheet flow layer thickness, $\theta_{\max}$ is maximum Shields parameter computed with maximum velocity, d_{50} is the median particle diameter,

β_t and R_V are the wave shape indices, and k_{Tt}:

$$k_{Tt} = \left(\frac{T_t}{T_{t,w}}\right)^{0.4} \tag{3.16}$$

where T_t is the half wave period of collinear waves and currents, and Tt, w is the half wave period for pure waves only. Dong et al. (2013) used the optical illumination technique to measure the thickness of sheet flow layer and proposed an expression for the maximum thickness of sheet flow layer under collinear waves and currents by considering the influence of flow acceleration and wavecurrent interaction effect. The proposed relation was:

$$\frac{\Delta_S}{d_{50}} = \begin{cases} 13 k_{Ti}\theta_{\max} \text{ for } d_{50} \geq 0.20 \text{ mm} \\ 22 k_{Ti}\theta_{\max} \text{ for } d_{50} \leq 0.15 \text{ mm} \\ \left[22 - \dfrac{9\,(d_{50} - 0.15)}{0.05}\right] k_{Ti}\theta_{\max} \text{ for } 0.16 < d_{50} < 0.20 \text{ mm} \end{cases} \tag{3.17}$$

where k_{Ti} is the correction factor, Δ_S is the maximum sheet flow layer thickness, and $\theta_{\max}$ is the maximum Shields parameter. Revil-Baudard and Chauchat (2013) proposed an analytical model by using the dense granular rheology and dilatancy law coupled with a mixing length approach and found the non-dimensional relation between the sheet flow layer thickness with Shields parameter (θ), static friction coefficient (μ), mean sheet flow layer concentration (C_m) and median particle diameterΔ_S:

$$\frac{\Delta_S}{d_{50}} = \frac{\theta}{\mu C_m} \tag{3.18}$$

Recently, Lanckriet et al. (2014) in their field study of swash-zone hydrodynamics and sediment transport used conductivity concentration profiler (CCP) instrument for the measurement of sheet flow layer thickness. Lanckriet et al. (2014) proposed relation of sheet flow layer thickness (Δ_S) with median particle diameter (d_{50}) and

a mobility number (Ψ) which does not depend on friction factor:

$$\frac{\Delta_S}{d_{50}} = 0.108\psi \tag{3.19}$$

$$\psi = \frac{u^2}{(s-1)\,gd_{50}} \tag{3.20}$$

where 'u' is the flow velocity, and 's' is the specific gravity. It is clear from the studies discussed above that seepage has not been considered in the study of sheet flow layer anywhere in the literature.

3.4.1 Distortion of the Channel Banks with Downward Seepage

Lane's (1953) geometric profile was stable during the no seepage experiments. No erosion or deposition of bed material was observed anywhere in the entire channel length and all the particles on the channel boundary were on the condition of incipient motion. After the application of downward seepage to these channels it has been observed that erosion of the sediment particles from channel banks and its deposition on the channel bed and further movement of the bed material in the form of sheet flow layer towards downstream follow a regular pattern under seepage experimentation. Figure 3.31 to Figure 3.36 show the cross-sectional area of both the banks that are eroded from channel upstream towards the downstream and the area of deposition of the eroded bank material on the channel bed for both the sands of median diameter 0.62 mm and 1.1 mm respectively, used in this study.

From the close observation of these Figures (3.31 to 3.36) we can see that the area of bank erosion at a cross-section decreases towards downstream whereas the area of deposition of the eroded material from the banks on channel bed at a cross-section increases from upstream towards the channel downstream. A definition sketch of the area of bank erosion and the area of deposition of bank material on the channel bed at a cross-section has been depicted in Figure 3.37. Snapshots of

the undistorted channel bank after the no seepage experiment and the distorted channel bank during the seepage experiment are given in Figure 3.38 and Figure 3.39, respectively.

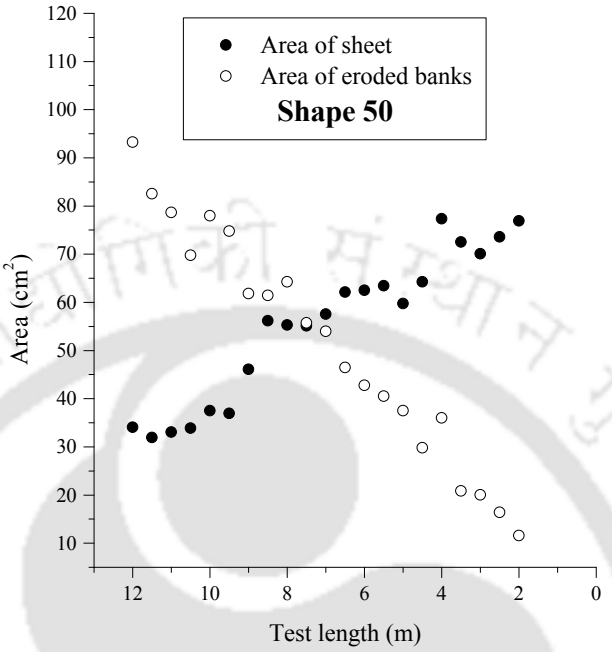

FIGURE 3.31: Area of eroded banks and sheet for the sand of d_{50} = 0.62 mm and shape 50

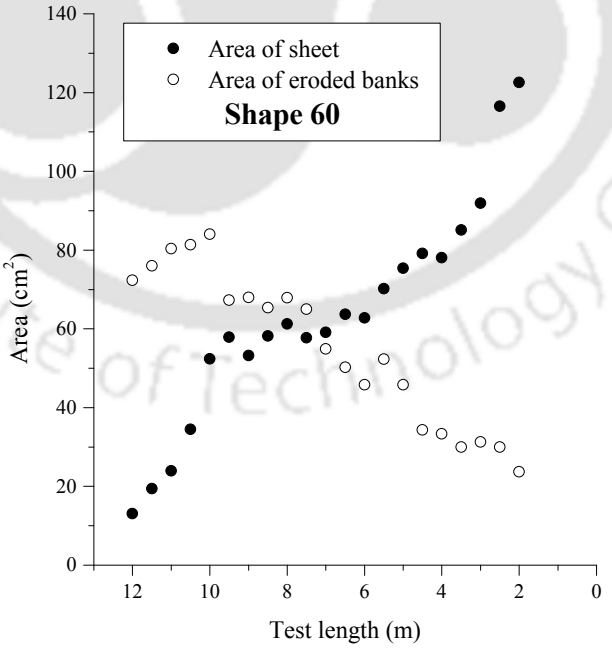

FIGURE 3.32: Area of eroded banks and sheet for the sand of d_{50} = 0.62 mm and shape 60

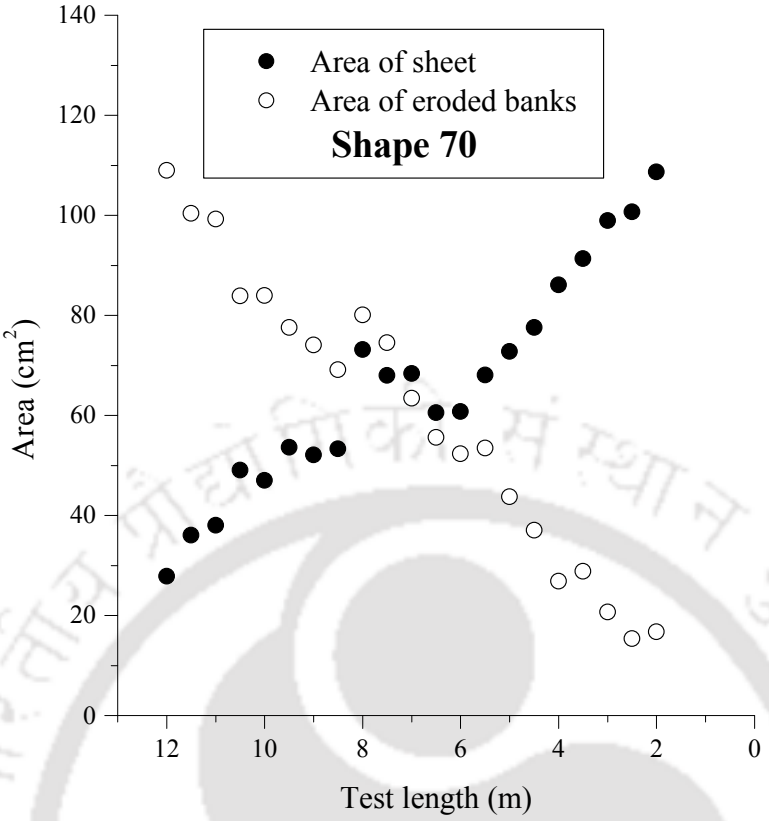

FIGURE 3.33: Area of eroded banks and sheet for the sand of $d_{50} = 0.62$ mm and shape 70

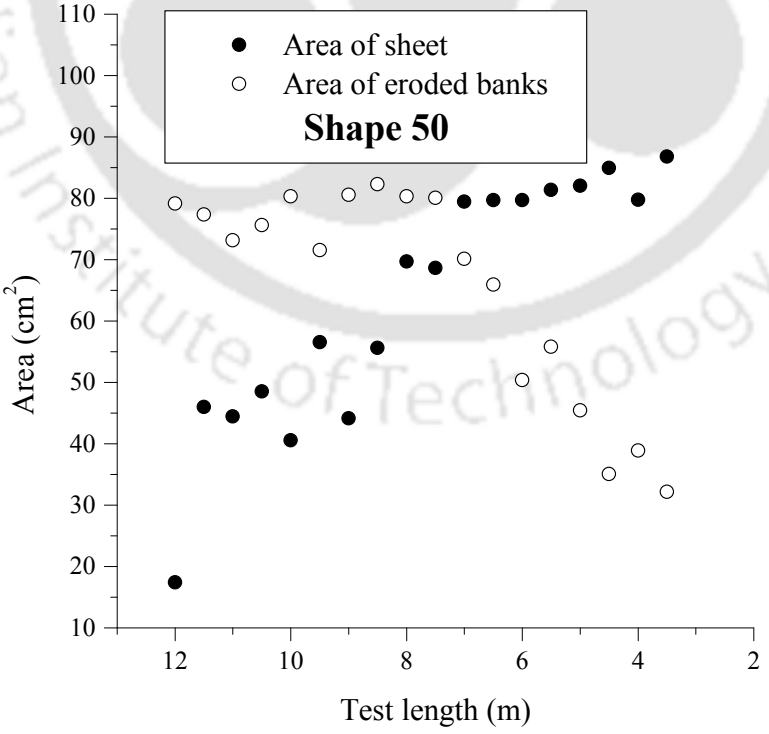

FIGURE 3.34: Area of eroded banks and sheet for the sand of $d_{50} = 1.1$ mm and shape 50

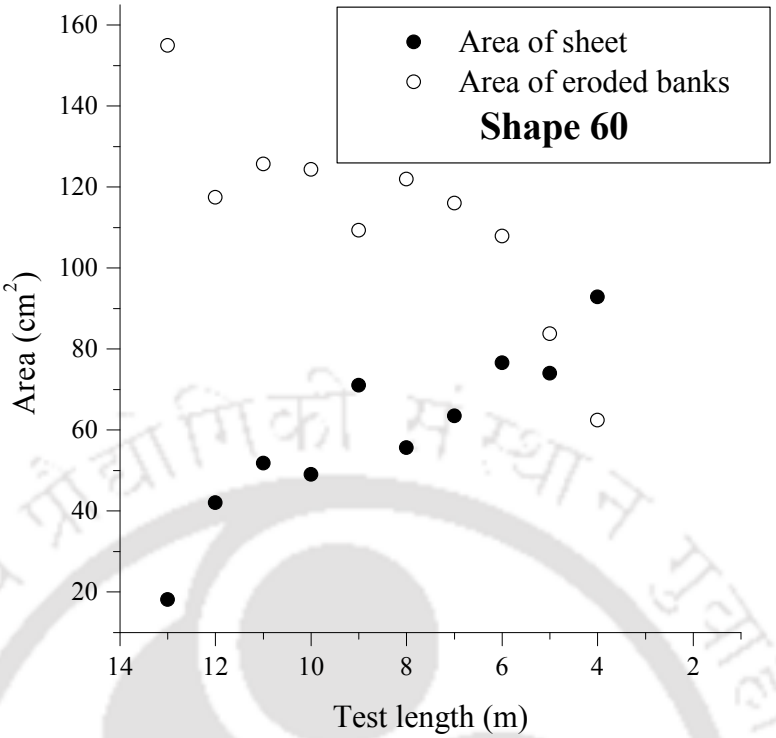

FIGURE 3.35: Area of eroded banks and sheet for the sand of d_{50} = 1.1 mm and shape 60

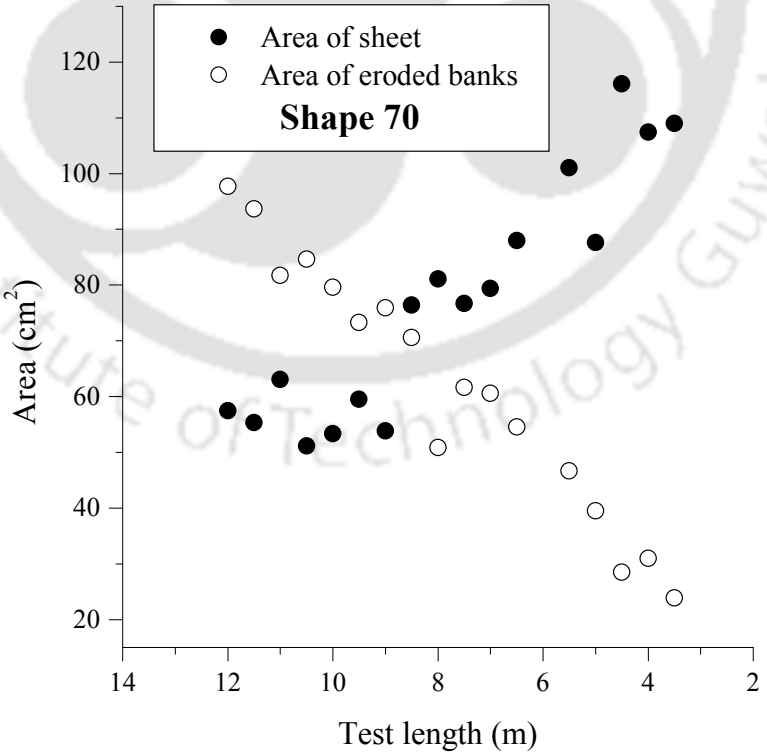

FIGURE 3.36: Area of eroded banks and sheet for the sand of d_{50} = 1.1 mm and shape 70

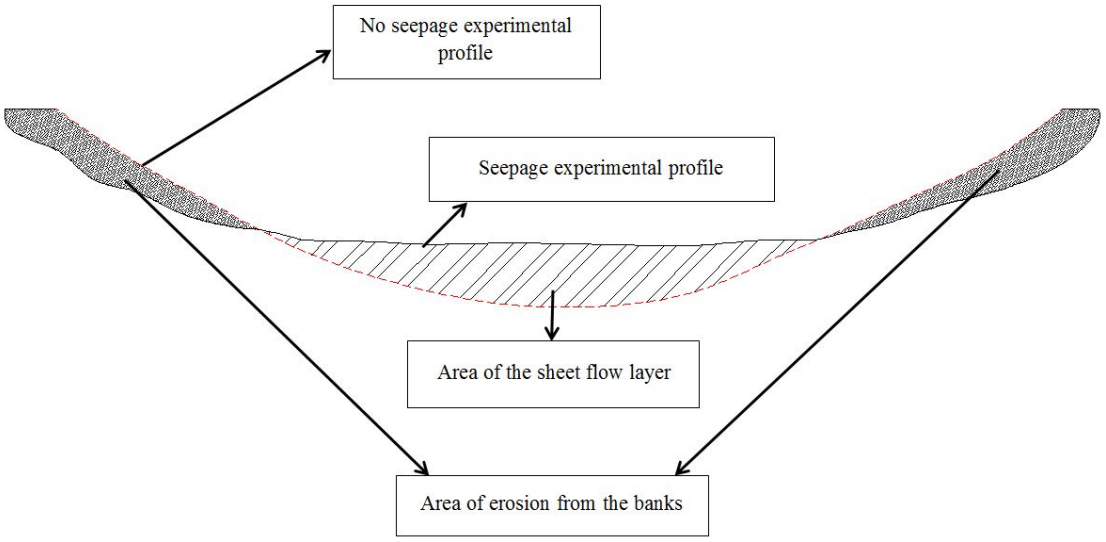

FIGURE 3.37: Definition Sketch for the area of bank erosion and the area of sheet flow layer

FIGURE 3.38: Undistorted channel bank obtained after the no seepage experiment

FIGURE 3.39: Distorted channel bank during the seepage experiment

During the no seepage experimental runs, Lane's (1953) geometric profile was stable and there was no erosion or deposition observed in the entire test length of the channel as it has been stated earlier that sediment particles on the entire periphery of Lane's (1953) geometric profile are on the verge of motion i.e. at the threshold condition where the tractive stress exerted by the flowing water equals the resistive stress of sediment particles.

This proves that this (Lane's (1953) geometric profile) is the ideal channel cross-section where the banks are stable and channel does not transport sediment. But during the seepage experiments, it has been observed that the bed shear stress was increased significantly from its value of no seepage experimental runs. This increase of bed shear stress caused the erosion of banks. Figure 3.40 to Figure 3.45 show the bed shear stress for seepage and no seepage experimental runs for shape 50, shape 60 and shape 70 for both the sands of median diameter 0.62 mm and 1.1 mm, respectively.

The eroded material from the banks at a cross-section is deposited on the channel bed and carried forward by the flow. Thus the sediment transport occurs in the channel which is in accordance of the natural channels which do transport sediment. After running the experiment for several hours, the channel geometry

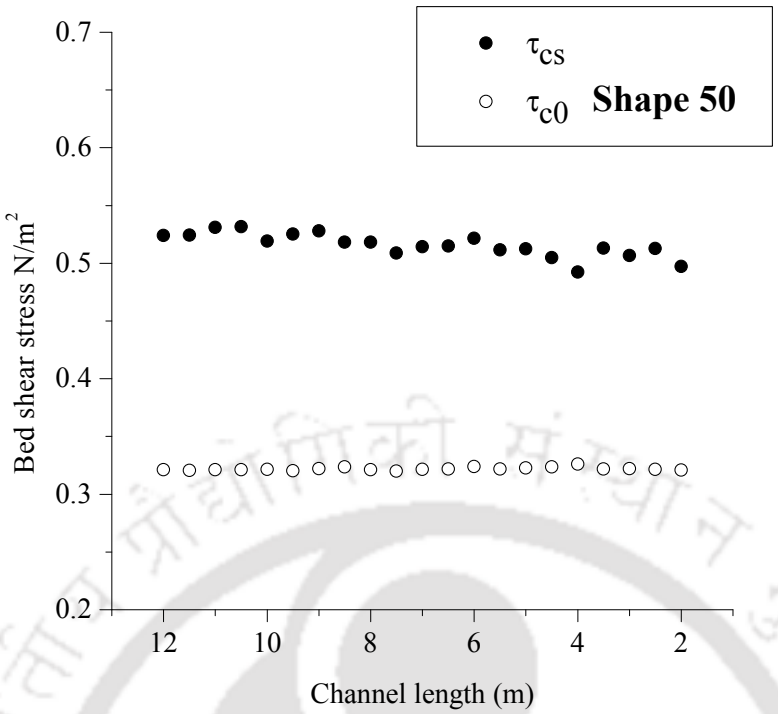

FIGURE 3.40: Bed shear stress after no seepage and seepage experimental runs for the sand of d_{50} = 0.62 mm and shape 50

in adjusted on its own so that the bed shear stress (τ_{bs}) becomes equal to the critical bed shear stress (τ_{cs}) and the channel becomes stable.

More erosion of banks takes place at the upstream side because of the higher stream power associated with the flow and towards the downstream as the stream power reduces gradually, the erosion of banks also decreases along the length of the channel. Figure 3.46 to Figure 3.51 show the gradual decrease of stream power along the length of the channel from upstream to downstream for shape 50, shape 60 and shape 70 for both the sands of median diameter 0.62 mm and 1.1 mm, respectively.

The new channel cross-section after seepage experiments is such that the banks are eroded and the central part is enhanced. Thus the geometric profile proposed by Lane (1953) is converted into a new shape which is similar to the cross-sectional profiles (trapezoidal with curved banks) of natural stable channels proposed by several researchers among Parker (1978), Diplas (1990), Pizzuto (1990), Diplas and Vigilar (1992) and Cao and Knight (1998) as shown in Figure 3.15. Figure 3.15(A) shows the channel shape after no seepage runs. It can be seen from the Figure 3.15

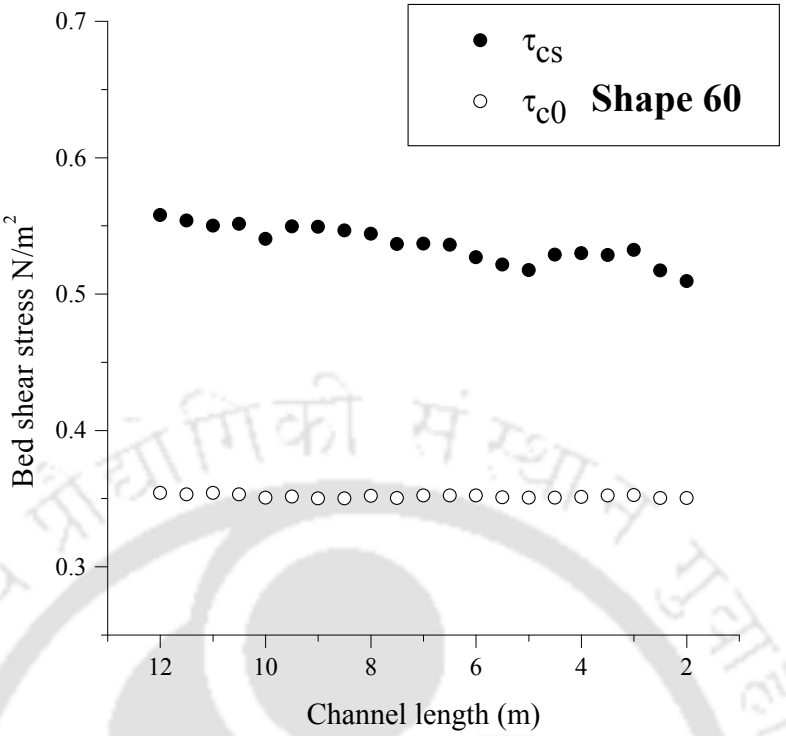

FIGURE 3.41: Bed shear stress after no seepage and seepage experimental runs for the sand of $d_{50} = 0.62$ mm and shape 60

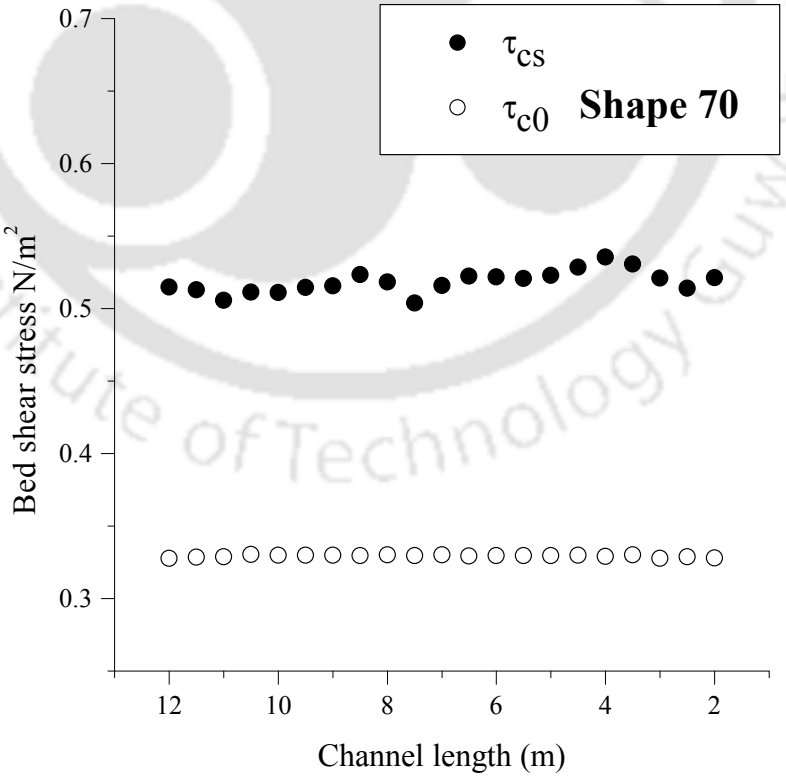

FIGURE 3.42: Bed shear stress after no seepage and seepage experimental runs for the sand of $d_{50} = 0.62$ mm and shape 70

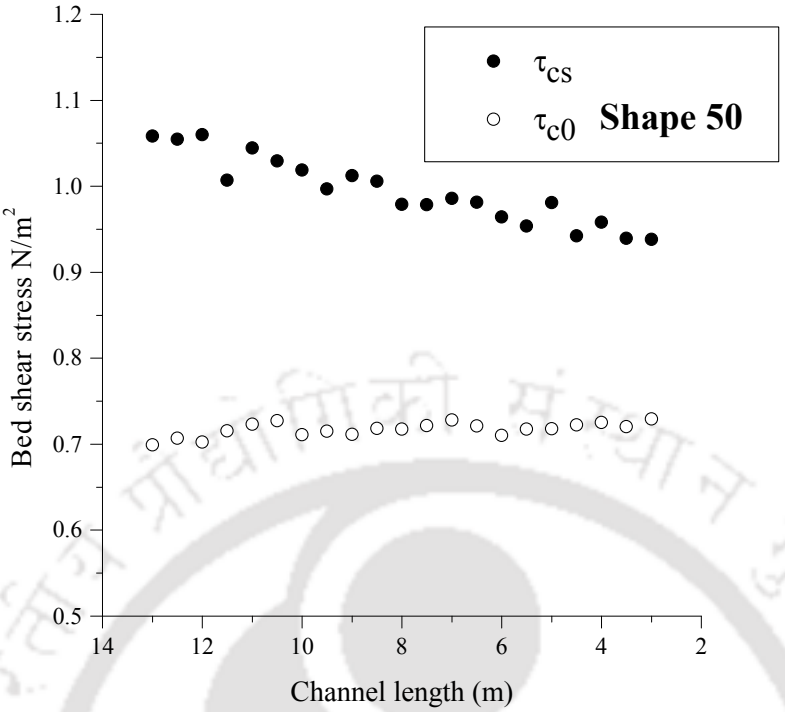

FIGURE 3.43: Bed shear stress after no seepage and seepage experimental runs for the sand of $d_{50} = 1.1$ mm and shape 50

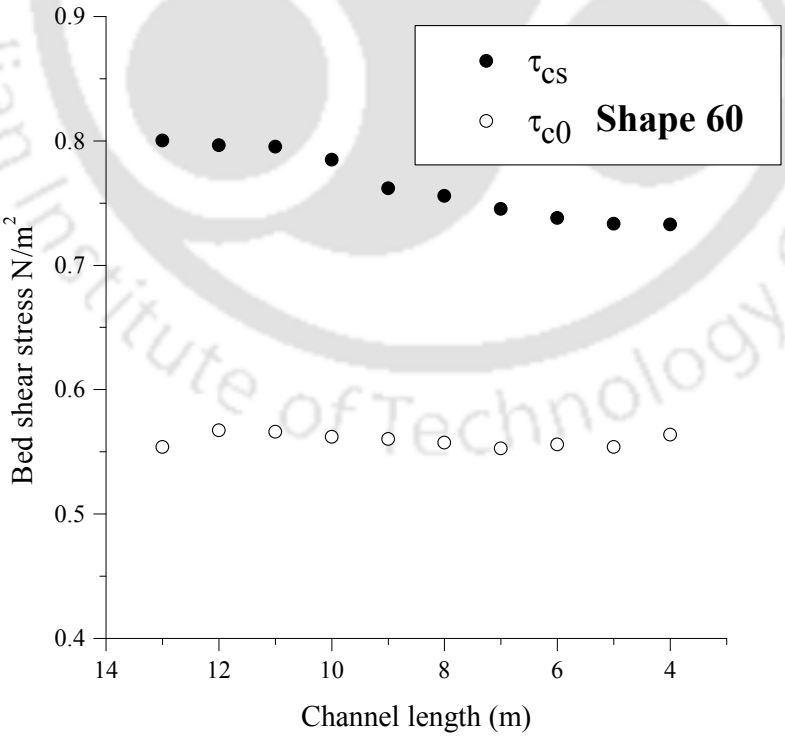

FIGURE 3.44: Bed shear stress after no seepage and seepage experimental runs for the sand of $d_{50} = 1.1$ mm and shape 60

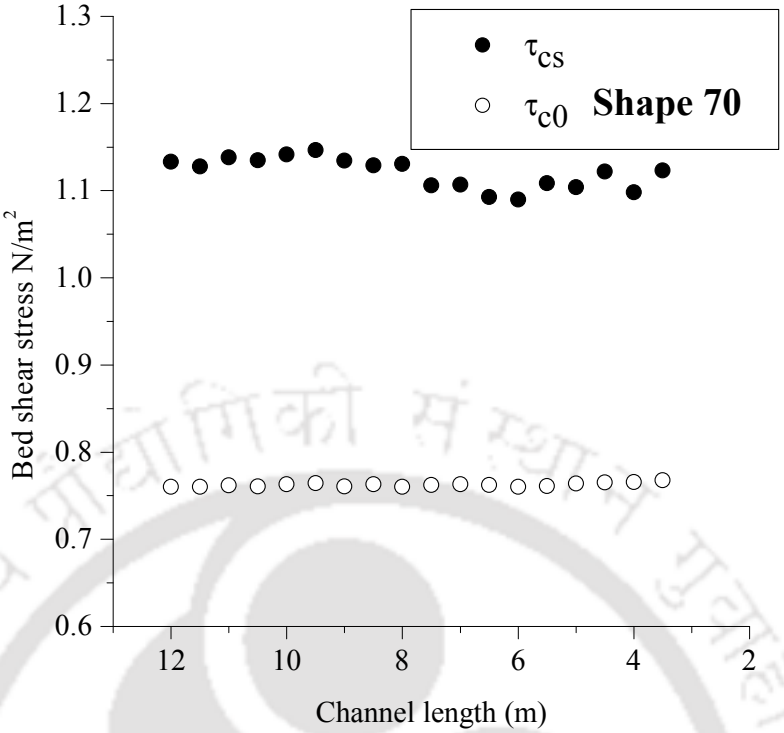

FIGURE 3.45: Bed shear stress after no seepage and seepage experimental runs for the sand of d_{50} = 1.1 mm and shape 70

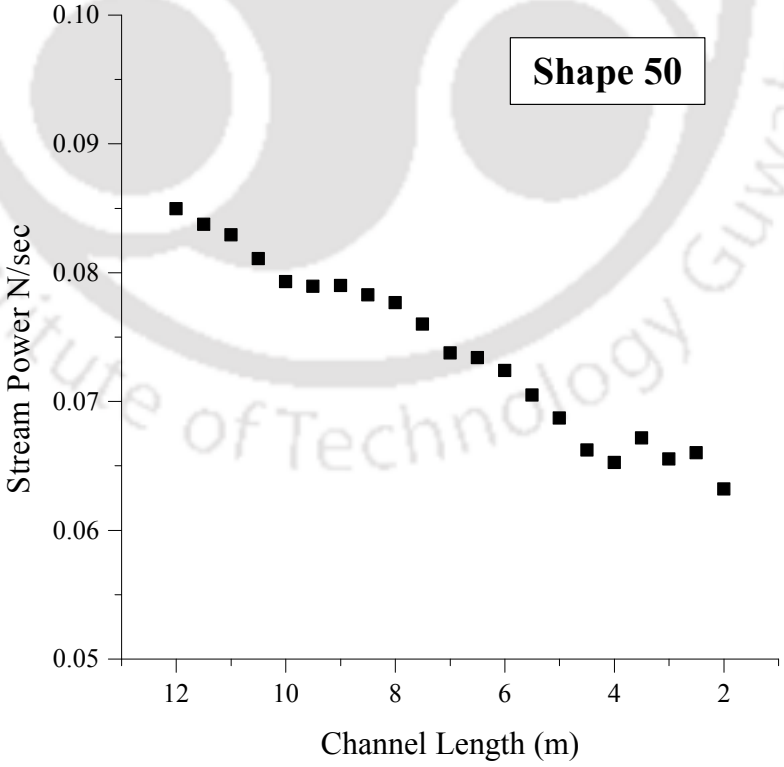

FIGURE 3.46: Variation of stream power during seepage experiments for the sand of d_{50} = 0.62 mm and shape 50

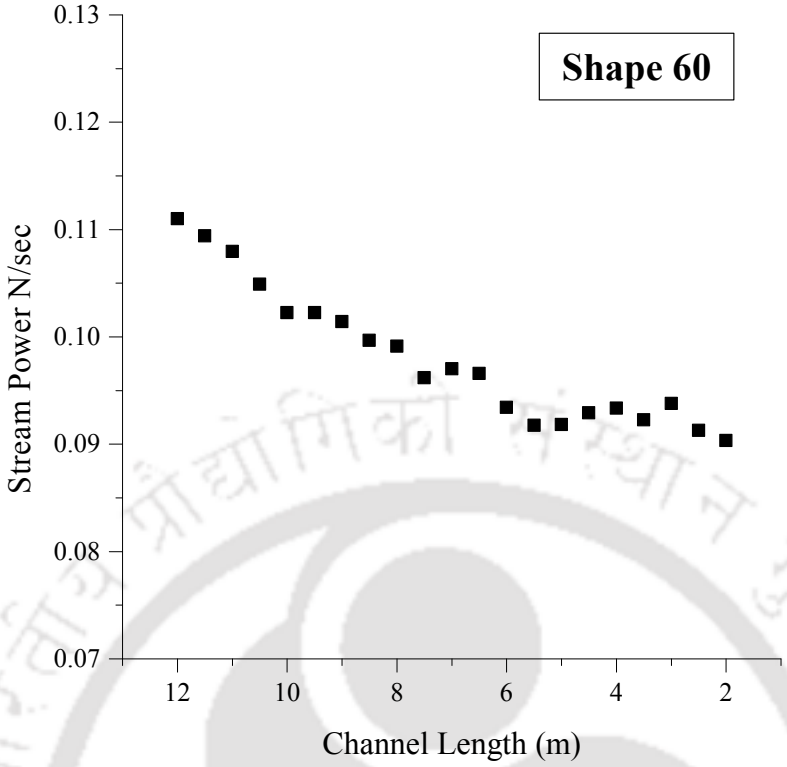

FIGURE 3.47: Variation of stream power during seepage experiments for the sand of $d_{50} = 0.62$ mm and shape 60

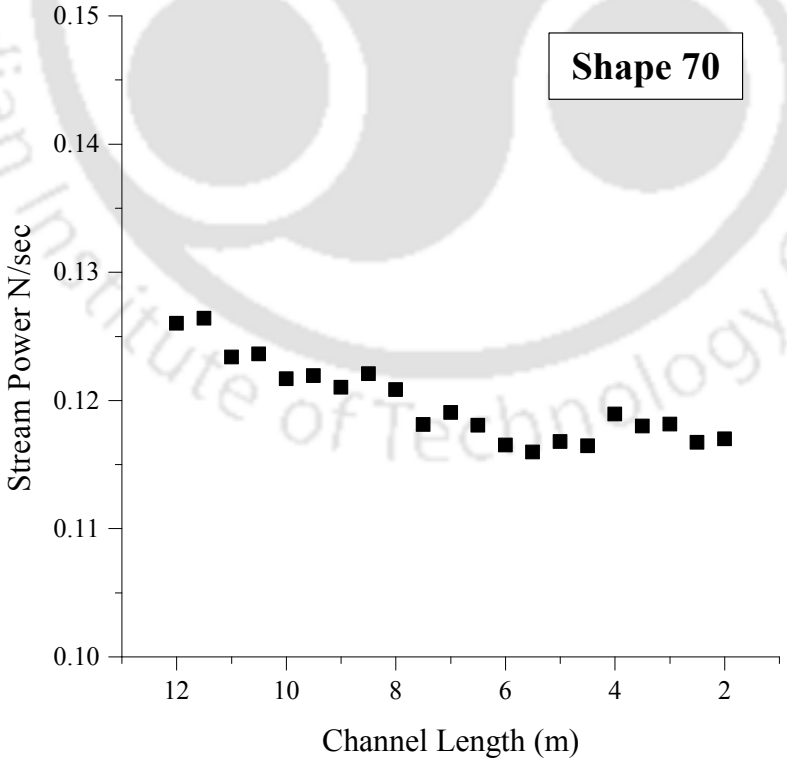

FIGURE 3.48: Variation of stream power during seepage experiments for the sand of $d_{50} = 0.62$ mm and shape 70

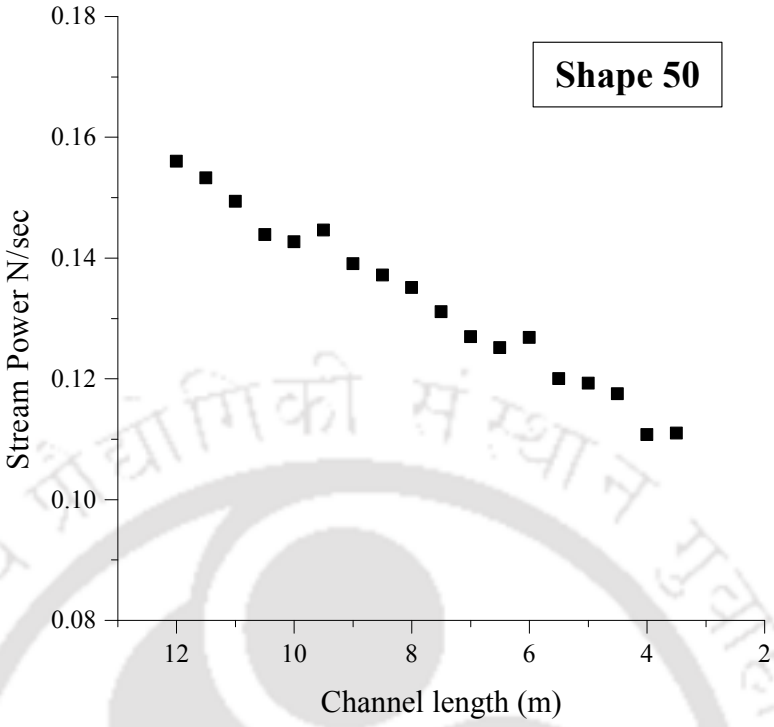

FIGURE 3.49: Variation of stream power during seepage experiments for the sand of d_{50} = 1.1 mm and shape 50

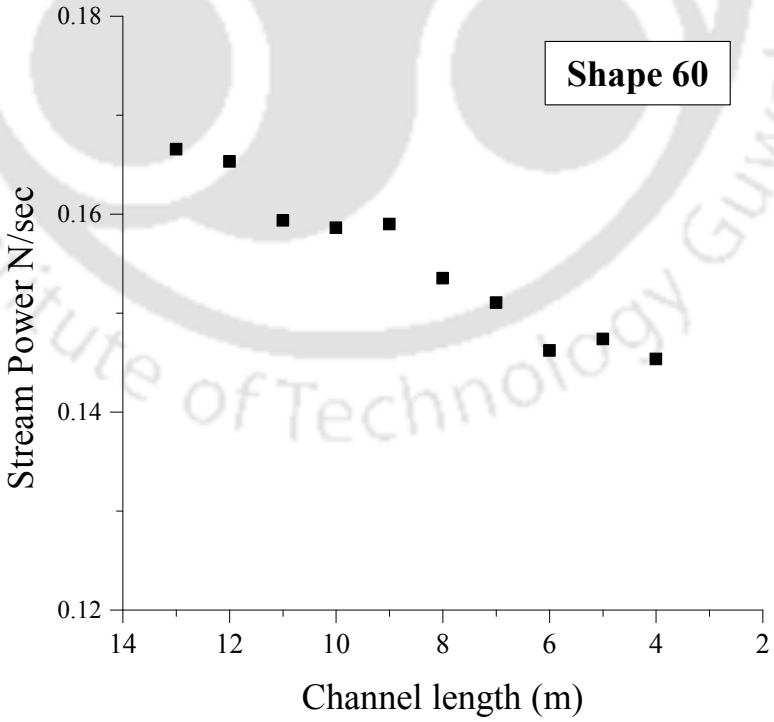

FIGURE 3.50: Variation of stream power during seepage experiments for the sand of d_{50} = 1.1 mm and shape 60

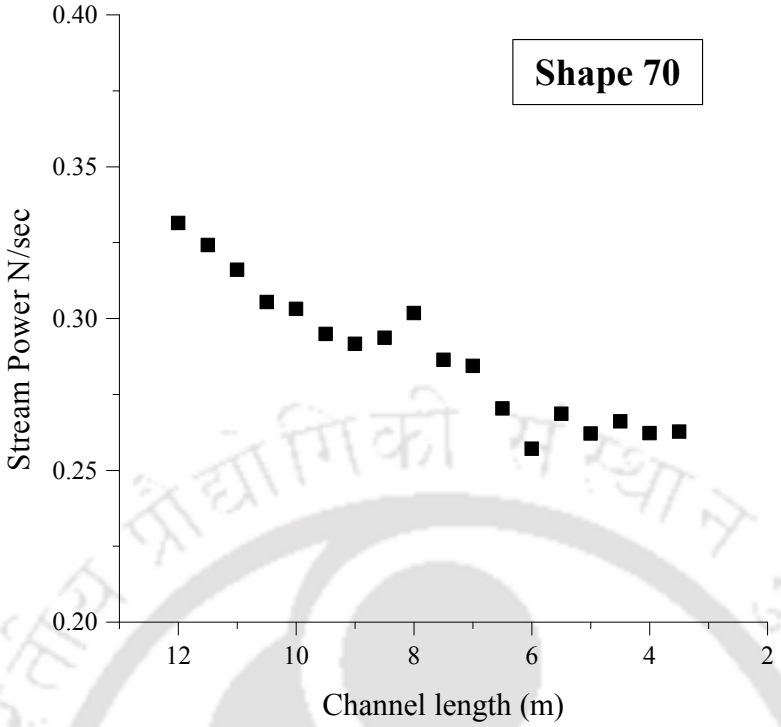

FIGURE 3.51: Variation of stream power during seepage experiments for the sand of d_{50} = 1.1 mm and shape 70

(A) that channel holds its shape during no seepage runs. Figure 3.15(B) shows the channel shape after seepage runs. There is very marked difference between Figure 3.15(A) and Figure 3.15(B). The channel during no seepage runs has been changed into a trapezoidal shape.

3.4.2 Bed Material Transport in the Form of Sheet Flow

During seepage experiments the channel banks were eroded because of the increased bed shear stress and the eroded material from the banks at a section was deposited on the channel bed at the adjacent section towards downstream. This deposited material is carried forward by the water along the length of channel in the form of sheet flow layer as shown in the Figure 3.52. Large amount of sediment eroded from the banks is transported in the form of sheet flow over the bed and the sediment particles move in such a way that the particles roll over one another.

According to the studies carried out by several researchers (Asano, 1992; Gotoh and Sakai, 1997; Flores and Sleath, 1998; Malarkey et al., 2003; Dong et al., 2013;

FIGURE 3.52: Front view of sheet flow layer

Revil-Baudard and Chauchat, 2013), sheet flow is observed when the Shields parameter is higher that its threshold value. In the present study the sheet flow layer has been observed during seepage experiments which indicate that Shields parameter becomes higher during seepage experiments and eventually it justifies that the bed shear stress becomes higher when downward seepage is applied to the channel.

In order to find the effect of seepage on the transport of bed material in the form of sheet flow, a formal dimensional analysis has been performed to generate an empirical relationship for the thickness of the sheet flow of bed material which incorporates seepage as an explicit variable. The thickness of sheet flow Δ can be considered as function of following independent variables:

$$\Delta = f\left(y_s, d_{50}, u_s, V_s, \tau_{c0}, \gamma_s, \gamma, g, R_{hs}, \nu\right) \tag{3.21}$$

where y_s is the depth of flow for seepage case, d_{50} is median particle size, g is acceleration due to gravity, ν is kinematic viscosity, γ_s and γ are the specific weight of sediment particles and water, respectively. This dimensional analysis indicated that the dimensionless sheet thickness δ was a function of four dimensionless parameters:

1. Critical Shields parameter θ_c;
2. Seepage intensity parameter N (Equation (2.19));
3. Froude number F_s (Equation (2.12)); and
4. Particle Reynolds number R_S with seepage.

The particle Reynolds number with seepage can be defined as:

$$R_S = V_s d_{50}/\nu \tag{3.22}$$

The non-dimensional sheet thickness δ was assumed to be proportional to the product of the following dimensionless parameters:

$$\delta = \frac{\Delta}{y_s} = a\left(\frac{\tau_{c0}}{(\gamma_s - \gamma)\, d_{50}}\right)^b \left(\frac{2\rho u_s V_s}{\tau_{c0}}\right)^c \left(\frac{u_s}{(gR_{hs})^{1/2}}\right)^d \left(\frac{V_s d_{50}}{\nu}\right)^e \tag{3.23}$$

Experimental data from both the sands i.e. sands of median particle diameter 0.62 mm and 1.1 mm have been used to determine the values of empirical coefficient a and exponents b, c, d and e. The resulting equation for the dimensionless thickness of the sheet flow of bed material comes out to be:

$$\delta = 1.1\theta c^{-0.45} N^{0.5} {F_s}^{1.7} Rs^{-0.13} \tag{3.24}$$

Figure 3.53 shows the prediction of dimensionless thickness of the sheet flow by Equation (3.24) with the corresponding experimental values. The performance of Equation (3.24) has been found to be very good in accordance with the experimental data and with the value of the coefficient of multiple determination (R^2) 0.77.

It can be seen from Figure 3.53 that around 90% of the observation falls within 20% variation from the prediction. The range of standard error in estimation of coefficient is 1.2E-3 to 4.3E-2. The standard error of the estimate is 6.1E-2.

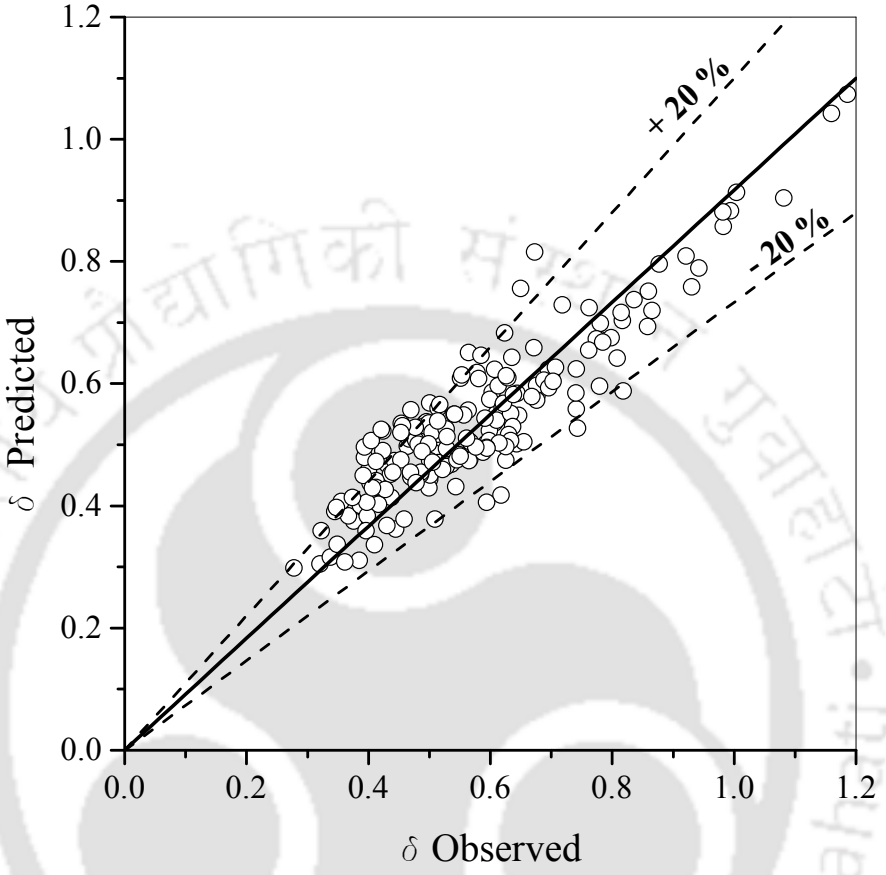

FIGURE 3.53: Predicted dimensionless thickness of the sheet flow by Equation (3.24) versus observed values

The predictive power of Equation (3.24) can be assessed through the NashSutcliffe efficiency index E proposed by Nash and Sutcliffe (1970). It can be calculated as:

$$E = 1 - \frac{\sum_{i=1}^{n} \left(\delta_{i,\text{Observed}} - \delta_{i,\text{Predicted}}\right)^2}{\sum_{i=1}^{n} \left(\delta_{i,\text{Observed}} - \overline{\delta_{\text{Observed}}}\right)^2} \tag{3.25}$$

where, $\delta_{Observed}$ is the observed values of dimensionless sheet thickness, $\delta_{Predicted}$ is the predicted values and $\overline{\delta_{\text{Observed}}}$ is mean of the observed values of dimensionless sheet thickness, and n is the sample size. E ranges from $-\infty$ to 1, $E = 1$ corresponds to a perfect match of predicted values with the observed values. $E = 0$

shows that the predictions are as accurate as the mean of the observed data, and $E < 0$ occurs when the observed mean is a better predictor than the model. Nash-Sutcliffe efficiency index for Equation (3.24) is 0.76 which makes it a very good predictor for the thickness of the sheet flow layer.

3.5 Conclusions

It has been observed that after the application of seepage parabolic shape of channels based on Lane's (1953) theory was distorted and channels attained new cross-sectional shape with flat bed and curved banks at the end of seepage experiments and achieved stability. In the previous studies various authors (Parker, 1978; Diplas, 1990; Pizzuto, 1990; Diplas and Vigilar, 1992; Cao and Knight, 1998) have supported this cross-sectional shape of threshold alluvial channels. But, in their analysis seepage in the downward direction has not been considered as an explicit governing parameter. Variation in various parameters like channel perimeter, hydraulic radius and top width has also been observed for the channel after seepage experiments. The rate of erosion became higher during seepage experiments because of the increase in bed shear stress. The values of channel shape parameter for the channels obtained after seepage experiments have been found to be greater than 2, which suggest that the channels obtained after seepage experiments exhibit similarity with the natural stable alluvial channels composed of curved banks and flat bed. Seepage in the downward direction has been considered for the evaluation of bank profiles and an empirically derived exponential expression has been suggested which predicts satisfactorily the bank profiles at various cross-sections of the natural alluvial rivers. After the application of seepage in the downward direction, channels went into upper flow regime and the concentration of sediment material coming from the banks became so high that the sheet flow layer on channel beds were formed. An empirical equation has been generated to predict the thickness of the sheet flow layer as a function of Shields parameter, Froude number, seepage intensity parameter and seepage particle Reynolds number.

Chapter 4

Geometry of Stable Alluvial Channels with Downward Seepage

The equilibrium geometry of alluvial channels remained a topic of fundamental scientific and engineering interest for years. Cross-sectional geometry and slope of alluvial channels change with the variation in the sediment load transported by them. The phenomenon of sedimentation and erosion has been observed in alluvial channels when heavily silt-laden water flows through them. A large amount of expenditure is incurred on maintenance of channels in desilting and on the other hand scouring of the bed, hinders the capacity of the channel.

An alluvial channel typically has three degrees of freedom i.e. width, depth and slope. In order to determine channel geometry completely, a set of three independent equations are thus required. These three equations can be obtained either empirically or analytically (Cao and Knight, 2002). In empirical approach, the required equations are obtained by analyzing the available data from stable alluvial channels with the laws of statistics. This empirical approach of attaining a set of three independent equations by analyzing the available data from existing

stable channels is frequently known as 'the regime theory' and was originated by the engineers working on irrigation canals of India and Pakistan.

In the analytical approach on the other hand, the required equations are obtained theoretically and according to White et al. (1982) "The analytical methods rely on specifying equations which describe the dominant individual processes such as sediment transport, flow resistance and bank stability. These approaches can only be successful if the dominant processes are correctly identified and appropriate equations exist to describe them adequately".

4.1 Empirical Approaches

Empirical approaches are those in which the set of three equations is sought by analyzing the available data from the existing stable alluvial channels, with the laws of statistics in order to derive the hydraulic geometry.

4.1.1 The Regime Concept

In regime methods, the stable channel is designated as 'regime channel'. One common observation that alluvial channel adjusts its dimensions in response to the variations in the size and quantity of sediments carried by it, lays the foundation of regime concept.

4.1.1.1 Kennedy's Study

Kennedy (1895) stated that a channel is said to be in a state of 'regime' if there is neither silting nor scouring in the channel. Empirical relationship between mean velocity and depth of flow has been proposed by Kennedy by utilizing the obtained data from twenty-two channels of Upper Bari Doab system which had permanent

and established cross-sections and neither silting nor scouring of bed occurred.

$$U_{cr} = 0.55y^{0.64} \tag{4.1}$$

where, U_{cr} is the critical velocity at which for a given depth y, silting is just prevented i.e. maintaining the entire sediment load without eroding the channel. Further, Kennedy reassessed his research by introducing a factor named as critical velocity ratio and designated by m, which was dependent upon silt grade, to account for the type of soil through which the channel was to pass. The equation thus modified as:

$$U_{cr} = 0.55my^{0.64} \tag{4.2}$$

This equation together with the flow resistance formula of Kutter's or Mannings's, can be used to determine the channel dimensions.

4.1.1.2 Lindley's Study

Lindley (1919) proposed equations for depth and channel width recognizing that the bed and the banks as well are subjected to scour or fill, which were:

$$U_{cr} = 0.95y^{0.57} \tag{4.3}$$

$$U_{cr} = 0.57B^{0.355} \tag{4.4}$$

where, B is the average width between banks of channel. Geometry of the channel can be obtained with these equations proposed by Lindley, together with any flow resistance formula of Kutter or Manning.

4.1.1.3 Lacey's Study

Lacey's regime method was published from 1930 to 1958 in a series of papers. It has been stated by Lacey that when water flows through an excavated channel, the silt carried by the water may get deposited in the upper reaches. Consequently the bed slope and therefore the velocity are increased and equilibrium is established in which there is no silting taking place. Banks of such channels may not be eroded due to their rigidity. Hence, there will be neither silting nor scouring in such channels and regime is appeared to be established in such channels but in fact, it is not. Such channels are termed as 'channels in initial regime', regime theory is not applicable to such channels.

When there is no resistance offered to lateral adjustment from the boundaries of channel then depth, width and slope etc. vary freely and finally get adjusted according to the incoming water and sediment discharges. The channel is said to have achieved permanent stability and is called in 'final regime'. Regime theory is applicable to such channels only. Lacey's regime method is summarized briefly in three regime equations, first one, which is a flow resistance equation, has two forms (Chang, 1988):

$$u = 1.15(f_l y)^{0.5} \tag{4.5}$$

$$u = \frac{1.34}{N_a} y^{0.25} {R_h}^{0.5} S_0^{0.5} \tag{4.6}$$

$$f_l = 1.59 {d_{50}}^{1/2} \tag{4.7}$$

$$N_a = 0.225 f_l^{1/4} \tag{4.8}$$

where:

u : is the mean velocity in feet per second.

y : is mean depth in feet.

R_h : is hydraulic radius.

S_0 : is channel slope.

f_l : is Lacey's silt factor.

N_a : is absolute rugosity.

d_{50} : is median bed-material size (in millimeters).

The second regime equation relates the wetted perimeter with water discharge Q and has a form:

$$p = 2.67Q^{1/2} \tag{4.9}$$

where:

p : is the wetted perimeter in feet.

Q : is the discharge in cubic feet per second.

When the discharges of large alluvial rivers are considered, the wetted perimeter closely approximates the water surface width. Lacey (1930) developed the following formula to determine the approximate width of stable alluvial channel:

$$B = 2.67Q^{1/2} \tag{4.10}$$

where B is water surface width in feet. Third regime equation gives the channel slope S_0:

$$S_0 = \frac{f_l^{5/3}}{1830Q^{1/6}} \tag{4.11}$$

These equations given by Lacey provide required stable width, depth and slope of the channel. This method should be applied when bed-material size is in the range of 0.15 to 0.40 mm and discharge between 5 and 5000 cfs.

4.1.1.4 Blench's Study

Blench (Chang, 1988) extended the previous regime methods to include the bank material characteristics. The regime method proposed by Blench consist three independent equations from which the required stable width, depth and slope of the channel can be determined. The first equation defines the bed factor F_{bed} and is known as 'bed factor equation':

$$F_{bed} = \frac{u^2}{y} \tag{4.12}$$

where:

u : is the mean velocity in feet per second.

y : is the depth of flow in feet.

The second equation gives the side factor F_{side} and is known as 'side factor equation':

$$F_{side} = \frac{u^3}{B} \tag{4.13}$$

where B is the average width in feet and is equal to the cross-sectional area divided by y.

The third equation is known as the regime slope equation and has form of flow resistance equation as:

$$\frac{u^2}{gyS} = 3.63\,(1 + C/2330)\left(\frac{uB}{v}\right)^{1/4} \tag{4.14}$$

where:

ν : is kinematic viscosity.

C : is suspended-sediment concentration in parts per million by weight.

g : is the acceleration due to gravity in feet per square second.

In a more practical form, we obtain for average width and mean depth:

$$B = \frac{A}{y} = \left(\frac{F_{bed}Q}{F_{side}}\right)^{1/2},\ y = \left(\frac{F_{side}Q}{F_{bed}^2}\right)^{1/3} \tag{4.15}$$

and slope:

$$S_0 = \frac{F_{bed}^{5/6} F_{side}^{1/12} v^{1/4}}{3.63\,(1 + C/2330)\,gQ^{1/6}} \tag{4.16}$$

The flow velocity can be obtained from these equations as (Graf, 1998):

$$u = \sqrt[6]{F_{bed} F_{side} Q} \tag{4.17}$$

Relation for the determination of bed factor given by Blench (1957) Blench (1964) as (Chang, 1988) :

$$F_{bed} = 1.9\sqrt{d_{50}} \tag{4.18}$$

where d_{50} is median sediment size in millimeters.

For side factor, Blench (1957) recommended following values (Graf, 1998):

F_{side} : = 0.1 for slightly cohesive loams
= 0.2 for medium cohesive loams
= 0.3 for highly cohesive loams

By observing these equations carefully, one can conclude that the bank slope of a channel is directly related to bank material and channels with more cohesive banks are narrower and deeper than those with less cohesive banks.

4.1.1.5 Simons and Albertson's Study

Simons and Albertson (1960) studied the canals of India-Pakistan and USA and classified them into five types (Table 4.1) on the basis of the different geotechnical channel conditions. The range of discharges studied was 5 to more than 9000 cusecs, with an average sediment discharge of 156 to 8000 ppm. The mean size of the bed material varied from 0.1 mm to 7.5 mm. Regime equations given by Simons and Albertson for regime width, depth and slope are as follows (Chang,

1988) . For regime width:

$$p = K_1 Q^{1/2} \tag{4.19}$$

$$B' = 0.9p \tag{4.20}$$

$$B' = 0.92B - 2.0 \tag{4.21}$$

where:

p : is the wetted perimeter.

B : is the surface width.

K_1 : is the coefficient related to the canal type.

For depth:

$$R_h = K_2 Q^{0.36} \tag{4.22}$$

$$y = 1.21 R_h \text{ for } R_h < 7 \text{ ft} \tag{4.23}$$

$$y = 2.0 + 0.93 R_h \text{ for } R_h \geq 7 \text{ ft} \tag{4.24}$$

where:

R_h : is the hydraulic radius.

K_2 : is the coefficient related to canal type.

and for slope:

$$u = K_3 \left(R^2 S_0\right)^{m_e} \tag{4.25}$$

$$\frac{u^2}{gyS} = K_4 \left(\frac{uB'}{\nu}\right)^{0.37} \tag{4.26}$$

where:

m_e : is an exponent.

K_3 and K_4 : are coefficients.

The effects of bed and bank materials on the geometry of stable channel are incorporated in this method.

TABLE 4.1: Values of exponent and coefficients for different canal types (after (Chang, 1988))

Canal Type	K_1	K_2	K_3	K_4	m_e
Sand bed and banks	3.5	0.52	13.9	0.33	0.33
Sand bed and cohesive banks	2.6	0.44	16	0.54	0.33
Cohesive bed and banks	2.2	0.37	–	0.87	–
Coarse non-cohesive material	1.75	0.23	17.9	–	0.29
Sand bed and cohesive banks with heavy sediment loads, 2000-8000 ppm.	1.7	0.34	16	–	0.29

4.1.2 Power Function Theory

Leopold and Maddock (1953) developed a set of empirical equations to express the variation of water surface width, mean depth and velocity for a channel in form of power functions of discharge for both at-a-station and downstream the channel. The relations are:

$$B = aQ^{b_p} \tag{4.27}$$

$$y = cQ^{f_p} \tag{4.28}$$

$$u = kQ^{m_p} \tag{4.29}$$

where:

B : is the channel width.

y : is mean flow depth.

u : is velocity.

Q : is the discharge.

b_p , f_p and m_p : are the exponents and represent the slope of the three lines on the graph of variation of width, depth and velocity with mean annual discharge, respectively

a , c and k : are the constants that represent the values of width, depth and velocity, respectively, when the discharge is unity.

From the continuity equation:

$$Q = Byu = aQ^{b_p} cQ^{f_p} kQ^{m_p} \tag{4.30}$$

hence:

$$b_p + f_p + m_p = 1, \text{ and } ack = 1 \tag{4.31}$$

The average values of b_p, f_p, and m_p for 20 river cross-sections of United States found by Leopold and Maddock (1953) were 0.5, 0.4 and 0.1 respectively. The work of Leopold and Maddock (1953) shows that discharge, width and depth increase in a similar manner for most of the streams in the downstream direction due to increase in drainage area but slight increase is observed in the velocity because of decreasing slope downstream. Average values of exponents, b_p, f_p, and m_p for the downstream hydraulic geometry, given by various authors (Singh, 2003) are compiled in Table 4.2.

4.2 Analytical Approaches

Analytical approaches constitute the derivation of hydraulic geometry of stable alluvial channels, from theoretical considerations of laws governing fluvial hydraulics and sediment transport under the dynamic equilibrium.

TABLE 4.2: Average values of exponents, b_p, f_p, and m_p by various authors (after Singh (2003))

Author	Exponents		
	b_p	f_p	m_p
Leopold and Maddock (1953)	0.5	0.4	0.1
Wolman (1955)	0.42	0.45	0.05
Ackers (1964)	0.42	0.43	0.15
	0.43	0.43	0.14
	0.53	0.35	0.12
Langbein (1964)	0.53	0.37	0.1
Carlston (1969)	0.461	0.383	0.155
	0.499	0.32	0.18
Thornes (1970)	0.4	0.34	0.25
Knighton (1974)	0.61	0.31	0.08
Smith (1974b)	0.54	0.23	0.23
	0.46	0.16	0.38
Parker (1979)	0.5	0.415	0.085
Lane and Foster (1980)	0.46	0.46	0.081
Allen et al. (1994)	0.557	0.341	0.104

4.2.1 Theory of Conservation of Mass and Momentum

Smith (1974b) derived the form parameters of width, depth, velocity and slope for the downstream changes in the channel geometry from three necessary conditions for the existence of steady state, finite width channel as a surface of $z = z(x, y, t)$; (1) sediment mass is conserved during transport, (2) the channel has the form just sufficient to carry its total water discharge and (3) the channel has the form just sufficient to carry its total sediment discharge. The hydraulic geometry thus theoretically derived from a mathematical expression with the following assumptions; (1) the channel has finite width, which is important as it specifies certain essential boundary conditions, (2) the channel be carved in non-cohesive materials, with most of the sediment transport occurring near the channel bed, which is a fair approximation to reality for larger class of channels and (3) freedom is there to

choose a time scale for which the channel has an essentially steady-state form, which is reasonable in the light of Schumm and Lichty's (1965) argument. By applying the continuity equation for water discharge, Manning's equation for the magnitude of water flux in the downstream direction and conservation principle for the flux of sediment mass, he derived the following mathematical expression for the channel model:

$$\frac{\partial z}{\partial t} = \frac{\partial}{\partial x}\left(k_1^n k_2 d^{5n/3} S_w^{m+n/2}\right) - \frac{\partial}{\partial y}\left(k_1^n k_2 k_3 d^{5n/3} S_w^{m+n/2}\right)\frac{\partial d}{\partial y} \tag{4.32}$$

$$\int_{y_1}^{y_2} k_1 d^{5/3} S_w^{1/2} dy = Ax \tag{4.33}$$

$$\int_{y_1}^{y_2} k_1^n k_2 d^{5n/3} S_w^{m+n/2} dy = Lx \tag{4.34}$$

where:

z : is the elevation of the channel bed.

x and y : are the downstream and transverse directions, respectively.

K_1, K_2, A and L : are the constants.

S_w : is the water surface slop.

d : is the depth.

m and n : usually take the values between one and four.

A similarity solution was sought for the derivation of the hydraulic geometry as it according to Smith (1974b) has a physical significance in that it implies some form of self-similarity in the system under consideration, which in this case could reside in the form of cross-section as one move downstream. Smith (1974b) obtained the following hydraulic geometry for the reasonable values of $m = n = 2$:

$$\text{Width} \propto Q^{7/11} \tag{4.35}$$

$$\text{Depth} \propto Q^{3/11} \tag{4.36}$$

$$\text{Velocity} \propto Q^{1/11} \tag{4.37}$$

$$\text{Slope} \propto Q^{-2/11} \tag{4.38}$$

which is in a good agreement with that obtained by Leopold and Maddock (1953).

4.2.2 Hydraulic Geometry by Echelon Matrix Procedure

Martin (1996) in his work demonstrated the development of the approach which was based on the work of Kawas (1985) and Martin (1988), for the prediction of stable channel geometry in alluvium by the application of echelon matrix procedure of dimensional analysis. The study is based on the normalization of the cross-sectional data obtained from different sources. The echelon matrix procedure of dimensional analysis was used to evolve the potential basis of correlation of alluvial channel data. The correlation in terms of non-dimensional functional form:

$$\left[\frac{B}{y}, \frac{Qg^2}{v_s^5}, \frac{Q_s g^2}{v_s^5}, \frac{v_s}{(gy)^{1/2}}\right] = 0 \tag{4.39}$$

The expression for relative width was given as:

$$\frac{B_n}{y} = 10^{-a}\left(\frac{Q_n g^2}{v_s^5}\right)^b \tag{4.40}$$

where:

a and b : are the constants which depend on fall velocity Froude number.

Q_n and B_n : are the discharge and width for the normalized channel.

v_s : is the fall velocity.

y : is the depth of flow.

Expression for flow depth was given as:

$$y = 0.067Q^{0.284}S_0^{-2.44} \tag{4.41}$$

Flow depth with the influence of the sediment concentration:

$$yc = \frac{y(1+\psi_C)}{1+0.13C^{0.32}\psi_C} \tag{4.42}$$

$$\psi_C = 3.432(540/C)^{-5.682} \tag{4.43}$$

where C is the sediment concentration. The expression for the longitudinal slope:

$$S_0 = 10^{-3}\left(\frac{1+1.56Q^{1.36}}{1+5.06Q^{1.36}}\right)Q^{-0.255} \tag{4.44}$$

Lacey's regime equations were compared against available data and some corrections were made and comparison was made between available observed data and that of data obtained from Lacey's modified equations and with this approach, which showed this approach can be applied successfully over a wide range of channel sizes.

4.3 Extremal Hypotheses

As described earlier in this study that for the derivation of stable channel hydraulic geometry, three independent equations are required. While the two equations are readily available in the form of sediment transport equation and flow resistance equation, the third necessary equation in order to find a unique solution of the system, is given in some form of a constraint or an extremal hypothesis based on the minimization or maximization of certain parameter for the channel flow.

4.3.1 Theory of Minimum Energy Degradation Rate

Brebner and Wilson (1967) derived a equation for the hydraulic geometry of stable channel by applying the principle of minimum rate of energy degradation which is the isothermal form of the thermodynamic principle of minimum entropy production rate and is similar to the principle of least work, to a generalized excess energy gradient equation of Durand type, for two phase flow. They used the minimization principle in the form, "For an isothermal system in equilibrium the rate of energy degradation is the minimum allowed by the boundary conditions and the applicable phenomenological laws". From the energy balance, the total power production in a uniform stream is $\rho gQiL$ and if the total weight of fluid is ρgAL then, Energy degradation rate:

$$\frac{\rho gQiL}{\rho gAL} = ui \tag{4.45}$$

Durand equation for two phase flow may be given as:

$$\frac{j - i_w}{Ci_w} = Z\left(\frac{gR_h}{u^2}\right)^{1.5} \tag{4.46}$$

where:

ρ : is the density of liquid phase.

g : is the gravitational acceleration.

Q : is the discharge.

i : is the hydraulic gradient.

L : is the length.

V : is the mean flow velocity.

j : is the friction gradient.

i_w : is the hydraulic gradient of equivalent clear water flow.

Z : is the function of particle properties.

R_h : is the hydraulic radius.

They stated that a certain value of Froude number is obtained, by the adjustment of the hydraulic radius of the waterway for the minimization of the energy

degradation rate, which is a function of particle properties and concentration and is independent of the discharge. The derived hydraulic geometry for a stable channel was:

$$B_r = Q_r^{0.471},\ R_r = Q_r^{0.353},\ i_r = Q_r^{-0.118} \tag{4.47}$$

where $Q_r = Q/Q_d$, $B_r = B/B_d$, $R_r = R/R_d$, $i_r = i/i_d$, Q_d, B_d, R_d, and i_d are the discharge, width, depth and slope for the reference canal. The method of application of the principle of minimum rate of energy degradation to the Durand type equation successfully derived the hydraulic relations for stable channel in the laboratory experiments.

4.3.2 Theory of Minimum Stream Power

Chang (1979a) defined the hypothesis of minimum stream power as "for an alluvial channel, the necessary and sufficient condition of equilibrium occurs when the stream power per unit channel length γQS is minimum subject to given constraints. Hence, an alluvial channel with water discharge Q and sediment load Q_s as independent variables tends to establish its width, depth and slope such that γQS is a minimum. Since Q is a given parameter, minimum γQS also means minimum channel slope S_0". For a hydraulic system, the hypothesis of minimum stream power may be derived from the principle of virtual work for a mechanical system. Chang (1982) extended the hypothesis of minimum stream power as "the equilibrium geometry of an alluvial channel reach of equal discharge is so adjusted that the power expenditure is a minimum subject to the given constraints. Minimum power expenditure for the channel reach is equivalent to equal power expenditure per unit channel length or uniform energy gradient along the channel". Chang (1980a) derived relations for channel width, depth and slope by using Engelund and Hansen's (1967) flow resistance equation and DuBoys' (Graf, 1998) bed load equation. Chang (1980a) needs observations on sediment concentration, which limits the scope osf designing a new channel.

4.3.3 Theory of Minimum Energy Dissipation Rate

Yang et al. (1981) derived the exponents of the hydraulic geometry relationship given by Leopold and Maddock (1953), theoretically by the application of the theory of minimum rate of energy dissipation. The general statement of this theory is "a system is in equilibrium condition when its rate of energy dissipation is at its minimum value. This minimum value depends on the constraints applied to the system. When a system is not in an equilibrium condition, its rate of energy dissipation is not at its minimum value. However, the system will adjust in such a manner that the rate of energy dissipation can be reduced until it reaches the minimum and regains equilibrium". The exponents of hydraulic geometry relationship proposed by Leopold and Maddock (1953) were determined by using the theory of minimum rate of energy dissipation in conjunction with the Manning-Strickler equation and the dimensionless unit stream power equation for sediment transport (Yang, 1972). The rate of energy dissipation was given as:

$$\Phi = \frac{n^2 l Q^2 \left(\gamma Q + \gamma_s Q_{sed}\right) \left(B + 2y\right)^{4/3}}{\left(By\right)^{10/3}} \tag{4.48}$$

where B is the channel width, y is the average depth, Q is the water discharge, γ is the specific weight of water, γ_s is the specific weight of sediments, Q_{sed} is the sediment discharge, n is the roughness coefficient and l is reach length.

It was assumed that the total rate of energy dissipation of a river is the sum of that due to transportation of water and sediments. It was further assumed that water and sediment discharges are constraints which can be determined by the characteristics of the watershed. They restricted their analysis to the channels which were approximately rectangular in shape and the hydraulic exponents for width, depth and slope were 9/22, 9/22 and -2/11 respectively. These values were in good agreement with laboratory data published by Barr et al. (1980) and the theoretically derived hydraulic geometry exponents were in general agreement with observed at-a-station values from natural river gauging stations.

4.3.4 Theory of Maximum Sediment Transport Rate

White et al. (1982) derived the geometric and hydraulic parameters of a stable channel by using a variational principle which is according to them, "for a particular water discharge and slope, the width of the channel adjusts itself to maximize the sediment transport rate".

It has been explained as well by White et al. (1982) that this hypothesis of maximum sediment transport rate is equivalent to the concept of minimum stream power i.e. for a give discharge and slope, the maximum in sediment concentration corresponds to the minimum slope for the given discharge and the previously calculated maximum sediment concentration. Six variable were considered in this study that describe the channel system; average velocity u, average depth y, slope S_0, discharge Q, sediment concentration C and channel width B. The equations to relate these variables were the continuity equation of water flow, sediment transport formula of Ackers and White (1973), flow resistance formula of White et al. (1980) together with the condition that the sediment transport should be maximized.

In the work by White et al. (1982) the discharge and slope were assumed to be imposed and corresponding values of u, y, C and B were determined with the assumption of steady uniform flow and non-cohesive bed and bank material. Comparison with the data obtained from laboratory experiments showed reasonable agreement with the wide range of practical applications except the prediction of slope where there was slight tendency to overestimate and the prediction of width where there was a tendency to under predict for very large sand channels and for meandering laboratory channels.

4.3.5 Theory of Maximum Friction Factor (MFF)

Davies and Sutherland (1980, 1983) hypothesized this theory. According to them "if the flow of a fluid past an originally plane boundary is able to deform the boundary to a non-planar shape, it will do so in such a way that the friction factor increases. The deformation will cease when the shape of the boundary is

that which gives rise to a local maximum friction factor. Thus, the equilibrium shape of a non-planar self-deformed flow boundary or channel corresponds to a local maximum friction factor".

Davies (1980) successfully tested the hypothesis for lower flow regime bedforms. Whittaker and Jaeggi (1982) also observed the maximum friction factor for bank-full stage in meander bends and in a laboratory channel respectively. The Darcy-Weisbach friction factor with the continuity equation $Q = Byu$, can be defined as:

$$f_{Darcy} = \frac{8gB^2y^3S}{Q^2} \tag{4.49}$$

Maximization of friction factor thus implies:

$$MFF \Rightarrow \max \frac{B^2y^3S}{Q^2} \tag{4.50}$$

where B and y are the channel width and depth, Q is the water discharge and S is the mean channel slope. Davies and Sutherland (1983) compared their hypothesis with that of minimization hypotheses, the comparison is summarized in Table 4.3.

Davies and Sutherland (1983) concluded that the minimization hypotheses will give the correct predictions if they are implied under similar conditions to that of MFF. A significant fact is that Q and Q_{sed} have always been assumed as independent variables in Chang's MSP hypothesis and most of the employed data reflect constraints of independent Q and S or of Q and Q_{sed} in Yang's MUSP hypothesis as well. It is demonstrated that Chang's MSP hypothesis and Yang's MUSP hypothesis are the special cases of Davies and Sutherland's (1980) maximum friction factor hypothesis.

4.3.6 Theory of Rate of Change of Unit Stream Power

Cheema et al. (1997) utilized the concept of unit stream power (Yang, 1972) and presented an extremal hypothesis, namely, the rate of change of unit stream power

TABLE 4.3: Summary of implication of hypotheses (Davies and Sutherland, 1983)

Independent variables	Hypotheses		
	Minimum unit stream power (MUSP) (Yang, 1976)	Minimum stream power (MSP) (Chang, 1979a) (Chang, 1979b) (Chang, 1980a) Chang (1980b)	Maximum friction factor (MFF) (Davies and Sutherland, 1983)
Q, Q_{sed} $(Q_{sed} = fn(\tau))$	max y, min S	max y, min S	max y, min S
Q, Q_{sed} $(Q_{sed} = fn(QS))$	max y, S fixed	NA	max y, S fixed
Q, S $(G_s = fn(\tau))$	max y, max G_s	NA	max y, max G_s
Q, S $(G_s = fn(QS))$	max y, G_s fixed	NA	max y, G_s fixed
Q, y	min S, min G_s	min S, min G_s	max S, max G_s

with respect to the channel width which then resulted in the form of a width control parameter for the determination of stable width of an alluvial channel.

In the hypothesis the stable width of an alluvial channel has been defined as a width at which a channel could adopt a new width with minimal change in energy expenditure per unit change in width (minimal change in the unit stream power with respect to the channel width for a fixed slope). For a fixed slope, the rate of change of unit stream power with respect to the top width was represented as:

$$\frac{d\left(uS\right)}{dB} = -S\frac{Q}{A^2}\frac{dA}{dB} \tag{4.51}$$

and the change rate of kinetic energy as:

$$\frac{d\left(\frac{u^2}{2g}\right)}{dB} = -S\frac{Q^2}{gA^3}\frac{dA}{dB} \tag{4.52}$$

The width control parameter W_p, was then given as

$$W_p = \frac{Q^2}{gA^3}\left(y + bS_d\right) \tag{4.53}$$

where u is the average velocity of flow, S is the slope of energy grade line, B is the

top width of channel, Q is the flow discharge, A is cross-sectional area of channel, y is the depth of channel, b is the bed width and S_d is the slope of depth-width curve given by

$$S_d = 1.82\left(\frac{y}{t}\right)^2 - 1.42\left(\frac{y}{t}\right) + 0.026 \tag{4.54}$$

For a given discharge and slope, a minimum value of the width control parameter has been regarded as the criterion for stable width of a channel. In the work, Cheema et al. (1997) criticized the approach of Chang (1980a) and subsequently the approach of White et al. (1982) by stating "in an environment where channels flow by gravity, the bed slope is usually one of the given design parameters. An approach based on minimizing the slope cannot be used for designing a channel for a fixed slope".

4.3.7 Theory of Maximum Flow Efficiency (MFE)

Huang and Nanson (2000) justified the use of extremal hypotheses in explaining appropriately the self-adjusting mechanism of alluvial channels and explained the mechanism with the basic flow relations of continuity, resistance and sediment transport by introducing a channel form factor (width/depth ratio). According to Huang and Nanson (2000) "natural channel flow is able to reach an optimum state (Maximum Flow Efficiency (MFE), defined as the maximum sediment transporting capacity per unit available stream power) with regard to the adjustment of channel form such that rivers exhibit regular hydraulic geometry relations at dominant or bankfull stage".

By using width/depth ratio as a non-dimensional channel shape factor ($\zeta = B/y$) the unknown dependent variables were brought down from four to three (width/depth ratio, slope and velocity). With width/depth ratio, Lacey's (1958) flow equation and DuBoys' (Graf, 1998) sediment transport formula, the averaged

optimal channel geometry relations were derived:

$$B \propto Q_b^{0.04} Q^{0.426} \propto \left(\frac{Q_b}{Q}\right)^{0.04} Q^{0.466} \tag{4.55}$$

$$y \propto Q_b^{-0.184} Q^{0.526} \propto \left(\frac{Q_b}{Q}\right)^{-0.184} Q^{0.342} \tag{4.56}$$

$$S_0 \propto Q_b^{0.526} Q^{-0.678} \propto \left(\frac{Q_b}{Q}\right)^{0.526} Q^{-0.152} \tag{4.57}$$

where B, y, S_0, Q, and Q_b are width, depth, slope, dominant or bank-full discharge and total bed load discharge, respectively. In practical circumstances when the Q_b is not known, the following form of downstream hydraulic geometry relations was given:

$$B \propto Q^{0.478} S_0^{0.076} \tag{4.58}$$

$$B \propto Q^{0.289} S_0^{-0.350} \tag{4.59}$$

$$u \propto Q^{0.233} S_0^{0.274} \tag{4.60}$$

This theory is thus the combination of the theory of maximum sediment transport capacity and the theory of minimum stream power. Huang and Nanson (2000) also reasoned that the existence of the optimum conditions of maximum flow efficiency can be physically explained by the general principle of least action in the variational theory of mechanics.

4.3.8 Family of Hydraulic Geometry Relations (Downstream Hydraulic Geometry)

Singh et al. (2003a,b) derived the family of downstream hydraulic geometry relations for a river in its dynamic equilibrium by applying the combination of two hypotheses, namely; principle of maximum entropy and minimum energy dissipation rate. In the work of Singh et al. (2003a,b), it has been hypothesized that for a given discharge the spatial variation of the stream power of a channel is accomplished by the spatial variation in channel form and hydraulic variables and the change in stream power is distributed among the changes in channel form and hydraulic variables. Considering the channel roughness, width and depth of flow as the controlling variables and using Manning's equation, Singh et al. (2003a,b) derived a set of three equations as:

$$P_n = \frac{2n\gamma Q^3}{B^2 y^{10/3}} \frac{(dn/dx)}{(d\Omega/dx)} \tag{4.61}$$

$$P_B = -\frac{2n^2\gamma Q^3}{B^3 y^{10/3}} \frac{(dB/dx)}{(d\Omega/dx)} \tag{4.62}$$

$$P_y = -\frac{10n^2\gamma Q^3}{3B^2 y^{13/3}} \frac{(dh/dx)}{(d\Omega/dx)} \tag{4.63}$$

where P_n, P_B and P_y are the proportions of the adjustment of stream power by friction, channel width and depth of flow respectively, n, γ, Q, Ω, y, B and x are Manning's roughness coefficient, weight density of water, flow discharge, stream power, flow depth, channel width and the direction of flow, respectively. Application of the principle of maximum entropy to a river in its dynamic equilibrium resulted in following four possibilities: (1) $P_n = P_B$, (2) $P_B = P_y$, (3) $P_n = P_y$, and (4) $P_n = P_B = P_y$. Using Engelund and Hansen's sediment transport equation, the hydraulic geometry relations for gravel rivers and sandy or alluvial rivers were derived for all the possibilities mentioned above.

4.3.9 Family of Hydraulic Geometry Relations (At-a-station Hydraulic Geometry)

Singh and Zhang (2008a,b) utilized the combination of two hypotheses namely principle of maximum entropy and minimum energy dissipation rate and extended the work of Singh et al. (2003a,b) to derive the at-a-station hydraulic geometry of alluvial channels. It has been hypothesized that at a given station with varying discharge, the temporal variation of the stream power of a channel is accomplished by the temporal variation in channel form and hydraulic variables and the change in stream power is distributed among the changes in channel form and hydraulic variables. The stream power of a channel was expressed as:

$$\Omega = \gamma \alpha B y^{\beta_1} S_e^{3/2} \tag{4.64}$$

where, α is the roughness measure, S_e is energy slope and β_1 is an exponent. It has been hypothesized that, the four variables on the right side of this equation: B, y, α, S will be adjusted by the channel cross-section in order to adjust or minimize its stream power for the influx of discharge varying with time and can be regarded as the controlling variables. Following equations representing the proportions of the temporal changes of stream power due to the temporal rates of adjustment of controlling variables were obtained:

$$P_B = \frac{\gamma \alpha y^{\beta_1} S_e^{3/2} dB/dt}{d\Omega/dt} \tag{4.65}$$

$$P_y = \frac{\gamma \alpha B y^{\beta_1 - 1} \beta S_e^{3/2} dh/dt}{d\Omega/dt} \tag{4.66}$$

$$P_\alpha = \frac{\gamma B y^{\beta_1} S_e^{3/2} d\alpha/dt}{d\Omega/dt} \tag{4.67}$$

$$P_S = \frac{3}{2}\frac{\gamma\alpha B y^{\beta_1} S_e^{1/2} dB/dt}{d\Omega/dt} \tag{4.68}$$

where P_B, P_y, P_α, and P_S are the proportions of the temporal changes of stream power due to the temporal rates of adjustment of width, depth, friction and slope, respectively. Application of the principle of maximum entropy to the cross-section in dynamic equilibrium gives rise to following eleven possibilities: (I) $P_B = P_y$, (II) $P_B = P_\alpha$, (III) $P_B = P_S$, (IV) $P_y = P_\alpha$, (V) $P_y = P_S$, (VI) $P_\alpha = P_S$, (VII) $P_B = P_y = P_\alpha$,(VIII) $P_B = P_\alpha = P_S$, (IX) $P_B = P_y = P_S$, (X) $P_y = P_\alpha = P_S$, and (XI) $P_B = P_y = P_\alpha = P_S$. Subsequently the at-a-station hydraulic geometry relations were derived.

4.3.10 Theory of Maximum Sediment Transport Efficiency

Millar (2005) derived a system of rational equations for gravel-bed rivers with stable banks by using the optimality theory which was based on the assumption that there corresponds an optimal solution for reach-averaged equilibrium hydraulic geometry under the constraints of the imposed discharge, sediment transport and bank stability. The optimum condition was defined as the maximum sediment transport efficiency, η:

$$\eta = \frac{G_b}{\rho Q_f i_a} \tag{4.69}$$

where G_b is bed material transport rate at the formative (bank-full) discharge (kg/s), ρ is the density of water (kg/m^3), Q_f is formative discharge, and i_a is the average channel gradient. Here it is to be noted that minimization of η is equivalent to maximizing G_b under conditions of constant $\rho Q_f i_a$ (White et al., 1982) and is equivalent to minimization of i_a or $\rho Q_f i_a$ under condition of constant G_b (Chang, 1979a, 1980a). Theoretical dimensionless equations for width, depth, slope, width/depth ratio, and meandering-braiding transition were derived by employing dimensionless variables such as discharge, sediment concentration, and relative bank strength, μ', which has been defined as the ratio of the critical

shear stresses for bank and bed sediments are as follows:

$$B^* = 16.5 Q^{*0.70} i_a^{0.60} \mu'^{-1.10} \tag{4.70}$$

$$y^* = 0.125 Q^{*0.16} i_a^{-0.62} \mu'^{0.64} \tag{4.71}$$

$$B/y = 155 Q^{*0.53} i_a^{1.23} \mu'^{-1.74} \tag{4.72}$$

where $Q^* = Q_f/(d_{50}^2\sqrt{g d_{50}(s-1)})$, $B^* = B/d_{50}$, $y^* = y/d_{50}$, B is channel width, y is average channel depth, d_{50} is median particle size, and s is specific gravity of bank sediment (2.65 assumed). Relative bank strength, μ', has been used to parameterize the influence of riparian vegetation on bank strength and has been evaluated by calibrating against observed width/depth ratio.

4.3.11 Griffiths' Study on Extremal Hypotheses (1984)

It has been illustrated in the study of Griffiths (1984) that the results obtained by combining the various extremal hypotheses with conventional sediment transport and flow resistance equations lead to conclusions that are incompatible with data obtained from flume channels in equilibrium and with observations from stable natural rivers. The extremal hypotheses he used in his study were, minimum stream power (MSP) (Chang, 1980a), minimum unit stream power (MUSP) (Yang and Song, 1979), minimum energy dissipation rate (MEDR) (Yang et al., 1981), maximum friction factor (MFF) (Davies and Sutherland, 1980) and maximum sediment transport rate (MSTR) (White et al., 1982). Following conclusions can be drawn out of the study:

1. For all the hypotheses except MSTR, where channel slope replaces sediment discharge as a specified quantity, it is assumed that water discharge, sediment discharge and sediment size are independent and specified and all these

hypotheses are incompatible with conventional sediment transport and flow resistance equations.

2. The result that the Einstein sediment discharge and Schields entrainment function are nearly constant in wide, straight and unconstrained alluvial reaches in equilibrium is obtained when these hypotheses are combined with conventional equations and the magnitude of the constants depends on the hypothesis and the equations used. But the data from flume channels in equilibrium demonstrate that Einstein sediment discharge and Schields entrainment function satisfy a highly variable bed load function and Schields entrainment function is highly variable for both, gravel and sand bed, stable natural channels at bank full flow.

3. Friction factor exhibits no maximum value when channel width, depth and slope are dependent variables in MFF hypothesis.

It was justified that redefinition is required in formulations of the mentioned hypotheses to turn the illusion of attractively simple solution into fact.

4.4 Verification with Datasets

Verification of the approaches discussed in the previous section has been carried out by applying the methods with the field data of Church and Rood (1983).

4.4.1 Description of the Dataset

Church and Rood (1983) published a catalogue of hydraulic geometry measurements for the study of alluvial rivers channels in regime (in the sense of Inglis and Lacey) through the extensive search of the published literature. The catalogue defines a set of consistent criteria for description of river channels. Although more or less arbitrary, they confirm with usually preferred field practices. Ten river

channel morphological types are defined as a basis for discriminating channels that may be compared meaningfully.

The catalogue contains 499 sets of data out of which about 40 percent represent Canadian rivers, 50 percent American rivers and about 10 percent British rivers. Almost all are located in humid or semi-arid temperate environments. The range of data for various hydraulic parameters as has been given in Church and Rood (1983) catalogue is compiled in Table 4.4. Each data set pertains either to an individual cross-section, or to the average of a set of adjacent sections within the homogeneous reach. The data in the catalogue have been selected on the following criteria (Church and Rood, 1983):

1. The method of measurement is known, so that the analysis may be carried out on assuredly comparable measurements.
2. River channel type is classified so that, within the limits of the scheme of classification, comparable regime types may be abstracted and compared.
3. Data are internally consistent for each station.
4. Each data set is relatively complete: at least, information of channel bed material must be included.

For the verification of the methods of stable alluvial channel design, discussed in this study, Church and Rood's (1983) river channel data have been subdivided in to three categories based on the median bed material sizes, namely: sand range ($0.063 \text{ mm} \leq d_{50} < 1 \text{ mm}$), gravel range ($1 \text{ mm} \leq d_{50} < 64 \text{ mm}$) and cobble or boulder range ($64 \text{ mm} \leq d_{50}$).

For the verification of the methods based on power function theory, values of coefficients, a, c, and k of Equation (4.30) are required. According to Leopold and Maddock (1953), "width and depth for a given discharge vary widely from one cross-section to another and, therefore, the intercept values, a, c, and k will vary". In order to obtain the values of coefficients mentioned above, about 33% of data from each of the data range (i.e. sand, gravel and cobble or boulder) have

TABLE 4.4: Ranges of various hydraulic parameters

Hydraulic Parameters	Range
Bank-full discharge Q, cumecs	0.06 – 16950
Slope S	0.00004 – 0.081
Water surface width B, m	2 – 900
Hydraulic mean depth D, m	0.04 – 13.92
Mean velocity u, m/s	0.09 – 4.7
Median bed material size, mm	0.15 – 268

been taken and the coefficients thus calibrated for each set of exponents, b_p, f_p, and m_p given by various authors. Average values of calculated coefficients were used to compute widths and depths. Average values of calculated coefficients were used to compute widths and depths (Figure 4.1). Therefore, for all the methods including those which are based on power function theory, widths and depths were computed for the remaining sets of data.

4.4.2 Results and Discussion

Prediction of width by Lacey's method for the entire dataset was good and when the method was applied to the subcategories of dataset, the prediction of width was better for gavel range of data (Figure 4.2). For the Blench's method of stable alluvial channel design, the prediction of channel width was good for gravel range and the prediction of flow depth was good for cobble or boulder range (Figure 4.3). Figure 4.4 shows the prediction of channel width and flow depth for Simons and Albertson's (1960) approach. It is apparent that the method predicted the width very good in gravel range and the depth prediction was very good for cobble or boulder range of data. The results are shown in Figure 4.5 for the power function theory (Leopold and Maddock, 1953). Prediction of width and depth by Smith's (1974b) theory of conservation of mass and momentum are shown in Figure 4.6. For the theory of minimum energy degradation rate Brebner and Wilson (1967) the results are depicted in Figure 4.7. For the exponents of hydraulic geometry derived by Yang et al.'s (1981) theory of minimum energy dissipation

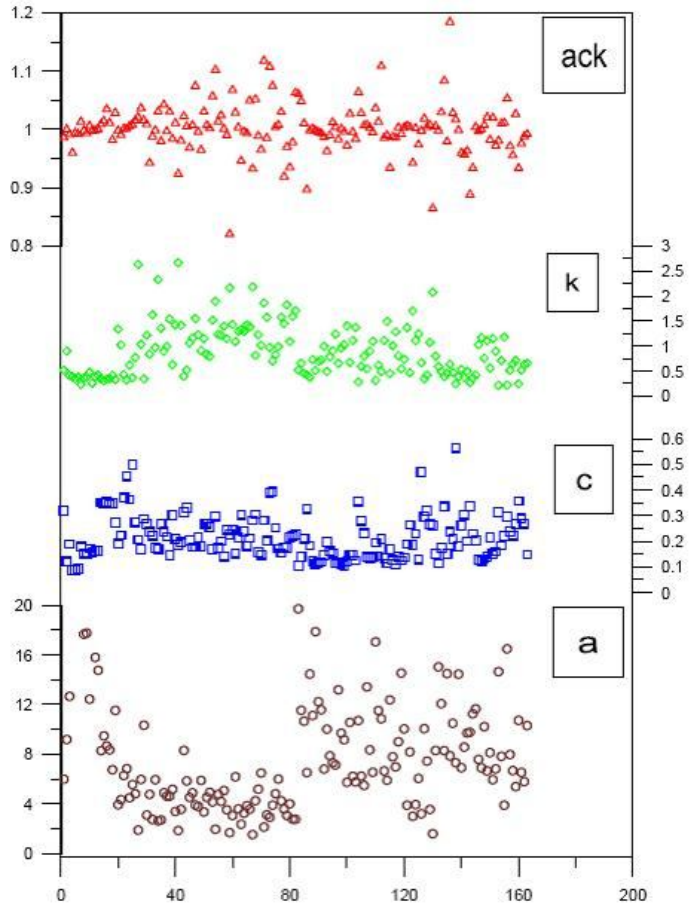

FIGURE 4.1: Calibration of coefficients

rate (MEDR), the predicted values of width and depth are shown in Figure 4.8. Prediction of hydraulic geometry (width and depth) of stable alluvial channel by the theory of maximum flow efficiency (Huang and Nanson, 2000) is shown in Figure 4.9. Channel side slopes for the prediction of downstream hydraulic geometry by Singh et al.'s (2003b) approach were calculated using Smith's (1974a) equation and Manning's roughness coefficients were calculated by Strickler's formula (Chang, 1988) and the results for the predicted values of width and depth are depicted in Figure 4.10.

4.4.3 Summary of the Results

Comparison among the results has been made on the basis of the coefficient of determination, R^2. In hydraulic geometry analysis, R^2 numerically represents the

amount of variation that can be explained by the selected independent variable. If R^2 is 1.0, there is no variation. The closer the R^2 value is to zero, the less useful the relation, and the wider the scatter in the data.

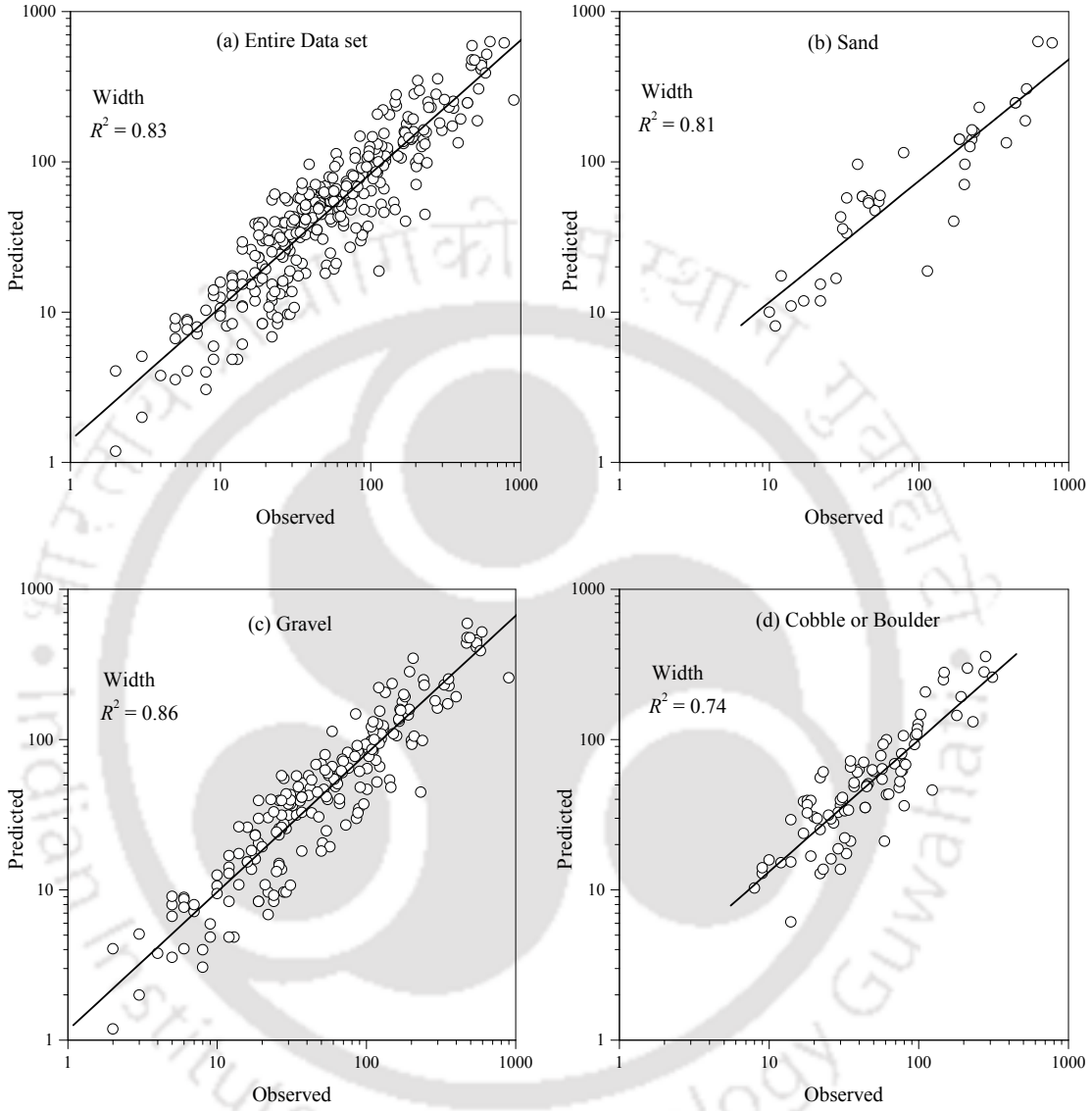

FIGURE 4.2: Prediction by Lacey's method

By inspection of R^2 values (Table 4.5), it is clear that the methods based on regime concept predicted the width and depth well in the entire range of data and especially in the gravel range. Theory of conservation of mass and momentum (Smith, 1974b), theory of minimum energy degradation rate Brebner and Wilson (1967), and the theory of minimum energy dissipation rate (Yang et al., 1981) predicted the depth very well in the cobble and boulder range with R^2 value of 0.87 and the prediction was good for rest of the ranges. Prediction of width

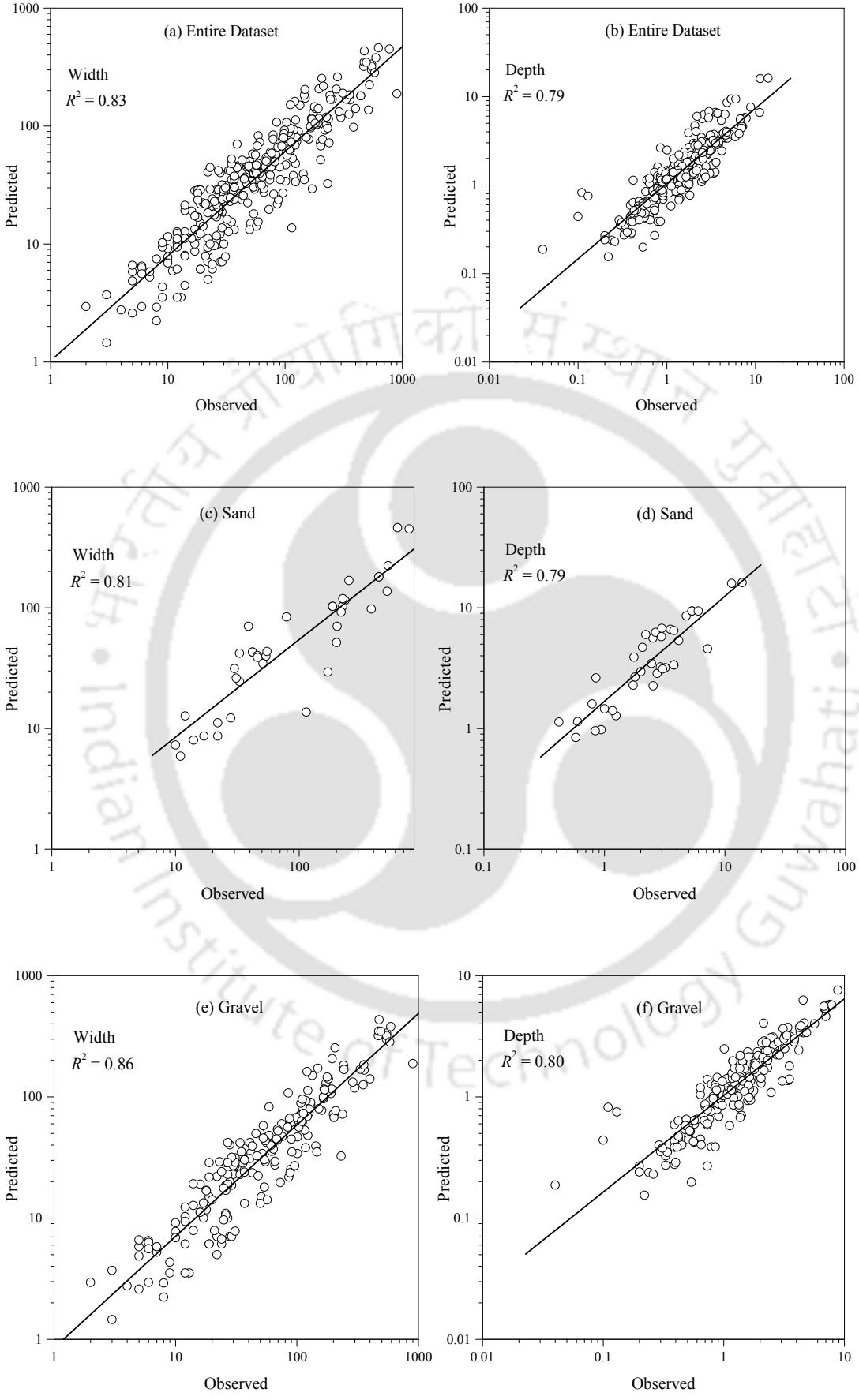

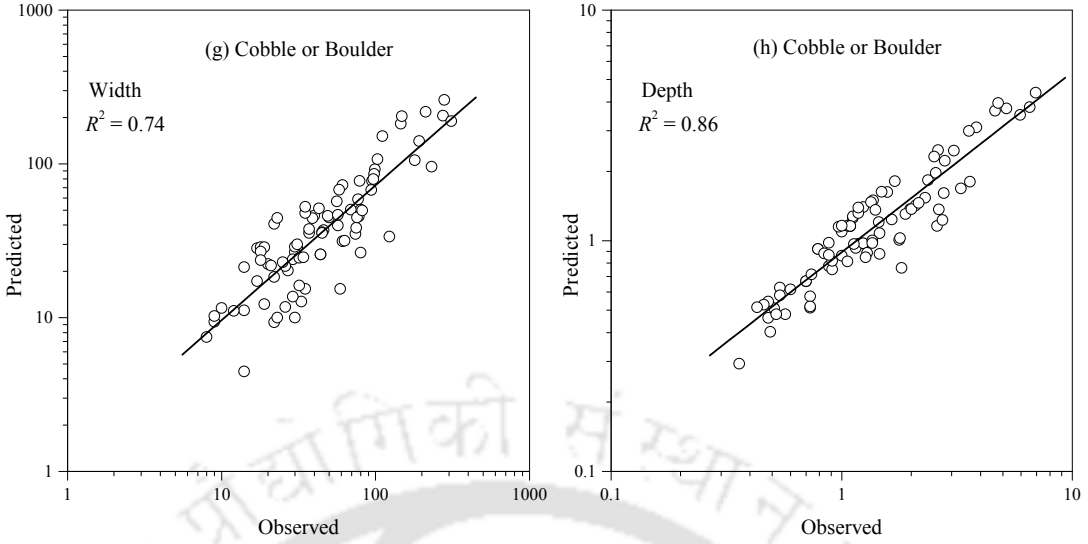

FIGURE 4.3: Prediction by Blench's method

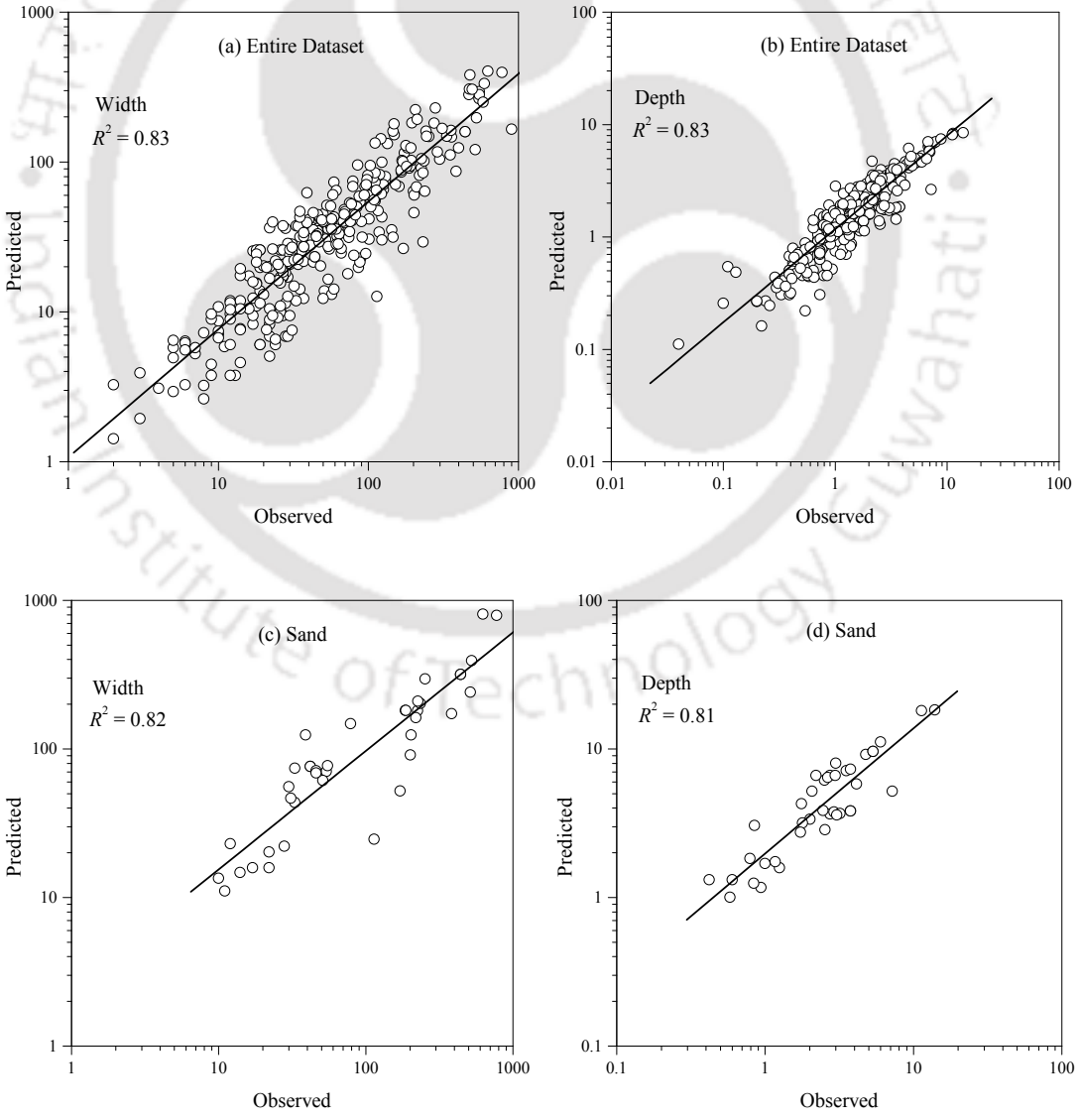

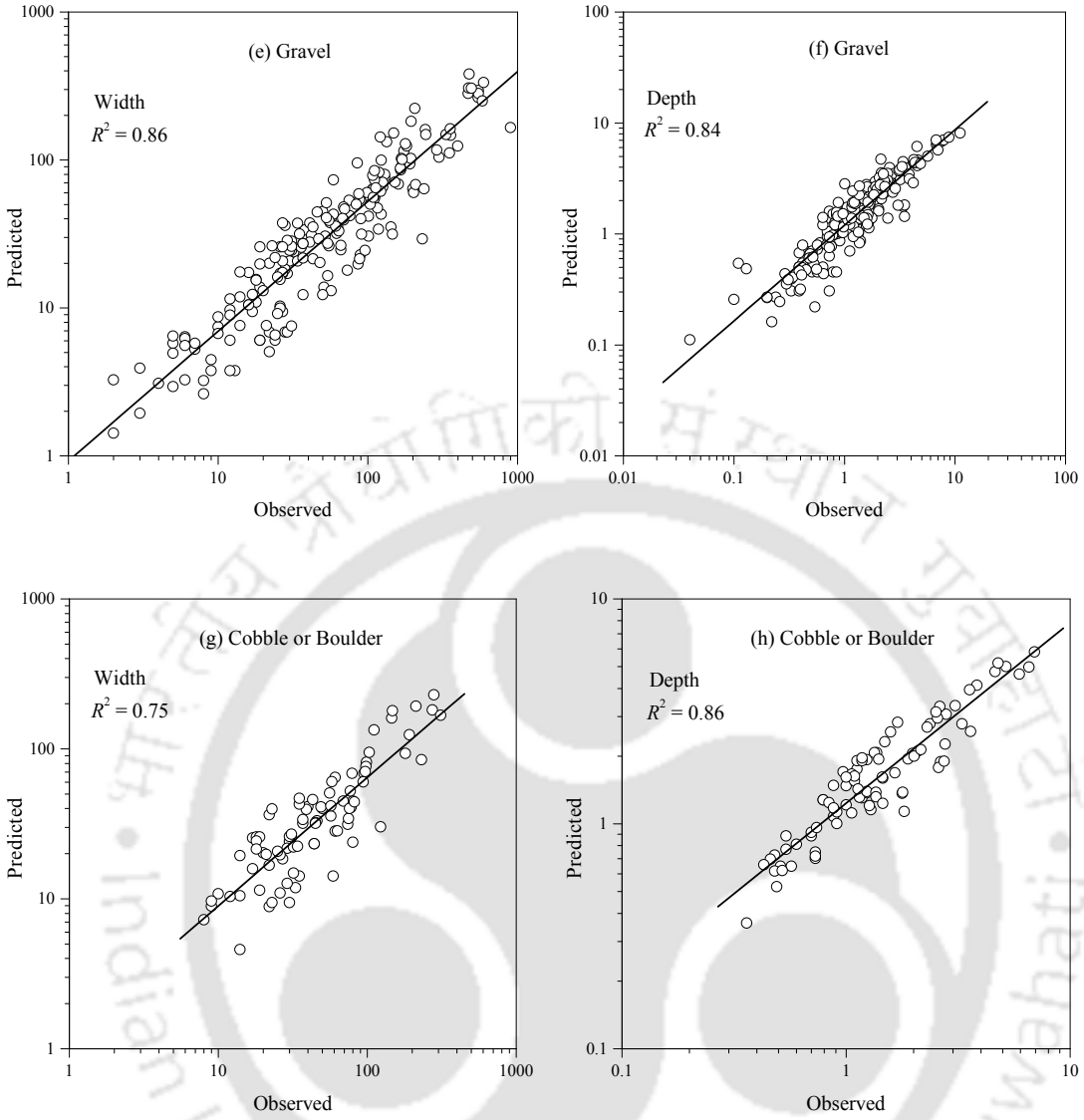

FIGURE 4.4: Prediction by Simons and Albertson's method

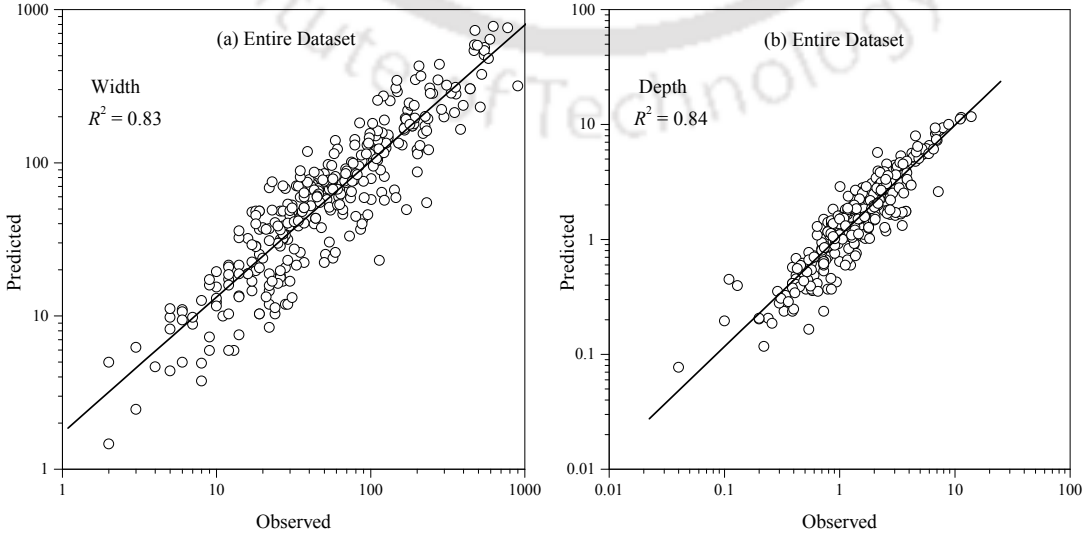

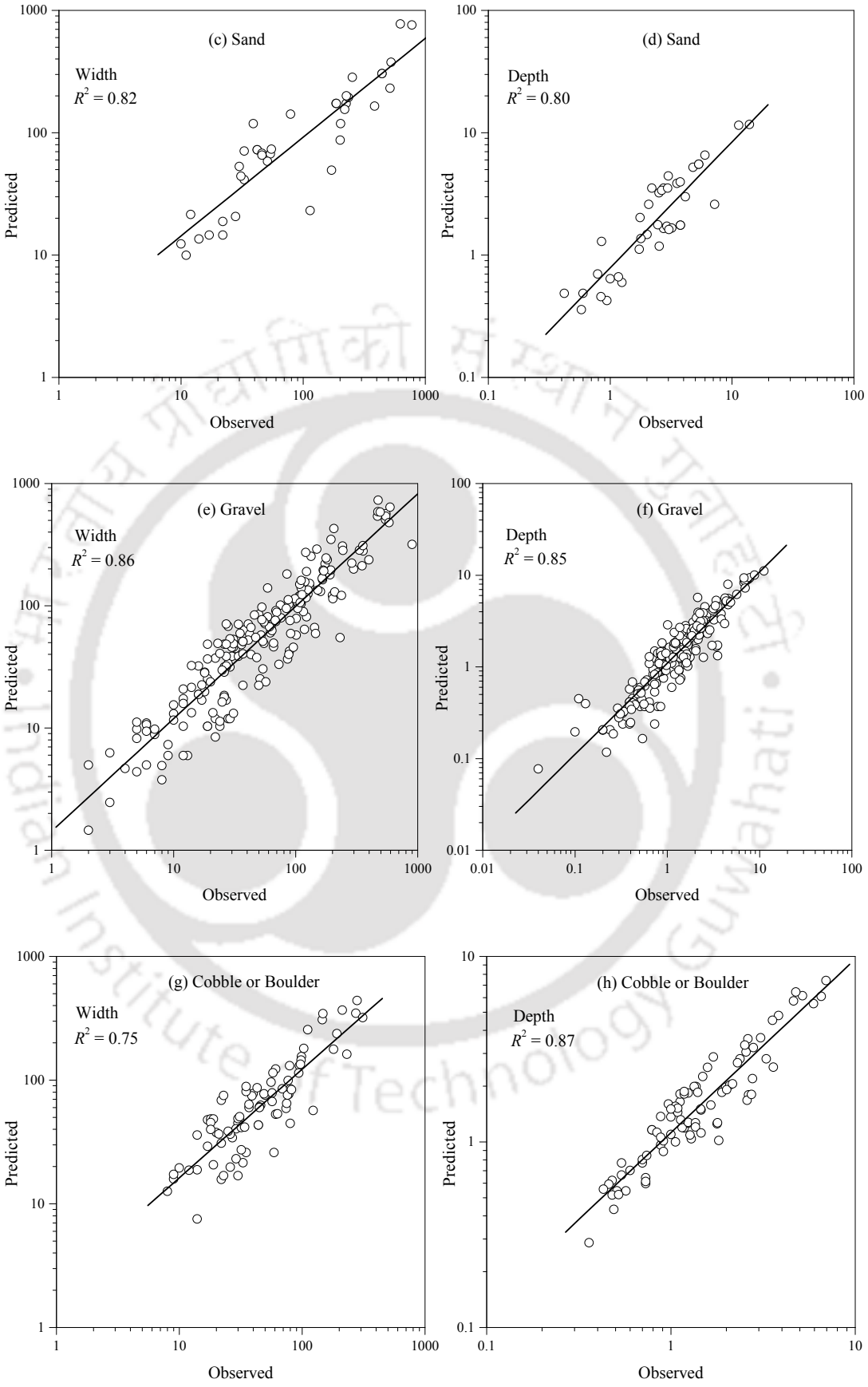

FIGURE 4.5: Prediction by power function theory (Leopold and Maddock, 1953)

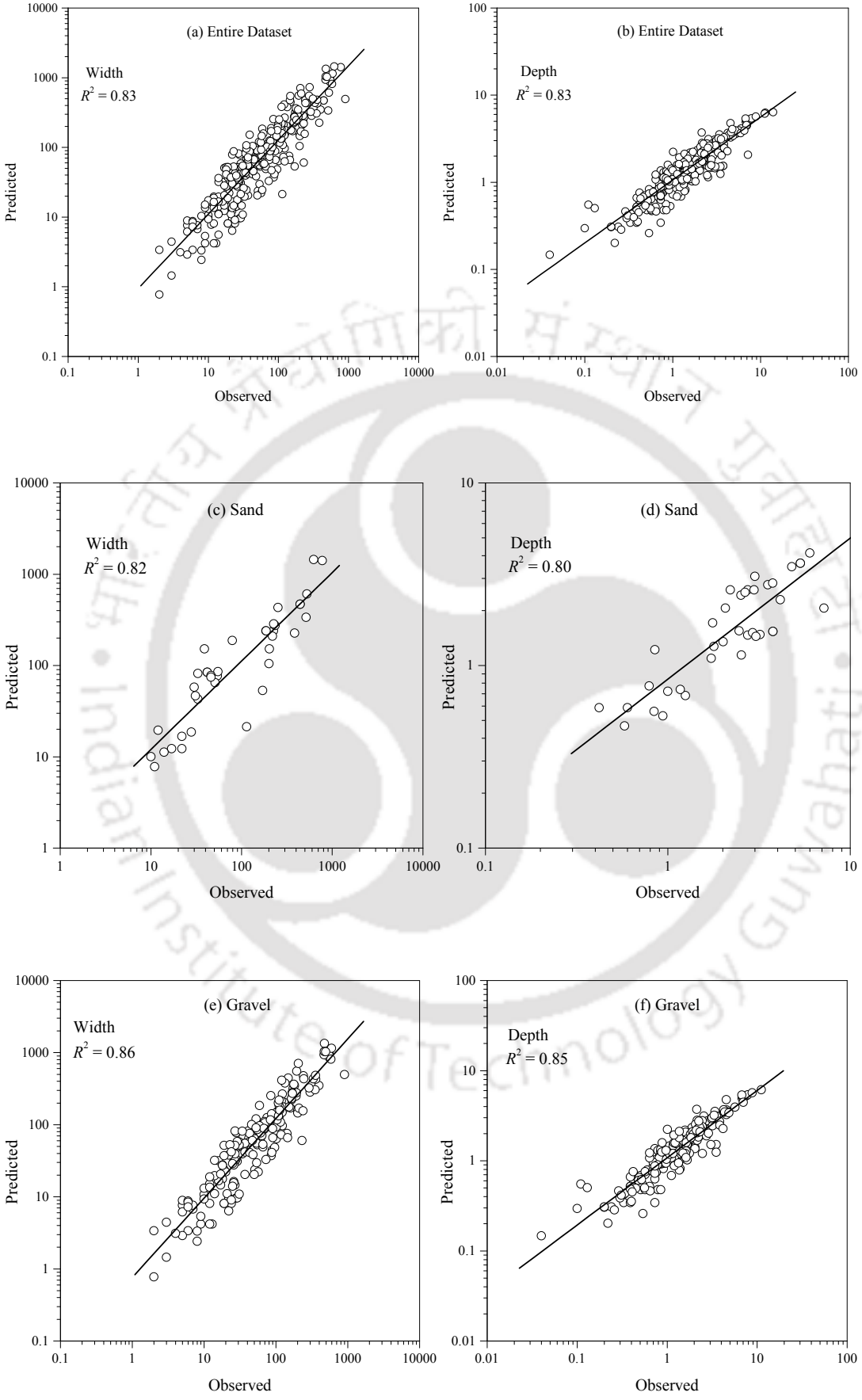

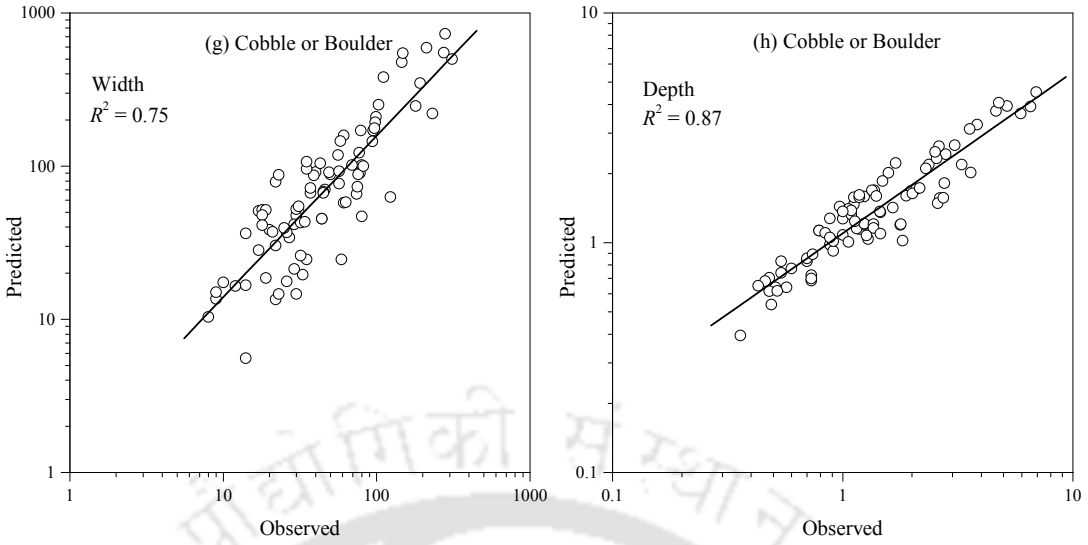

FIGURE 4.6: Prediction by the theory of conservation of mass and momentum (Smith, 1974b)

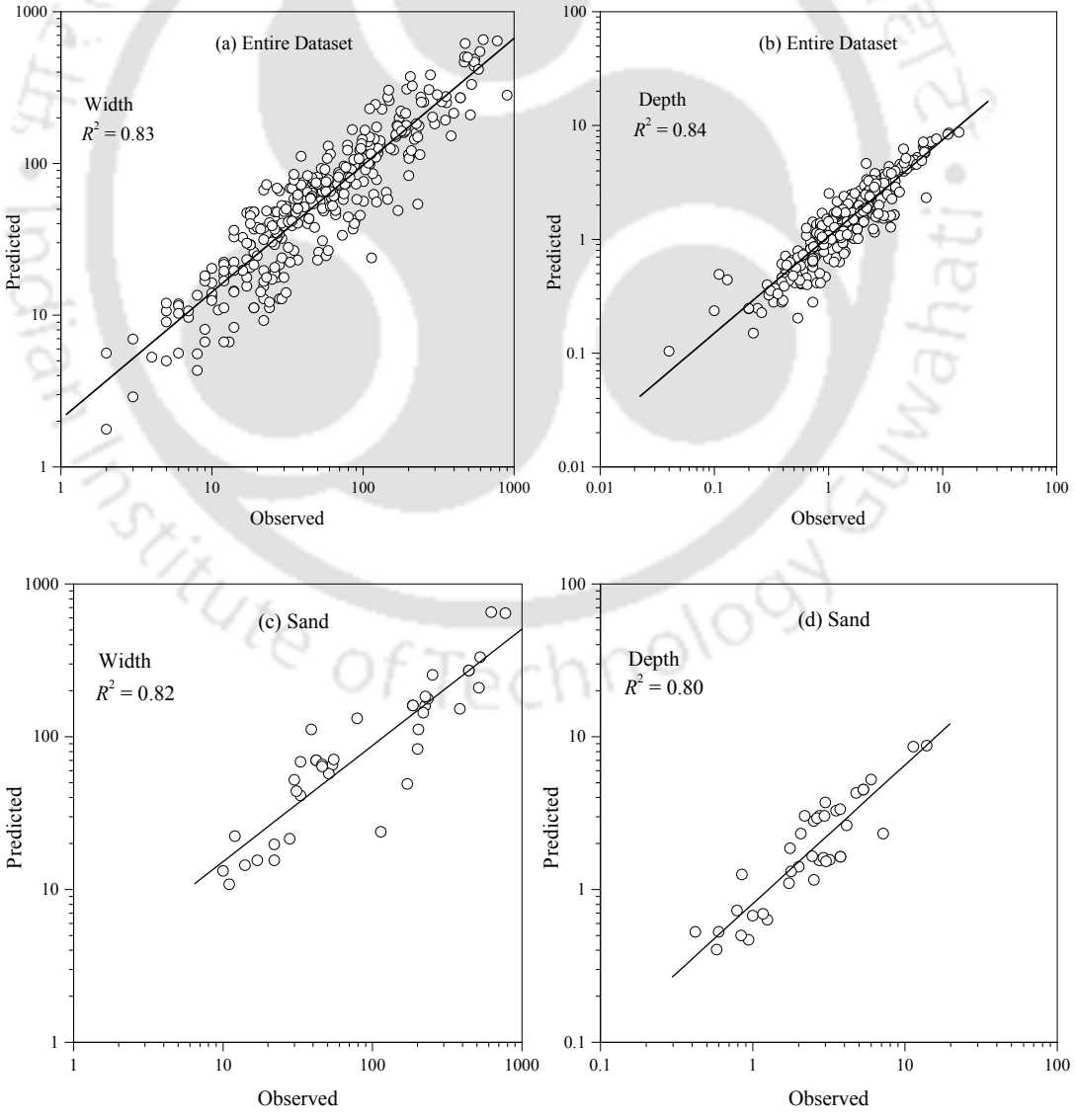

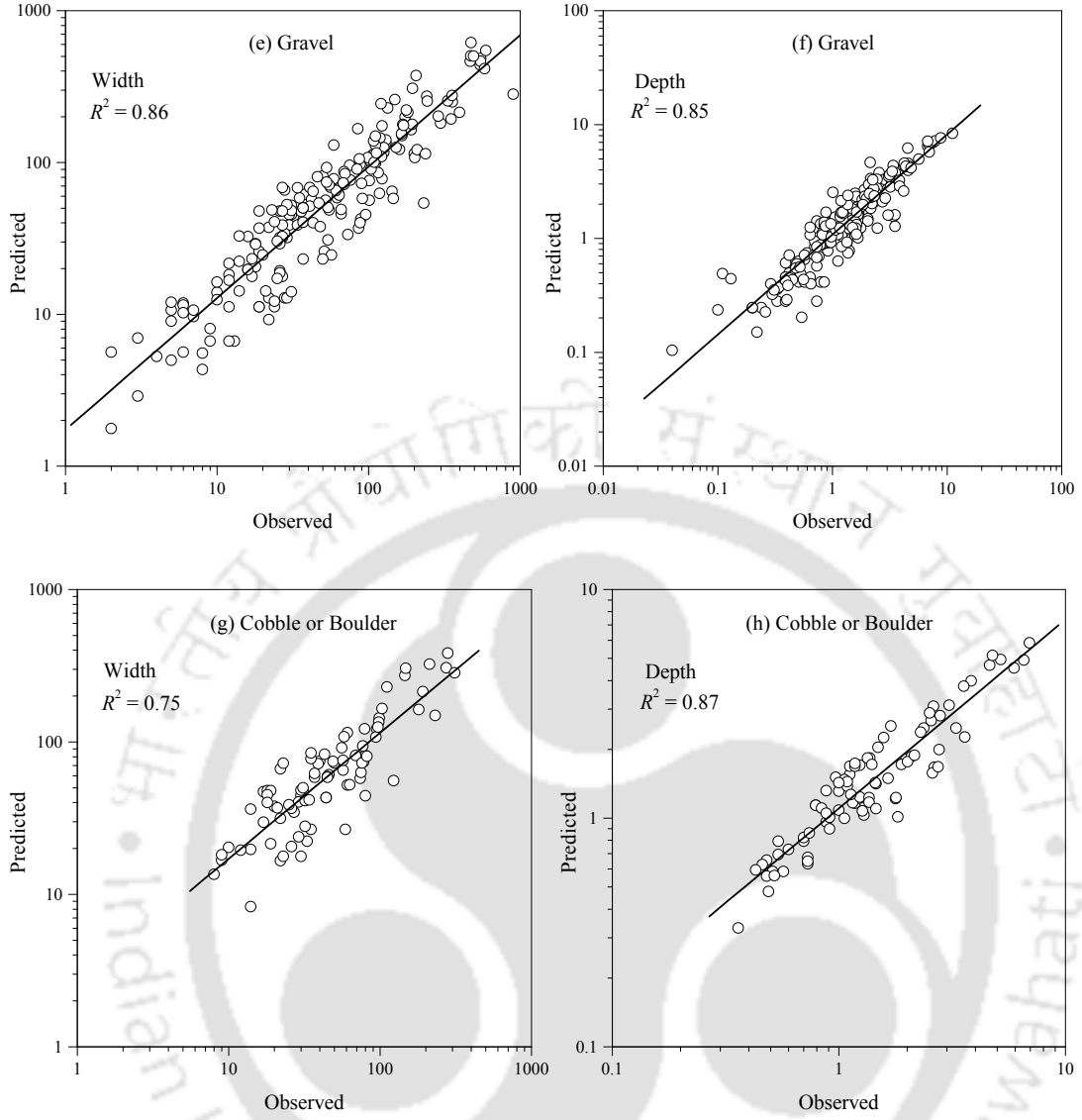

FIGURE 4.7: Prediction by theory of minimum energy degradation rate (Brebner and Wilson, 1967)

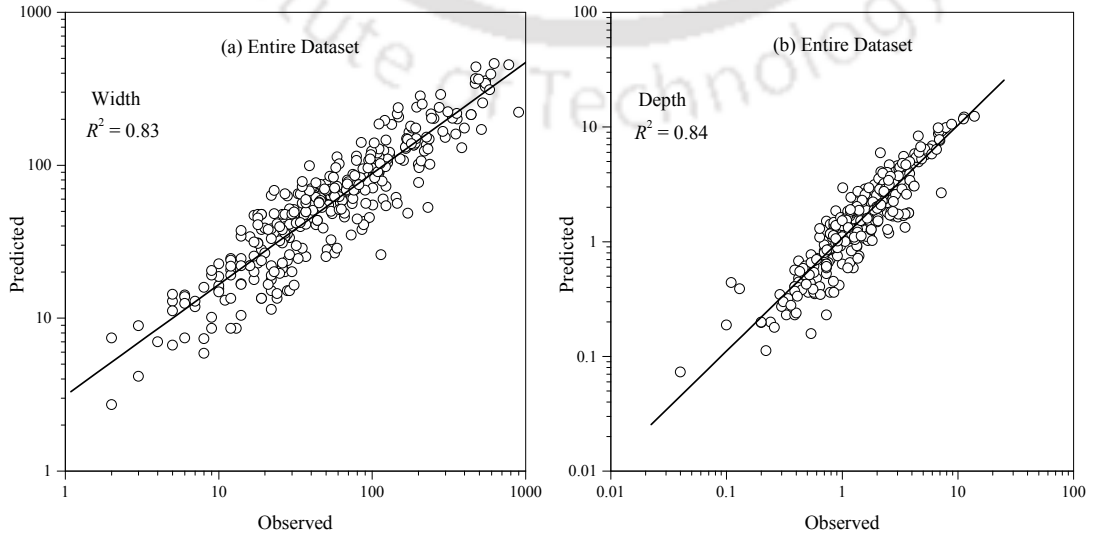

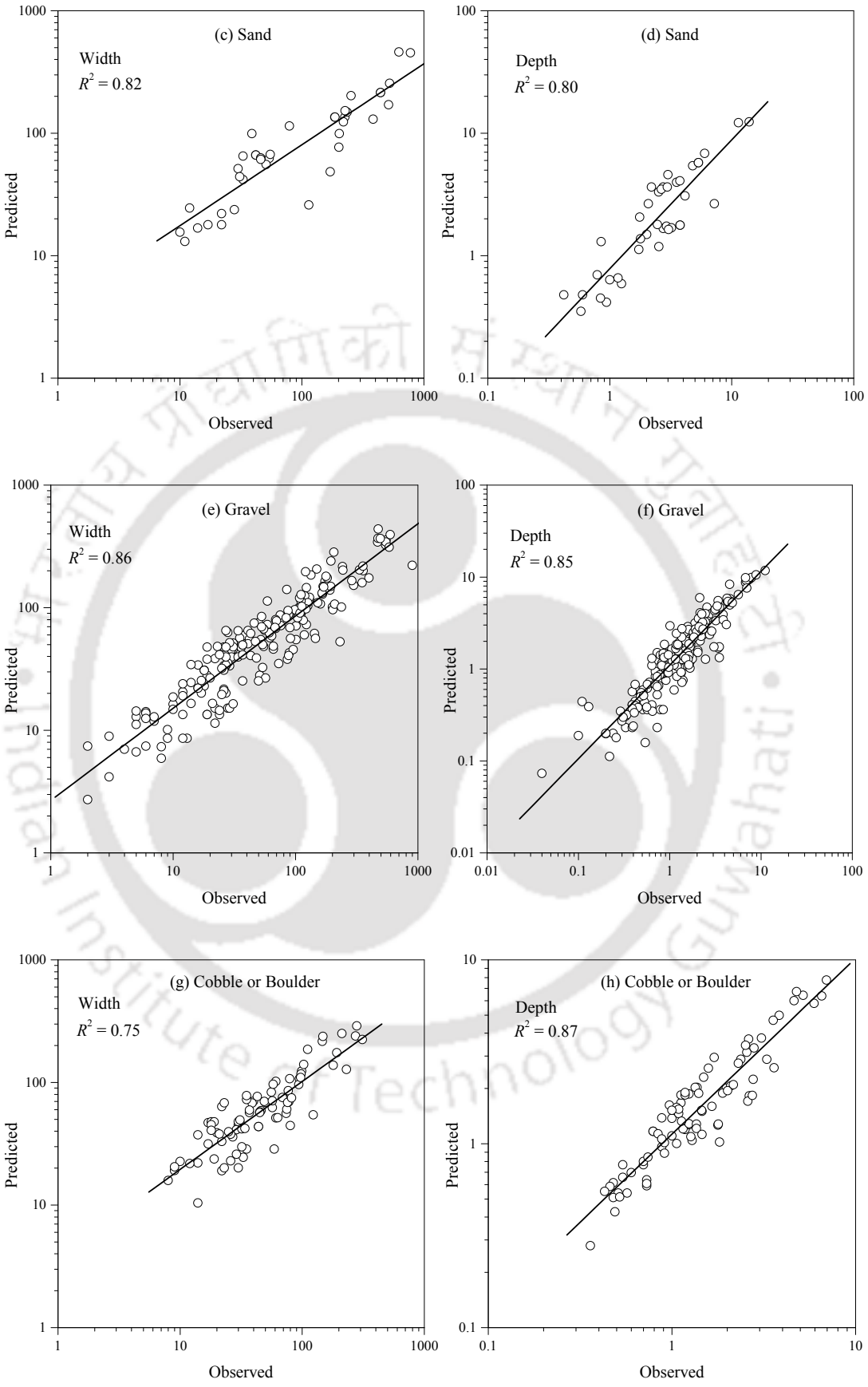

FIGURE 4.8: Prediction by MEDR (Yang et al., 1981)

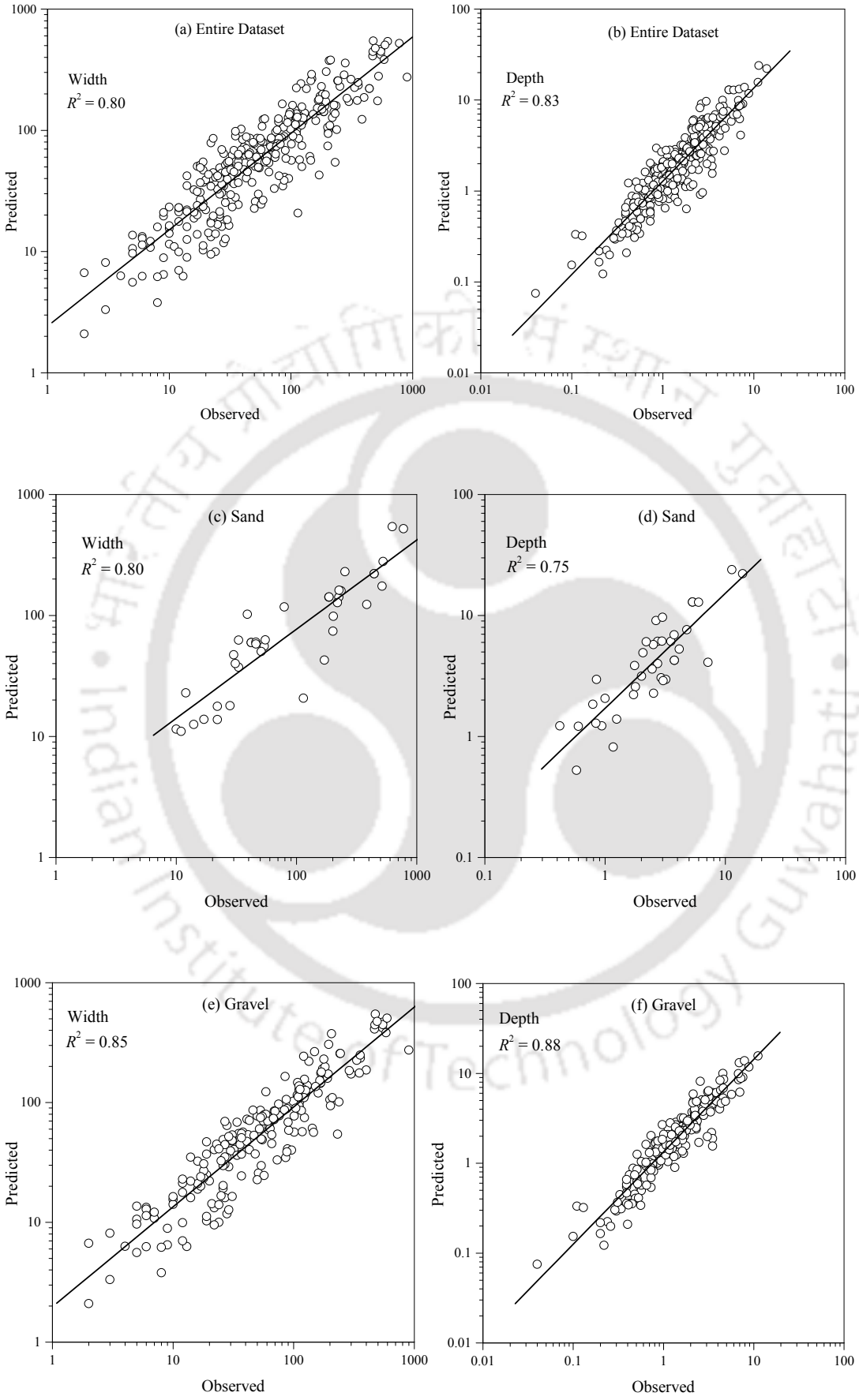

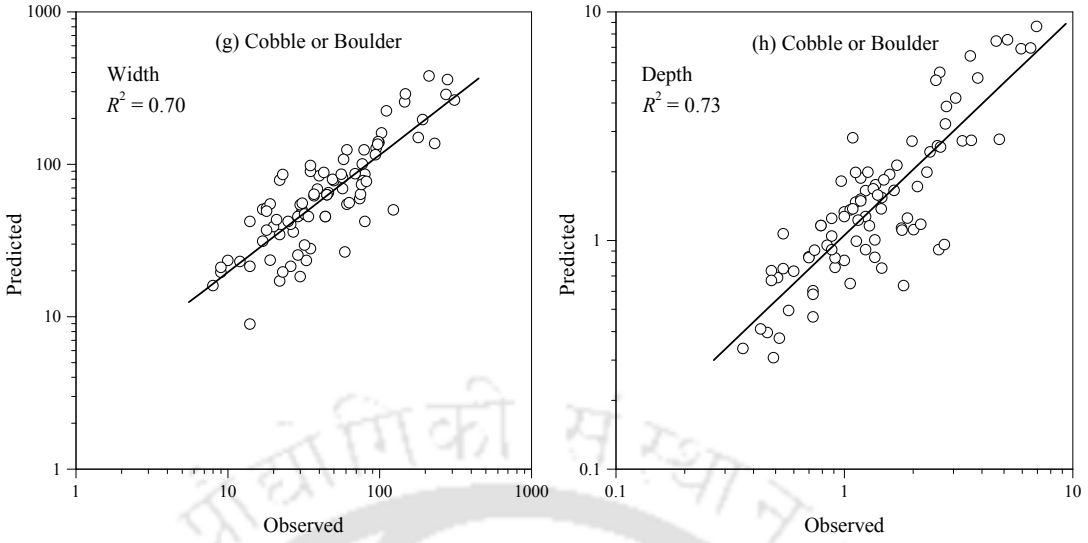

FIGURE 4.9: Prediction by the theory of maximum flow efficiency (Huang and Nanson, 2000)

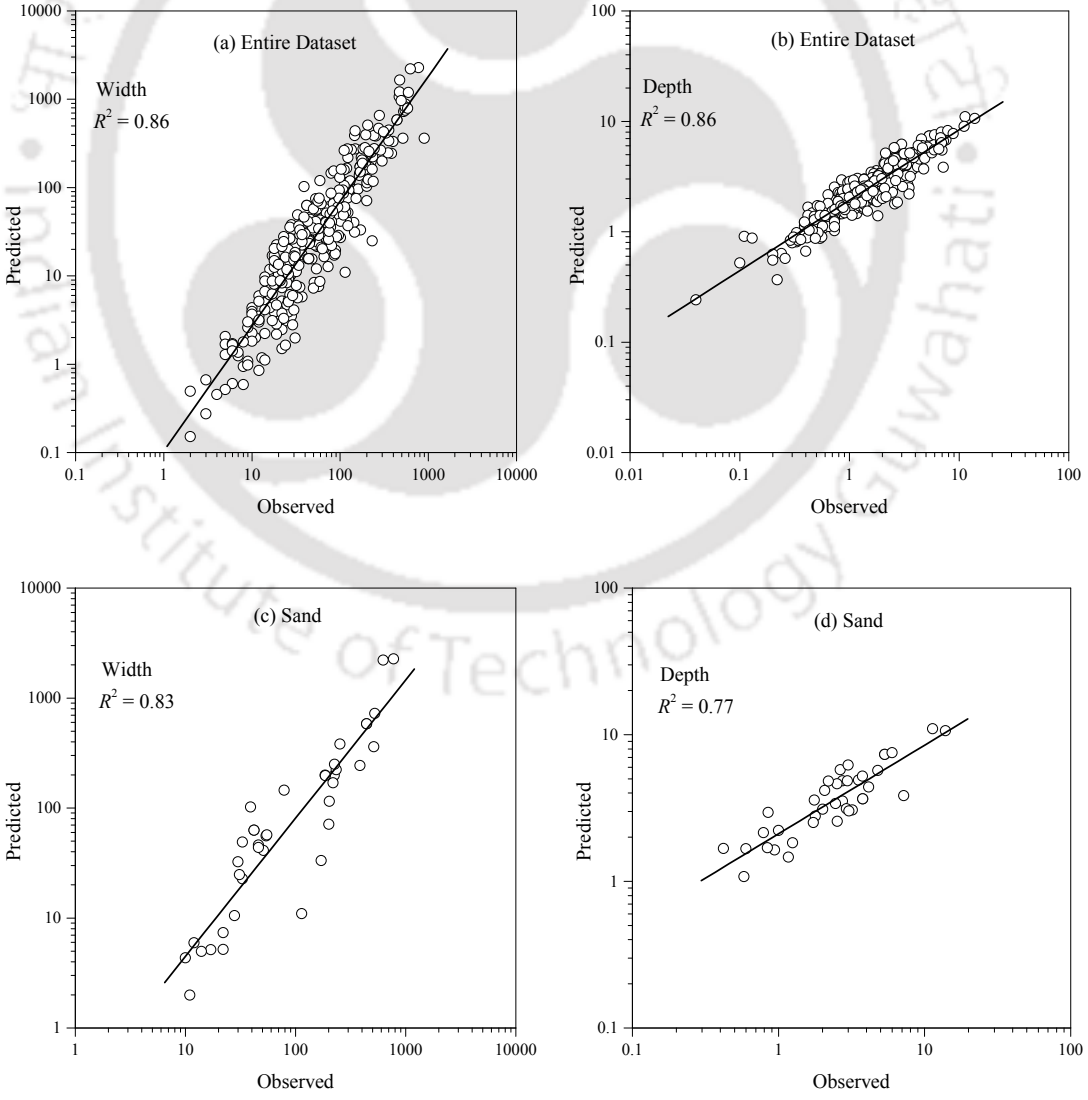

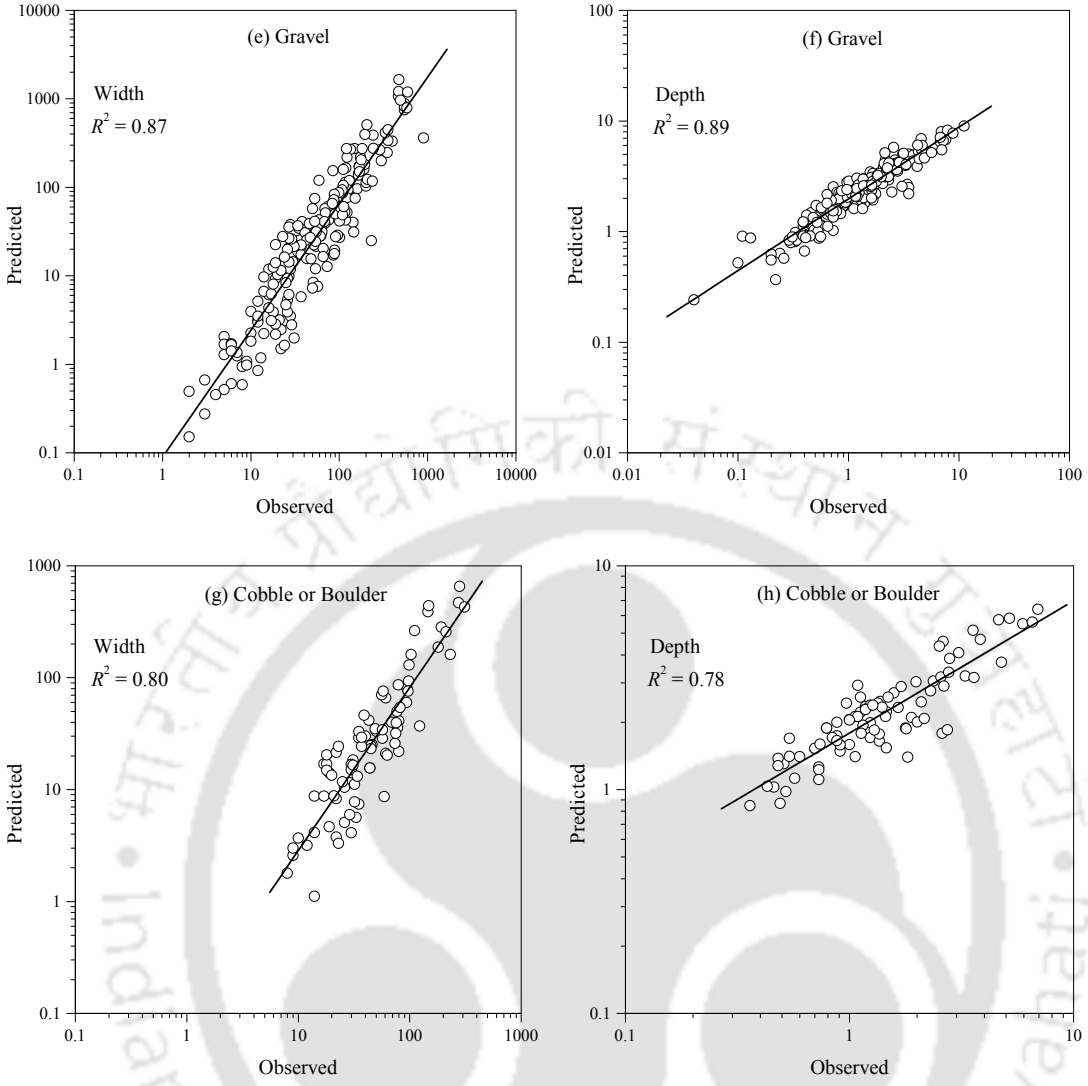

FIGURE 4.10: Prediction by the approach of Singh et al. (2003b)

and depth by theory of maximum flow efficiency (Huang and Nanson, 2000) was excellent in gravel range with R^2 value of 0.85 and 0.88 respectively for width and depth. Prediction of downstream hydraulic geometry by the method of Singh et al. (2003b) was very good in the entire range of data with R^2 value of 0.86 for width and depth and especially in the gravel range with R^2 value of 0.87 and 0.89 for width and depth respectively. Calculated R^2 values in the prediction for width and depth by various methods are compiled in Table 4.5.

In the prediction of width and depth by power function theory and the b_p, f_p, and m_p values of Table 4.2 and for some methods namely: the theory of conservation of mass and momentum (Smith, 1974b), theory of minimum energy degradation

rate Brebner and Wilson (1967), and theory of minimum energy dissipation rate (Yang et al., 1981) for which the coefficients of proportionalities were obtained in a similar manner as was followed for the power function theory (Leopold and Maddock, 1953) the R^2 values were very much same and hence, the comparison among them has been made on the basis of average discrepancy ratio based on logarithm ratio (Table 4.6) between predicted and measured values of width and depth. The discrepancy ratio indicates the goodness-of-fit between the predicted and observed results. For a perfect fit, the average discrepancy ratio should be equal to zero. The calculation procedure is as follows Islam and Karim (2005):

$$D_i = \log\left(\frac{\psi_c}{\psi_m}\right) \tag{4.73}$$

$$D_a = \frac{\sum_{i=1}^{j} D_i}{j} \tag{4.74}$$

where, D_i is discrepancy ratio based on logarithm ratio, ψ_c is calculated value, ψ_m is measured value, D_a is averaged discrepancy ratio based on logarithm ratio, and j is the total number of data used. Inspection of D_a from Table 4.6 reveals that for the power function theory, the prediction for width was very good for the values of exponents given by Thornes (1970) and the prediction of depth was excellent for the exponents given by Allen et al. (1994) with least value of average discrepancy ratio in the entire range of data. Slopes have also been predicted by various methods but the predictions were not good.

The calculated R^2 and D_a values in the prediction for slope by various methods have been arranged in Table 4.7. It is to note that all the methods which are discussed in this paper could not be verified because of the limitations of dataset and in some cases because of the nature of the particular method itself. For example some methods such as the theory of maximum sediment transport rate (White et al., 1982) and hydraulic geometry by echelon matrix procedure (Martin, 1996) require sediment concentration as an independent variable, which was not available in the dataset of Church and Rood (1983).

TABLE 4.5: R^2 values in the prediction of width and depth

Author	R^2 for width				R^2 for depth			
	Entire Dataset	Sand	Gravel	Cobble or Boulder	Entire Dataset	Sand	Gravel	Cobble or Boulder
Lacey (1930)	0.83	0.82	0.86	0.74	NA	NA	NA	NA
Blench (1957)	0.83	0.81	0.86	0.74	0.79	0.79	0.8	0.86
Simons and Albertson (1960)	0.83	0.82	0.86	0.75	0.83	0.81	0.84	0.86
Leopold and Maddock (1953)	0.83	0.82	0.86	0.75	0.84	0.8	0.85	0.87
Smith (1974b)	0.83	0.82	0.86	0.75	0.83	0.8	0.85	0.87
Brebner and Wilson (1967)	0.83	0.82	0.86	0.75	0.84	0.8	0.85	0.87
Yang et al. (1981)	0.83	0.82	0.86	0.75	0.84	0.8	0.85	0.87
Huang and Nanson (2000)	0.8	0.8	0.85	0.7	0.83	0.75	0.88	0.73
Singh et al. (2003b)	0.86	0.83	0.87	0.8	0.86	0.77	0.89	0.78

TABLE 4.6: Average discrepancy ratio between predicted and measured hydraulic geometry parameters (for the exponents of Table 4.2)

Author	D_a for width				D_a for depth			
	Entire Dataset	Sand	Gravel	Cobble or Boulder	Entire Dataset	Sand	Gravel	Cobble or Boulder
Leopold and Maddock (1953)	0.044	-0.022	0.019	0.132	0.025	-0.093	0.04	0.041
Wolman (1955)	0.025	-0.064	0.006	0.111	0.052	-0.051	0.064	0.07
Ackers (1964)	0.025	-0.064	0.006	0.111	0.04	-0.069	0.054	0.058
	0.027	-0.06	0.007	0.112	0.04	-0.069	0.054	0.058
	0.055	-0.002	0.028	0.144	0.003	-0.129	0.022	0.018
Langbein (1964)	0.055	-0.002	0.028	0.144	0.011	-0.115	0.028	0.027
Carlston (1969)	0.033	-0.045	0.011	0.12	0.017	-0.106	0.033	0.033
	0.044	-0.023	0.019	0.132	-0.007	-0.148	0.014	0.007
Thornes (1970)	0.023	-0.072	0.005	0.108	-0.001	-0.136	0.019	0.014
Knighton (1974)	0.094	0.06	0.062	0.185	-0.01	-0.154	0.012	0.004
Smith (1974b)	0.059	0.005	0.032	0.148	-0.024	-0.191	0.003	-0.012
	0.033	-0.045	0.011	0.119	-0.022	-0.21	0.01	-0.013
Parker (1979)	0.044	-0.022	0.019	0.132	0.032	-0.081	0.046	0.049
Lane and Foster (1980)	0.033	-0.045	0.011	0.119	0.058	-0.042	0.069	0.076
Allen et al. (1994)	0.067	0.017	0.038	0.156	0	-0.135	0.019	0.015
Smith (1974b)	0.088	0.052	0.057	0.179	-0.013	-0.159	0.01	0.001
Brebner and Wilson (1967)	0.035	-0.039	0.013	0.122	0.004	-0.127	0.023	0.02
Yang et al. (1981)	0.024	-0.069	0.005	0.109	0.029	-0.086	0.044	0.046

TABLE 4.7: Prediction for slope

Author	R^2 for slope				D_a for slope			
	Entire Dataset	Sand	Gravel	Cobble or Boulder	Entire Dataset	Sand	Gravel	Cobble or Boulder
Lacey (1930)	0.38	0.45	0.1	0.43	0.45	-0.47	0.56	0.59
Simons and Albertson (1960)	0.46	0.16	0.39	0.27	-0.61	-0.73	-0.62	-0.58
Smith (1974b)	0.32	0.48	0.41	0.36	0.57	1.25	0.57	0.26
Brebner and Wilson (1967)	0.32	0.48	0.41	0.36	0.63	1.33	0.63	0.32
Yang et al. (1981)	0.32	0.48	0.41	0.36	0.57	1.25	0.57	0.26

4.5 Generalized Downstream Hydraulic Geometry Relations

To derive the downstream hydraulic geometry relations for a river in its dynamic equilibrium, Singh et al. (2003b) combined two hypotheses, namely; principle of maximum entropy and minimum energy dissipation rate. In the theoretical development, application of the principle of maximum entropy to a river in its dynamic equilibrium resulted in following four possibilities: (1) $P_n = P_B$, (2) $P_B = P_y$, (3) $P_n = P_y$, and (4) $P_n = P_B = P_y$. These possibilities were based on the hypothesis that for a give discharge the spatial variation of the stream power of a channel is accomplished by the spatial variation in channel form and hydraulic variables and the change in stream power is distributed among the changes in channel form and hydraulic variables.

The calibration of derived equations for hydraulic geometry and the determination of morphological coefficients were carried out for an assumed V-shaped channel cross section. It was justified by Singh et al. (2003b) through the sensitivity analysis that for most of the natural channels, $B/y > 10$ and hence they can effectively be treated as rectangular in shape and their hydraulic geometry can be described by the proposed model which was calibrated for a V-shaped cross section.

However, authors of the present study have a view that the calibration of equations for natural river cross section which can be termed as wide rectangular if $B/y > 10$, should not be carried out for a V-shaped cross section. For this, a wide

trapezoidal channel section, central rectangular part of which can be treated as wide rectangular for width-to-depth ratio > 10 is assumed. For stable straight rivers, Chang (1988) found that $B/y = 21$ (Deng et al., 2001). The calibration of morphological coefficients and theoretically derived equations by Singh et al. (2003b) has been carried out for the assumed wide trapezoidal channel cross section with the central wide rectangular part for which $B/y = 21$. Derived equations for channel top width and depth are:

$$B = 0.1489\,(z + 10.5)\,\frac{Q^{0.462}}{S^{0.231}} \tag{4.75}$$

$$y = 3.135\left(\frac{n}{z + 10.5}\right)^{3/5}\frac{Q^{0.323}}{S^{0.161}} \tag{4.76}$$

Calibration of the equations and the morphological coefficients were derived by dividing the river regime data of Church and Rood (1983) in exactly the same manner which was applied for the determination of the coefficients of proportionality in the power function theory (Leopold and Maddock, 1953) as described in the previous section. Marginal improvement has been observed when the results were compared with the model proposed by Singh et al. (2003b). Results of prediction in different ranges of data for width and depth by the proposed modified model in this study are shown in Figure 4.11. Table 4.8 shows the comparison among the results on the basis of R^2 values between the model of Singh et al. (2003b) and the modified model proposed in this study.

Through the careful inspection of the R^2 values from Table 4.8, it is clear that there is a marginal improvement in the results for the model proposed in this study, especially for the width in cobble or boulder range and for depth in sand and cobble or boulder ranges of data. This improvement in the results may be attributed to the fact that a wide trapezoidal channel section with the central wide rectangular part ($B/y = 21$) assumed in present study, represents the natural river cross-section better than a V-shaped cross-section assumed by Singh et al. (2003b).

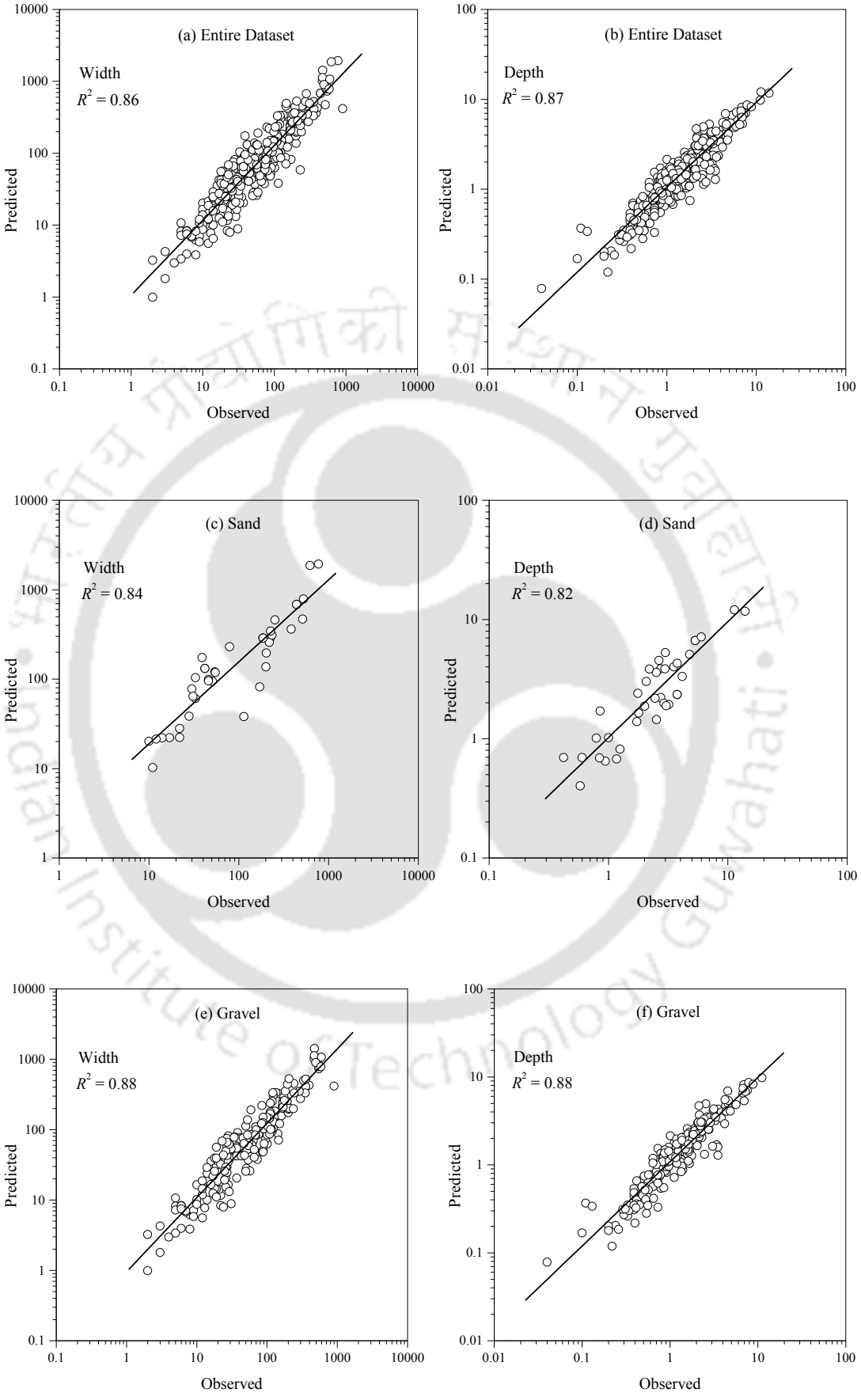

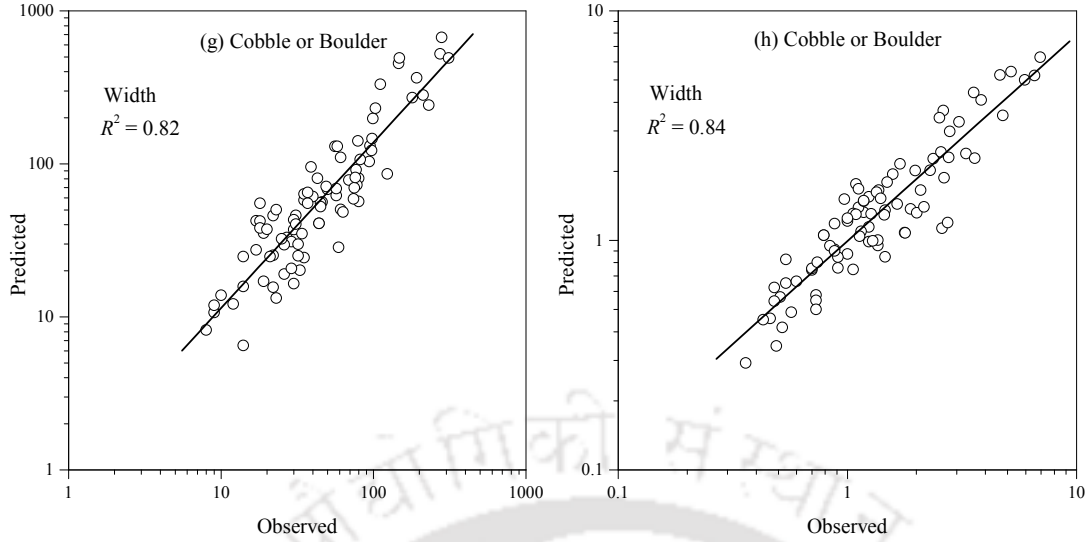

FIGURE 4.11: Prediction for width and depth for the proposed model in this study

TABLE 4.8: Comparison among the results based on R^2 values

Author	R^2 for width				R^2 for depth			
	Entire Dataset	Sand	Gravel	Cobble or Boulder	Entire Dataset	Sand	Gravel	Cobble or Boulder
Singh et al. (2003b)	0.86	0.83	0.87	0.8	0.86	0.77	0.89	0.78
Present study	0.86	0.84	0.88	0.82	0.87	0.82	0.88	0.84

4.6 Development of Regime Equations with Downward Seepage

There are great numbers of methods available in the published literature for the prediction of hydraulic geometry of stable alluvial channels. Some of the methods are fundamentally similar and some are based on quite different ideas and the data required for all these methods are different in its nature.

Engineers have largely relied on empirical formulae for the design of hydraulic structures. Such formulae are often based on experimental measurement, intuition and trial and error in the field. Functional analysis and laboratory experiments are two tools which (together with the process of reasoning) help in interpreting the various flow phenomena. Functional analysis is used to incorporate all the relevant variables in to a basic functional form of the system. This is the basic of

the regime theory. Design of alluvial channels has traditionally been accomplished using regime methods. Regime methods rely on regression equations that are used to determine the dependent variables. The independent variables of discharge and sediment concentration are single-valued functions and, therefore, are applicable to cases where the discharge is relatively uniform with time. Regime methods are applicable for low-energy systems with low sediment transport. Various regime equations have been proposed which relate channel characteristics primarily to flow discharge, however Julien and Wargadalam (1995) has shown that channel characteristics is also dependent on sediment size and Shields parameter other than discharge and proposed following relations:

$$\left.\begin{aligned} B &= 0.512 Q^{0.533} d_{50}^{-0.333} \theta^{-0.267} \\ y &= 0.133 Q^{0.4} \theta^{-0.2} \\ S_w &= 12.4 Q^{-0.4} d_{50} \theta^{1.2} \end{aligned}\right\} \tag{4.77}$$

where B is the top width, Q is the flow discharge, θ is the Shields parameter, y is flow depth and S_w is the water surface slope. Afzalimehr et al. (2010) has developed the similar relationship:

$$\left.\begin{aligned} B &= 4.92 Q^{0.726} d_{50}^{-0.035} \theta^{-0.018} \\ y &= 0.346 Q^{0.363} d_{50}^{0.073} \theta^{0.048} \\ S_w &= 1.441 Q^{0.033} d_{50}^{0.814} \theta^{0.846} \end{aligned}\right\} \tag{4.78}$$

Here, it can be said that Shields parameter and sand size are interrelated. As has been discussed earlier, existing regime equations do not consider the seepage as an explicit parameter. The variables affecting the channel bed stability with seepage should be as follows (Vanoni, 1975):

- Physical system: g
- Fluid properties: γ (specific weight of fluid), ν (kinematic viscosity)
- Sediment properties: γ_s (specific weight of sediment), d_{50}(particle size), τ_c (Shields critical stress)

- Cross section: p (perimeter), y (flow depth) , B (Top width), R_h (Hydraulic radius), A (Area of cross section)
- Flow properties: Q (discharge at particular section), q_s (seepage discharge), S_f (frictional slope)

With seepage as an independent parameter, Rao et al. (2011) developed a set of regime equations:

$$\left.\begin{aligned} y &= 0.30Q^{0.27}N^{0.44}p^{-0.72} \\ S_f &= 0.0007Q^{-0.044}N^{-0.032}p^{0.38} \end{aligned}\right\} \tag{4.79}$$

The major limitation of Rao et al. (2011) is that the equations do not reduce to the form of known regime equations as the seepage term vanishes. Here it has been proposed that these variables are the function of channel discharge, seepage discharge and sand size. In equation form, it can be written as:

$$\left.\begin{aligned} p &= f\left(Q, q_s, d_{50}\right) \\ R_h &= f\left(Q, q_s, d_{50}\right) \\ S_f &= f\left(Q, q_s, d_{50}\right) \end{aligned}\right\} \tag{4.80}$$

In the development of governing function for channel geometric characteristics, experimental observations of both seepage and no seepage runs have been considered. A nonlinear regression analysis was performed with experimental observations to find the functional form of Equation (4.80). The derived equations for the prediction of stable channel characteristics with seepage are expressed as:

$$\left.\begin{aligned} p &= 1.6Q^{0.41}d_{50}^{-0.12}e^{31.42q_s} \\ R_h &= 0.3Q^{0.39}d_{50}^{-0.02}e^{-8.54q_s} \\ S_f &= 0.16Q^{-0.49}d_{50}^{1.03}e^{q_s} \end{aligned}\right\} \tag{4.81}$$

The parity plot of Equation (4.81) has been shown in the Figure 4.12 to Figure 4.14. As shown, the value of R^2 is high. Thus, it shows that the predictability of the relationship is quite high.

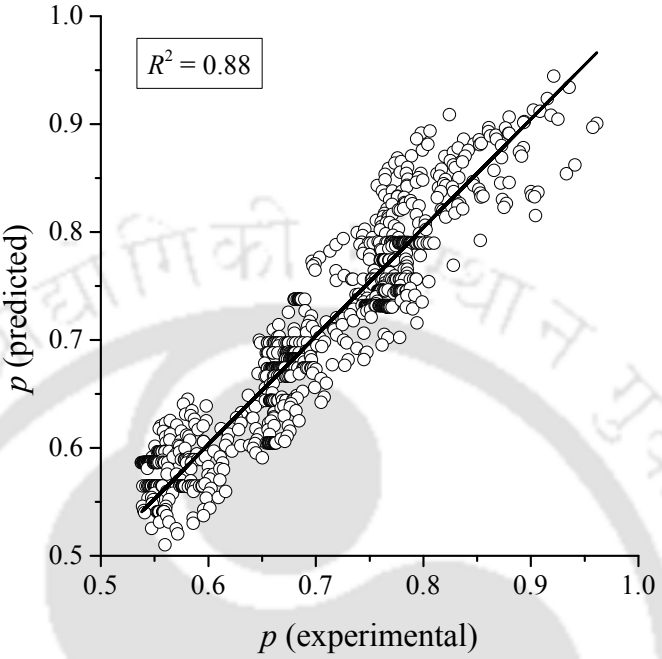

FIGURE 4.12: Regime relationship for perimeter with downward seepage

Behavior of the multivariate problem and interpretation of the complex interaction of variables involving them can be better understood by non-dimensional analysis. In non-dimensional analysis suitable substitution of variables is carried out for the partial or full removal of units of an equation. Here, the function can be expressed as:

$$f\left(p, R_h, B, S_f, u, \nu, d_{50}, V_s, \gamma_s, \gamma\right) = 0 \tag{4.82}$$

As has been defined earlier in Equation (3.22), R_S is a function of V_s, d_{50}, ν and incorporating other non-dimensional parameters such as Shields parameter (θ_C) and flow Reynolds number (R_e), Equation (4.82) reduces to:

$$f\left(p, R_h, S_f, B, Rs, \theta_C, R_e\right) = 0 \tag{4.83}$$

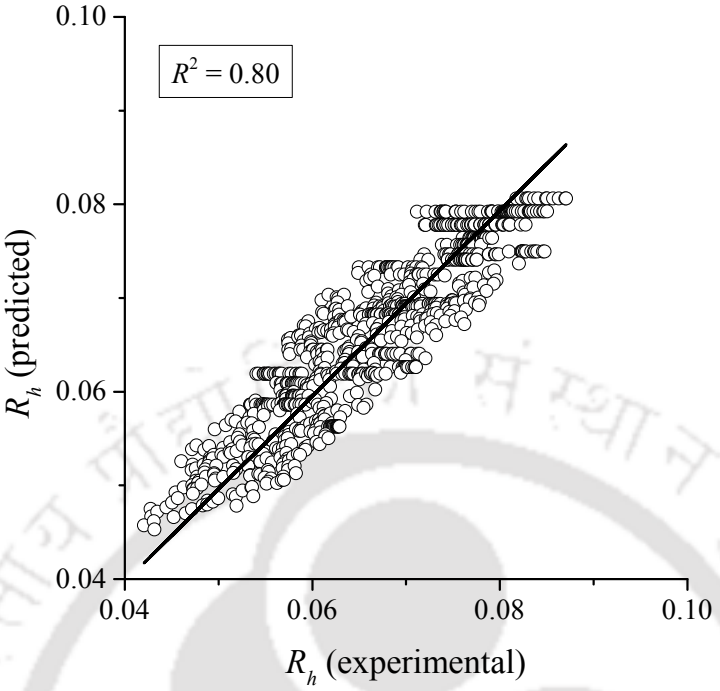

FIGURE 4.13: Regime relationship for hydraulic radius with downward seepage

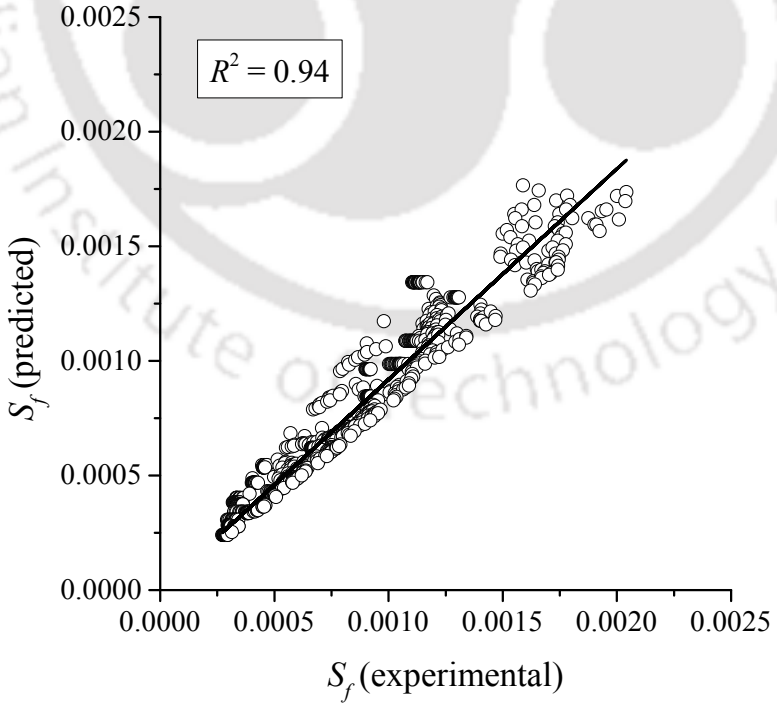

FIGURE 4.14: Regime relationship for friction slope with downward seepage

Segregating the parameters in the form of non-dimensional way may be expressed as:

$$f\left(\frac{p}{R_h}, \frac{B}{R_h}, S_f, R_S, \theta_C, R_e\right) = 0 \tag{4.84}$$

The variables can be grouped into a set of non-dimensional tri-variate relations as follows:

$$\left.\begin{aligned} \frac{p}{R_h} &= f\left(R_e, R_S, \theta_C\right) \\ \frac{B}{R_h} &= f\left(R_e, R_S, \theta_C\right) \\ S_f &= f\left(R_e, R_S, \theta_C\right) \end{aligned}\right\} \tag{4.85}$$

Functional for of Equation (4.85) has been obtained by performing regression analysis and following non-dimensional relations for the prediction of cross-sectional geometry of stable channel have been derived:

$$\left.\begin{aligned} \frac{p}{R_h} &= \frac{1.42 \exp\left({R_S}^{0.0216}\right)}{\ln\left(R_e\right) \theta_C^{1.2}} \\ \frac{B}{R_h} &= \frac{1.0 \exp\left({R_S}^{0.00302}\right)}{\ln\left(R_e\right) \theta_C^{1.17}} \\ S_f &= \frac{1.6 \exp\left({R_S}^{0.0128}\right)}{\ln\left(R_e\right) \theta_C^{-1.85}} \end{aligned}\right\} \tag{4.86}$$

Predictability of the relations given in Equation (4.86) has been shown in Figure 4.15 to Figure 4.17 which suggests that Equation (4.86) is a good predictor for the stable channel dimensions.

Predictability of the dimensional relations given in Equation (4.81) and non-dimensional relations presented in Equation (4.86) cannot be tested by the independent set of data from the natural stable rivers (Church and Rood, 1983) as has been carried out for previous studies because the dataset does not provide

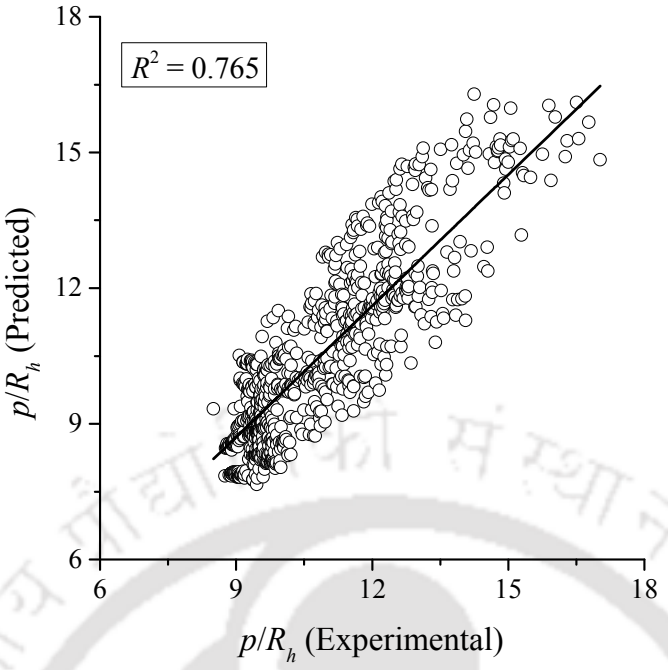

FIGURE 4.15: Non-dimensional relationship for channel perimeter with downward seepage

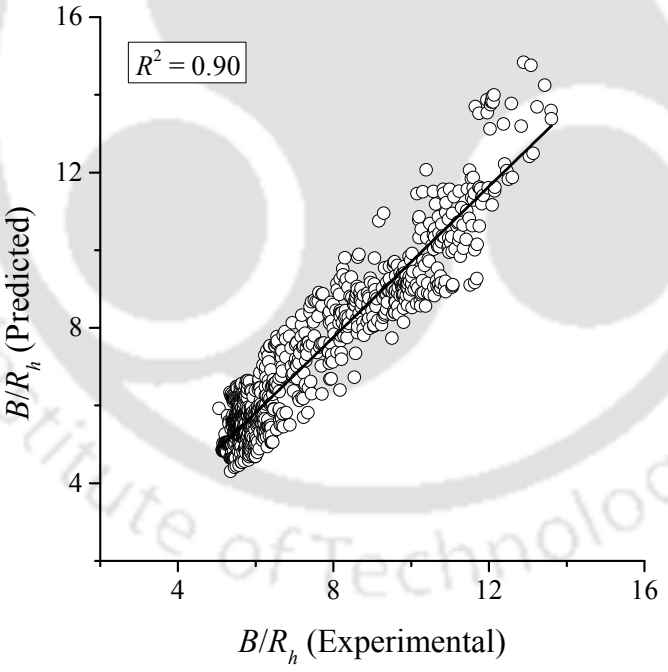

FIGURE 4.16: Non-dimensional relationship for channel width with downward seepage

information on the seepage discharge from the rivers.

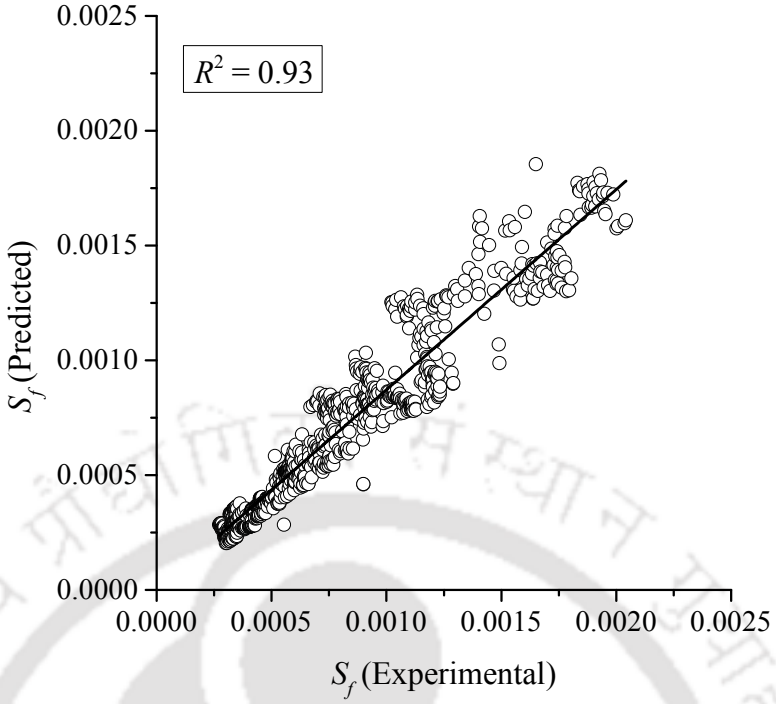

FIGURE 4.17: Non-dimensional relationship for friction slope with downward seepage

4.7 Conclusions

Various theories available in the literature for the design of stable alluvial channels are presented. Comparative study for the predictability is carried out among the previous studies for the design of stable channels using an independent dataset which contains 499 sets of data out of which about 40 percent represent Canadian rivers, 50 percent American rivers and about 10 percent British rivers. For the verification of the methods of stable alluvial channel design, the river channel data have been subdivided into three categories based on the median bed material sizes, namely: sand range (0.063 mm $\leq d_{50} <$ 1 mm), gravel range (1 mm $\leq d_{50} <$ 64 mm) and cobble or boulder range (64 mm $\leq d_{50}$).

It has been observed that the prediction of downstream hydraulic geometry by the method of Singh et al. (2003b) was very good in the entire range of data. The proposed model by Singh et al. (2003b) has been modified by considering a wide trapezoidal channel section and marginal improvement in the predictions has been observed. These previous studies for the design of stable channels for

which the comparative analysis has been carried out do not contain seepage as an explicit parameter. Here, a new set of regime equations have been developed for perimeter, flow depth and frictional slope of a stable channel with the consideration of downward seepage as an explicit parameter. Non-dimensional relations have also been developed for perimeter, top width and frictional slope considering them to be functions of flow Reynolds number, seepage particle Reynolds number and Shields parameter.

Chapter 5

Turbulent Structures of Flow in Alluvial Channels with Curved Cross-sections under Downward Seepage

State of the flow can be either laminar or turbulent. The laminar state can be characterized by a smooth variation of the flow variables and well defined flow characteristics, while the state of turbulent flow can be characterized by a large range of scales of irregular, diffusive, dissipative and highly three-dimensional motions (Tennekes and Lumley, 1972). Turbulent flow can be experienced in everyday life such as clouds, smoke rising from a chimney or from an incense stick, or flames of a bonfire. Turbulent flow has fascinated mankind for a very long time, while some authors observe the importance of turbulence to the hydraulic structures of the ancient civilizations as an indication that the effects of turbulence must have been understood by the responsible engineers (Rouse and Ince, 1957; Batchelor et al., 2002). The beginning of modern turbulence research is commonly related to the mid 19^{th} century, when detailed measurements of the pressure drops in turbulent pipe flow were carried out by Hagen (1854) and Darcy (1857). Boussinesq (1877)

two decades later introduced the concept of an enhanced eddy viscosity and suggested a statistical treatment of turbulent flows. Reynolds (1883) carried out a detailed study on the transition from the laminar to the turbulent flow regime and proposed the criterion based on a non-dimensional number that now bears his name. The concept of flow decomposition was later introduced by Reynolds (1895). It became clearer with the beginning of the 20^{th} century that a phenomenon such as turbulence can emerge from a set of deterministic equations and it is now commonly accepted that the description of turbulent flow can appropriately be given by the NavierStokes equations.

The work of A. N. Kolmogorov (Kolmogorov, 1941) made a major step in understanding the nature of turbulence. Kolmogorov advanced and quantified the energy cascade concept described by Richardson (1922). The concept of energy cascade states that the turbulent energy is injected in the large scales and transferred to smaller scales by an inviscid process. The viscosity becomes important and dissipates all energy in the small scales as the Reynolds number of the smallest scales is low. An explanation of this model can be provided as the rate of dissipation might be specified by the inviscid processes related to the large scales and not by the viscosity itself. A review of the work of Kolmogorov can be found in the book by Frisch (1995).

5.1 Velocity Decomposition

Turbulence has been evaluated traditionally by decomposing the instantaneous velocity samples (U_i) into the time-averaged (U) and fluctuating components of velocity ($u^{'}$):

$$U_i = U + u' \tag{5.1}$$

This process is called the Reynolds decomposition (Tennekes and Lumley, 1972) and it requires a steady or quasi-steady flow. Time averaged streamwise (U) and

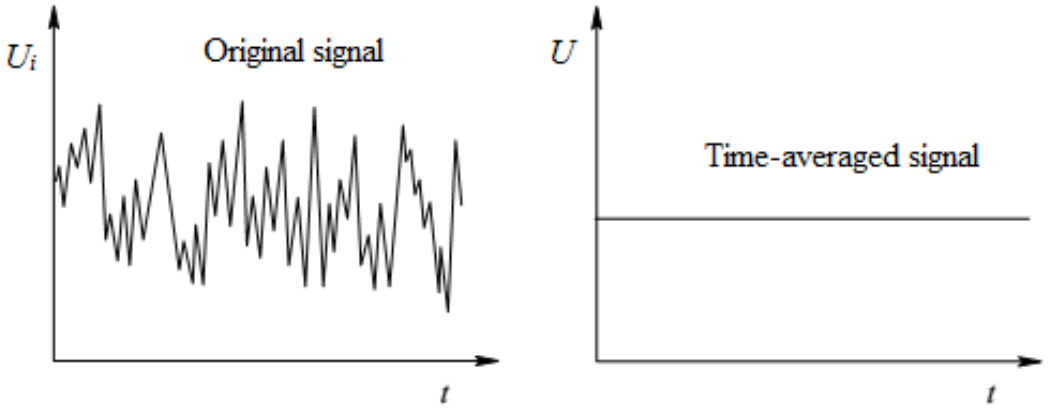

FIGURE 5.1: Comparison between original and time-averaged signal

vertical (W) velocities have been calculated as:

$$\left.\begin{aligned} U &= \frac{1}{n}\sum_{i=1}^{n} U_i \\ W &= \frac{1}{n}\sum_{i=1}^{n} W_i \end{aligned}\right\} \tag{5.2}$$

where:

U_i : is the instantaneous velocity in the streamwise direction.

W_i : is the instantaneous velocity in the vertical direction.

n : is the number of samples taken.

Averaging fundamentally results in a loss of information. Indeed, it is the purpose of averagingto remove'non-essential' details, while leaving only the core information. With respect to this, Reynolds' (1895) proposal should be recalled that it would be impossible to understand turbulence in detail, and it would thus be more useful to consider only statistical properties of the turbulent flow. Figure 5.1 depicts the loss of information due to averaging.

For flows over irregular boundaries, such as that of mobile or deformable sand bed, the time-averaged velocity U is dependent upon the spatial position over the bed. Turbulent fluctuations at a point are given by the deviations from the local time averaged velocity:

$$U_i\left(x,y,z,t\right) = U\left(x,y,z,t\right) + u_i{}'\left(x,y,z,t\right) \tag{5.3}$$

Water molecules move in very irregular paths in turbulent flow, causing an exchange of momentum from one portion of fluid to the other, and hence, the turbulent shear stresses (τ_{turb}) are generated also known as the Reynolds shear stresses (τ_{uw}). The Reynolds shear stresses can be given by time-averaging of the Navier-Stokes equation:

$$\left.\begin{aligned} \tau_{turb} = \tau_{uw} &= -\rho_w \overline{u'w'} \\ \overline{u'w'} &= \frac{1}{n}\sum_{i=1}^{n}\left(U_i - U\right)\left(W_i - W\right) \end{aligned}\right\} \tag{5.4}$$

In turbulent flow both viscosity and turbulence contribute to shear stress. The total shear stress (τ_{total}): where:

ρ_w : is the density of water.

$u^{'}$: is the fluctuating component of velocity in the streamwise direction.

$w^{'}$: is the fluctuating component of velocity in the vertical direction.

$$\tau_{total} = \tau_{visc} + \tau_{turb} = \rho\nu\frac{dU}{dz} + \left(-\rho\overline{u'w'}\right) \tag{5.5}$$

where:

τ_{visc} : is the shear stress due to viscosity.

ν : is the kinematic viscosity.

5.2 Turbulence in 3-Dimensional Flow Field

The level of turbulence in a sampled velocity traditionally been described by the average magnitude of velocity fluctuations, commonly the RMS $\sqrt{\overline{u_i'^2}}$, or standard deviation of the velocity sample. This is commonly expressed as the non-dimensional turbulence intensity (σ_u^+) of velocity components, and the turbulent kinetic energy (TKE). Semi-empirical universal functions for (σ_u^+) and non-dimensional TKE in open-channel flow are proposed by Nezu and Nakagawa

(1993), based on the $k-\epsilon$ turbulence model:

$$\left.\begin{aligned} \sigma_u^+ &= \left(\frac{\sqrt{\overline{u'u'}}}{U_*}\right) = D_u e^{(-C_u z^+)} \\ TKE &= \frac{1}{2}\left(\overline{u'^2} + \overline{v'^2} + \overline{w'^2}\right) \end{aligned}\right\} \tag{5.6}$$

where:

z^+ : is the non-dimensional depth.

D_u and C_u : are the coefficients set to 2.3 and 1 respectively as suggested by Nezu and Nakagawa (1993).

These functions are applicable throughout the depth of flow over a smooth bed, except very near to the wall, where viscous effects dominate. Nezu and Nakagawa (1993) pointed out that there is limited data available for rough bed turbulence intensities in comparison to those for smooth beds. Turbulence intensities in the near-bed region are reduced by the effect of increasing roughness height. With increasing relative roughness Bayazit (1976) observed significant reduction in turbulence intensities.

The distribution of turbulence is further reflected by the higher moments of velocity fluctuations which aid in the identification of infrequent velocity fluctuations of large magnitude associated with sweep and ejection events (Grass, 1971). The third moment of turbulent velocity fluctuations or the coefficient of skewness $Sk(u_i)$ of a velocity time series describes the asymmetry in the probability density function of turbulent fluctuations. The coefficient of skewness is an important factor to describe infrequent velocity fluctuations of large magnitude such as bursting events (Nezu and Nakagawa, 1993) can be defined as:

$$Sk\left(u_i\right) = \frac{\overline{u_i'^3}}{\left(\overline{u_i'^2}\right)^{3/2}} \tag{5.7}$$

Grinvald and Nikora (1988) reported from investigations in flumes and rivers at moderate velocity that the skewness coefficient for velocity in the streamwise direction is usually positive near the bed, becomes negative in the intermediate region, and again positive near the water surface, with absolute values generally

less than 1. Measurements of Nikora and Smart (1997) in a gravel-bed river similarly show negative skewness coefficient for velocity in the streamwise direction over the majority of the flow depth. These negative values of skewness coefficient reflect the transport of turbulent energy from the bottom region to the upward direction (Nikora and Smart, 1997).

Turbulent characteristics presented here have been taken for the experiments on the geometric profile with top width 0.70 m. Set-1 stands for the measurements taken in the experiments on longitudinal bed slope 0.00116 and Set-2 stands for measurements taken in the experiments on bed slope 0.00176. Measurements were carried out along the centerline of the channel on a section located at distance of 8 m from the downstream end.

5.3 Mean Velocity

Comparison among the vertical distributions of the time averaged velocities in the streamwise direction for no seepage and seepage runs has been depicted in Figure 5.2 and 5.3 for Set-1 and Set-2 experiments.

Careful observation of Figure 5.2 and Figure 5.3 reveals that the velocity increased when the downward seepage was applied to the channel which was at the condition of incipient motion with no seepage earlier. Quantitative analysis suggests that at very near to the channel bed i.e. at $\frac{z}{y} \sim 0.03$ and $\frac{z}{y} \sim 0.013$ for Set-1 and Set-2 experiments, respectively, the streamwise velocity increased approximately by 3 - 6%. In the present experiments, it has been observed that the universal logarithmic law for the rough wall $U/U_* = 2.43 \ln(z/d_{50}) + 8.5$ (Dey et al., 2011b) is not applicable to the flows over curved deformable channel beds in both no seepage and seepage conditions.

Hence, the log law has been fitted in the inner layer ($\frac{z}{y}$<0.2) of the velocity profiles in the same manner as has been suggested by Dey et al. (2012) and have been depicted in Figure 5.4. Following non-dimensional expression has been considered

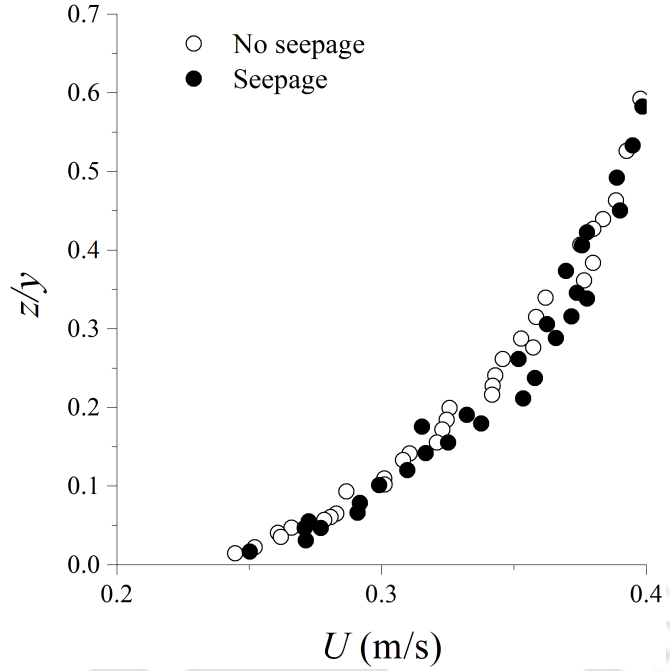

FIGURE 5.2: Vertical distribution of time-averaged velocities for Set-1 experiments

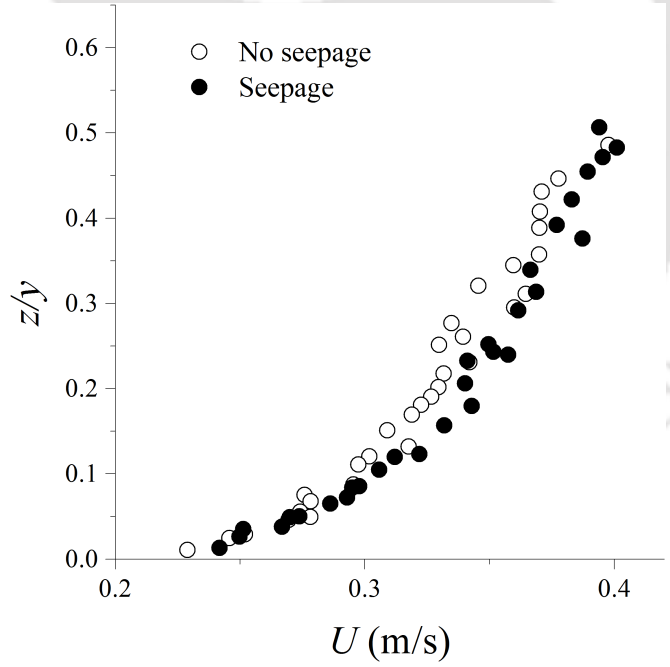

FIGURE 5.3: Vertical distribution of time-averaged velocities for Set-2 experiments

for the log law:

$$\frac{U}{U_*} = \frac{1}{k} \ln \left(\frac{z^+ + \Delta z^+}{\chi^+} \right) \tag{5.8}$$

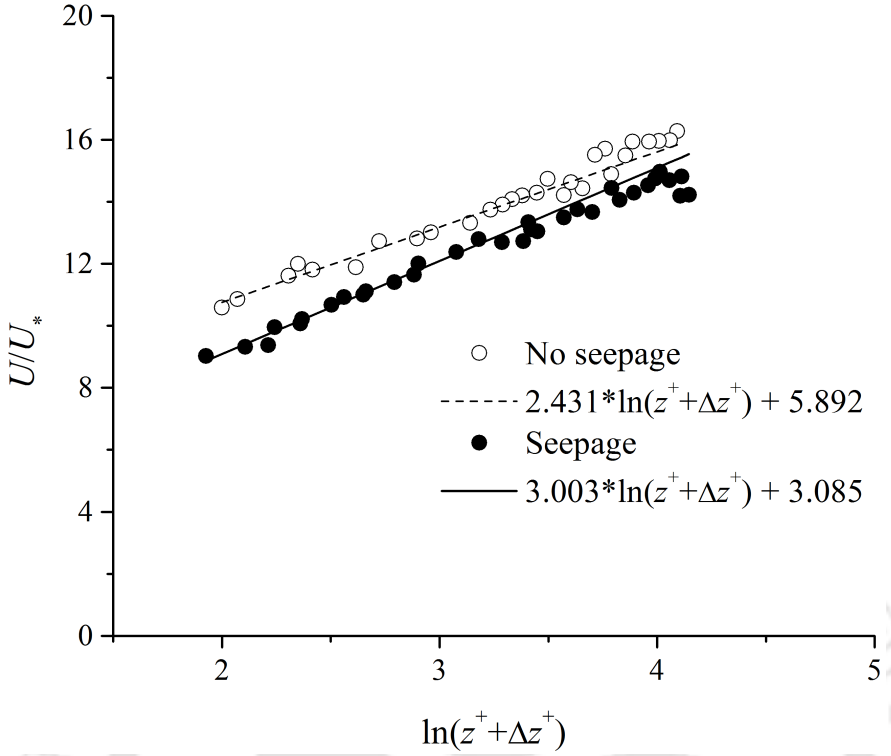

FIGURE 5.4: Logarithmic law for velocity distributions for no seepage and seepage experiments

here, $z^+ = \frac{z}{d_{50}}$, $\Delta z^+ = \frac{\Delta z}{d_{50}}$, Δz is the depth of the virtual bed below the bed surface, $\chi^+ = \frac{z_0}{d_{50}}$, z_0 is the zero velocity level, and k is the von Karman's constant.

One can observe from Figure 5.4 that the modified logarithmic law for no seepage condition does not hold for the streamwise velocity under seepage condition any longer as there is strong exchange of momentum between the flow in the streamwise direction and seepage flow in the vertically downward direction. Hence, the modified logarithmic law for no seepage condition has further been modified for the seepage condition. Average values of the von Karman's constant, depth of the virtual bed level, and the zero velocity level have been obtained as 0.402, 5.40 mm, and 0.12 mm, respectively, for no seepage condition and 0.340, 7.32 mm, and 0.39 mm, respectively, for seepage condition. Value of the k for no seepage condition has been observed to be in a good agreement with the universal value (0.41).

Right after the application of downward seepage to the non-transporting bed where the bed particles were on the verge of motion, the channel bed started transporting sediments and the value of k decreased significantly to 0.34, from its universal

value. Further, it has also been observed in the present experiments that the depth of virtual bed level and the level of zero velocity from the bed surface increased after the application of downward seepage, suggesting an exposure of increased velocity component in the streamwise direction to the particles on the bed surface.

5.4 Reynolds Stresses

Reynolds stresses provide crucial information on the characteristics of flows without seepage and after the seepage is applied. Reynolds stresses are the components of a symmetric second order tensor where the diagonal components are called the Reynolds normal stresses (RNS) and the off diagonal components are called the Reynolds shear stresses (RSS) (Pope, 2000).

5.4.1 Distribution of Reynolds Shear Stresses (RSS)

Vertical distribution of RSS for no seepage and seepage runs has been shown in Figure 5.5 and Figure 5.6 for Set-1 and Set-2 experiments, respectively, where the vertical ordinate (z) has been made non-dimensional with the flow depth (y). The friction velocity U^* has been evaluated by the linear projection of the RSS profile on the channel bed, $U_* = \left(-\overline{u'w'}\right)^{0.5}{}_{at\ z=0}$ as has been suggested by Nezu (1977) and Dey et al. (2012). The vertical distribution of the non-dimensional RSS ($\overline{uw}^+ = -\overline{u'w'}/{U_*}^2$) for no seepage and seepage runs has been plotted in Figure 5.7 and Figure 5.8 for Set-1 experiments and in Figure 5.9 and Figure 5.10 for Set-2 experiments, respectively.

Figure 5.7 to Figure 5.10 show that the distribution of the RSS in outer layer ($\frac{z}{y}$>0.1) for both, no seepage and seepage runs is reasonably consistent with the linear law of RSS for free surface flows with zero pressure gradient ($\overline{uw}^+ = -\overline{u'w'}/{U_*}^2 = 1 - z/y$). It can be seen from Figure 5.5 and Figure 5.6 that RSS

increases with decrease in the distance from the boundary and attains a maximum value somewhere between $0.01<z<0.03$ m and then again decrease towards the channel bed which indicates the presence of a roughness sublayer in the near bed region. Further, the distance of occurrence of maximum RSS from the bed increases when seepage in the downward direction is applied to the no seepage run, indicating thickness of the roughness sublayer under seepage. In the present experiments, the profiles of Reynolds shear stress distribution has been found similar for both no seepage and seepage runs, but the magnitude is higher in outer ($\frac{z}{y}>0.2$) as well as in inner ($\frac{z}{y}<0.2$) regions of flow.

The maximum RSS increased approximately by 21% and 22% after the application of seepage for Set-1 and Set-2 experiments, respectively. This increase in the RSS caused the subsequent increase (11.11% and 16% for Set-1 and Set-2 experiments, respectively) in the shear velocities.

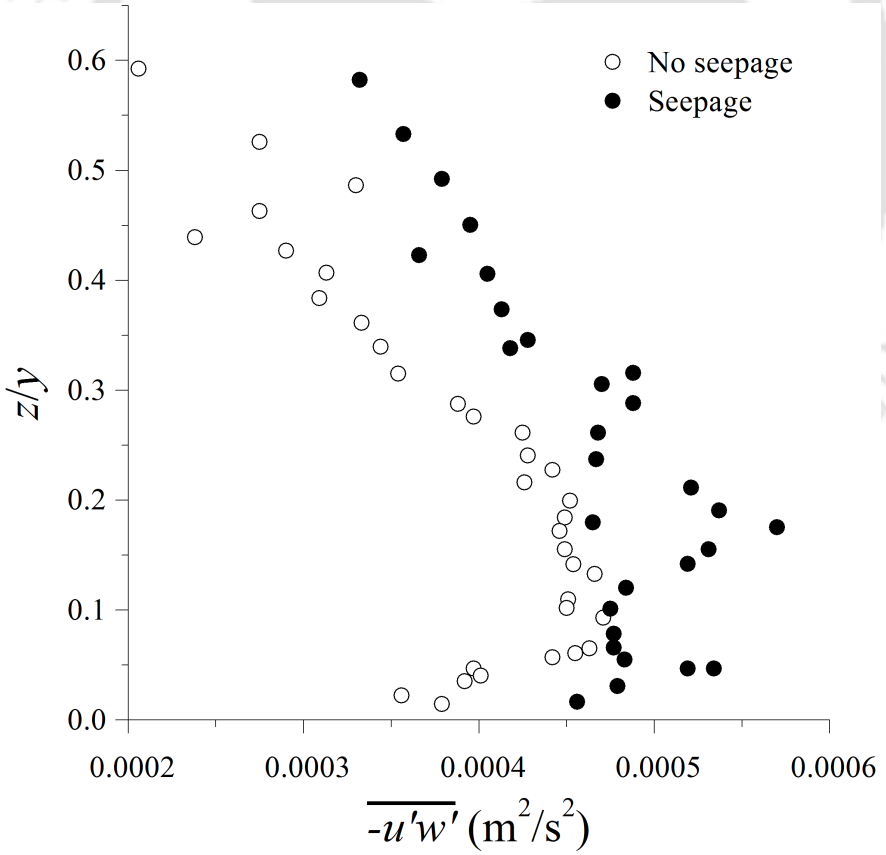

FIGURE 5.5: Vertical distribution of the Reynolds shear stresses for Set-1 experiments

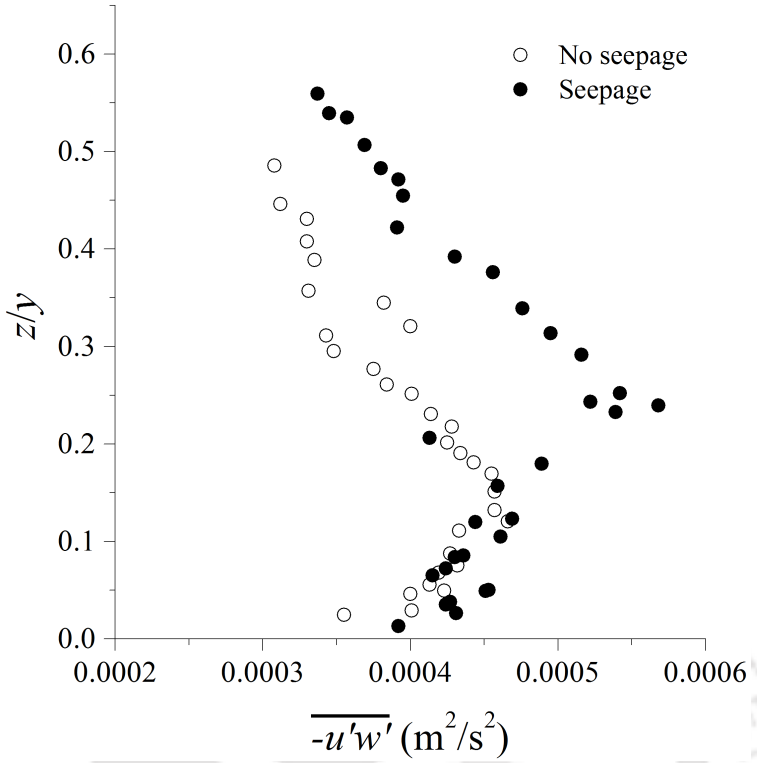

FIGURE 5.6: Vertical distribution of the Reynolds shear stresses for set-2 experiments

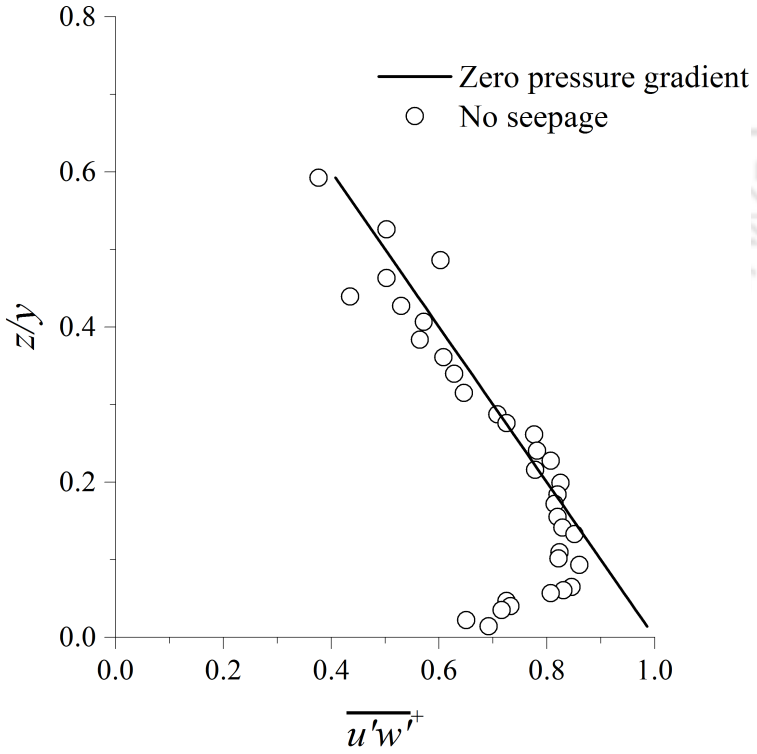

FIGURE 5.7: Distribution of non-dimensional RSS for Set-1 experiments in no seepage case

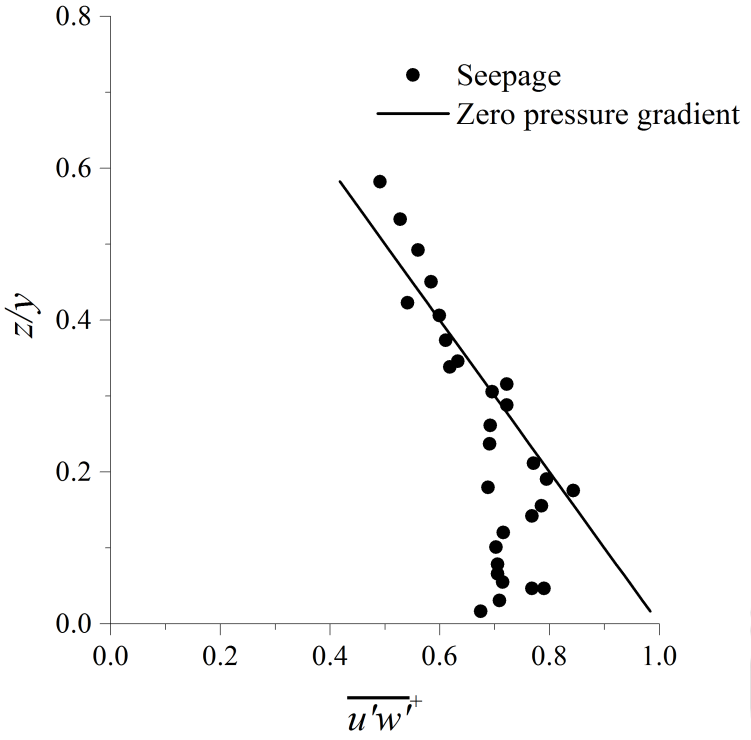

FIGURE 5.8: Distribution of non-dimensional RSS for Set-1 experiments in seepage case

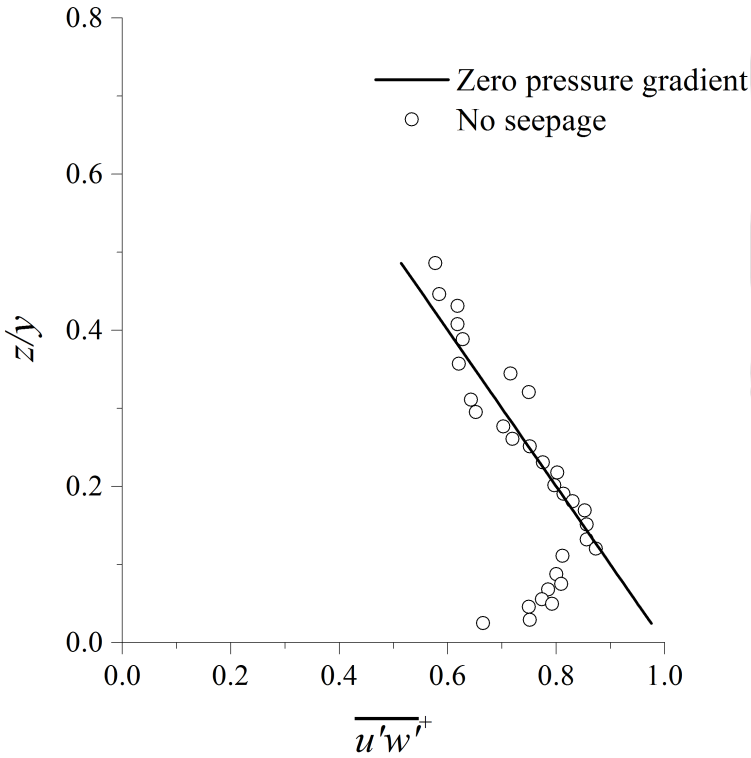

FIGURE 5.9: Distribution of non-dimensional RSS for Set-2 experiments in no seepage case

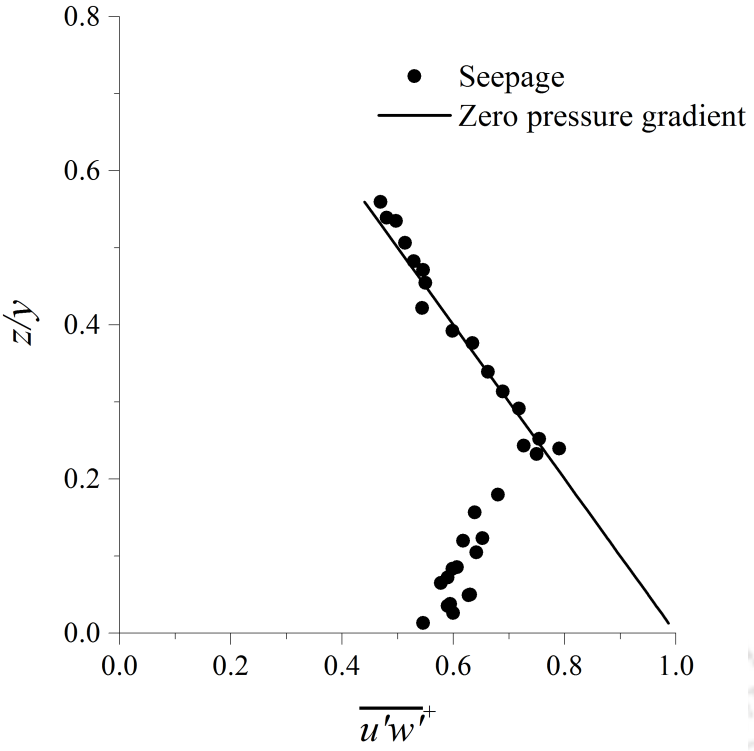

FIGURE 5.10: Distribution of non-dimensional RSS for Set-2 experiments in seepage case

5.4.2 Distribution of Reynolds Normal Stresses (RNS)

Vertical distribution of Reynolds normal stresses also called the turbulence intensities or the second moments of velocity, have been plotted in Figure 5.11 and Figure 5.12 for Set-1 experiments. Streamwise turbulence intensities (σ_u) and vertical turbulence intensities (σ_w) have been made non-dimensional with U^* and have also been depicted in Figure 5.13 and Figure 5.14.

$$\left.\begin{aligned} {\sigma_u}^+ &= \frac{\sigma_u}{U_*} = \frac{\sqrt{\overline{u'u'}}}{U_*} \\ {\sigma_w}^+ &= \frac{\sigma_w}{U_*} = \frac{\sqrt{\overline{w'w'}}}{U_*} \end{aligned}\right\} \tag{5.9}$$

It is clear from Figure 5.11 and Figure 5.12 that turbulent intensities increased in the seepage runs and attained significantly higher values than that of no seepage runs in outer ($\frac{z}{y}$>0.2) and in the inner ($\frac{z}{y}$<0.2) zones of flow while, the non-dimensional turbulent intensities (Figure 5.13 and Figure 5.14) decreased in the

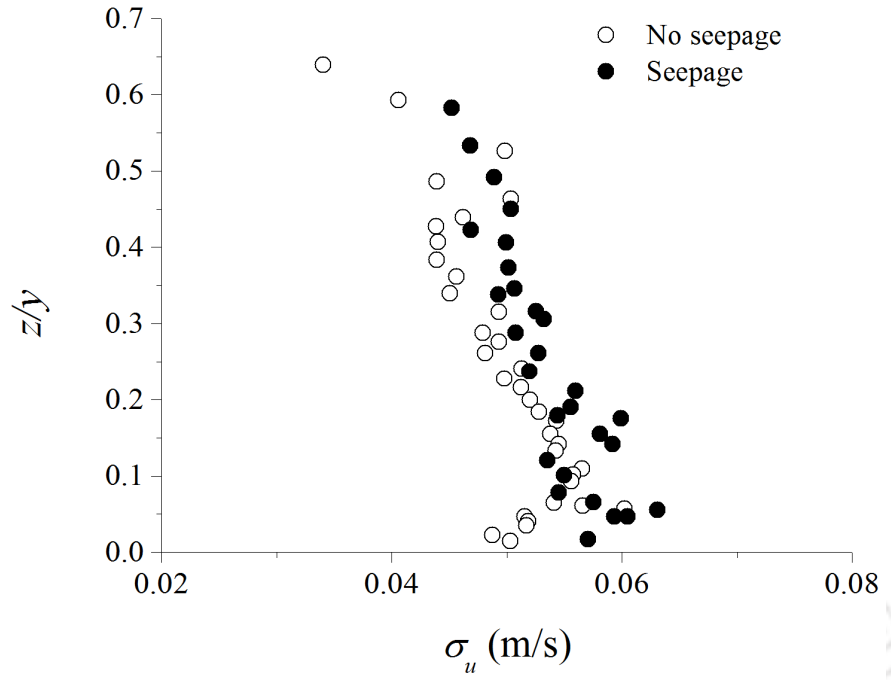

FIGURE 5.11: Distribution of the streamwise turbulence intensities for Set-1 experiments

seepage run. This decrease in the non-dimensional turbulent intensities may be attributed to the corresponding increase in the shear velocities. Similar results have been obtained for Set-2 experiments and the results are shown in Figure 5.15 to Figure 5.18. Comparison among the streamwise turbulent intensities with universal functions of turbulent intensity (Nezu and Nakagawa, 1993) and those provided by Nikora and Goring (1998) has been depicted for no seepage and seepage runs in Figure 5.19 and Figure 5.20 for Set-1 experiments and in Figure 5.21 and Figure 5.22 for Set-2 experiments, respectively.

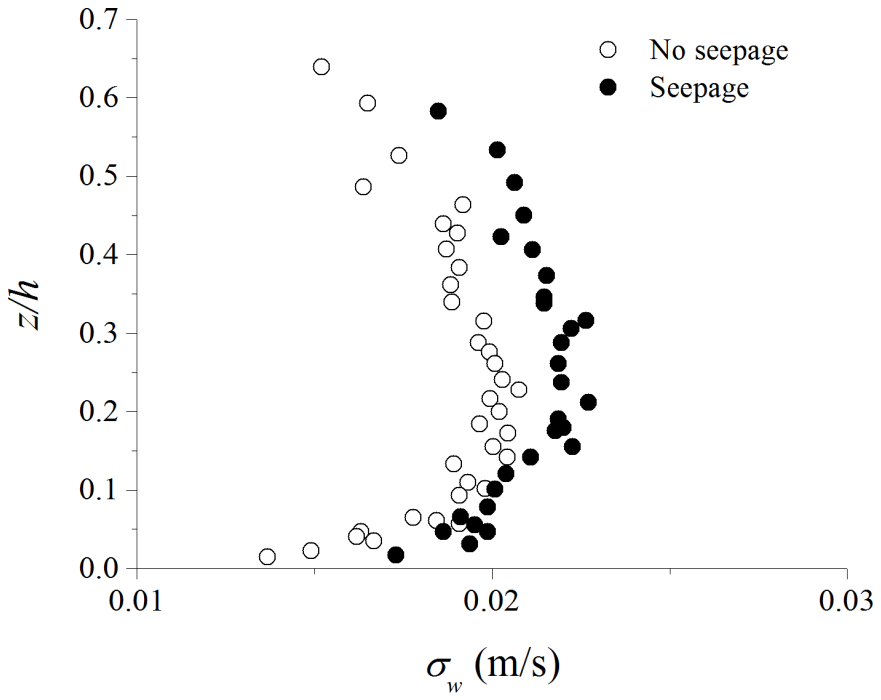

FIGURE 5.12: Distribution of the vertical turbulence intensities for Set-1 experiments

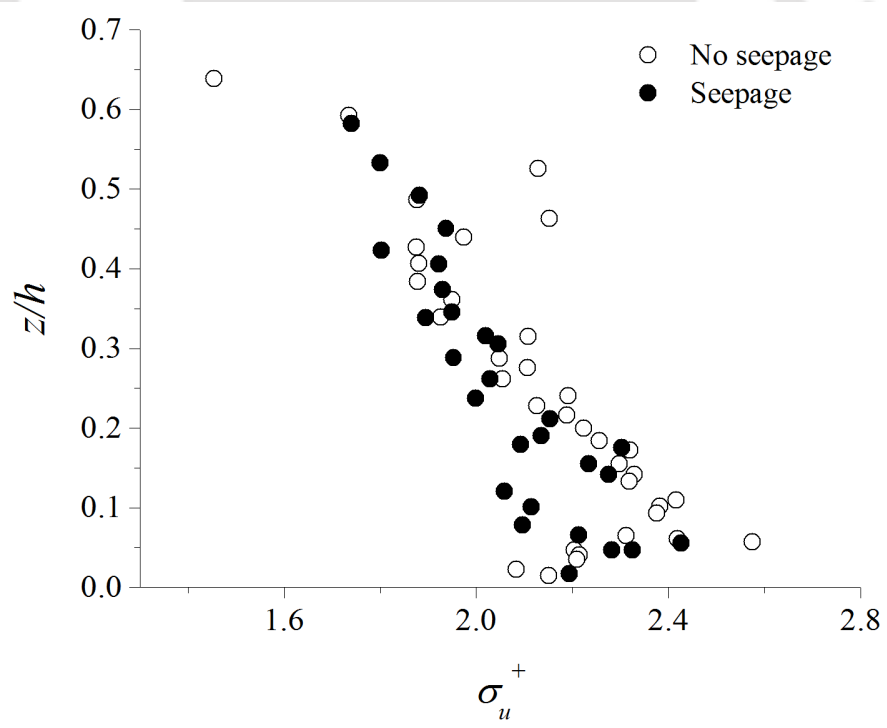

FIGURE 5.13: Distribution of the non-dimensional streamwise RNS for Set-1 experiments

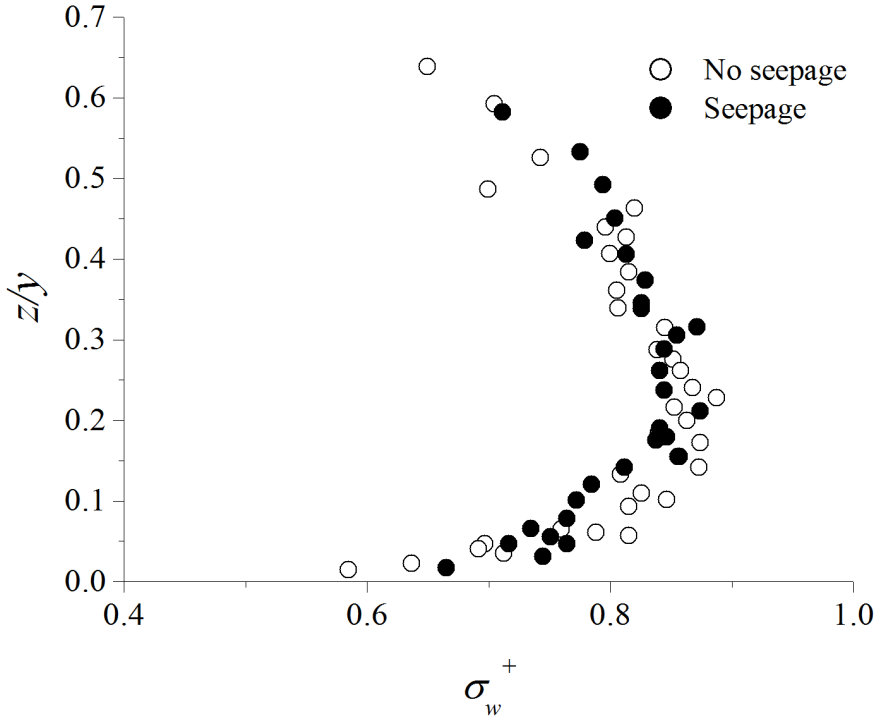

FIGURE 5.14: Distribution of the non-dimensional vertical RNS for Set-1 experiments

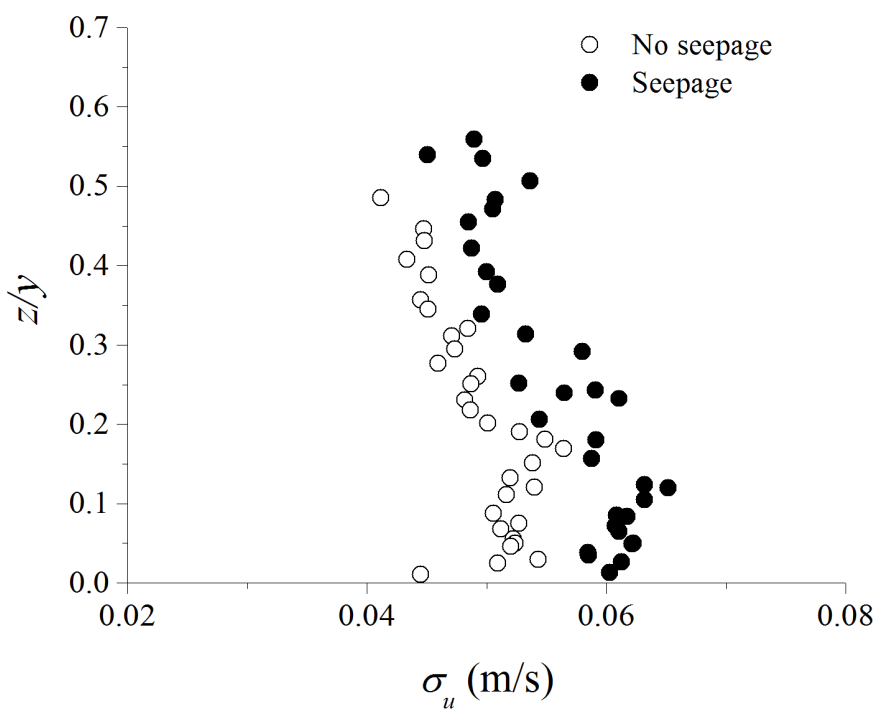

FIGURE 5.15: Distribution of the streamwise turbulence intensities for Set-2 experiments

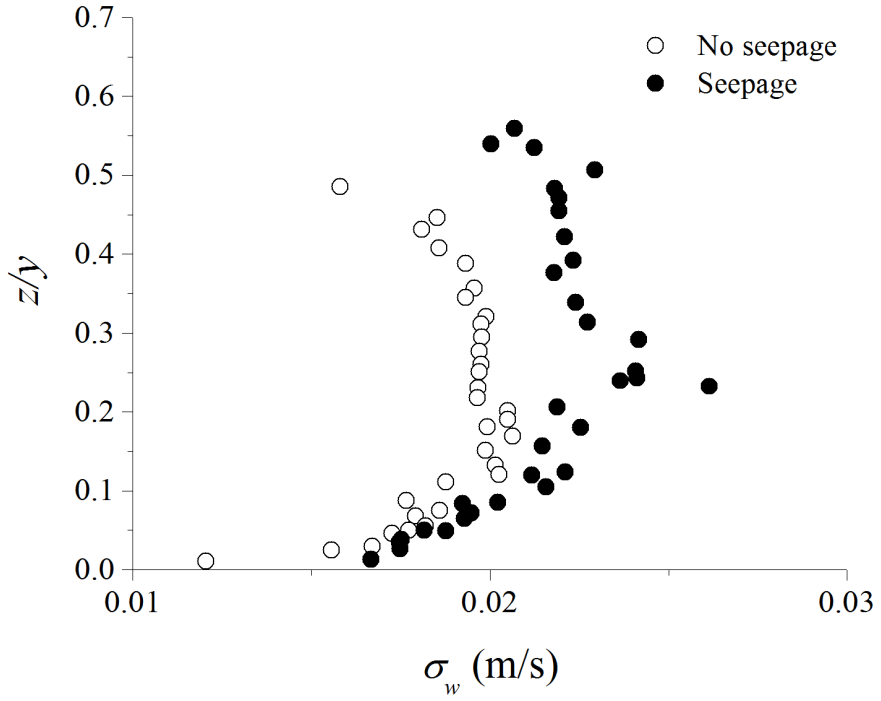

FIGURE 5.16: Distribution of the vertical turbulence intensities for Set-2 experiments

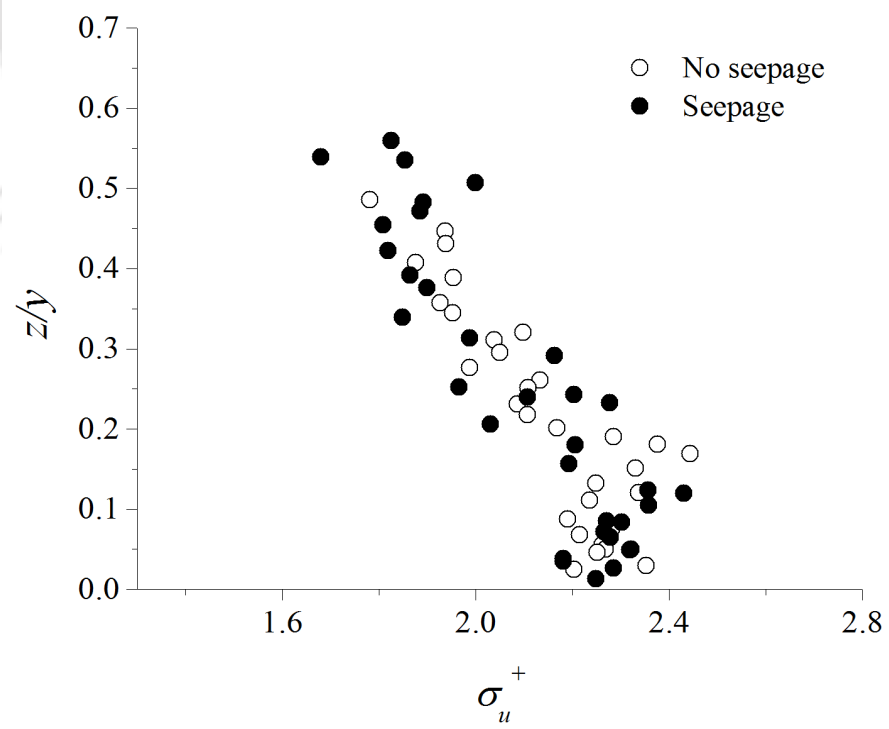

FIGURE 5.17: Distribution of the non-dimensional streamwise RNS for Set-2 experiments

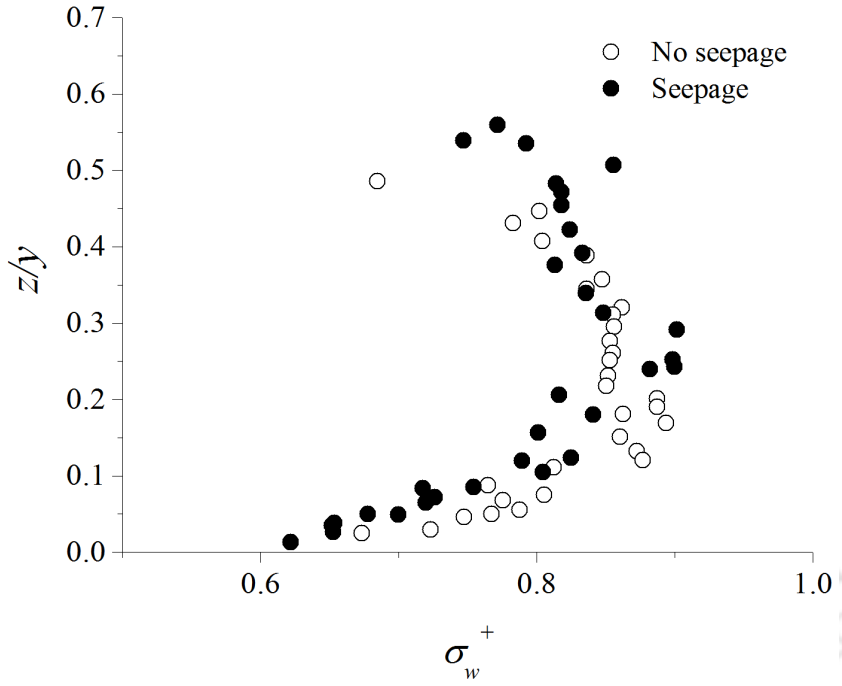

FIGURE 5.18: Distribution of the non-dimensional vertical RNS for Set-2 experiments

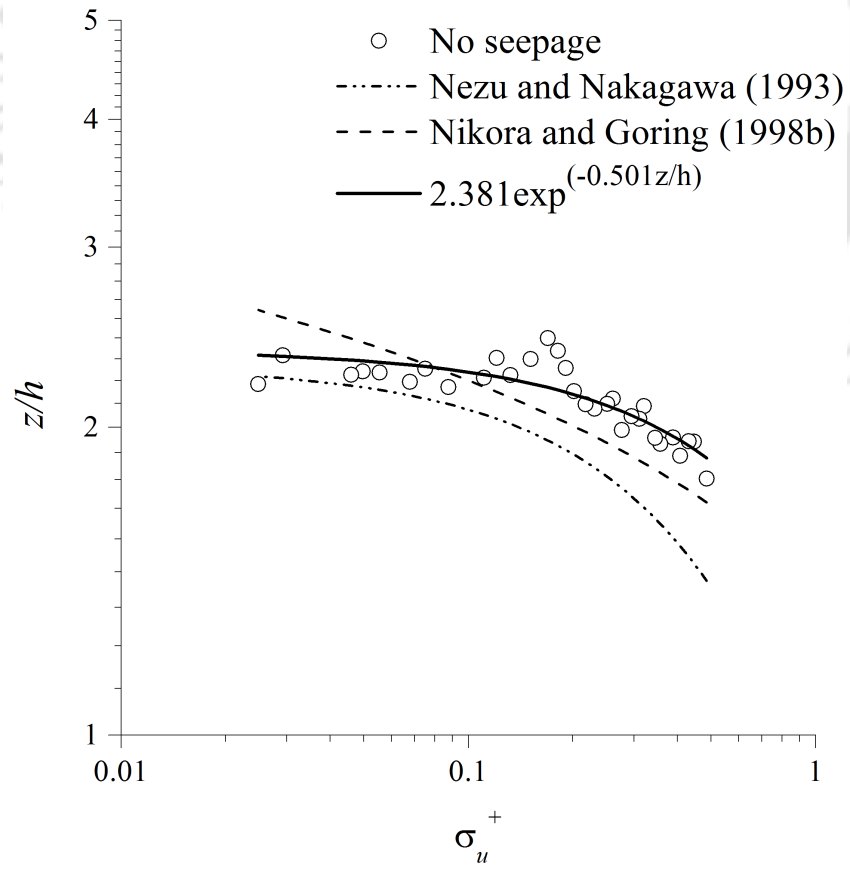

FIGURE 5.19: Comparison of turbulent intensities with Nezu and Nakagawa (1993) and Nikora and Goring (1998) for Set-1 experiments in no seepage case

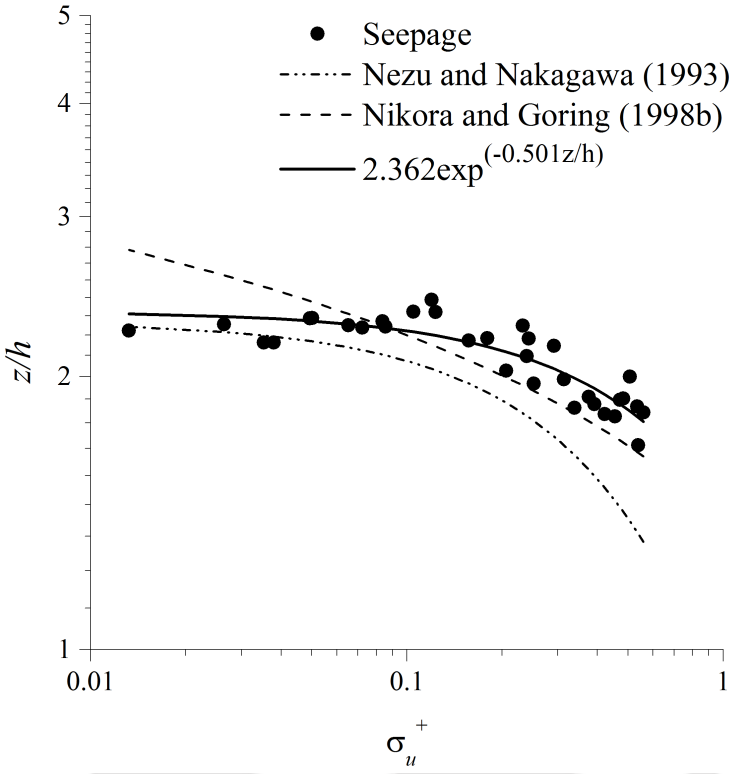

FIGURE 5.20: Comparison of turbulent intensities with Nezu and Nakagawa (1993) and Nikora and Goring (1998) for Set-1 experiments for seepage case

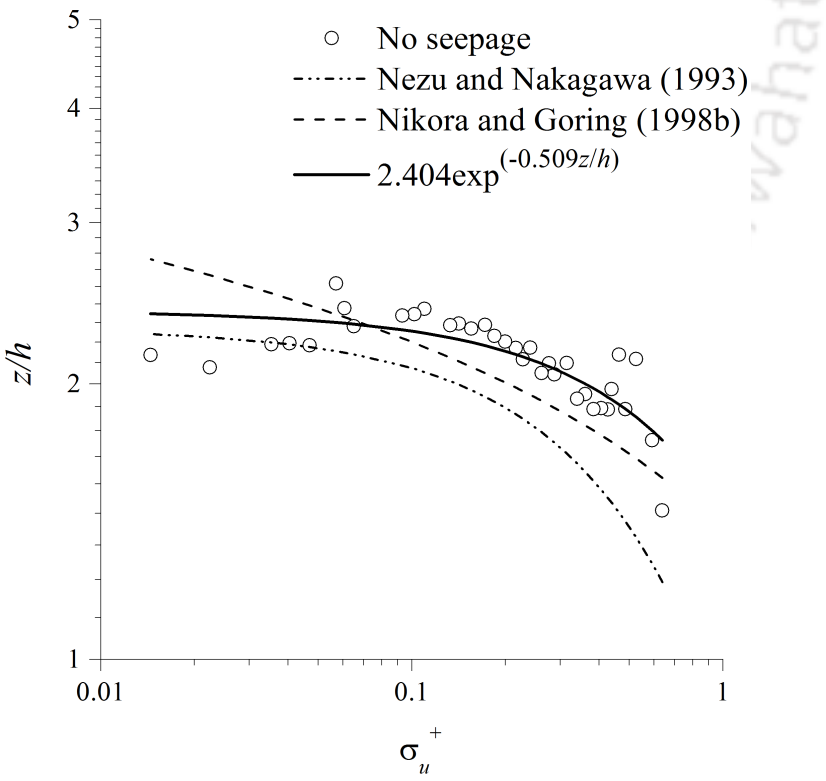

FIGURE 5.21: Comparison of turbulent intensities with Nezu and Nakagawa (1993) and Nikora and Goring (1998) for Set-2 experiments in no seepage case

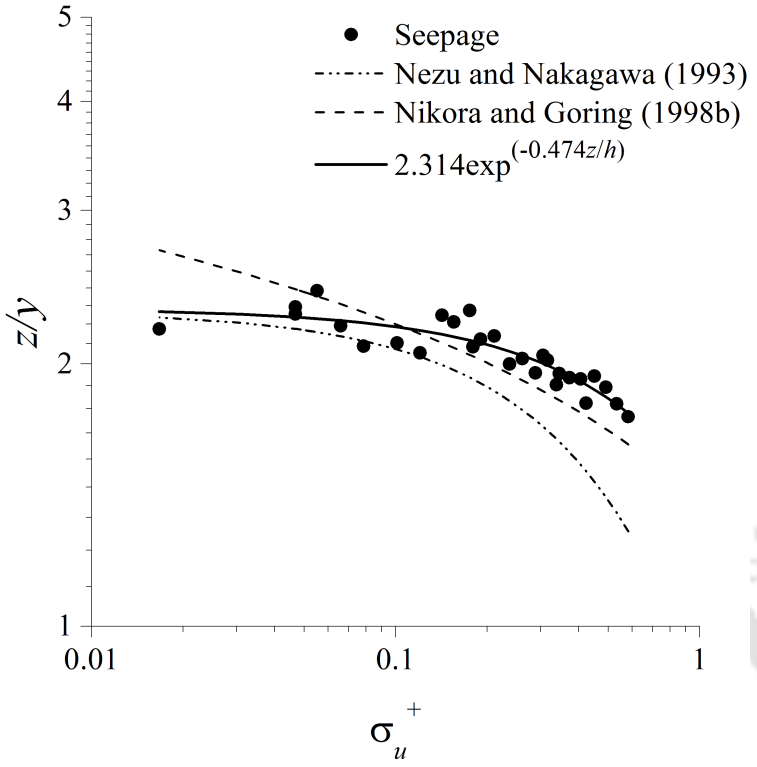

FIGURE 5.22: Comparison of turbulent intensities with Nezu and Nakagawa (1993) and Nikora and Goring (1998) for Set-2 experiments in seepage case

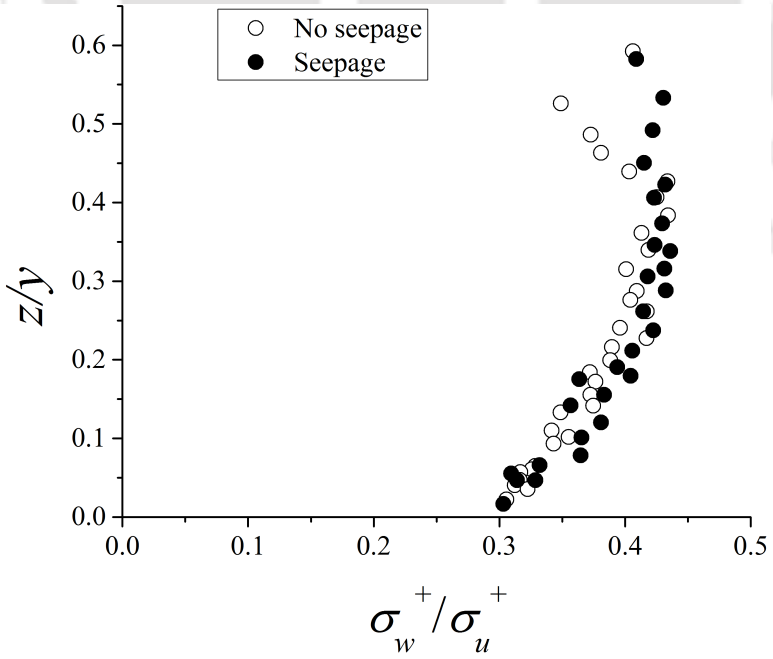

FIGURE 5.23: Vertical distribution of flow anisotropy for Set-1 experiments

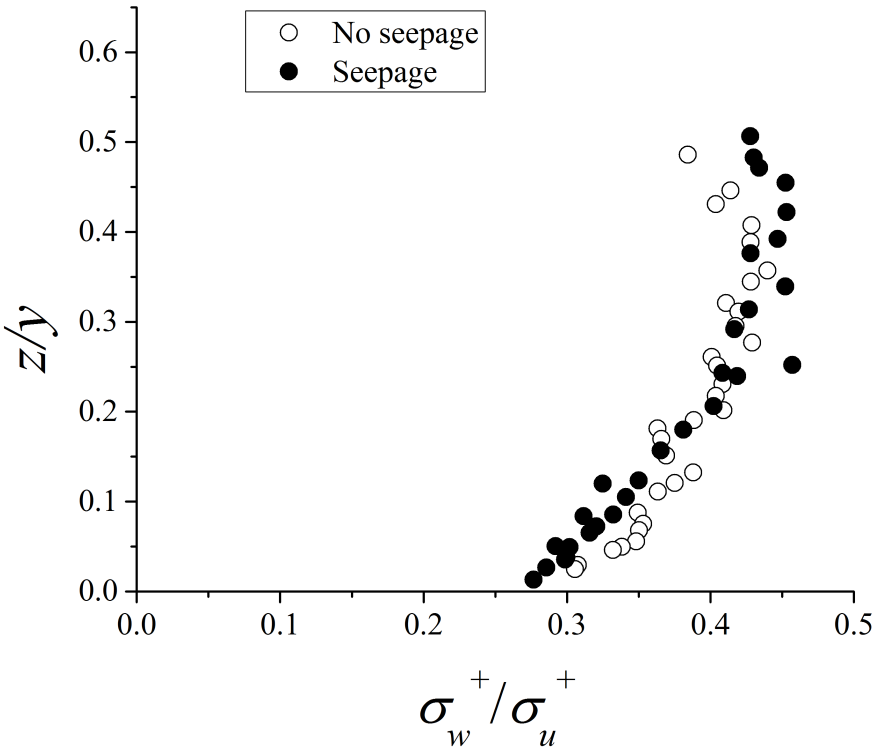

FIGURE 5.24: Vertical distribution of flow anisotropy for Set-2 experiments

TABLE 5.1: Values of the empirical constants

Experiments	Case	D_u	C_u
Set-1	No seepage	2.381	0.501
	Seepage	2.362	0.501
Set-2	No seepage	2.404	0.509
	Seepage	2.314	0.474

New empirical constants (Table 5.1) have been derived using the regression analysis for flows over curved deformable boundaries with no seepage and seepage affected channels:

$$\sigma_u{}^+ = D_u \exp\left(-C_u \frac{z}{y}\right) \tag{5.10}$$

Degree of flow anisotropy is measured by the ratio, $(\frac{\sigma_w^+}{\sigma_u^+})$. Figure 5.23 and Figure 5.24 depict the vertical distribution of $\frac{\sigma_w^+}{\sigma_u^+}$ as plotted against $\frac{z}{y}$ for Set-1 and Set-2 experiments from where it is evident that the flow is highly anisotropic as $(\frac{\sigma_w^+}{\sigma_u^+}<1)$.

It has been predicted by Nezu and Nakagawa (1993) that the ratio is universal and has a constant value (0.55) throughout the flow depth but in the present study, it has been found that the ratio does not have a constant value whereas, it is a function of depth and has a minimum value ($\frac{\sigma_w^+}{\sigma_u^+} \sim 0.3$) close to the channel bed irrespective of the flow condition i.e., for both, no seepage and seepage runs and increase linearly up to $\frac{z}{y} \sim 0.3$.

5.5 Flux of the Turbulent Kinetic Energy

Figure 5.25 and Figure 5.26 show the distribution of the non-dimensional flux of turbulent kinetic energy in the streamwise $F_{TKEu} = \frac{f_{TKEu}}{U_*^3}$ and vertical directions $F_{TKEw} = \frac{f_{TKEw}}{U_*^3}$ of Set-1 experiments for no seepage and seepage runs, respectively, which can be calculated as (Raupach, 1981; Krogstadt and Antonia, 1999; Dey et al., 2011b):

$$\left.\begin{aligned} f_{TKEu} &= \frac{3}{4}\left(\overline{u'^3} + \overline{u'w'^2}\right) \\ f_{TKEw} &= \frac{3}{4}\left(\overline{u'^2w'} + \overline{w'^3}\right) \end{aligned}\right\} \tag{5.11}$$

It can be observed from Figure 5.25 that for no seepage run in the near bed region, F_{TKEu} initiates from positive value and starts decreasing with the increasing distance from the bed and becomes negative for $\frac{z}{y}$>0.07 while, F_{TKEw} (Figure 5.26) starts with small negative value in the near bed region and increases with the increasing distance from the bed and changes sign for $\frac{z}{y}$>0.07 . In the near bed region, positive values of F_{TKEu} indicate the streamwise flux of turbulent kinetic energy in the streamwise direction while, negative values of F_{TKEw} imply the vertical flux of turbulent kinetic energy in the downward direction.

Similarly, for $\frac{z}{y}$>0.07, negative F_{TKEu} and positive F_{TKEw} correspond to the streamwise flux of turbulent kinetic energy opposite to the flow direction and vertical flux of turbulent kinetic energy in the upward direction, respectively. Similar patterns for F_{TKEu} and F_{TKEw} have been observed for the seepage runs but close

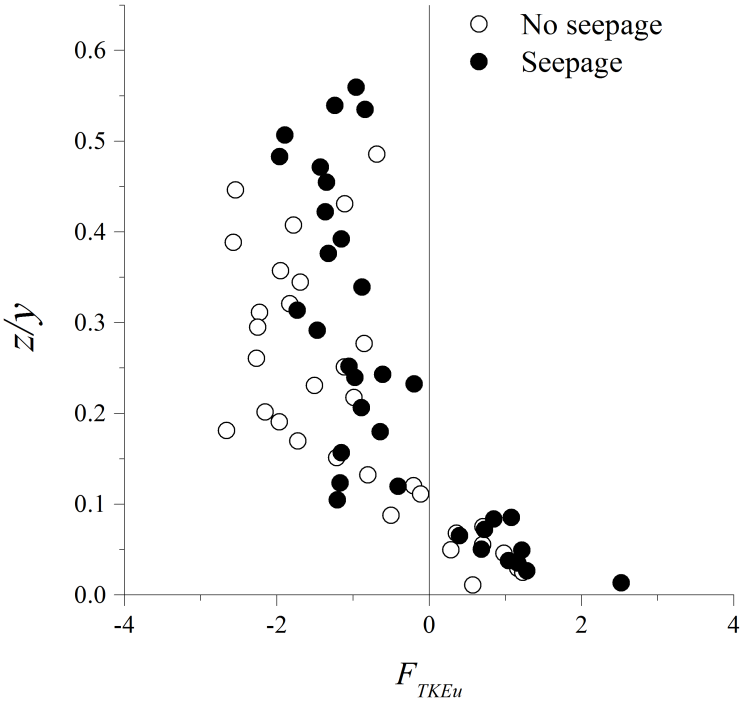

FIGURE 5.25: Vertical distribution of streamwise TKE fluxes for Set-1 experiments

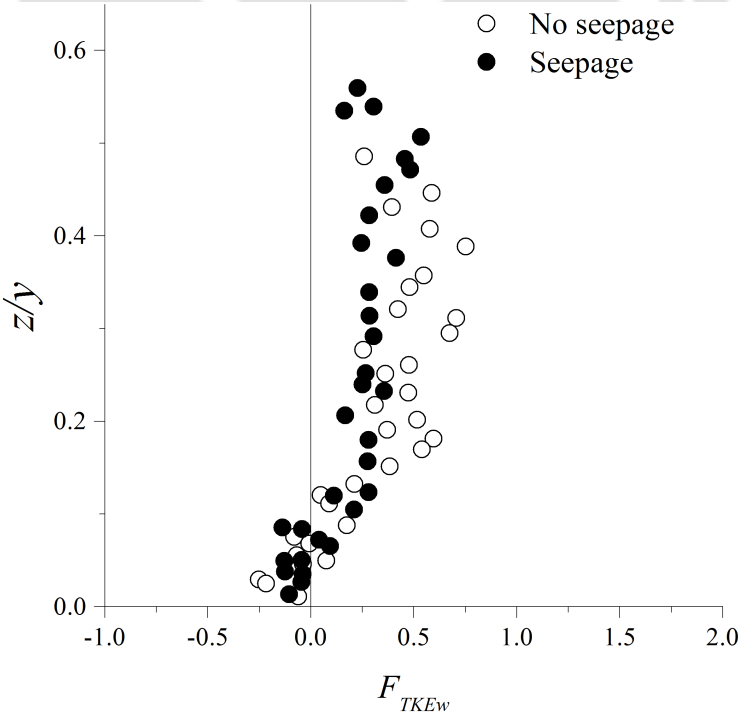

FIGURE 5.26: Distribution of vertical TKE fluxes for Set-1 experiments

observation of Figure 5.25 together with Figure 5.26 reveals an important information that in seepage runs, F_{TKEu} starts with positive value greater than that of no seepage runs in near bed region and becomes lesser negative for the rest of the depth than for no seepage runs.

Near the bed the length of the zone of negative F_{TKEw} and positive F_{TKEu} increases in the seepage runs. Positive F_{TKEu} and negative F_{TKEw} are associated to the mobility of the bed particles where, small negative F_{TKEw} and small positive F_{TKEu} in near bed region for no seepage runs indicate the prevailing condition of the incipient motion of the bed particles while, greater negative F_{TKEw} and greater positive F_{TKEw} in near bed region for seepage runs imply the mobile bed condition immediately after the application of downward seepage. Similar results in the near-bed region and away from the bed have been observed in Set-2 experiments and are shown in Figure 5.27 and Figure 5.28 for F_{TKEu} and F_{TKEw}, respectively.

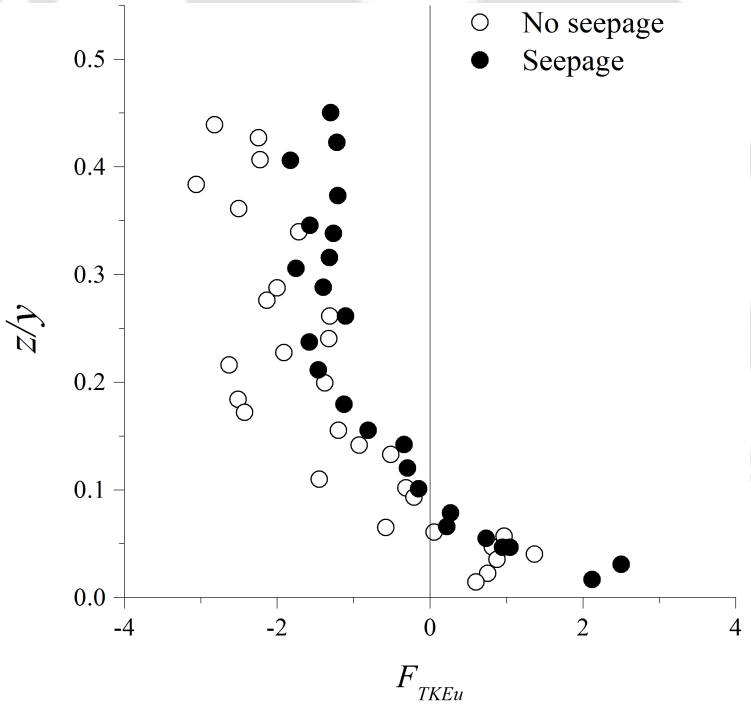

FIGURE 5.27: Vertical distribution of streamwise TKE fluxes for Set-2 experiments

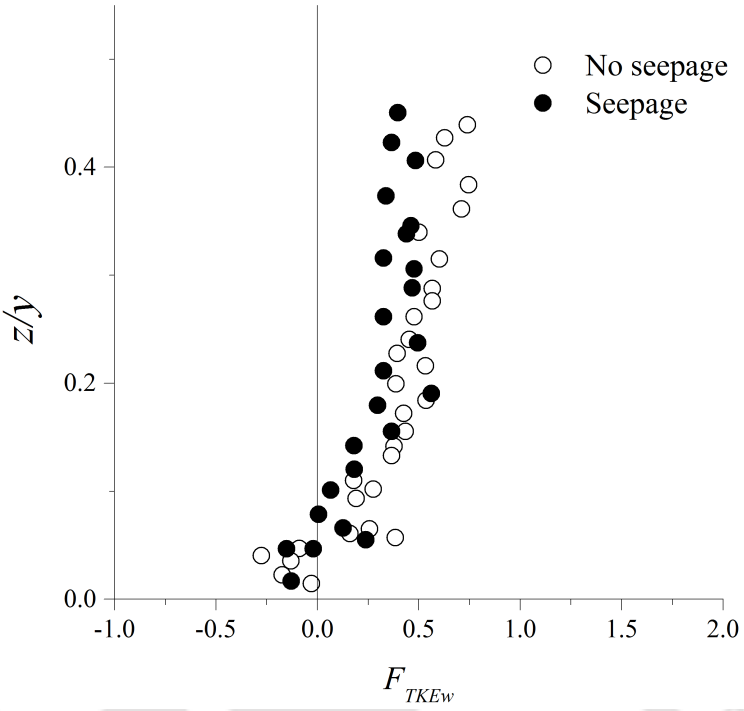

FIGURE 5.28: Distribution of vertical TKE fluxes for Set-2 experiments

5.6 Conditional Statistics for Reynolds Shear Stress Distribution

The total Reynolds shear stress ($-\overline{u'w'}$) at any given point is the sum of different types of bursting events. Thus, depending upon the relative sign of instantaneous values of velocity fluctuations u and w, the bursting events can be plotted in four different quadrants ($i = 1, 2, 3, 4$) of (u, w) plane (Lu and Willmarth, 1973) i.e. outward interactions ($i = 1 : u{>}0, w{>}0$), ejections ($i = 2 : u{<}0, w{>}0$), inward interactions ($i = 3 : u{<}0, w{<}0$), and sweeps ($i = 4 : u{>}0, w{<}0$). At any point in the flow field, the contribution to the total Reynolds shear stress through different ways of momentum transfer can be calculated as:

$$\langle u'w' \rangle_{i,H} = \lim_{T \to 0} \frac{1}{T} \int_0^T u'(t)\, w'(t)\, \delta_{i,H} \left[u'(t), w'(t) \right] dt \tag{5.12}$$

where angle brackets correspond to conditional averaging, T is the sampling time, and $\delta_{i,H}$ is the indicator function. The definition of indicator function can be given

as:

$$\delta_{i,H}\left[u'(t), w'(t)\right] = \begin{cases} 1, \text{ if } (u', w') \text{ are in quadrant } i \text{ and if } |u'w'| \geq H\sigma_u\sigma_w \\ 0, \text{ otherwise.} \end{cases} \tag{5.13}$$

where H is the parameter defined by the hyperbolic hole region (Nezu and Nakagawa, 1993) which allows the investigation of larger contribution to total Reynolds shear stress from various quadrants. Schematic diagram of four quadrants and hole region has been depicted in Figure 5.29. Pairs of ($u^{'}$, $w^{'}$) in Cartesian coordinate system are shown in Figure 5.30 and Figure 5.31 for no seepage and seepage experiments, respectively, at $\frac{z}{y} \sim 0.015$. Fractional contribution to the total Reynolds shear stress from different quadrants can be defined as:

$$S_{i,H} = \frac{\langle u'w' \rangle_{i,H}}{\overline{u'w'}} \tag{5.14}$$

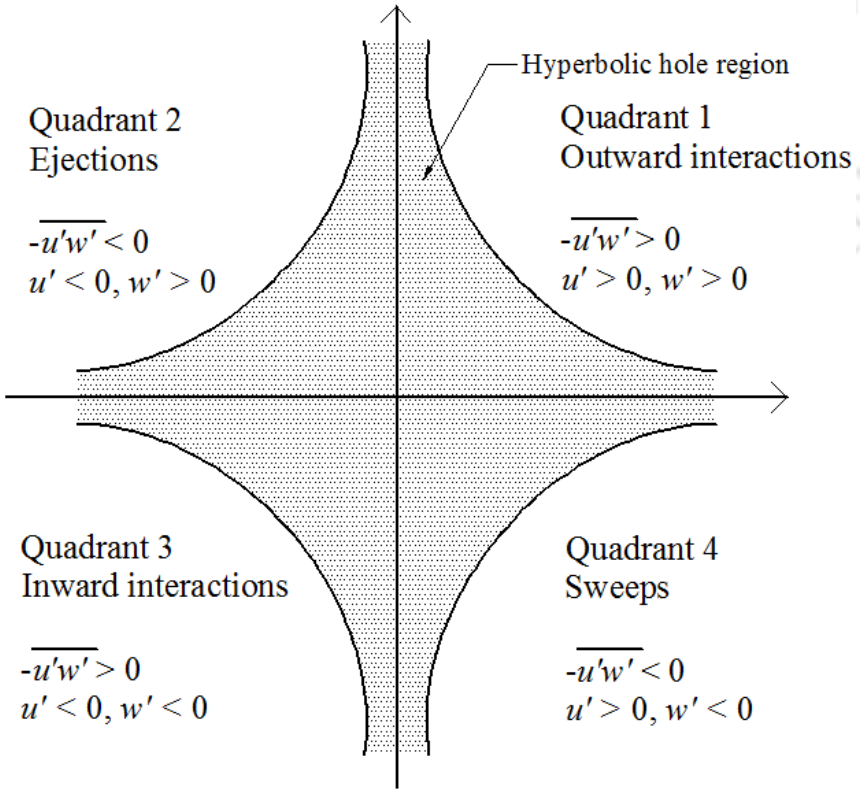

FIGURE 5.29: Schematic diagram of quadrants and hole region

$S_{i,H}$ is positive for outward and inward interactions ($i = 1, 3$) and is negative for ejections and sweeps ($i = 2, 4$). Equation (5.14) implies that for $H = 0$ when hole size disappears, sum of the fractional contributions from all the quadrants equals to unity ($\sum_{i=1}^{4} S_{i,0} = 1$).

Conditional statistics through the quadrant analysis provides essential information of the coherent structure of turbulent flow in the near wall region. It has been observed through the flow visualization techniques (Kline et al., 1967) that relatively slow moving fluid parcel in the region very near to the wall, drifts away from the wall. At some distance, it moves violently away from the wall, oscillates, breaks down and merges in the flow layers. This process in which the fluid parcel moves slowly away from the wall is called ejection. In order to maintain continuity, high speed fluid moves towards the wall which is called sweeps. These combined events are called bursting and provide characteristic behavior to the turbulence.

Grass (1971), Nakagawa and Nezu (1977), and Raupach (1981) have observed that largest contribution to the Reynolds shear stress come from both ejections and sweeps throughout the boundary layer. Although ejections dominate in most of the thickness of boundary layer, sweeps are prevalent in the near boundary region. Thus, the roughness characteristics and sediment transport are associated mainly to the sweep events which are dominant in contribution to the momentum transfer in the region close to the boundary.

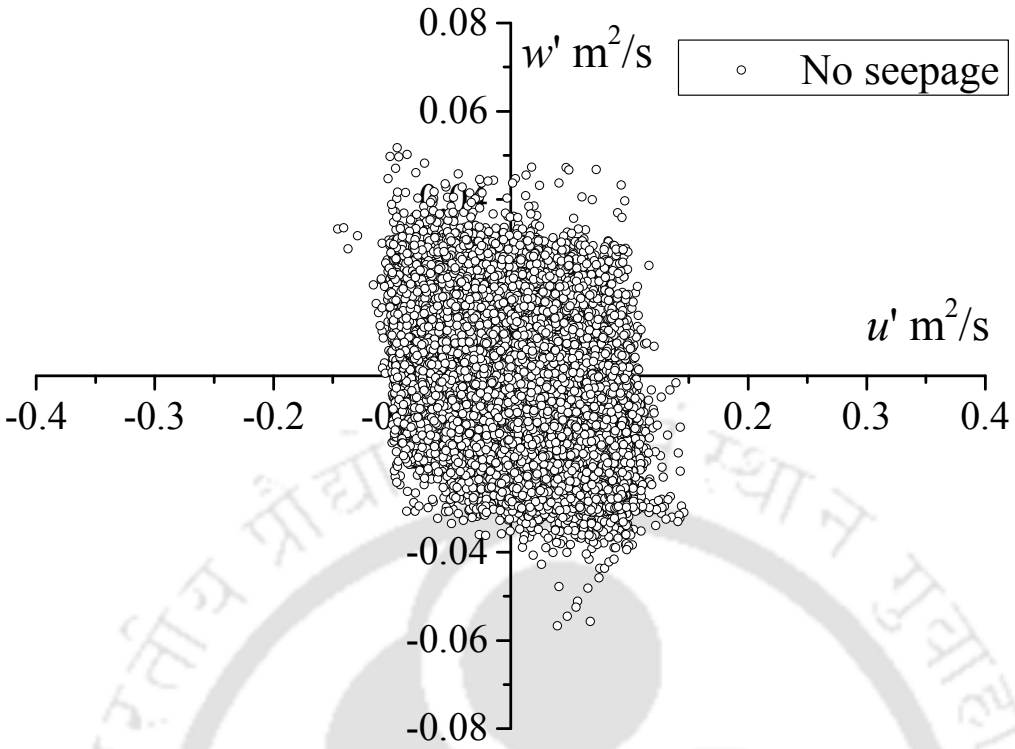

FIGURE 5.30: (u', w') for no seepage experiment

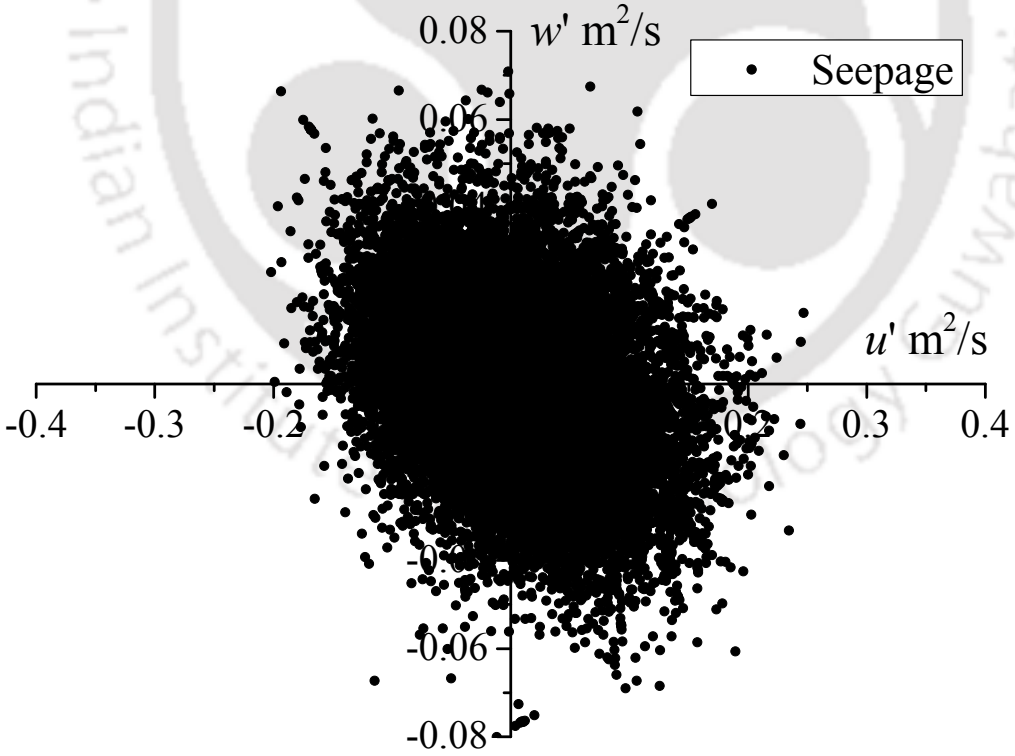

FIGURE 5.31: (u', w') for seepage experiment

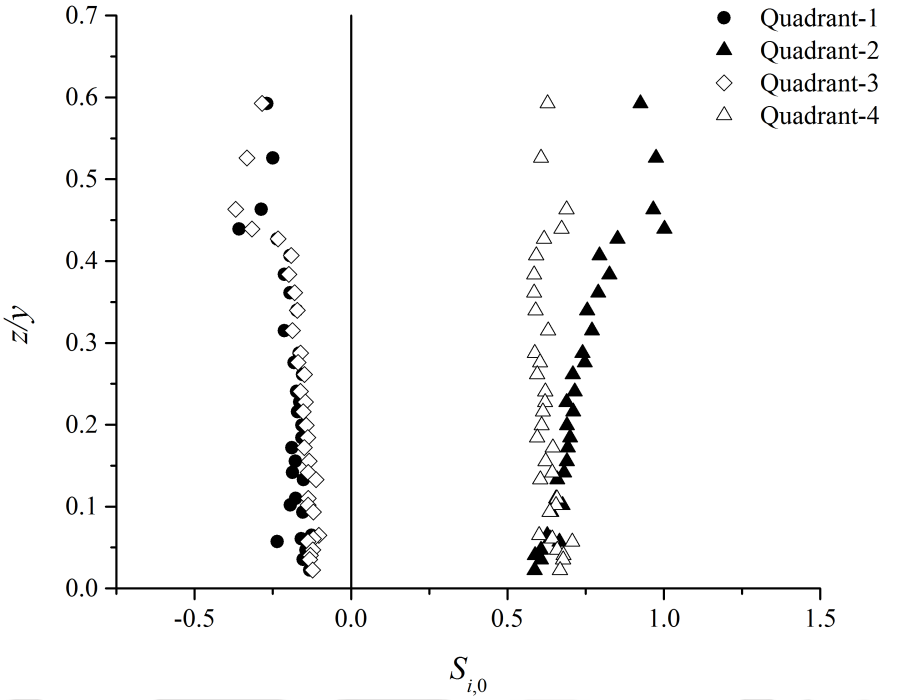

FIGURE 5.32: Quadrant analysis for no seepage and $H = 0$ for Set-1 experiments

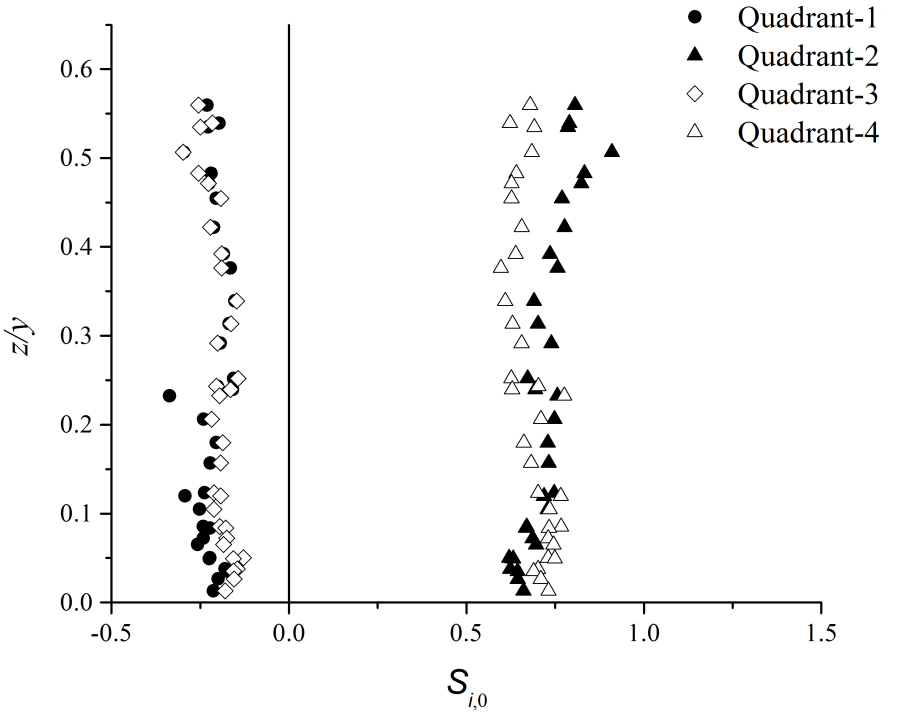

FIGURE 5.33: Quadrant analysis for seepage and $H = 0$ for Set-1 experiments

Vertical distributions of the fractional contribution towards Reynolds shear stresses $S_{i,H}$ for $H = 0$ for no seepage and seepage runs have been plotted in Figure 5.32 and Figure 5.33, respectively, for Set-1 experiments. For $H = 0$, all the pairs of (u', w') are plotted which is helpful to understand the near bed characteristics of turbulent flow. Throughout the measured depth, most of the contribution comes from ejection and sweep events while, outward and inward interactions contribute weakly toward the Reynolds shear stress production.

From Figure 5.32, it can be observed that at very near to the bed ($\frac{z}{y} \sim 0.025$) contribution from the sweep events towards the Reynolds shear stress production is highest (67%) and that from the ejections is 59% while, the contributions from the quadrant-1 and quadrant-3 events are very small ($\sim$ 13%) for no seepage run where the particles on the channel bed are on the threshold of motion.

Thickness of the sweep dominated region extends nearly up to $\frac{z}{y} \sim 0.06$. Moving further away from the bed ($\frac{z}{y}$>0.06), ejection events dominate in contributing to the Reynolds shear stresses. In this flow layer (0<$\frac{z}{y}$<0.06), average contributions from ejections and sweeps are 61% and 66%, respectively.

In the seepage run (Figure 5.33), the contribution from all the events towards RSS production increases from that of no seepage run. At very near to the bed $\frac{z}{y} \sim 0.025$, the contribution from sweeps in seepage run is 71% while, that from ejections is 64%. Weak contributions about 20% and 15% from outward and inward interactions are observed. Thickness of the zone of sweep dominance increases from $\frac{z}{y} \sim 0.06$ of no seepage to $\frac{z}{y} \sim 0.12$ in the seepage run. Average contributions from ejections and sweeps in the flow layer (0<$\frac{z}{y}$<0.12) are 67% and 73%, respectively.

These increased values of contribution from sweep events and thickness of the zone of sweep dominance in seepage run corresponds to the mobile bed condition that takes place when downward seepage is applied to the channel which was on the incipient motion of the bed particles at no seepage.

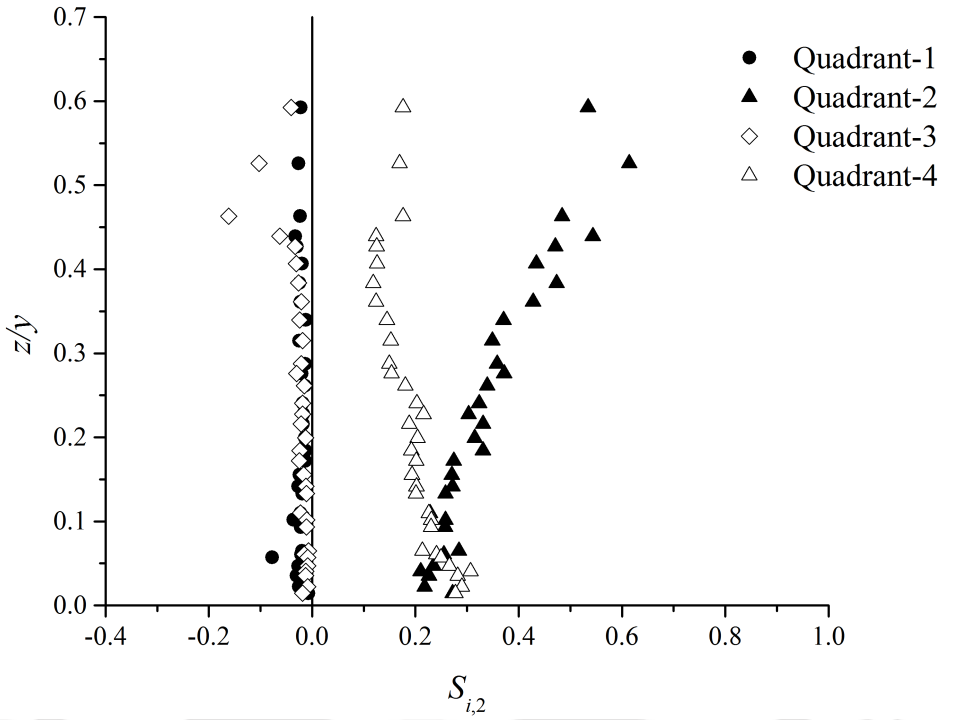

FIGURE 5.34: Quadrant analysis for no seepage and $H = 2$ for Set-1 experiments

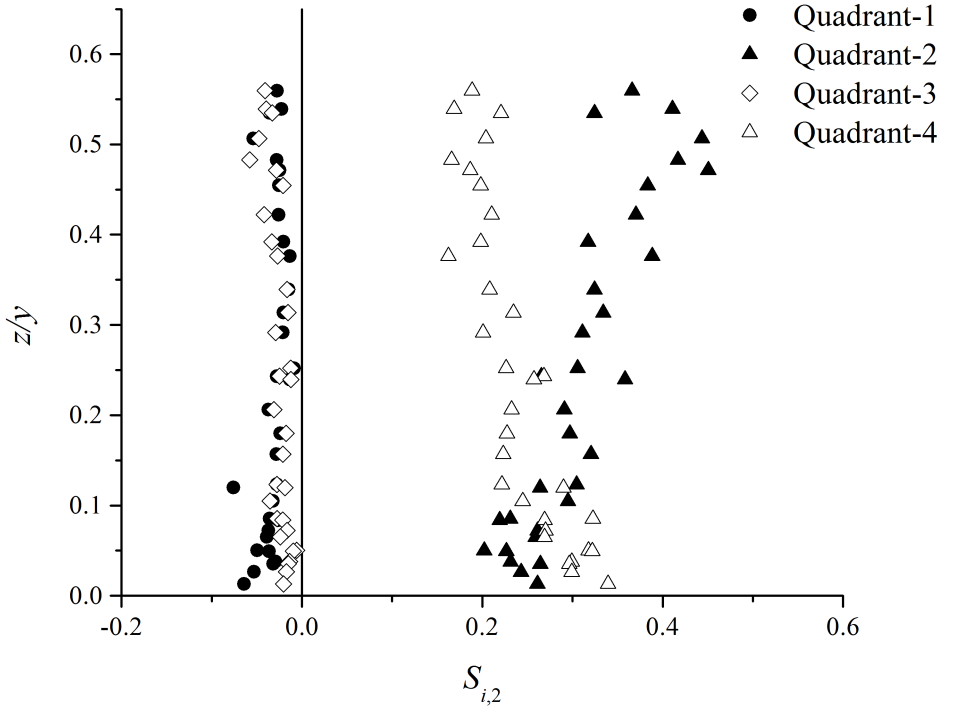

FIGURE 5.35: Quadrant analysis for seepage and $H = 2$ for Set-1 experiments

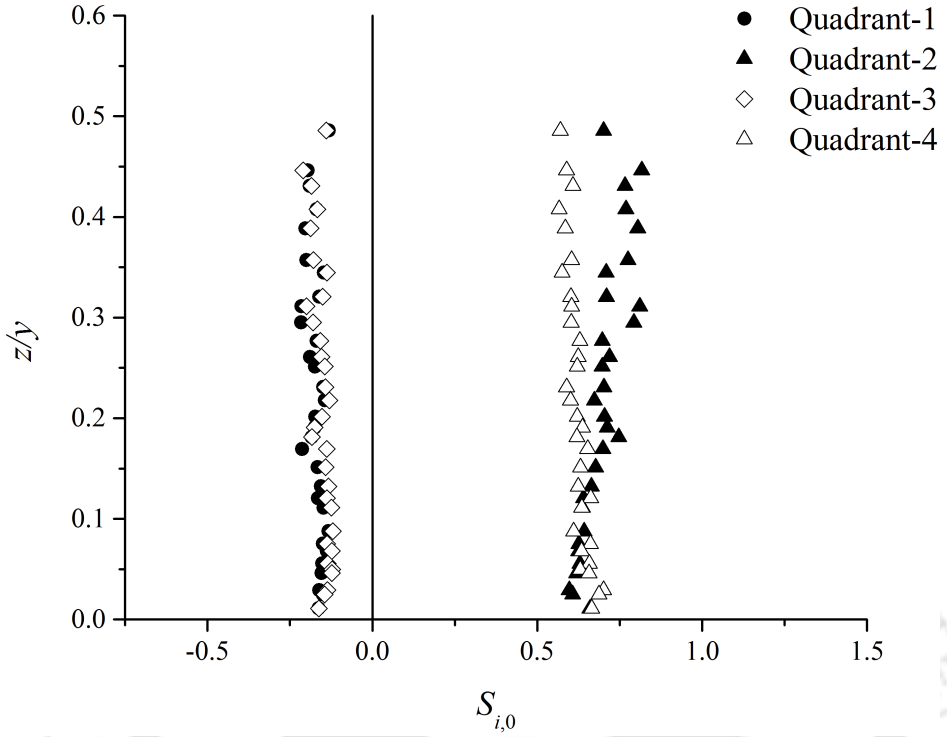

FIGURE 5.36: Quadrant analysis for no seepage and $H = 0$ for Set-2 experiments

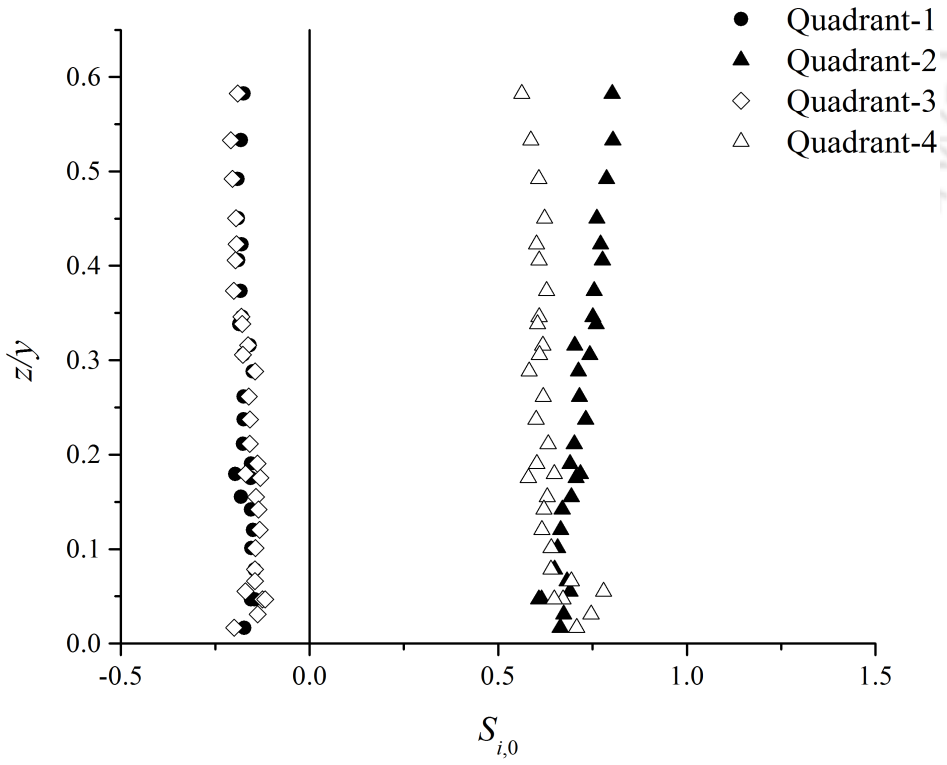

FIGURE 5.37: Quadrant analysis for seepage and $H = 0$ for Set-2 experiments

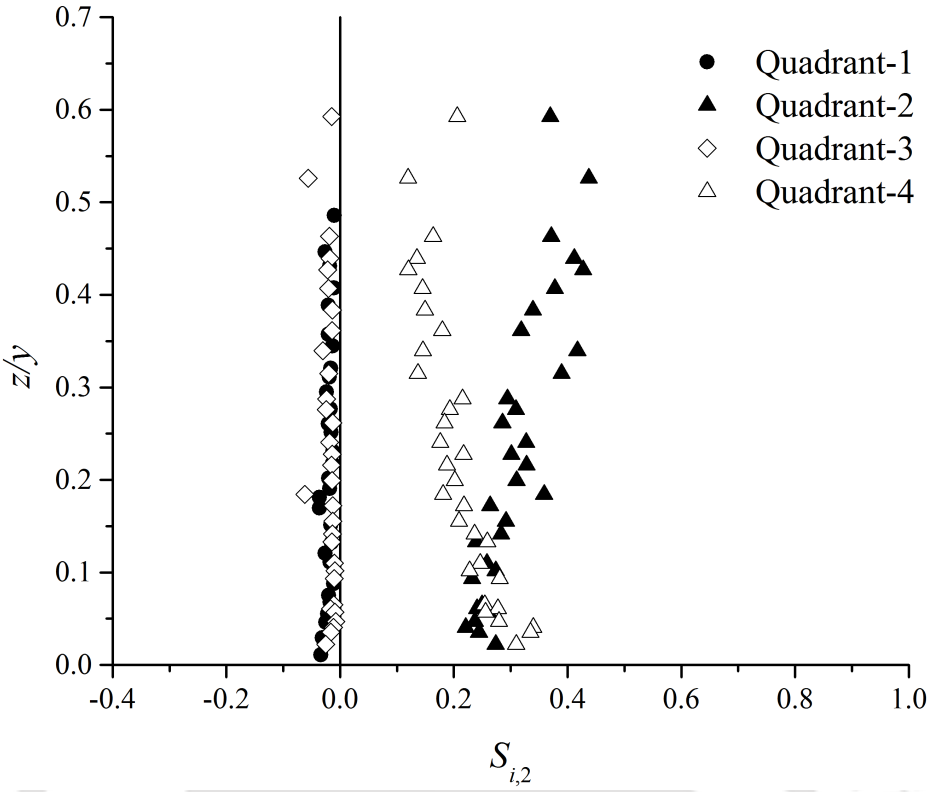

FIGURE 5.38: Quadrant analysis for no seepage and $H = 2$ for Set-2 experiments

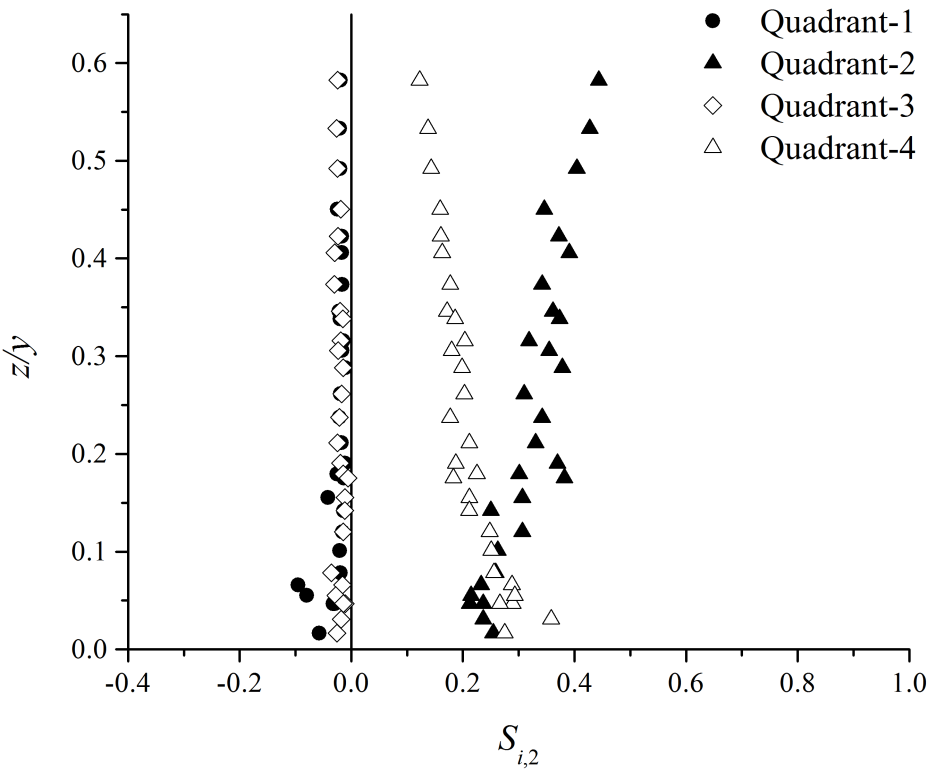

FIGURE 5.39: Quadrant analysis for seepage and $H = 2$ for Set-2 experiments

In order to observe the vertical distribution of larger contributions the analysis has also been carried out with $H = 2$ for both no seepage and seepage runs (Figure 5.34 and Figure 5.35). It is evident from Figure 5.34 that sweep events are the largest contributors for up to $\frac{z}{y} \sim 0.05$ for no seepage run while in seepage run (Figure 5.35), sweep events dominate up to $\frac{z}{y} \sim 0.09$ in contribution towards the Reynolds shear stress production.

Similar results of quadrant analysis have also been observed for Set-2 experiments and are shown in Figure 5.36 and Figure 5.37 for $H = 0$ under no seepage and seepage experimental conditions, respectively. Results for $H = 2$ are plotted in Figure 5.38 and Figure 5.39 for no seepage and seepage runs, respectively.

Variation of stress fraction (S_i, H) with different hole sizes (H) has been plotted in Figure 5.40 to understand the contribution of even larger events at $\frac{z}{y} = 0.03$. Close observation of Figure 5.40 reveals that the fractional contribution from interactions for no seepage run vanishes for $H \geq 5$. On the other hand, contribution from the ejection events vanishes for $H \geq 7$ while, that from sweeps vanishes for $H \geq 8$. In seepage run, the contributions from outward and inward interactions cease for $H \geq 7$ and $H \geq 8$, respectively. Ejections and sweep events dominate even for $H > 10$ with sweeps still being the largest contributor towards the momentum transfer.

Vertical distribution of the difference in the fractional contributions towards Reynolds shear stress production from sweep and ejection events ($\Delta S_{i,0} = S_{4,0} - S_{2,0}$) has been plotted in Figure 5.41 and Figure 5.42 for Set-1 and Set-2 experiments, respectively. It is evident from the observation of Figure 5.41 and Figure 5.42 that due to increase in roughness concentration in the seepage runs, $\Delta S_{i,0}$ also increases which clearly indicates that dominance of the sweep events in contribution towards the production of Reynolds shear stresses increases when downward seepage is applied to the channel.

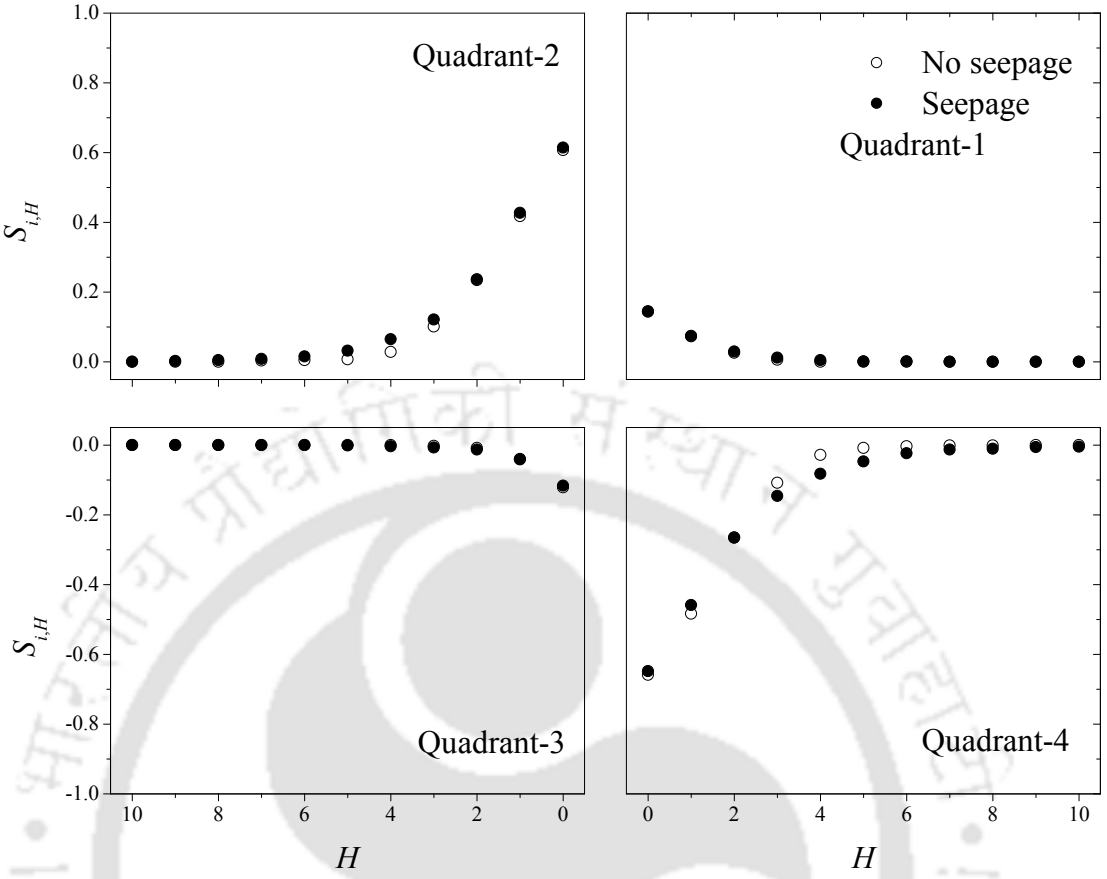

FIGURE 5.40: Variation of fractional contributions with hole sizes

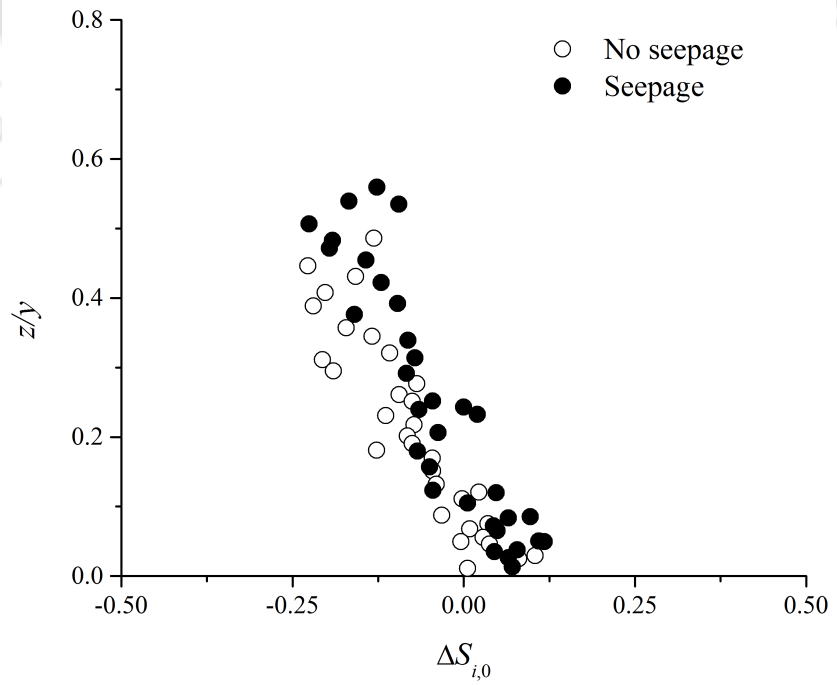

FIGURE 5.41: Vertical distribution of $\Delta S_{i,0}$ for Set-1 experiments

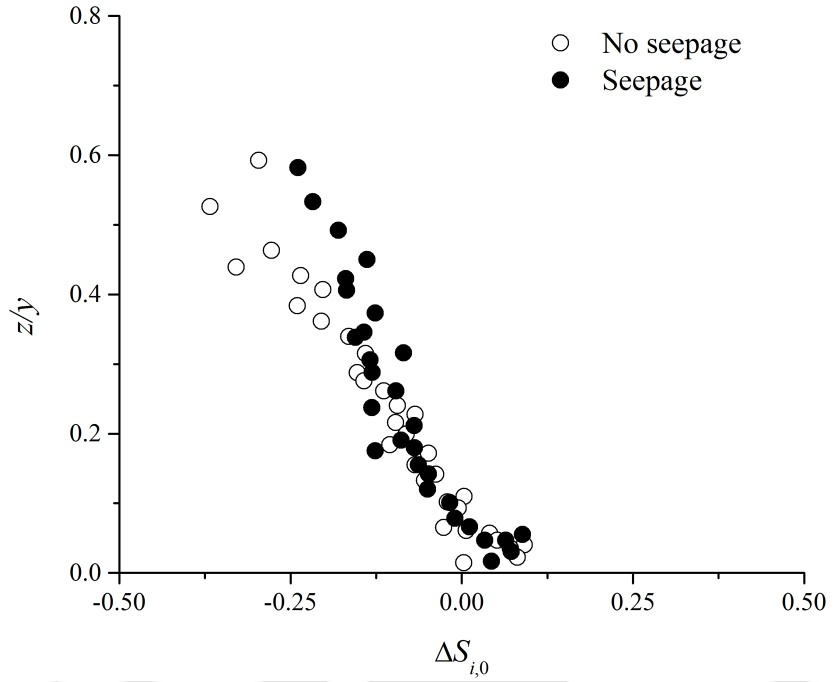

FIGURE 5.42: Vertical distribution of $\Delta S_{i,0}$ for Set-2 experiments

5.7 Third Moments of Velocity Fluctuation

The third statistical moments or the skewness indicate the non-symmetric distributions. Zero skewness indicate the symmetric distribution about the mean or the Gaussian distribution while, the negative and positive values of skewness show the distribution skewed towards left and right, respectively, of the mean. According to Raupach (1981), the third moments of velocity fluctuations can be expressed as:

$$\left.\begin{aligned} M_{jk} &= \overline{\widehat{u}^j \widehat{w}^k} \text{ where } j+k=3 \\ \widehat{u} &= \frac{u'}{\left(\overline{u'u'}\right)^{0.5}}, \widehat{w} = \frac{w'}{\left(\overline{w'w'}\right)^{0.5}} \end{aligned}\right\} \tag{5.15}$$

$$\left.\begin{aligned} M_{30} &= \frac{\overline{u'^3}}{\left(\overline{u'u'}\right)^{1.5}} \\ M_{03} &= \frac{\overline{w'^3}}{\left(\overline{w'w'}\right)^{1.5}} \\ M_{21} &= \frac{\overline{u'^2 w'}}{\left(\overline{u'u'}\right)\left(\overline{w'w'}\right)^{0.5}} \\ M_{12} &= \frac{\overline{u'w'^2}}{\left(\overline{u'u'}\right)^{0.5}\left(\overline{w'w'}\right)} \end{aligned}\right\} \tag{5.16}$$

Where M_{30} represents the flux of the streamwise Reynolds normal stress in the streamwise direction of the skewness of $u^{'}$, M_{03} represents the vertical flux of RNS in vertical direction or the skewness of $w^{'}$, M_{21} defines the advection of streamwise RNS in the vertical direction, and M_{12} stands for advection of vertical RNS in the streamwise direction. Figure 5.43 to Figure 5.46 display the vertical profiles of third moments with comparison between no seepage and seepage runs.

Raupach (1981) observed that irrespective of the surface roughness, third moments follow universal patterns except very near to the boundary. It can be observed from Figure 5.43 that for no seepage run, M_{30} initiates with small positive and M_{03} (Figure 5.44) starts with small negative value near to the boundary. Magnitude of the positive M_{30} near the bed is increased after the application of the downward seepage suggesting the strong influence of increased streamwise flux of streamwise RNS on increased roughness concentration and increased particle mobility in the seepage run.

Similar trend in the distribution of M_{12} is observed (Figure 5.46) which reflects the increase in advection of vertical RNS in streamwise direction in seepage run. Magnitude of the negative values of M_{03} and M_{21} (Figure 5.45) in the near bed region increases after the application of downward seepage as compared to their negative values in no seepage run, suggests the increase in vertical flux of RNS and also the increase in advection of streamwise RNS in downward direction.

Similar trends in the third order correlations have been observed for Set-2 experiments under no seepage and seepage experimental conditions. Profiles of M_{30} are shown in Figure 5.47, M_{03} are shown in Figure 5.48, M_{21} are depicted in Figure 5.49, M_{12} are plotted in Figure 5.50 for Set-2 experiments. In the near-bed region, M_{30} starts with small positive value and M_{03} starts with small negative value for no seepage run. After the application of the downward seepage magnitude of the positive M_{30} and M_{12} in the near-bed region is increased while, the magnitude of the negative M_{03} and M_{21} in the near-bed region is increased after the application of downward seepage as compared to their negative values in no seepage run.

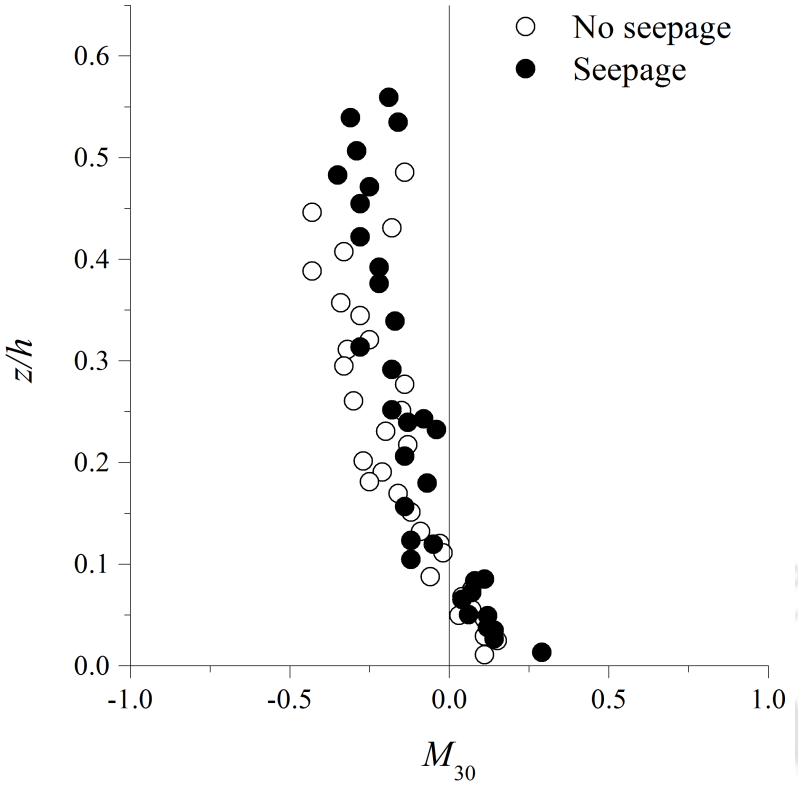

FIGURE 5.43: Vertical distributions of M_{30} for Set-1 experiments

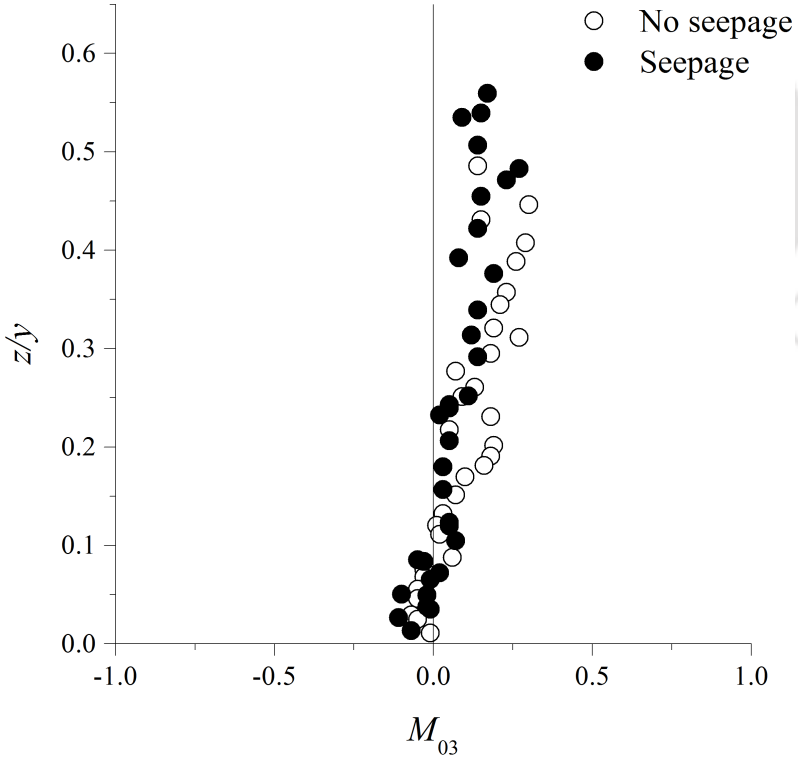

FIGURE 5.44: Vertical distributions of M_{03} for Set-1 experiments

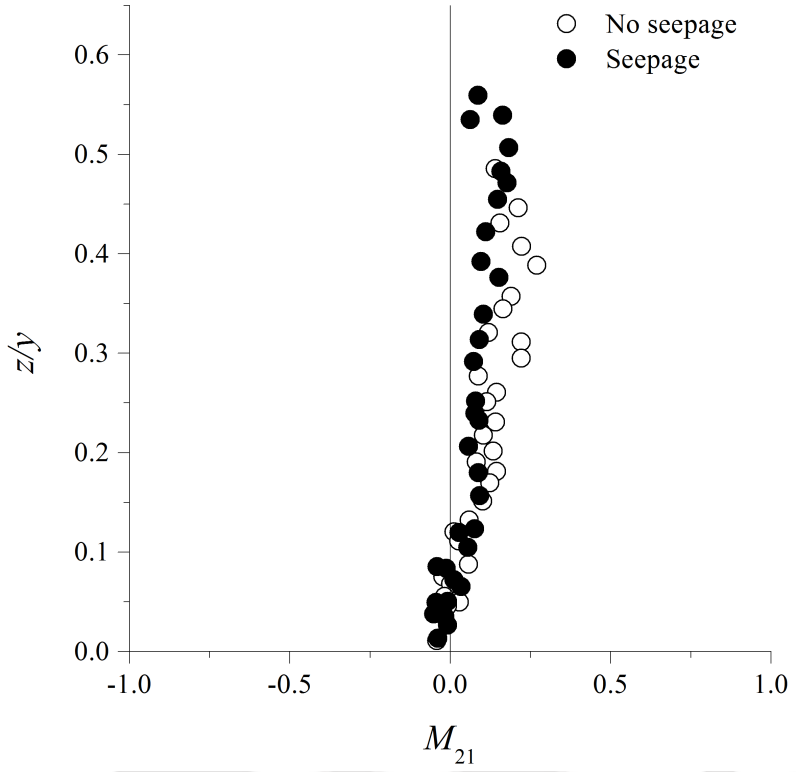

FIGURE 5.45: Vertical distributions of M_{21} for Set-1 experiments

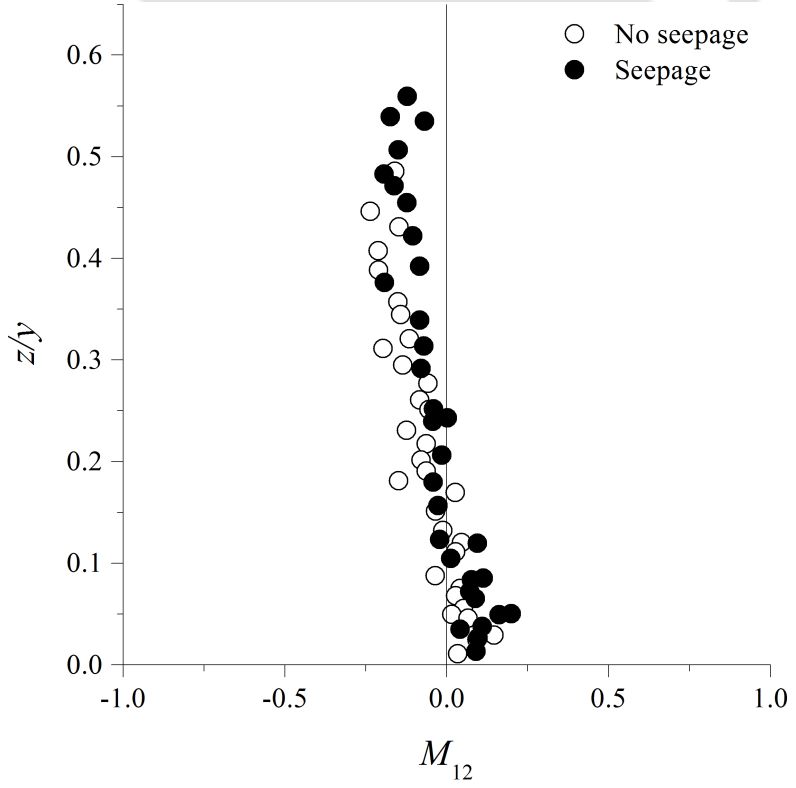

FIGURE 5.46: Vertical distributions of M_{12} for Set-1 experiments

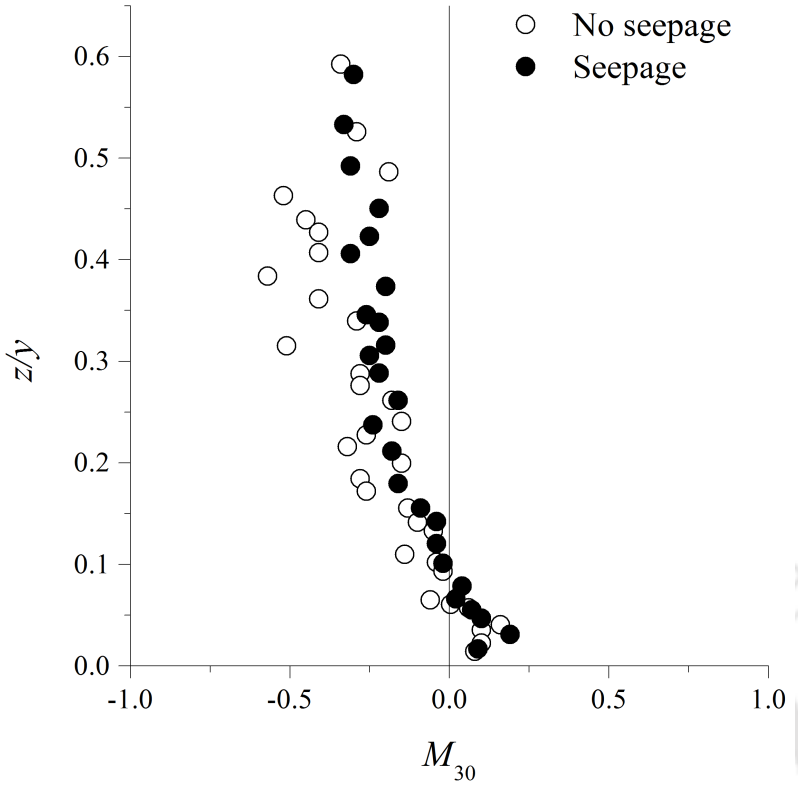

FIGURE 5.47: Vertical distributions of M_{30} for Set-2 experiments

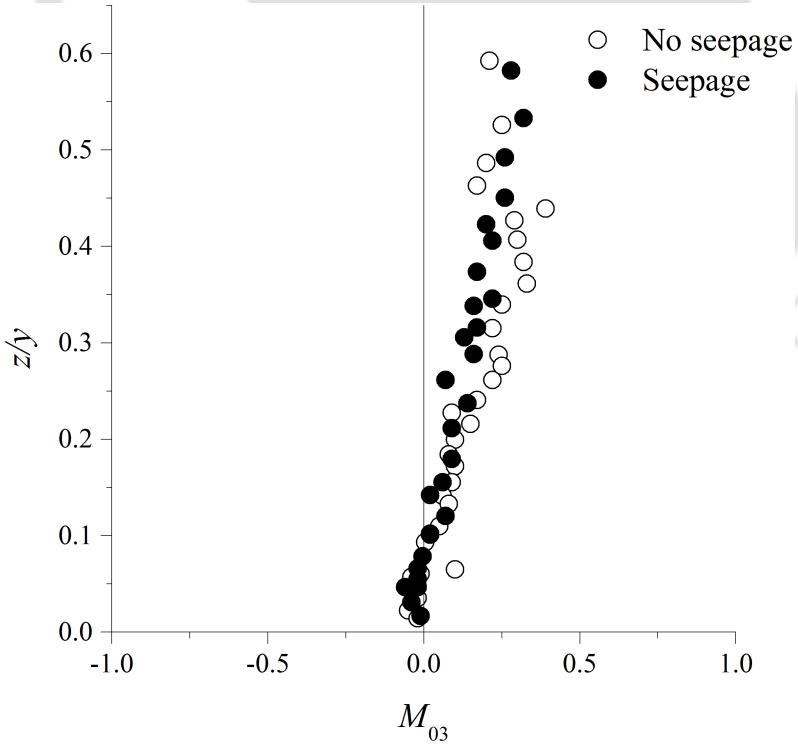

FIGURE 5.48: Vertical distributions of M_{03} for Set-2 experiments

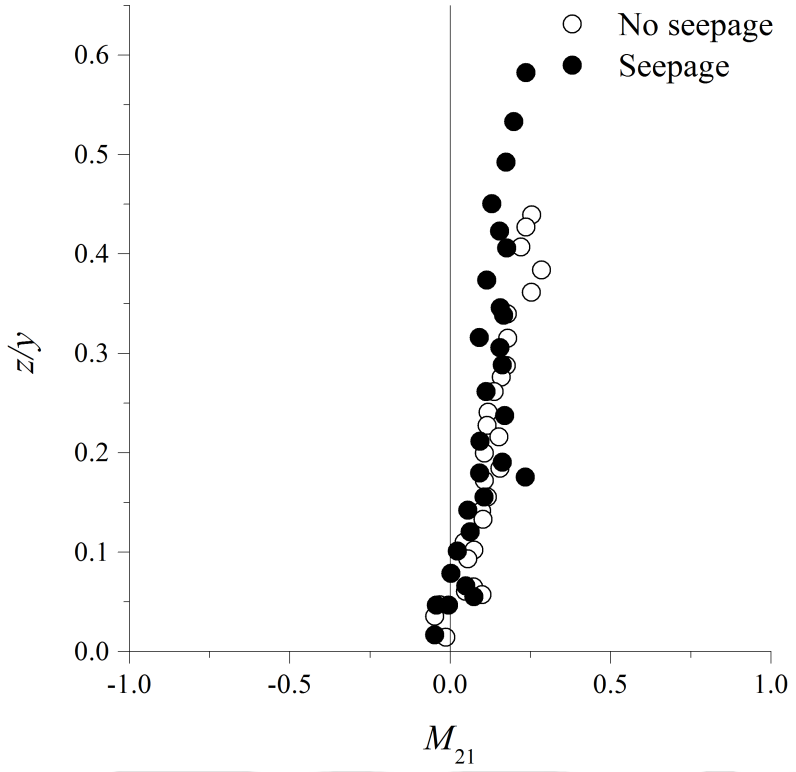

FIGURE 5.49: Vertical distributions of M_{21} for Set-2 experiments

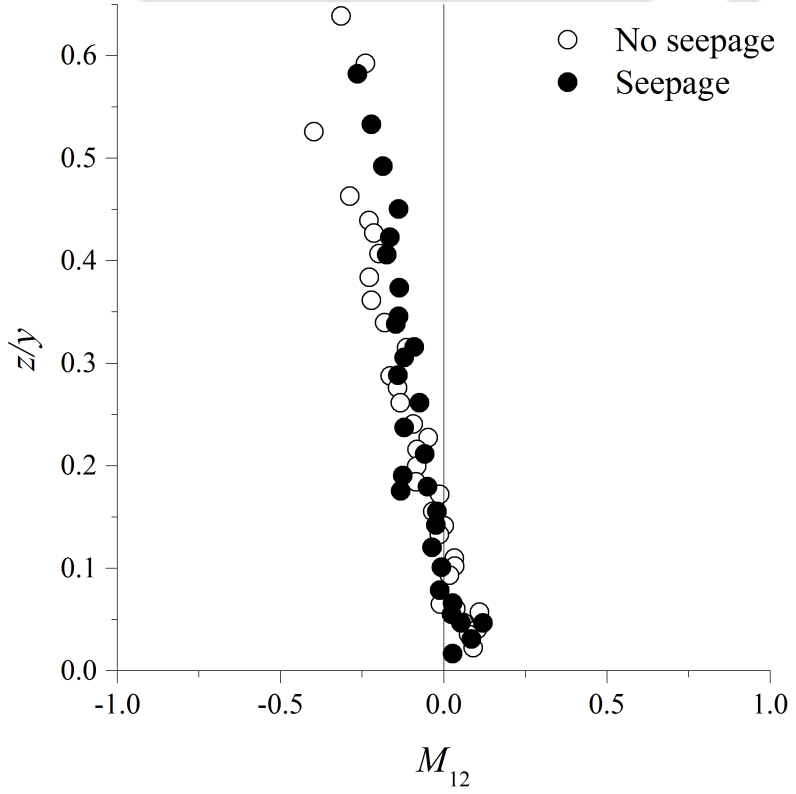

FIGURE 5.50: Vertical distributions of M_{12} for Set-2 experiments

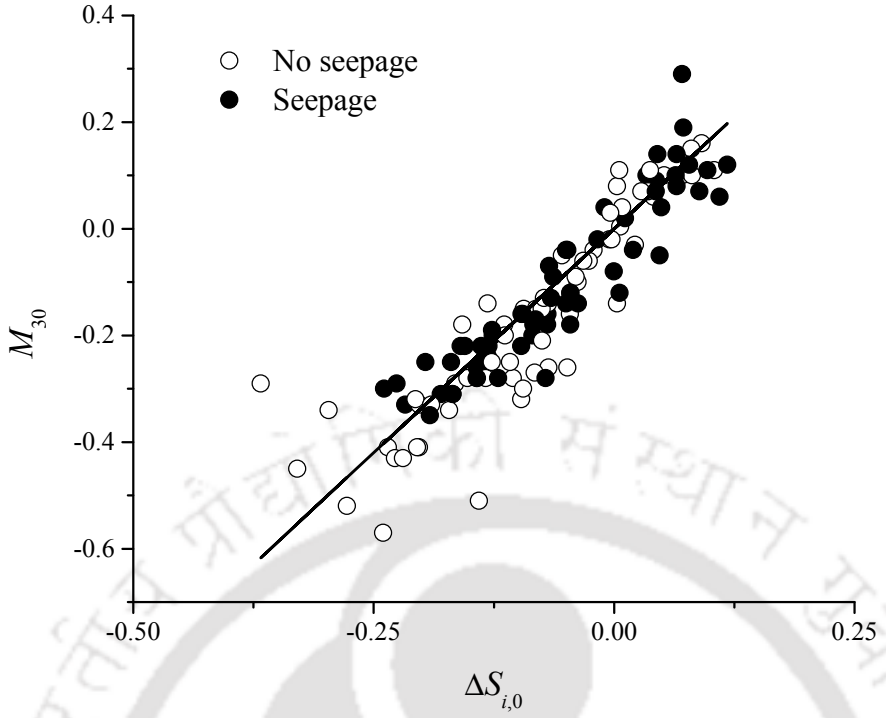

FIGURE 5.51: Relation between $\Delta S_{i,0}$ and M_{30}

Third moments of velocity fluctuations are important parameters to understand the behavior of bursting events (Nezu and Nakagawa, 1993) as they exhibit similitude with $\Delta S_{i,0}$ (Raupach, 1981). Variation of M_{30} has been plotted with $\Delta S_{i,0}$ in Figure 5.51 for no seepage and seepage runs. It should be observed from Figure 5.51 that irrespective of the roughness concentration caused by the change in flow conditions (application of downward seepage), there exist a linear relationship between $\Delta S_{i,0}$ and M_{30} which was also observed by Raupach (1981). However, without using different roughness elements on the boundary and after applying downward seepage to a curved deformable boundary, the linear relationship between $\Delta S_{i,0}$ and M_{30} changes to:

$$M_{30} = 1.68\Delta S_{i,0} \tag{5.17}$$

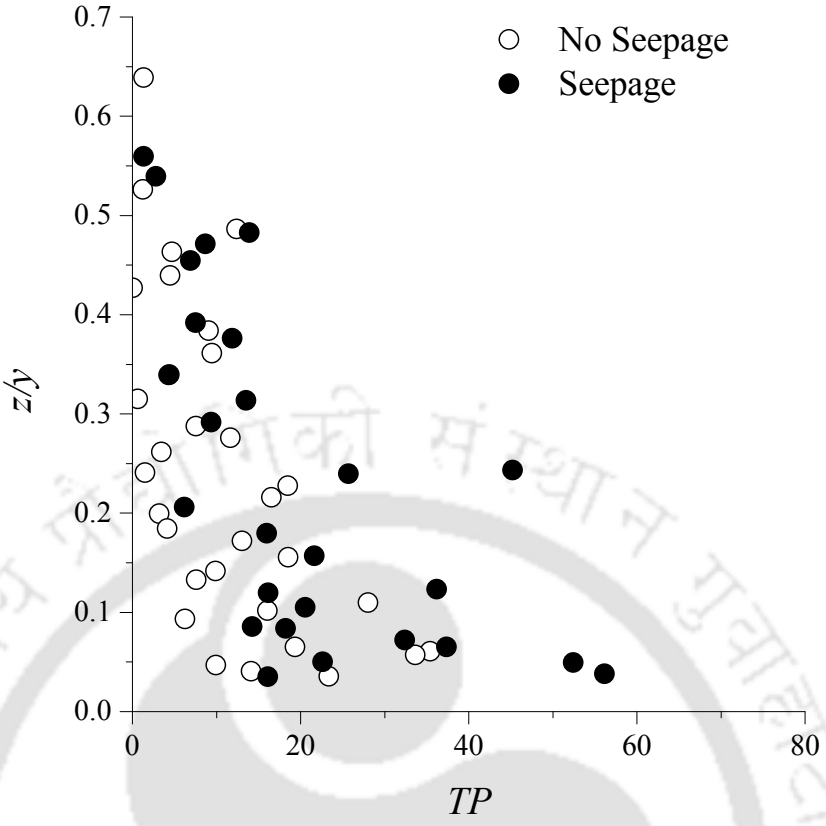

FIGURE 5.52: Vertical distributions of *TP* (turbulence production)

5.8 Turbulence Production, Dissipation and Diffusion

Figure 5.52, Figure 5.53, and Figure 5.54 depict the vertical distribution of the production of turbulence, dissipation of turbulent kinetic energy, and diffusion of turbulence, respectively, for both no seepage and seepage runs which can be calculated as (Krogstadt and Antonia, 1999; Dey et al., 2011b):

$$\left.\begin{aligned} &\text{Turbulence production } t_P = -\overline{u'w'}\frac{\partial U}{\partial z} \\ &\text{Turbulence dissipation } \varepsilon = \frac{15\upsilon}{U^2}\left(\frac{\partial u'}{\partial t}\right)^2 \\ &\text{Turbulence diffusion } t_D = \frac{\partial f_{kw}}{\partial z} \end{aligned}\right\} \tag{5.18}$$

All the terms (t_p, υ, and t_D) have been made non-dimension by multiplying $\frac{h}{U_*^3}$

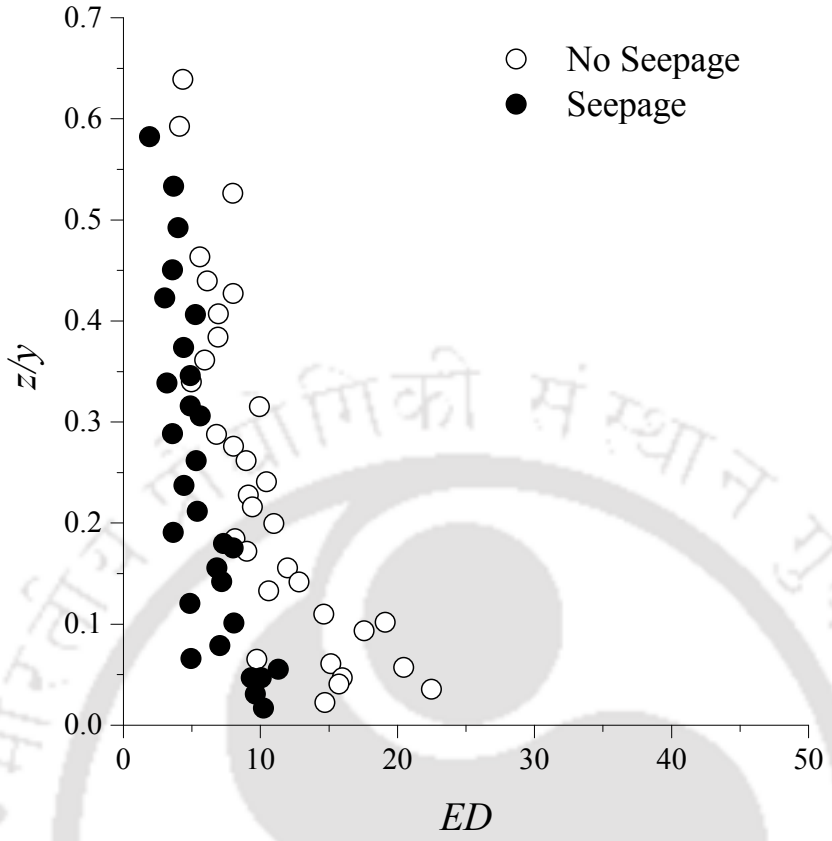

FIGURE 5.53: Vertical distributions of *ED* (energy dissipation)

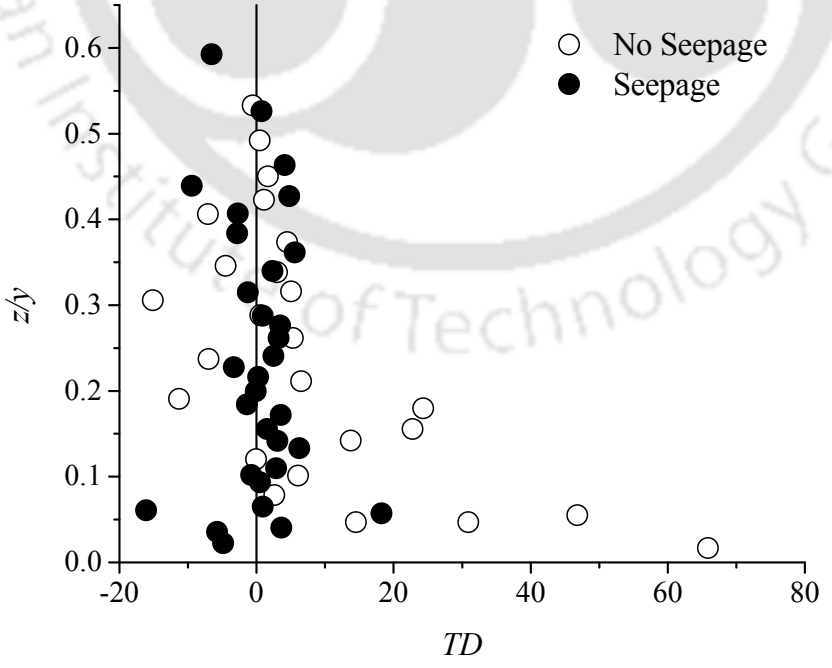

FIGURE 5.54: Vertical distributions of *TD* (turbulent diffusion)

and have been denoted as TP, ED and TD for turbulence production, energy dissipation, and turbulence diffusion respectively. As the term indicates, turbulence production comes from the interchange of mean flow energy to fluctuations. It is evident from Figure 5.52 that turbulence production becomes higher especially in the near bed region in the seepage run, suggesting the increased level of turbulence after the application of downward seepage. This increased level of turbulence is line with the increased turbulence intensities and increased momentum transfer when water is taken out of the channel in vertically downward direction through the send bed in the form of seepage flow.

Dissipation of turbulent kinetic energy indicates that it is reducing in magnitude or becoming less noticeable. After the application of seepage as more energy is converted to turbulent fluctuations, the gain in turbulent kinetic energy becomes higher while, its dissipation reduces. Figure 5.53 clearly indicates that in seepage run, dissipation of turbulent kinetic energy is less than that of no seepage run. Turbulence diffusion as the term refers to the spreading of turbulence is reduced in the near bed region in the seepage run which is evident in Figure 5.54 and which is also in agreement with the gain in turbulence production and subsequent reduction in the dissipation of turbulent kinetic energy when downward seepage is applied.

5.9 Turbulent Mixing Length

The distribution of the non-dimensional turbulent mixing length has been depicted in Figure 5.55 and Figure 5.56, respectively, for no seepage and seepage runs. Turbulent mixing length (l) can be calculated as (Krogstadt and Antonia, 1999):

$$l^+ = \frac{(\overline{uw}^+)^{0.5}}{\partial U^+ / \partial z^+} \tag{5.19}$$

where $l^+ = \frac{l}{y}$, $U^+ = \frac{U}{U^*}$ and $z^+ = \frac{z}{y}$.

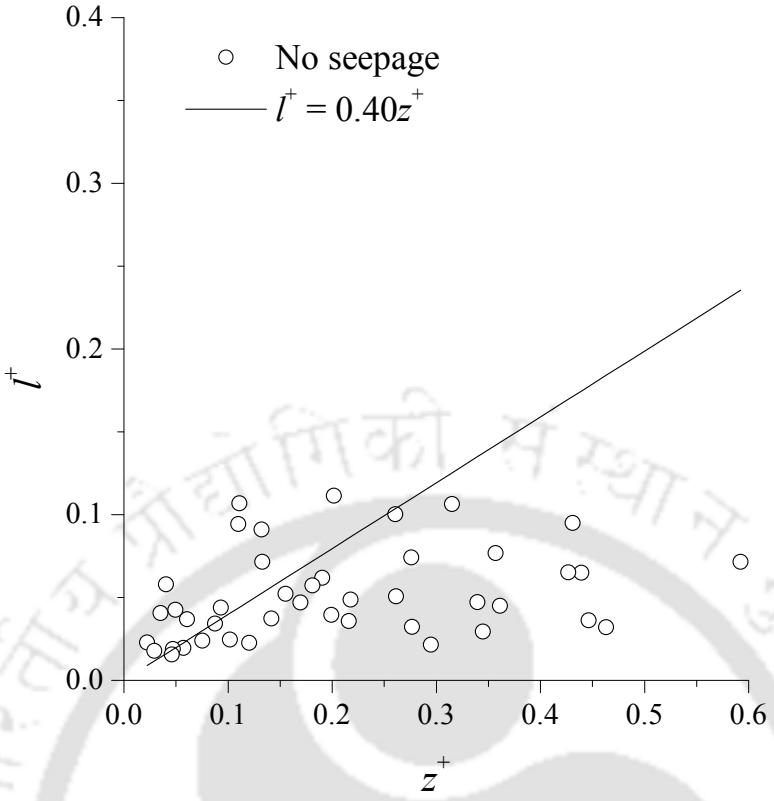

FIGURE 5.55: Distribution of the turbulent mixing length for no seepage

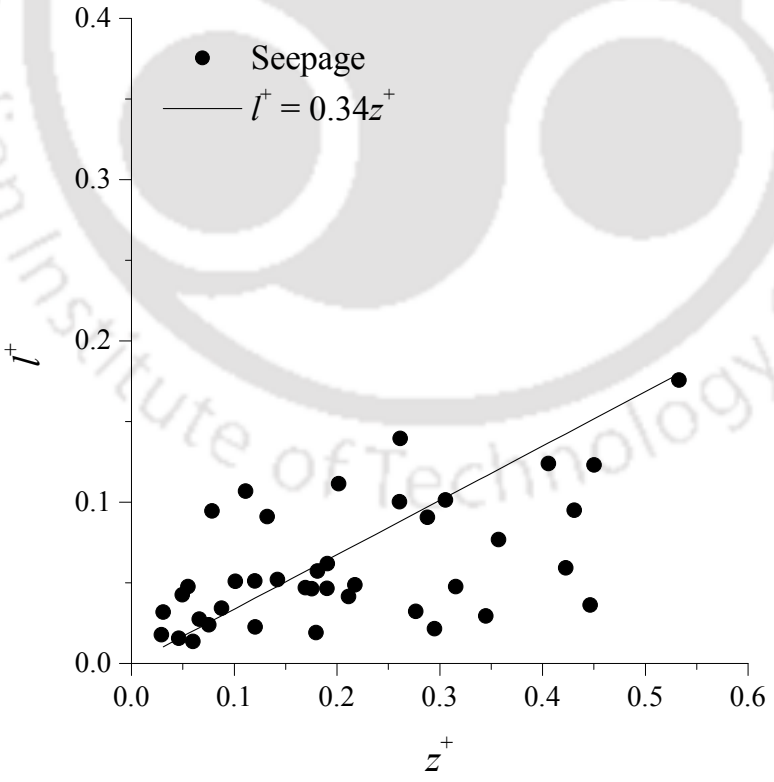

FIGURE 5.56: Distribution of the turbulent mixing length for seepage

In the inner flow layer ($0<\frac{z}{y}<0.2$) there is an acceptable linear fit between l^+ and z^+:

$$l^+ = kz^+ \tag{5.20}$$

The slope of this linear fit defines the von Karman's constant (k). Figure 5.55 and Figure 5.56 that the slope of the linear fit (i.e. von Karman's constant) decreases when downward seepage is applied to the channel. This decrease in the slope suggests that the mixing length of turbulent eddies decreases, which further signifies the prevailing mobile bed condition in the channel under the action of downward seepage.

5.10 Discussions

It has been observed that, a non-transporting channel started eroding and transporting bed material after seepage in the downward direction was applied to it. The curved cross-sectional profile, which was stable during the entire course of the no seepage run (dotted line in Figure 3.16), distorted in the seepage run and subsequently changed to some other shape (solid line in Figure 3.16).

Analysis of such behavior necessitates the close and careful observation of the flow structure being within the flow. Hence, instantaneous velocities were measured by ADV right after the application of downward seepage to understand the change in turbulent characteristics of flow. Close observation of all the turbulence parameters together discussed and their comparison between no seepage and seepage runs, leads to the solution up to a certain extent.

Analysis of the time averaged velocity profile reveals that for a channel with curved deformable boundaries consisting of bed particles which are on the verge of motion, an increase of $3\% - 6\%$ in velocities very near to bed caused the transport of bed materials. Increase in the depth of the virtual bed level and the zero velocity level reflect that the particles resting on the channel boundary were exposed to a

higher component of streamwise velocity. Decrease in the values of von Karman's constant from 0.402 for no seepage to 0.340 for seepage also suggests the prevalence of mobile bed condition. Decrease in the slope of turbulent mixing length has been observed which indicates lesser mixing length of turbulent eddies under the application of downward seepage.

Increase in maximum Reynolds shear stress ($\sim 21\% - 22\%$) after the application of seepage and subsequent increase in shear velocities ($\sim 11\% - 16\%$) suggest greater momentum transfer towards the boundary in seepage runs where, higher turbulence intensities have also been observed than that of no seepage runs. At near the bed in seepage runs, greater positive values of F_{TKEu} and greater negative values of F_{TKEw} than that of no seepage runs, correspond to increased flux of streamwise turbulent kinetic energy in streamwise direction and increased flux of vertical turbulent kinetic energy in the downward direction which in turn suggests the increased bed mobility in seepage runs.

While in the upper flow layer, negative F_{TKEu} suggests the flux of streamwise turbulent kinetic energy is transported in the opposite direction which can be related to the retardation caused by inertia of fluid layer. In seepage suns, lesser negative F_{TKEu} in upper flow layers and near the bed greater positive F_{TKEu} mean that retardation was reduced and effect of which can be thought of relative increase in velocities when the downward seepage was applied.

Further, the investigation of bursting events reveals increased contribution of ejections and sweeps towards the production of Reynolds shear stresses in seepage runs than that of no seepage runs. Analysis of contribution by stronger events also shows the dominance of sweep events in Reynolds shear stress production. This increase in high speed fluid towards the wall in seepage runs is responsible for the mobile bed condition.

Vertical distributions third moments of velocity fluctuations also give the insight of phenomena taking place after the application of downward seepage. In the region close to bed, greater flux of streamwise RNS in streamwise direction and greater vertical flux of RNS in downward direction indicate increased roughness

concentration and increased particle mobility in the seepage run. After the application of downward seepage, higher turbulence production associated with decreased turbulent diffusion with decrease in turbulent kinetic energy dissipation has been observed which indicate that there was increased level of turbulence in the main channel flow which may have caused the distortion of initial curvilinear cross-sectional profile.

5.11 Conclusions

Changes in the turbulent characteristics of flow have been observed in the experiments when seepage was applied in the downward direction to a curved channel cross-section. Increased bed materials transports were observed after the application of downward seepage to the channel, which was stable and non-transporting with no seepage.

Time-averaged streamwise velocities in the near bed region were increased after the application of downward seepage. This increase in streamwise velocities was enough to put the bed particles in a mobile condition which were on the verge of motion earlier. Enhanced momentum transfer towards the boundary has been observed through the significant increase in the Reynolds shear stresses.

Vertical and streamwise turbulent intensities increased after the application of seepage. Thickness of roughness sublayer and shear velocities were also increased under the action of downward seepage. Value of von Karman's constant reduced, which corresponds to the mobile bed condition in seepage experiments. In the near-bed region increased fluxes of streamwise turbulent kinetic energy in the streamwise direction and vertical turbulent kinetic energy in the downward direction have been observed.

Increased streamwise flux of streamwise RNS and increased vertical flux of RNS in the downward direction have been observed near the boundary. Increase in the contribution of sweep events towards Reynolds shear stress production near the

boundary with increased zone of sweep dominance was observed. Contribution of sweep events towards Reynolds shear stress production was increased near the boundary and thickness of the zone of sweep dominance was increased.

After the application of seepage in the downward direction increase in the level of turbulence in the flow has been observed associated with higher turbulence production, decreased turbulent diffusion and decrease in turbulent kinetic energy dissipation. The mixing length of turbulent eddies was decreased when the downward seepage was applied to the channel, which further signifies the prevailing mobile bed condition in the channel under the action of downward seepage.

Chapter 6

Conclusions and Recommendations for Future Work

Experimental study has been carried out on three sands of median diameter 1.1 mm, 0.418 mm, and 0.62 mm in two categories; no seepage experiments to check the stability of channels with curvilinear cross-sections and when seepage was applied in the downward direction to the channel. It has been observed that the curved cross-sectional profiles were no longer stable when downward seepage was applied to them and subsequently the cross-sectional geometry was distorted by the flow. Following conclusions are made from the study:

6.1 Cross-sectional Profile of Stable Alluvial Channels with Downward Seepage

The parabolic cross-sectional shape of channels was no longer stable during seepage experiments and channels attained new shape with flat bed and curved banks at the end of seepage experiments and achieved stability. This shape of threshold alluvial channels, i.e. flat-bed and two curved banks has been supported by various

authors (Parker, 1978; Diplas, 1990; Pizzuto, 1990; Diplas and Vigilar, 1992; Cao and Knight, 1998) but in their analysis, seepage has not been considered. It is clear from the available literature (Table 1.1) that seepage affects the hydrodynamics of alluvial channels. In the present study, seepage has been considered for the evaluation of bank profiles and an empirically derived exponential expression has been suggested which is in very good agreement of the experimental channel bank profile:

$$y* = 1 - \exp(-2.306\mu x*^{0.912}) \tag{6.1}$$

Developed empirical equation for bank profile predicts satisfactorily the bank profiles at various cross-sections of the natural alluvial rivers. Variation in various parameters like channel perimeter, hydraulic radius and top width has also been observed for the channel after seepage experiments and the corresponding parameters have been compared with the ones obtained after no seepage experiments. During seepage experiments, as the rate of erosion becomes higher because of the increase in bed shear stress, subsequently, the top width and the channel perimeter becomes higher than that of no seepage experiments.

As the eroded material from the upstream side of channels gets deposited on the downstream side, the hydraulic radius decreases along the length of channel towards the downstream and its value becomes lesser than that of no seepage experiments. Channel shape parameter β (Deng et al., 2001) has been calculated for the channels obtained after seepage experiments. The values of β, for all the cases have been found to be greater than 2, which suggest that the channels obtained after seepage experiments are similar to the natural stable alluvial channels with curved banks and flat bed.

6.2 Sheet Flow in Alluvial Channels with Downward Seepage

In the experiments channel bank erosion and the formation of sheet flow layer have been observed when downward seepage was applied to the channels of no seepage experiments. More erosion took place at the upstream of the channel because of the higher stream power associated with the flow there and eroded material from the banks at a section was deposited on the channel bed on the adjacent section. This process of erosion and deposition is continued till the channel achieves the threshold condition again with the applied seepage.

It has been observed that after the application of seepage in the downward direction, upper flow regime prevailed in the channel and the concentration of sediment material coming from the banks was so high that the sheet flow layer on channel bed was formed. It has also been observed and justified through the Shields parameter and the formation of sheet flow layer that the bed shear stress increases when downward seepage is applied to the channel. Finally, an empirical equation has been generated which related the Shields parameter, Froude number, seepage intensity parameter and seepage particle Reynolds number to the thickness of the sheet flow layer:

$$\delta = \frac{\Delta}{y_s} = 1.1\left(\frac{\tau_{c0}}{(\gamma_s - \gamma)\, d_{50}}\right)^{-0.45}\left(\frac{2\rho u_s V_s}{\tau_{c0}}\right)^{0.5}\left(\frac{u_s}{(gR_{hs})^{1/2}}\right)^{1.7}\left(\frac{V_s d_{50}}{\nu}\right)^{-0.13} \tag{6.2}$$

6.3 Regime Equations for the Design of Alluvial Channels with Downward Seepage

Regime theory has been used to define the regression equations for a channel's dimension under stable conditions. Regression relationships have been developed for the design of alluvial channels in the presence of downward seepage. Following

equations in the dimensional form have been proposed for channel perimeter, average flow depth and frictional slope which are the functions of channel discharge, seepage discharge and sand size:

$$p = 1.6Q^{0.41}d_{50}^{-0.12}e^{31.42q_s} \tag{6.3}$$

$$y = 0.3Q^{0.39}d_{50}^{-0.02}e^{-8.54q_s} \tag{6.4}$$

$$S_f = 0.16Q^{-0.49}d_{50}^{1.03}e^{q_s} \tag{6.5}$$

Predictability of the proposed relationships is quite high because of the high R^2 associated with them. The proposed relationships here have the ability to reduce to the form of known regime equations as the seepage term vanishes. Further, following non-dimensional relations have also been proposed for the perimeter, top width and frictional slope of an alluvial channel as functions of flow Reynolds number, seepage particle Reynolds number and Shields parameter:

$$\frac{p}{R_h} = \frac{1.42\exp\left({R_S}^{0.0216}\right)}{\ln\left(R_e\right)\theta_C^{1.2}} \tag{6.6}$$

$$\frac{B}{R_h} = \frac{1.0\exp\left({R_S}^{0.00302}\right)}{\ln\left(R_e\right)\theta_C^{1.17}} \tag{6.7}$$

$$S_f = \frac{1.6\exp\left({R_S}^{0.0128}\right)}{\ln\left(R_e\right)\theta_C^{-1.85}} \tag{6.8}$$

6.4 Turbulent Characteristics of the Flow in Curved Alluvial Channels with Downward Seepage

In the experimental study the changes in turbulent characteristics of flow have been observed when seepage in downward direction was applied to the curved channel with deformable boundaries. Particle on the entire periphery of the channels were at the condition of incipient motion earlier with no seepage. Deformation of the cross-sectional profile of the channel and increased bed load transport were observed after the application of downward seepage to the channel which was stable and non-transporting with no seepage. Close observation of the turbulent characteristics of flow leads to following conclusions about causes of increased bed material transport and deformed cross-sectional geometry after the application of downward seepage to the channel:

1. Increase of $3\% - 6\%$ in the time-averaged streamwise velocities in the near bed region was observed. For the bed particles at the verge of motion, this increase in streamwise velocities is enough for them to be in mobile condition.

2. Significant increase of $\sim 21\% - 22\%$ in the Reynolds shear stresses has been observed in seepage runs which indicate enhanced momentum transfer towards the boundary. Increase in vertical and streamwise turbulent intensities has also been observed.

3. After the application of downward seepage thickness of roughness sublayer was increased. Significant increase of $\sim 11\% - 16\%$ in shear velocities has also been observed.

4. Reduction in the value of von Karman's constant from 0.402 for no seepage to 0.340 for seepage experiments was observed which corresponds to the mobile bed condition prevailing in seepage runs.

5. Greater fluxes of streamwise turbulent kinetic energy in streamwise direction vertical turbulent kinetic energy in the downward direction has been

observed in the near bed region. Greater streamwise flux of streamwise RNS in streamwise direction and greater vertical flux of RNS have also been observed near the boundary.

6. Increase in the contribution of sweep events towards Reynolds shear stress production near the boundary with increased zone of sweep dominance was observed in seepage experiments. This increase is responsible for the mobile bed condition when the seepage in the downward direction is applied to initially non-transporting channels.

7. Increased level of turbulence in flow has been observed with higher turbulence production, decreased turbulent diffusion and decrease in turbulent kinetic energy dissipation after downward seepage was applied to the channel.

8. Decrease in the mixing length of turbulent eddies has been observed which further signifies the prevailing mobile bed condition in the channel under the action of downward seepage.

6.5 Recommendations for the Future Work

Lateral bank shifting of channels in fine-grained alluvium that produces sinuous serpentine meanders is a very common phenomenon which depends on longitudinal channel slope, bed particle size, strength of banks and supply of sediments. Experimental study in laboratory flumes has been carried out by several researchers (Whiting and Dietrich, 1993; Smith, 1998; Eaton and Church, 2004; Peakall et al., 2007; Braudrick et al., 2009; van Dijk et al., 2010) on channel meandering, but the possibility of lateral bank shift after the application of seepage in the downward direction to a threshold stable alluvial channel has not been investigated anywhere in the published literature. Channel cross-sections after no seepage experiments (dotted lines) and seepage experiments (solid lines) on the sand of median diameter 0.418 mm from downstream to upstream in the test length for shape 60 are depicted in Figure 6.1.

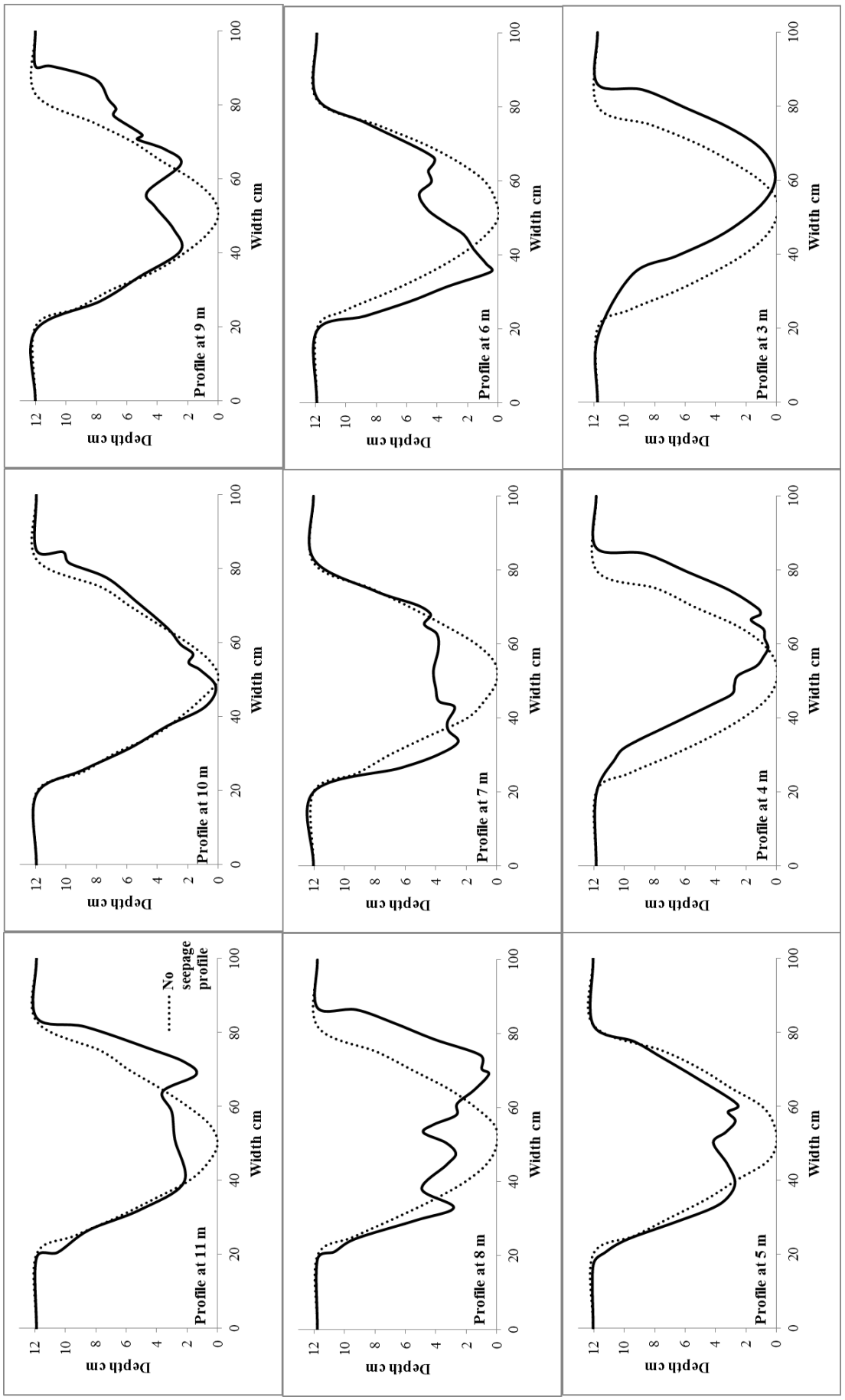

FIGURE 6.1: Cross-sectional profiles obtained after no seepage and seepage experiments for shape 60 ($d_{50} = 0.418$ mm)

Increase in bed shear stress along the length of the channel under seepage experimental conditions caused shifting of the channel in lateral directions i.e. erosion of one bank and deposition of the bed material on the other bank. Close observation of Figure 6.1 reveals that at upstream side in test length for shape 60 (11 m, 10 m, 9 m and 8 m), channel eroded the right bank then at 7 m, 6 m and 5 m channel shifted towards left side by eroding the left bank and then at 4 m and 3 m, channel again shifted towards right hand side by eroding the right bank.

This clearly indicates that the channel obtained after seepage experiment, followed a sinusoidal pattern which shows that downward seepage does have an effect on channel meandering. Work should be carried out in future to observe and understand the change in the turbulent characteristics of flow on the locations, where alluvial channels meander under the action of downward seepage.

Appendix A

Sensitivity and Uncertainty Analyses

Sensitivity analysis is a technique which is widely used to determine how different values of an independent variable will impact a particular dependent variable under a given set of assumptions. Sensitivity analysis is very useful when attempting to determine the impact the actual outcome of a particular variable will have if it differs from what was previously assumed. By creating a given set of scenarios, the analyst can determine how changes in one variable(s) will impact the target variable.

A mathematical model is defined by a series of equations, input variables and parameters aimed at characterizing some process under investigation. Quite often, some or all of the model inputs are subject to sources of uncertainty, including errors of measurement, absence of information and poor or partial understanding of the driving forces and mechanisms. This uncertainty imposes a limit on our confidence in the response or output of the model.

Further, models may have to cope with the natural intrinsic variability of the system, such as the occurrence of stochastic events. Good modeling practice requires that the modeler provides an evaluation of the confidence in the model. In models

involving many input variables, sensitivity analysis is an essential ingredient of model building and quality assurance.

A.1 Thickness of the Sheet Flow Layer

Sensitivity analysis for the non-dimensional thickness of the sheet flow layer (Equation 3.24) has been carried out and depicted in Figure A.1. Figure A.1A shows the sensitivity of the relation towards the variation in in the values of critical Shields parameter (θ_C) ($\pm$10%, $\pm$15%, $\pm$20% and $\pm$25%) while, keeping other variables fixed. Figure A.1B, A.1C and A.1D show the sensitivity of Equation (3.24) with the variation in the values of seepage intensity parameter (N), Froude number (F_S) and particle Reynolds number with seepage (R_S), respectively, in the similar fashion. It can be observed from Figure A.1 that the equation for the prediction of non-dimensional thickness of the sheet flow layer is highly sensitive towards the variation of Froude number.

A.2 Regime Relations for Alluvial Channels

Sensitivity of the proposed relations for the prediction of channel perimeter (P), hydraulic radius (R_h) and friction slope (S_f) in the dimensional form (Equation 4.81) has been shown in Figure A.2, Figure A.3 and Figure A.4, respectively. It can be observed that these relations are quite sensitive towards the variation of main channel discharge (Q) and less sensitive towards the variation of seepage discharge (q_s).

Regime relations in the non-dimensional form for the prediction of cross-sectional geometry of the stable channel have been proposed in Equation (4.86). sensitivity analysis for the prediction of non-dimensional channel perimeter, non-dimensional channel width, and frictional slope have been presented in Figure A.5, Figure A.6 and Figure A.7, respectively, towards the variation in the values of different

independent variables such as: flow Reynolds number (R_e), particle Reynolds number with seepage (R_S) and critical Shields parameter (θ_C). It can be observed that all the non-dimensional relations are highly sensitive towards the variation in the values of critical Shields parameter.

A.3 Uncertainty Analysis

Uncertainty analysis has been carried out for the measurements of main channel discharge (Q), seepage discharge from the electro magnetic flow meter (q_s) and distance measured from the SeaTek Ultrasonic Ranging System (z). 15 readings were collected from each of these instruments on the sand of median diameter 1.1 mm and shape 70. Seepage discharge was 30% of the main channel discharge at incipient motion condition of bed particles. Transducers for distance measurement were kept at 5 cm away from the channel bed and the results are presented in Table A.1.

TABLE A.1: Uncertainty associated with the measurements

Statistical parameters	Q	q_s	z
Standard deviation	0.00068	0.00036	0.00092
Standard deviation about the mean	0.03478	0.03768	0.01840
Uncertainty %	0.05285	0.03058	0.07260

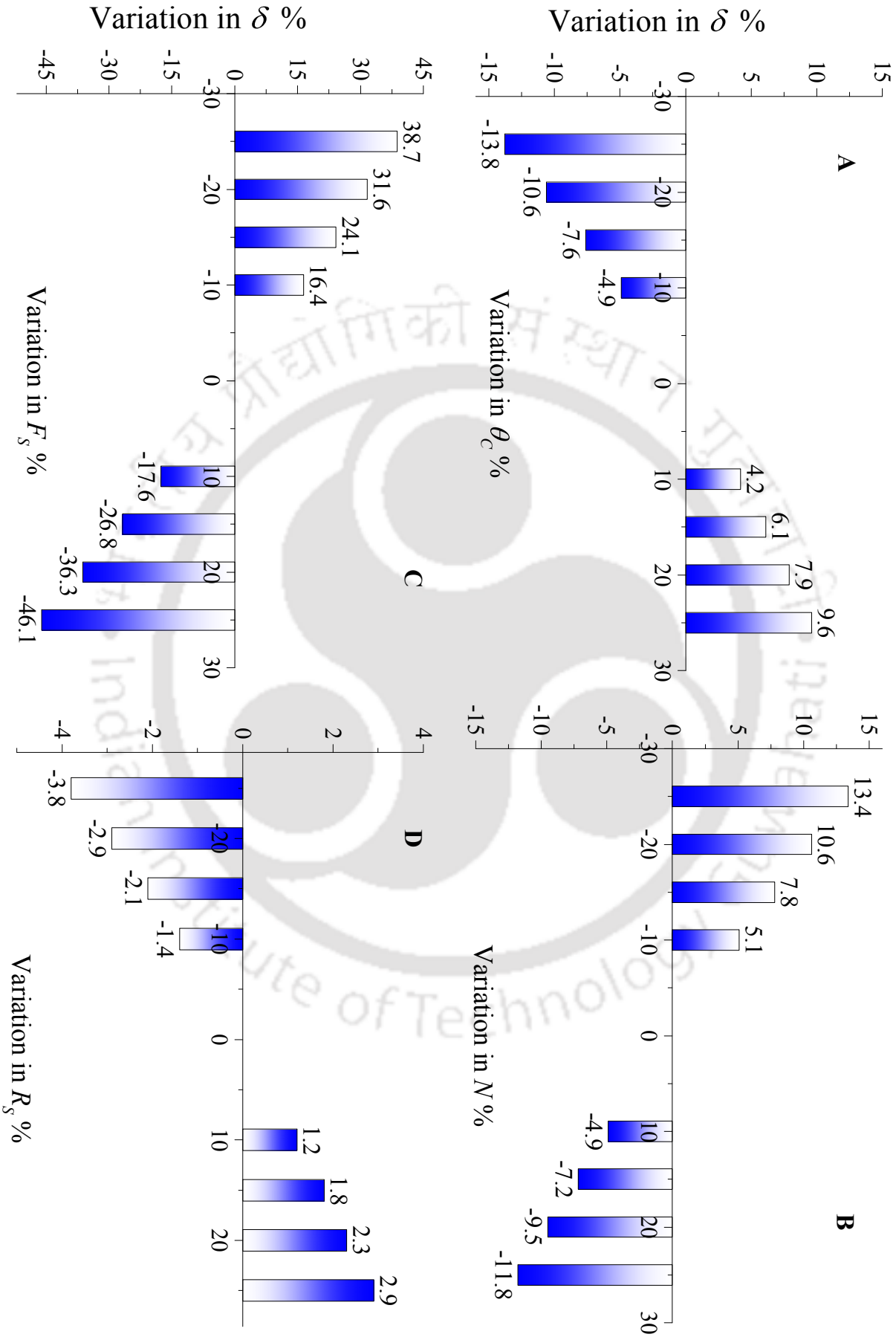

FIGURE A.1: Sensitivity analysis for the thickness of the sheet flow layer

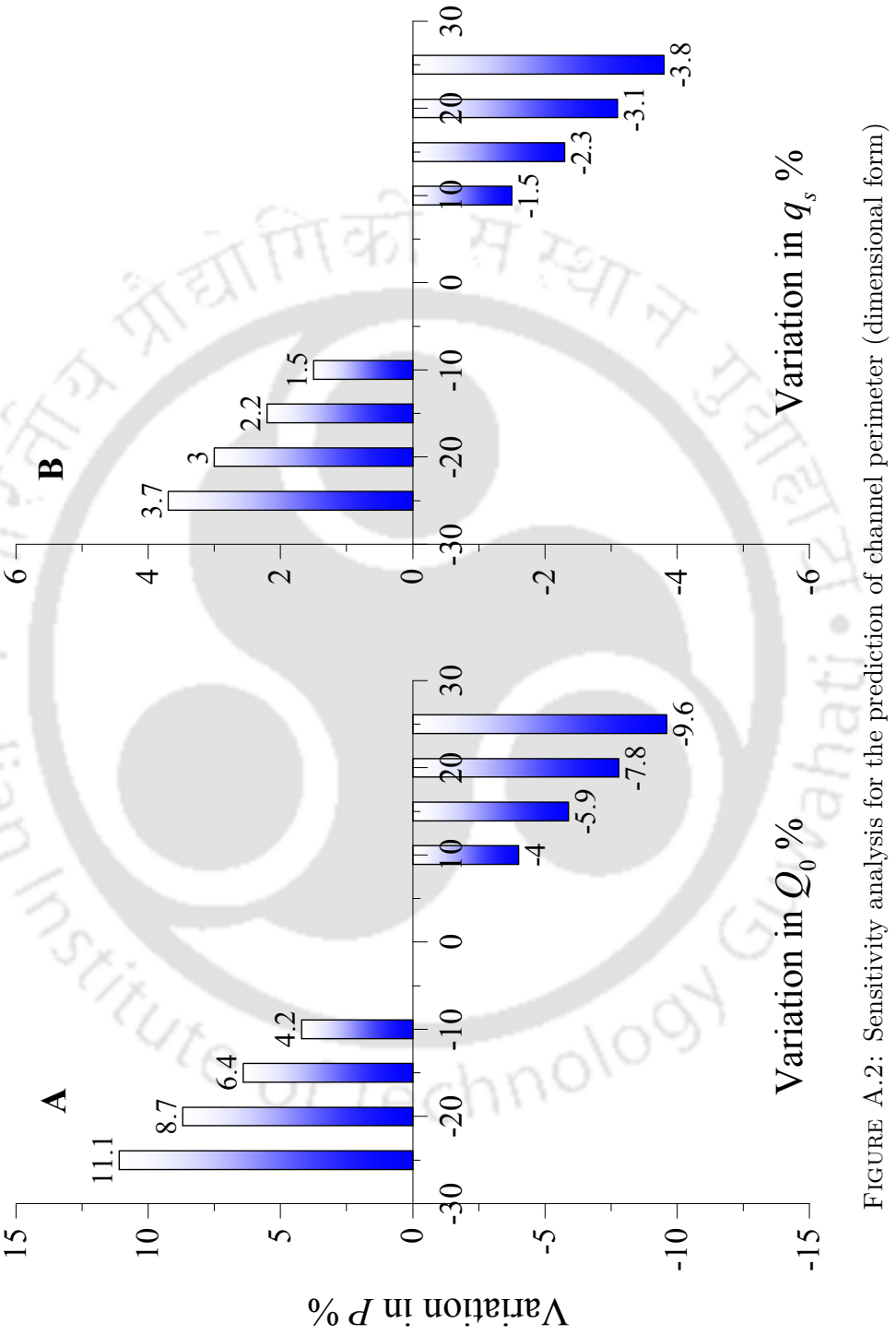

FIGURE A.2: Sensitivity analysis for the prediction of channel perimeter (dimensional form)

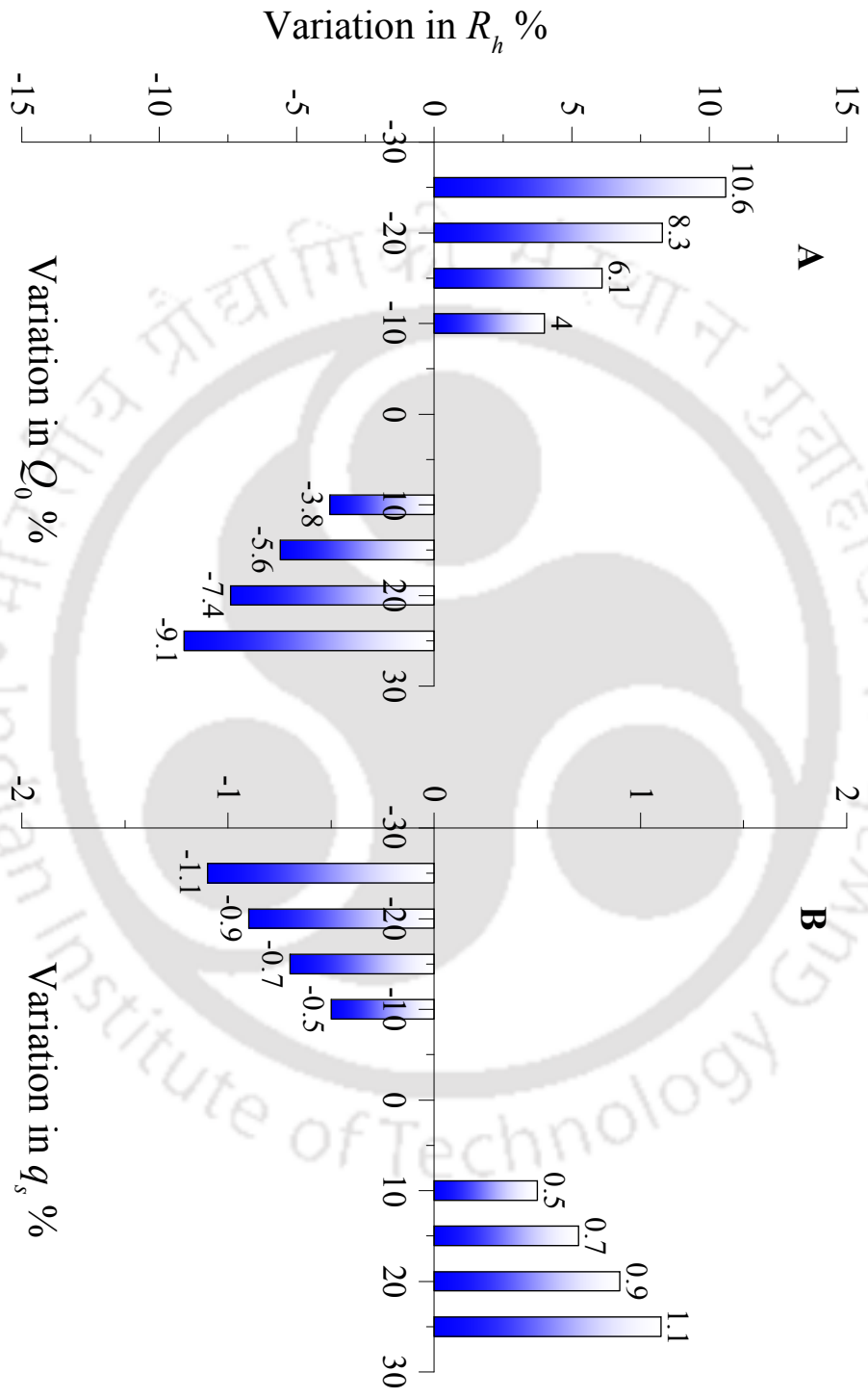

FIGURE A.3: Sensitivity analysis for the prediction of hydraulic radius (dimensional form)

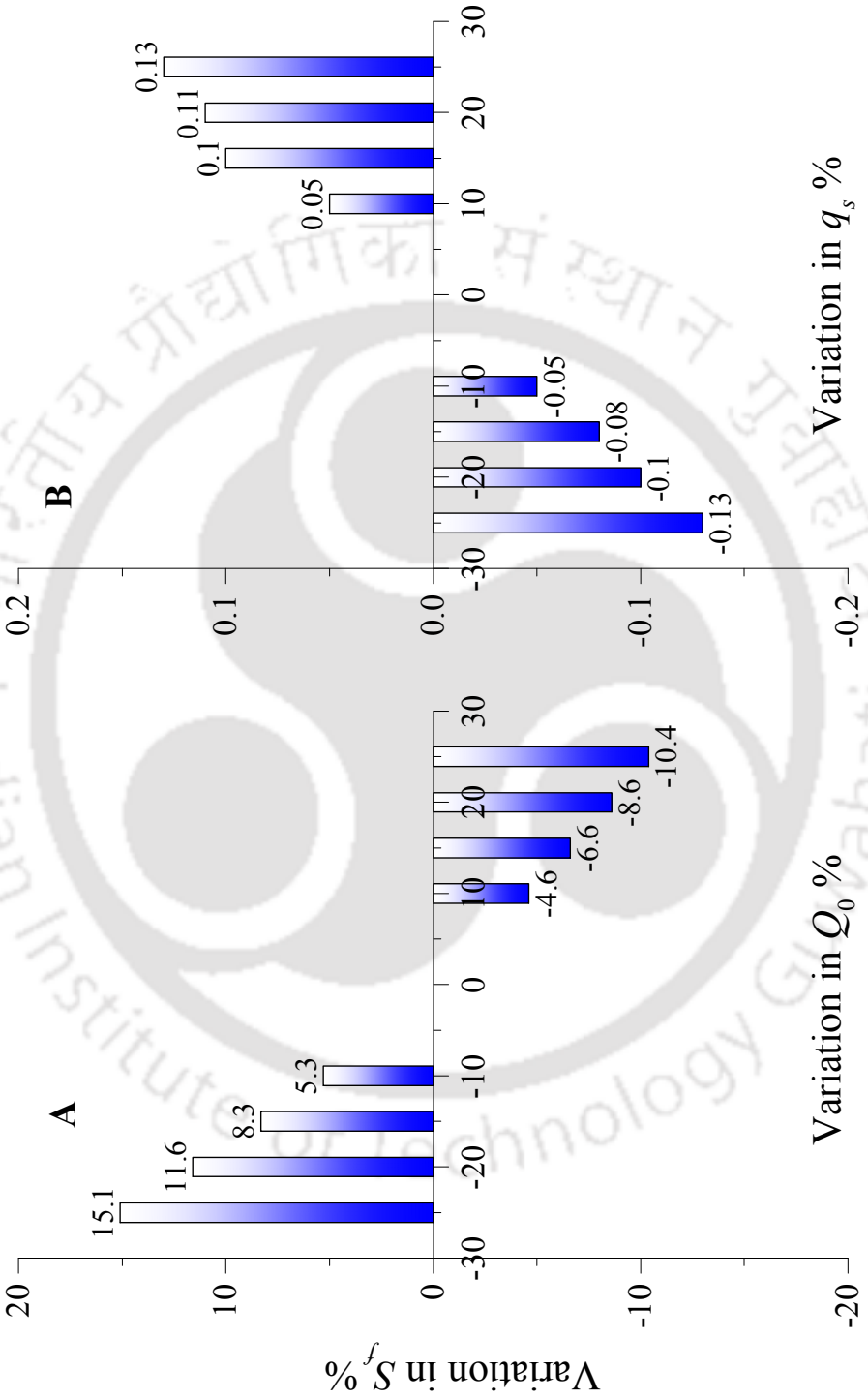

FIGURE A.4: Sensitivity analysis for the prediction of frictional slope (dimensional form)

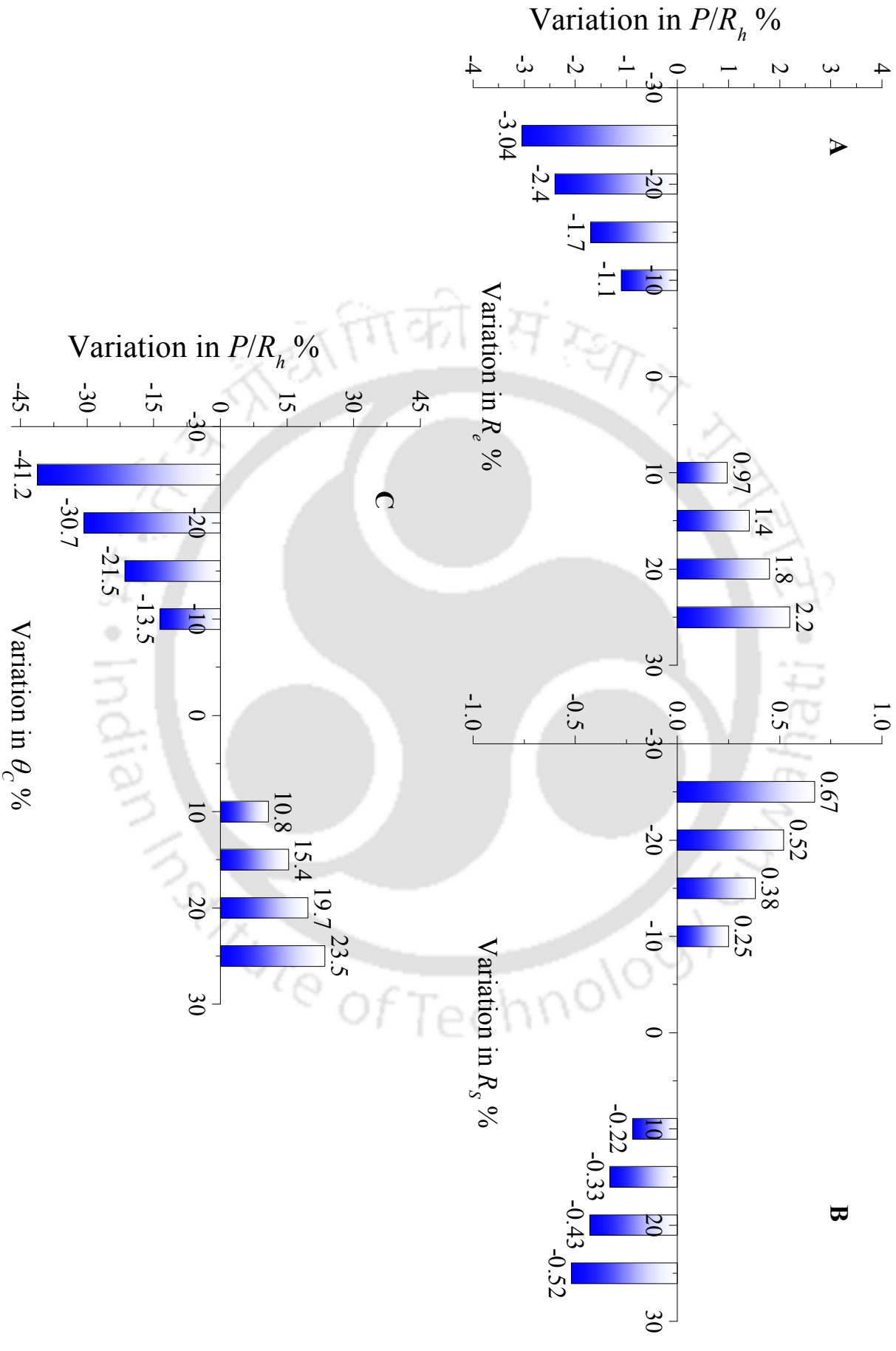

FIGURE A.5: Sensitivity analysis for the prediction of channel perimeter (non-dimensional form)

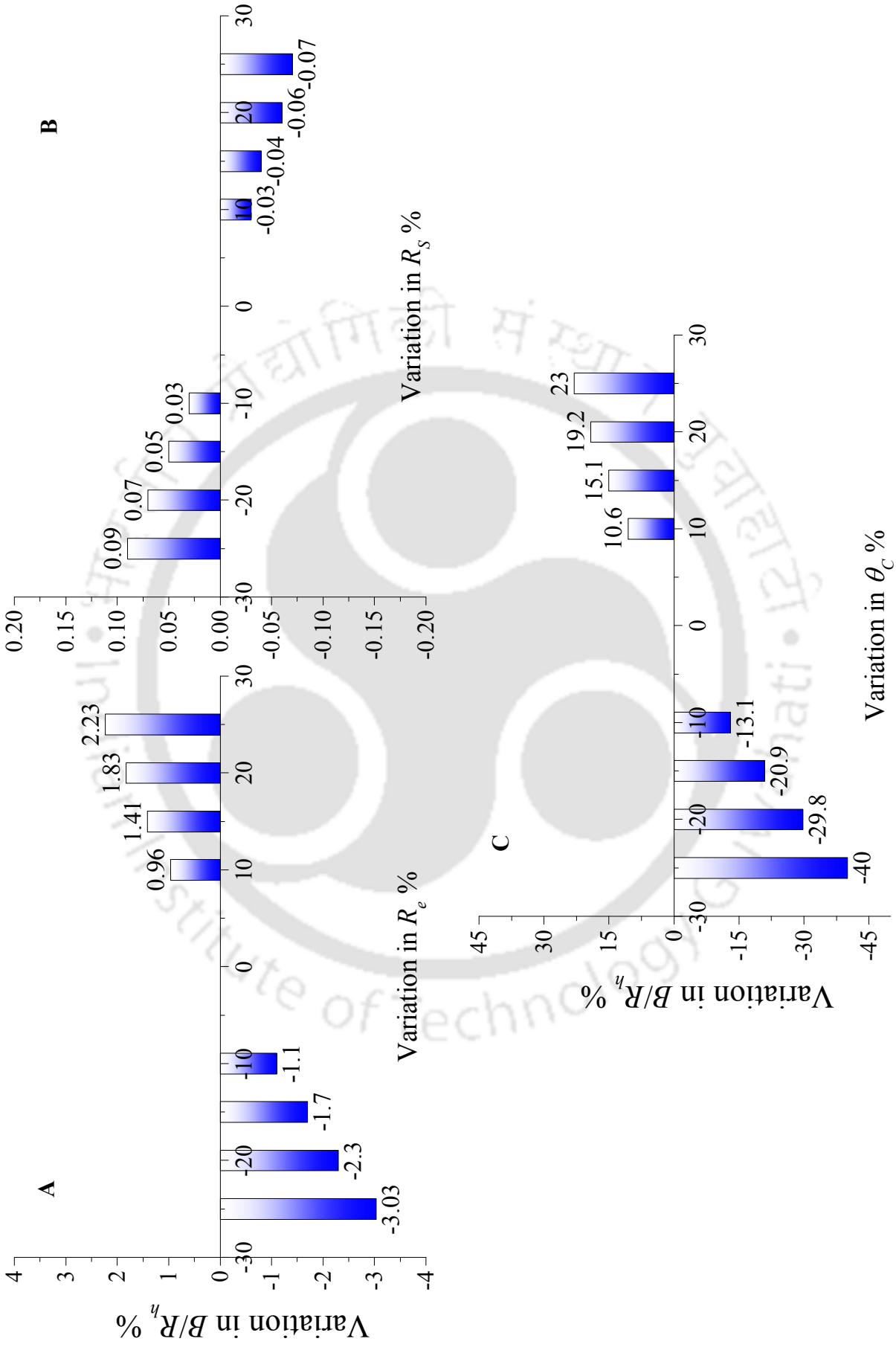

FIGURE A.6: Sensitivity analysis for the prediction of channel width (non-dimensional form)

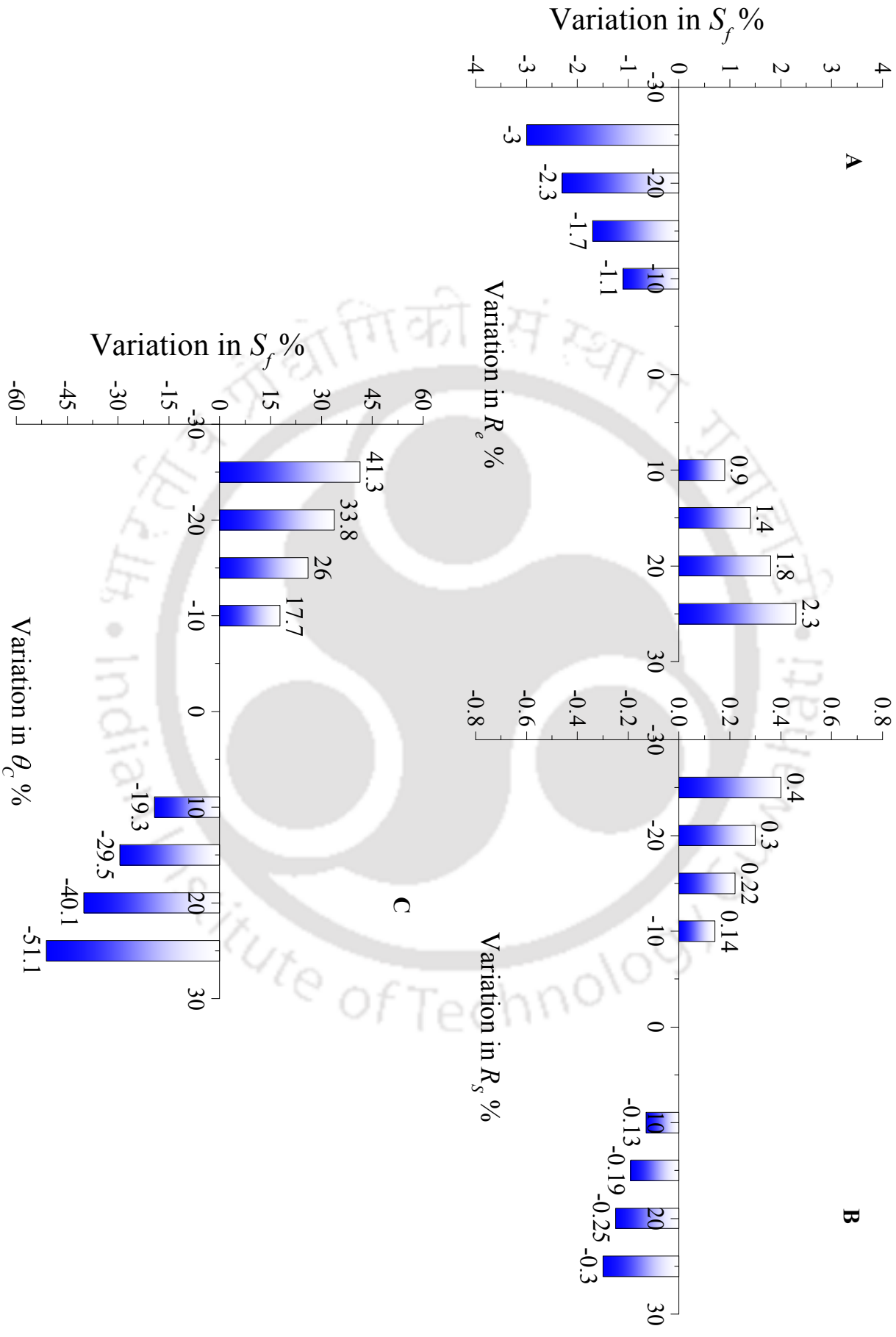

FIGURE A.7: Sensitivity analysis for the prediction of frictional slope (non-dimensional form)

Bibliography

Ackers, P. (1964). "Experiments on small streams in alluvium." *Journal of the Hydraulics Division*, 90, 1–37.

Ackers, P. and White, W. R. (1973). "Sediment transport: new approach and analysis." *Journal of the Hydraulics Division*, 99(hy11).

Afzalimehr, H., Abdolhosseini, M., and Singh, V. (2010). "Hydraulic geometry relations for stable channel design." *Journal of Hydrologic Engineering*, 15(10), 859–864.

Ahmed, A. S. M. and Sato, S. (2003). "A sheetflow transport model for asymmetric oscillatory flows: part ii: mixed grain size sediments." *Coastal Engineering Journal*, 45(03), 339–361.

Allen, P. M., Arnold, J. C., and Byars, B. W. (1994). "Downstream channel geometry for use in planning-level models." *JAWRA Journal of the American Water Resources Association*, 30(4), 663–671.

Antonia, R., Zhu, Y., and Sokolov, M. (1995). "Effect of concentrated wall suction on a turbulent boundary layer." *Physics of Fluids*, 7(10), 2465–2474.

Antonia, R. A., Fulachier, L., Krishnamoorthy, L. V., Benabid, T., and Anselmet, F. (1988). "Influence of wall suction on the organized motion in a turbulent boundary layer." *Journal of Fluid Mechanics*, 190, 217–240.

Asano, T. (1992). "Observations of granular-fluid mixture under an oscillatory sheet flow." *Coastal Engineering Proceedings*, 1(23).

Barr, D., Alam, M., Nishat, A., et al. (1980). "A contribution to regime theory relating principally to channel geometry." *ICE Proceedings*, Vol. 69, Thomas Telford, 651–670.

Batchelor, G., Moffatt, H., and Worster, M. (2002). *Perspectives in fluid dynamics, Edited by GK Batchelor and HK Moffatt and MG Worster*, Vol. 1. Cambridge, UK: Cambridge, University Press.

Bayazit, M. (1976). "Free surface flow in a channel of large relative roughness." *Journal of Hydraulic Research*, 14(2), 115–126.

Bennett, S. J. and Bridge, J. S. (1995). "The geometry and dynamics of low-relief bed forms in heterogeneous sediment in a laboratory channel, and their relationship to water flow and sediment transport." *Journal of Sedimentary Research*, 65(1a), 29–39.

Berenbrock, C. (1999). "Streamflow gains and losses in the lower boise river basin, idaho, 1996-97." *Report No. 99-4105*.

Best, J. (1992). "On the entrainment of sediment and initiation of bed defects: insights from recent developments within turbulent boundary layer research." *Sedimentology*, 39(5), 797–811.

Blench, T. (1957). *Regime behaviour of canals and rivers*. Butterworths Scientific Publications.

Boussinesq, J. (1877). "Essa sur latheories des eaux courantes, memoires presentes par divers savants a l." *Academic des Sciences de lInstitut Nationale de France*, 23(1).

Braudrick, C. A., Dietrich, W. E., Leverich, G. T., and Sklar, L. S. (2009). "Experimental evidence for the conditions necessary to sustain meandering in coarse-bedded rivers." 106(40), 16936–16941.

Brebner, A. and Wilson, K. C. (1967). "Derivation of the regime equations from relationships for pressurized flow by use of the principle of minimum energy-degradation rate.." *ICE Proceedings*, Vol. 36, Thomas Telford, 47–62.

Brunke, M. and Gonser, T. (1997). "The ecological significance of exchange processes between rivers and groundwater." *Freshwater Biology*, 37(1), 1–33.

Camenen, B., Bayram, A., and Larson, M. (2006). "Equivalent roughness height for plane bed under steady flow." *Journal of Hydraulic Engineering*, 132(11), 1146–1158.

Cao, D. and Chiew, Y.-M. (2014). "Suction effects on sediment transport in closed-conduit flows." *Journal of Hydraulic Engineering*, 140(5).

Cao, S. and Knight, D. (2002). "Review of regime theory of alluvial channels." *Journal of Hydrodynamics*, 3, 1–7.

Cao, S. and Knight, D. W. (1997). "Entropy-based design approach of threshold alluvial channels." *Journal of Hydraulic Research*, 35(4), 505–524.

Cao, S. and Knight, D. W. (1998). "Design for hydraulic geometry of alluvial channels." *Journal of Hydraulic Engineering*, 124(5), 484–492.

Cao, Z. (1997). "Turbulent bursting-based sediment entrainment function." *Journal of Hydraulic Engineering*, 123(3), 233–236.

Carlson, R. and Petrich, C. (1999). "New york canal geologic cross-section, seepage gain/loss data, and ground water hydrographs: compilation and interim findings." *Report No. IWRRI-2002-09*.

Carlston, C. W. (1969). "Downstream variations in the hydraulic geometry of streams; special emphasis on mean velocity." *American journal of science*, 267(4), 499–509.

Carr, J. E., Chase, E. B., Paulson, R. W., and Moody, D. W. (1990). "National water summary 1987: hydrologic events and water supply and use." *Report No. 2350*, United States Geological Survey.

Chang, H. H. (1979a). "Geometry of rivers in regime." *Journal of the Hydraulics Division*, 105(6), 691–706.

Chang, H. H. (1979b). "Minimum stream power and river channel patterns." *Journal of Hydrology*, 41(3), 303–327.

Chang, H. H. (1980a). "Geometry of gravel streams." *Journal of the Hydraulics Division*, 106(9), 1443–1456.

Chang, H. H. (1980b). "Stable alluvial canal design." *Journal of the Hydraulics Division*, 106(5), 873–891.

Chang, H. H. (1982). "Mathematical model for erodible channels." *Journal of the Hydraulics Division*, 108(5), 678–689.

Chang, H. H. (1988). *Fluvial processes in river engineering*.

Cheema, M. N., Mariño, M. A., and DeVries, J. J. (1997). "Stable width of an alluvial channel." *Journal of irrigation and drainage engineering*, 123(1), 55–61.

Chen, X. and Chiew, Y.-M. (2004). "Velocity distribution of turbulent open-channel flow with bed suction." *Journal of Hydraulic Engineering*, 130(2), 140–148.

Cheng, N.-S. (1997). "Seepage effect on open-channel flow and incipient sediment motion." Ph.D. thesis, Ph.D. thesis.

Cheng, N.-S. and Chiew, Y.-M. (1998a). "Modified logarithmic law for velocity distribution subjected to upward seepage." *Journal of Hydraulic Engineering*, 124(12), 1235–1241.

Cheng, N.-S. and Chiew, Y.-M. (1998b). "Turbulent open-channel flow with upward seepage." *Journal of Hydraulic Research*, 36(3), 415–431.

Cheng, N.-S. and Chiew, Y.-M. (1999). "Incipient sediment motion with upward seepage." *Journal of Hydraulic Research*, 37(5), 665–681.

Church, M. and Rood, K. (1983). "Catalogue of alluvial river channel regime data." *Report No. B0007BZ5I4*.

Clifford, N., McClatchey, J., and French, J. (1991). "Measurements of turbulence in the benthic boundary layer over a gravel bed and comparison between acoustic measurements and predictions of the bedload transport of marine gravels." *Sedimentology*, 38(1), 161–166.

Darcy, H. (1857). *Recherches expérimentales relatives au mouvement de l'eau dans les tuyaux*, Vol. 1. Mallet-Bachelier, Paris.

Davies, T. and Sutherland, A. (1980). "Resistance to flow past deformable boundaries." *Earth Surface Processes*, 5(2), 175–179.

Davies, T. R. (1980). "Bedform spacing and flow resistance." *Journal of the Hydraulics Division*, 106(3), 423–433.

Davies, T. R. and Sutherland, A. J. (1983). "Extremal hypotheses for river behavior." *Water Resources Research*, 19(1), 141–148.

Deng, Z.-Q., Singh, V. P., and Bengtsson, L. (2001). "Longitudinal dispersion coefficient in straight rivers." *Journal of Hydraulic Engineering*, 127(11), 919–927.

Dey, S., Das, R., Gaudio, R., and Bose, S. K. (2012). "Turbulence in mobile-bed streams." *Acta Geophysica*, 60(6), 1547–1588.

Dey, S. and Nath, T. K. (2010). "Turbulence characteristics in flows subjected to boundary injection and suction." *Journal of engineering mechanics*, 136(7), 877–888.

Dey, S. and Raikar, R. V. (2007). "Characteristics of loose rough boundary streams at near-threshold." *Journal of Hydraulic Engineering*, 133(3), 288–304.

Dey, S., Sarkar, S., and Ballio, F. (2011a). "Double-averaging turbulence characteristics in seeping rough-bed streams." *Journal of Geophysical Research: Earth Surface*, 116(F3).

Dey, S., Sarkar, S., and Solari, L. (2011b). "Near-bed turbulence characteristics at the entrainment threshold of sediment beds." *Journal of Hydraulic Engineering*, 137(9), 945–958.

Diplas, P. (1990). "Characteristics of self-formed straight channels." *Journal of Hydraulic Engineering*, 116(5), 707–728.

Diplas, P. and Vigilar, G. (1992). "Hydraulic geometry of threshold channels." *Journal of Hydraulic Engineering*, 118(4), 597–614.

Dohmen-Janssen, C. M. (1999). "Grain size influence on sediment transport in oscillatory sheet flow; phase lags and mobile-bed effects." Ph.D. thesis, Ph.D. thesis.

Dohmen-Janssen, C. M., Hassan, W. N., and Ribberink, J. S. (2001). "Mobile-bed effects in oscillatory sheet flow." *Journal of Geophysical Research: Oceans (1978–2012)*, 106(C11), 27103–27115.

Dohmen-Janssen, C. M., Kroekenstoel, D. F., Hassan, W. N., and Ribberink, J. S. (2002). "Phase lags in oscillatory sheet flow: experiments and bed load modelling." *Coastal Engineering*, 46(1), 61–87.

Dong, L. and Sato, S. (2011). "Sheetflow sediment transport under asymmetric waves and strong currents." *Coastal Engineering Proceedings*, 1(32), sediment–17.

Dong, L. P., Sato, S., and Liu, H. (2013). "A sheetflow sediment transport model for skewed-asymmetric waves combined with strong opposite currents." *Coastal Engineering*, 71, 87–101.

Drake, T. G., Shreve, R. L., Dietrich, W. E., Whiting, P. J., and Leopold, L. B. (1988). "Bedload transport of fine gravel observed by motion-picture photography." *Journal of Fluid Mechanics*, 192, 193–217.

Dukker, P. (1994). *Seepage Losses from the Lower Gugera Branch Canal, Punjab, Pakistan*, Vol. 134. IWASRI.

Dwivedi, A., Melville, B., and Shamseldin, A. Y. (2010). "Hydrodynamic forces generated on a spherical sediment particle during entrainment." *Journal of Hydraulic Engineering*, 136(10), 756–769.

Eaton, B. C. and Church, M. (2004). "A graded stream response relation for bed load-dominated streams." *Journal of Geophysical Research: Earth Surface*, 109(F03011).

Engelund, F. and Hansen, E. (1967). "A monograph on sediment transport in alluvial streams." *Report no.*, Tekniskforlag Skelbrekgade 4 Copenhagen V, Denmark.

Fipps, G. (2005). "Potential water savings in irrigated agriculture for the rio grande planning region (region m)." *Texas Cooperative Extension, Texas A&M University System*.

Flores, N. Z. and Sleath, J. F. (1998). "Mobile layer in oscillatory sheet flow." *Journal of Geophysical Research: Oceans (1978–2012)*, 103(C6), 12783–12793.

Francalanci, S., Parker, G., and Solari, L. (2008). "Effect of seepage-induced nonhydrostatic pressure distribution on bed-load transport and bed morphodynamics." *Journal of Hydraulic Engineering*, 134(4), 378–389.

Frisch, U. (1995). *Turbulence: the legacy of AN Kolmogorov*. Cambridge university press.

Gallagher, M., McEwan, I., and Nikora, V. (1999). "The changing structure of turbulence over a self-stabilising sediment bed." *Report No. 21*.

Garde, R. (1995). *History of fluvial hydraulics*. New Age International.

Glover, R. E. and Florey, Q. (1951). "Stable channel profiles." *Report No. Hyd-325*.

Goring, D. G. and Nikora, V. I. (2002). "Despiking acoustic doppler velocimeter data." *Journal of Hydraulic Engineering*, 128(1), 117–126.

Gotoh, H. and Sakai, T. (1997). "Numerical simulation of sheetflow as granular material." *Journal of waterway, port, coastal, and ocean engineering*, 123(6), 329–336.

Graf, W. H. (1998). *Hydraulics of sediment transport*, Vol. 513. McGraw-Hill New York.

Grass, A. (1971). "Structural features of turbulent flow over smooth and rough boundaries." *Journal of Fluid Mechanics*, 50(02), 233–255.

Griffiths, G. A. (1983). "Stable-channel design in alluvial rivers." *Journal of Hydrology*, 65(4), 259–270.

Griffiths, G. A. (1984). "Extremal hypotheses for river regime: an illusion of progress." *Water Resources Research*, 20(1), 113–118.

Grinvald, D. and Nikora, V. (1988). "River turbulence." *Hydrometeoizdat, Leningrad, Russia*.

Hagen, G. H. L. (1854). *Über den einfluss der temperatur auf die bewegung des wassers in röhren–*. Druckerei der Königl. akademie der wissenschaften.

Hanson, B. and Lin, W. (2008). "The use of channel characteristics for the calibration of index velocity ratings for acoustic doppler velocity meters." *Report No. ND08 - 07*, North Dakota Water Resources Research Institute, North Dakota State University, Fargo, North Dakota.

Heathershaw, A. and Thorne, P. (1985). "Sea-bed noises reveal role of turbulent bursting phenomenon in sediment transport by tidal currents.

Hey, R. D. and Thorne, C. R. (1986). "Stable channels with mobile gravel beds." *Journal of Hydraulic Engineering*, 112(8), 671–689.

Huang, H. Q. and Nanson, G. C. (2000). "Hydraulic geometry and maximum flow efficiency as products of the principle of least action." *Earth Surface Processes and Landforms*, 25(1), 1–16.

Ikeda, S. (1981). "Self-formed straight channels in sandy beds." *Journal of the hydraulics division*, 107(4), 389–406.

Ikeda, S. (1982). "Incipient motion of sand particles on side slopes." *Journal of the Hydraulics Division*, 108(1), 95–114.

Islam, T. and Karim, R. (2005). "Predicting downstream hydraulic geometry of the gorai river." *J. Civil Eng*, 33, 55–63.

Jones, J. and Mulholland, P. (2000). *Streams and Groundwaters*. Academic Press, San Diego.

Julien, P. Y. and Wargadalam, J. (1995). "Alluvial channel geometry: theory and applications." *Journal of Hydraulic Engineering*, 121(4), 312–325.

Karambas, T. V. (2003). "Modelling of infiltration-exfiltration effects of cross-shore sediment transport in the swash zone." *Coastal Engineering Journal*, 45(1), 63–82.

Kawas, M. (1985). "Studies of sediment erosion and of the geometry of sediment carrying watercourses.." Ph.D. thesis, University of Strathclyde, University of Strathclyde.

Kellerhals, R. (1967). "Stable channels with gravel-paved beds." *Journal of the Waterways and Harbors Division*, 93(1), 63–84.

Kennedy, R. G. (1895). "The prevention of silting in irrigation canals.(including appendix).." *Proc. Inst. Civ. Engr.*, Vol. 119, Thomas Telford, 281–290.

Kinzli, K.-D., Martinez, M., Oad, R., Prior, A., and Gensler, D. (2010). "Using an adcp to determine canal seepage loss in an irrigation district." *Agricultural water management*, 97(6), 801–810.

Kline, S., Reynolds, W., Schraub, F., and Runstadler, P. (1967). "The structure of turbulent boundary layers." *Journal of Fluid Mechanics*, 30(4), 741–773.

Knighton, A. D. (1974). "Variation in width-discharge relation and some implications for hydraulic geometry." *Geological Society of America Bulletin*, 85(7), 1069–1076.

Kolmogorov, A. N. (1941). "The local structure of turbulence in incompressible viscous fluid for very large reynolds numbers." *Dokl. Akad. Nauk SSSR*, Vol. 30, 299–303.

Krishnamurthy, K. and Rao, S. (1969). "Theory and experiment in canal seepage estimation using radioisotopes." *Journal of Hydrology*, 9(3), 277–293.

Krogstad, P.-Å. and Kourakine, A. (2000). "Some effects of localized injection on the turbulence structure in a boundary layer." *Physics of Fluids (1994-present)*, 12(11), 2990–2999.

Krogstadt, P.-Å. and Antonia, R. (1999). "Surface roughness effects in turbulent boundary layers." *Experiments in Fluids*, 27(5), 450–460.

Lacey, G. (1930). "Stable channels in alluvium (includes appendices).." *Proc. Inst. Civ. Engr.*, Vol. 229, Thomas Telford, 259–292.

Lacey, G. (1958). "Flow in alluvial channels with sand mobile beds." *Proc. Inst. Civ. Engr. London*, number 9, 146–164.

Lanckriet, T., Puleo, J. A., Masselink, G., Turner, I. L., Conley, D., Blenkinsopp, C., and Russell, P. (2014). "Comprehensive field study of swash-zone processes. II: Sheet flow sediment concentrations during quasi-steady backwash." *Journal of Waterway, Port, Coastal, and Ocean Engineering*, 140(1), 29–42.

Lane, E. W. (1937). "Stable channels in erodible materials." *Transactions of the American Society of Civil Engineers*, 102(1), 123–142.

Lane, E. W. (1953). "Progress report on studies on the design of stable channels by the bureau of reclamation." Vol. 79, Separate 280, American Society of Civil Engineers, 1–31.

Lane, L. J. and Foster, G. R. (1980). "Modeling channel processes with changing land use." *Symposium on Watershed Management*, ASCE, 200–214.

Langbein, W. (1964). "Geometry of river channels." *J. Hydraul. Div. Am. Soc. Civ. Eng*, 90, 301–312.

Leopold, L. B. and Maddock, T. (1953). "The hydraulic geometry of stream channels and some physiographic implications." *USGS Publications Warehouse*, 252.

Lindley, E. (1919). "Regime channels." *Proceedings of Punjab Engineering Congress*, Vol. 7, 63–74.

Lu, S. and Willmarth, W. (1973). "Measurements of the structure of the reynolds stress in a turbulent boundary layer." *Journal of Fluid Mechanics*, 60(3), 481–511.

Lu, Y. and Chiew, Y.-M. (2007a). "Seepage effects on dune dimensions." *Journal of Hydraulic Engineering*, 133(5), 560–563.

Lu, Y. and Chiew, Y.-M. (2007b). "Suction effects on turbulence flows over a dune bed." *Journal of Hydraulic Research*, 45(5), 691–700.

Maclean, A. (1991a). "Open channel velocity profiles over a zone of rapid infiltration." *Journal of Hydraulic Research*, 29(1), 15–27.

Maclean, A. and Willetts, B. (1986). "Measurement of boundary shear stress in non-uniform open channel flow." *Journal of Hydraulic Research*, 24(1), 39–51.

Maclean, A. G. (1991b). "Bed shear stress and scour over bed-type river intake." *Journal of Hydraulic Engineering*, 117(4), 436–451.

Mahmood, K., Haque, M., and Choudri, A. (1988). *Mechanics of Alluvial Channels*. Water Resources Publications, Littleton, Colorado.

Malarkey, J., Davies, A., and Li, Z. (2003). "A simple model of unsteady sheet-flow sediment transport." *Coastal Engineering*, 48(3), 171–188.

Marsh, N. A., Western, A. W., and Grayson, R. B. (2004). "Comparison of methods for predicting incipient motion for sand beds." *Journal of Hydraulic Engineering*, 130(7), 616–621.

Martin, M. (1988). "The geometry of alluvial channels." Ph.D. thesis, Ph.D. thesis.

Martin, M. (1996). "Regime approach for predicting the alluvial channel geometry." *J. Civ. Eng. Inst. Engr. Ban*, 24(1), 27–40.

Millar, R. G. (2005). "Theoretical regime equations for mobile gravel-bed rivers with stable banks." *Geomorphology*, 64(3), 207–220.

Millar, R. G. and Quick, M. C. (1993). "Effect of bank stability on geometry of gravel rivers." *Journal of Hydraulic Engineering*, 119(12), 1343–1363.

Myrhaug, D. and Holmedal, L. E. (2007). "Mobile layer thickness in sheet flow beneath random waves." *Coastal engineering*, 54(8), 577–585.

Nakagawa, H. and Nezu, I. (1977). "Prediction of the contributions to the reynolds stress from bursting events in open-channel flows." *Journal of fluid mechanics*, 80(1), 99–128.

Nash, J. and Sutcliffe, J. V. (1970). "River flow forecasting through conceptual models part ia discussion of principles." *Journal of hydrology*, 10(3), 282–290.

Nelson, J. M., Shreve, R. L., McLean, S. R., and Drake, T. G. (1995). "Role of near-bed turbulence structure in bed load transport and bed form mechanics." *Water Resources Research*, 31(8), 2071–2086.

Nezu, I. (1977). "Turbulent structure in open-channel flows." Ph.D. thesis, Kyoto University, Kyoto University.

Nezu, I. and Nakagawa, H. (1993). *Turbulence in Open Channel Flows*. Balkema, Rotterdam, The Netherlands.

Nikora, V. and Goring, D. (1998). "Spectral scaling for gravel-bed open-channel flows." *Stochastic Models of Hydrological Processes and their Application to Problems of Environmental Preservation, Proceedings of the NATO Advanced Research Workshop. Russian Academy of Science: Moscow*, 239–245.

Nikora, V. and Goring, D. (1999). *Effects of bed mobility on turbulence structure*. National Institute of Water and Atmospheric Research.

Nikora, V. and Goring, D. (2000). "Flow turbulence over fixed and weakly mobile gravel beds." *Journal of Hydraulic Engineering*, 126(9), 679–690.

Nikora, V. and Smart, G. (1997). "Turbulence characteristics of new zealand gravel-bed rivers." *Journal of Hydraulic Engineering*, 123(9), 764–773.

Nowell, A. R. and Jumars, P. A. (1987). "Flumestheoretical and experimental considerations for simulation of benthic environments." *Oceanogr Mar Biol*, 25, 91–112.

O'Donoghue, T. and Wright, S. (2004). "Concentrations in oscillatory sheet flow for well sorted and graded sands." *Coastal Engineering*, 50(3), 117–138.

Oldenziel, D. M. and Brink, W. E. (1974). "Influence of suction and blowing on entrainment of sand particles." *Journal of the Hydraulics Division*, 100(7), 935–949.

Oyewola, O., Djenidi, L., and Antonia, R. (2004). "Influence of localised wall suction on the anisotropy of the reynolds stress tensor in a turbulent boundary layer." *Experiments in fluids*, 37(2), 187–193.

Parker, G. (1978). "Self-formed straight rivers with equilibrium banks and mobile bed. part 2. the gravel river." *Journal of Fluid Mechanics*, 89(1), 127–146.

Parker, G. (1979). "Hydraulic geometry of active gravel rivers." *Journal of the Hydraulics Division*, 105(9), 1185–1201.

Peakall, J., Ashworth, P. J., and Best, J. L. (2007). "Meander-bend evolution, alluvial architecture, and the role of cohesion in sinuous river channels: a flume study." *Journal of Sedimentary Research*, 77(3), 197–212.

Pizzuto, J. E. (1990). "Numerical simulation of gravel river widening." *Water Resources Research*, 26(9), 1971–1980.

Pope, S. B. (2000). *Turbulent flows*. Cambridge university press.

Prinos, P. (1995). "Bed-suction effects on structure of turbulent open-channel flow." *Journal of Hydraulic Engineering*, 121(5), 404–412.

Raja, R., Kumar, A., and Chhabra, S. (1983). "Estimation of seepage losses from an unlined channel- a field study by nuclear techniques." *Proceedings*, Vol. II, Hydraulics, CBIP, Fiftieth annual research and development session, Simla, Himachala Pradesh, India.

Rao, A. R. and Sitaram, N. (1999). "Stability and mobility of sand-bed channels affected by seepage." *Journal of Irrigation and Drainage Engineering*, 125(6), 370–379.

Rao, A. R., Sreenivasulu, G., and Kumar, B. (2011). "Geometry of sand-bed channels with seepage." *Geomorphology*, 128(3), 171–177.

Raupach, M. (1981). "Conditional statistics of reynolds stress in rough-wall and smooth-wall turbulent boundary layers." *Journal of Fluid Mechanics*, 108, 363–382.

Revil-Baudard, T. and Chauchat, J. (2013). "A two-phase model for sheet flow regime based on dense granular flow rheology." *Journal of Geophysical Research: Oceans*, 118(2), 619–634.

Reynolds, O. (1883). "An experimental investigation of the circumstances which determine whether the motion of water shall be direct or sinuous, and of the law of resistance in parallel channels.." *Philosophical Transactions of the Royal Society of London A*, 174, 935–982.

Reynolds, O. (1895). "On the dynamical theory of incompressible viscous fluids and the determination of the criterion.." *Philosophical Transactions of the Royal Society of London A*, 186, 123164.

Richardson, J., Abt, S., and Richardson, E. (1985). "Inflow seepage influence on straight alluvial channels." *Journal of Hydraulic Engineering*, 111(8), 1133–1147.

Richardson, L. F. (1922). *Weather prediction by numerical process*. Cambridge University Press.

Rosgen, D. L. (2006). "The natural channel design method for river restoration." *World Environmental and Water Resource Congress*.

Rouse, H. and Ince, S. (1957). *History of hydraulics*. Institute of hydraulic Research, the University of Iowa.

Savenije, H. H. (2003). "The width of a bankfull channel; lacey's formula explained." *Journal of Hydrology*, 276(1), 176–183.

Schumm, S. A. and Lichty, R. W. (1965). "Time, space, and causality in geomorphology." *American Journal of Science*, 263(2), 110–119.

Sharma, H. and Chawla, A. (1975). "Manual of canal lining." *Report No. 14*, Central Board of Irrigation and Power, New Delhi.

Shiono, K. and Knight, D. W. (1991). "Turbulent open-channel flows with variable depth across the channel." *Journal of Fluid Mechanics*, 222, 617–646.

Simons, D. B. and Albertson, M. L. (1960). "Uniform water conveyance channels in alluvial materials." *Journal of the Hydraulics Division*, 86(5), 33–71.

Simons, D. B. and Albertson, M. L. (1963). "Uniform water conveyance channels in alluvial material." *Transactions of the American Society of Civil Engineers*, 128(1), 65–106.

Singh, V. P. (2003). "On the theories of hydraulic geometry." *International Journal of Sediment Research*, 18(3), 196–218.

Singh, V. P., Yang, C. T., and Deng, Z. (2003a). "Downstream hydraulic geometry relations: 1. theoretical development." *Water Resources Research*, 39(12), SWC2–1–SWC2–15.

Singh, V. P., Yang, C. T., and Deng, Z.-Q. (2003b). "Downstream hydraulic geometry relations: 2. calibration and testing." *Water resources research*, 39(12), SWC3–1–SWC3–10.

Singh, V. P. and Zhang, L. (2008a). "At-a-station hydraulic geometry relations, 1: theoretical development." *Hydrological processes*, 22(2), 189–215.

Singh, V. P. and Zhang, L. (2008b). "At-a-station hydraulic geometry relations, 2: calibration and testing." *Hydrological processes*, 22(2), 216–228.

Smith, C. E. (1998). "Modeling high sinuosity meanders in a small flume." *Geomorphology*, 25(1), 19–30.

Smith, K. (1974a). "Comparison of prediction techniques with records of observations on the lower chenab canal system, university of southampton." *Report no.*, CE/5/74.

Smith, T. R. (1974b). "A derivation of the hydraulic geometry of steady-state channels from conservation principles and sediment transport laws." *The Journal of Geology*, 98–104.

Song, T. and Graf, W. (1994). "Non-uniform open-channel flow over a rough bed." *J. Hydrosci. Hydr. Eng*, 12(1), 1–25.

Sreenivasulu, G., Kumar, B., and Ramakrishna Rao, A. (2011). "Variation of stream power with seepage in sand-bed channels." *Water SA*, 37(1), 115–119.

Sreenivasulu, G., Rao, A. R., Kumar, B., and Tripathi, S. (2010). "Analysis of gradually and spatially varied flow in sand-bed channels." *Journal of Hydraulic Research*, 48(2), 274–279.

Stebbings, J. (1963). "The shapes of self-formed model alluvial channels." *ICE Proceedings*, Vol. 25, Thomas Telford, 485–510.

Sumer, B. M., Chua, L. H., Cheng, N.-S., and Fredsøe, J. (2003). "Influence of turbulence on bed load sediment transport." *Journal of Hydraulic Engineering*, 129(8), 585–596.

Sumer, B. M., Kozakiewicz, A., Fredsøe, J., and Deigaard, R. (1996). "Velocity and concentration profiles in sheet-flow layer of movable bed." *Journal of Hydraulic Engineering*, 122(10), 549–558.

Sutherland, A. J. (1967). "Proposed mechanism for sediment entrainment by turbulent flows." *Journal of Geophysical Research*, 72(24), 6183–6194.

Tanji, K. K. and Kielen, N. C. (2002). "Agricultural drainage water management in arid and semi-arid areas." *FAO irrigation and drainage paper*.

Tennekes, H. and Lumley, J. L. (1972). *A first course in turbulence*. MIT press.

Terrio, P. and Nazimek, J. (1997). "Changes in cross-section geometry and channel volume in two reaches of the kankakee river in illinois, 1959-94." *Report No. 96-4261*, U.S. Geological Survey.

Thorne, P. D., Williams, J. J., and Heathershaw, A. D. (1989). "In situ acoustic measurements of marine gravel threshold and transport." *Sedimentology*, 36(1), 61–74.

Thornes, J. B. (1970). "The hydraulic geometry of stream channels in the xingu-araguaia headwaters." *Geographical Journal*, 376–382.

Turner, I. L. (1995). "Simulating the influence of groundwater seepage on sediment transported by the sweep of the swash zone across macro-tidal beaches." *Marine Geology*, 125(1), 153–174.

van Dijk, W. M., van de Lageweg, W. I., Hoendervoogt, R., and Kleinhans, M. G. (2010). "Incipient meandering and self-formed floodplains in experiments." *Proc. River Flow*, Vol. 2, 1030–1038.

Van Rijn, L. C. (1993). *Principles of sediment transport in rivers, estuaries and coastal seas*, Vol. 2. Aqua publications Amsterdam.

Vanoni, V. (1975). *Sedimentation engineering, ASCE manuals and reports on engineering practiceNo. 54*.

Venditti, J. G., Church, M. A., and Bennett, S. J. (2005). "Bed form initiation from a flat sand bed." *Journal of Geophysical Research: Earth Surface (2003–2012)*, 110(F1).

Watters, G. Z. and Rao, M. V. (1971). "Hydrodynamic effects of seepage on bed particles." *Journal of the Hydraulics Division*, 97(3), 421–439.

Weller, J. and McAteer, P. (1993). "Seepage measurement techniques and accuracy." *Proceedings of the Workshop on Canal Lining and Seepage, Lahore*, 171–196.

White, W., Paris, E., Bettess, R., Einstein, H., Barbarossa, N., Engelund, F., Raudkivi, A., et al. (1980). "The frictional characteristics of alluvial streams: A new approach.." *ICE Proceedings*, Vol. 69, Thomas Telford, 737–750.

White, W. R., Bettess, R., and Paris, E. (1982). "Analytical approach to river regime." *Journal of the Hydraulics Division*, 108(10), 1179–1193.

Whiting, P. J. and Dietrich, W. E. (1993). "Experimental studies of bed topography and flow patterns in large-amplitude meanders: 1. observations." *Water Resources Research*, 29(11), 3605–3614.

Whittaker, J. G. and Jaeggi, M. N. (1982). "Origin of step-pool systems in mountain streams." *Journal of the Hydraulics Division*, 108(6), 758–773.

Willetts, B. B. and Drossos, M. E. (1975). "Local erosion caused by rapid forced infiltration." *Journal of the Hydraulics Division*, 101(ASCE# 11796 Proceeding).

Wilson, K. (1966). "Bed-load transport at high shear stress." *Journal of the Hydraulics Division*, 92(11), 49–59.

Wilson, K. (1989). "Friction of wave-induced sheet flow." *Coastal Engineering*, 12(4), 371–379.

Wilson, K. C. (1987). "Analysis of bed-load motion at high shear stress." *Journal of Hydraulic Engineering*, 113(1), 97–103.

Wobus, C. W., Kean, J. W., Tucker, G. E., and Anderson, R. S. (2008). "Modeling the evolution of channel shape: Balancing computational efficiency with hydraulic fidelity." *Journal of Geophysical Research: Earth Surface (2003–2012)*, 113(F2).

Wolman, M. G. (1955). "The natural channel of brandywine creek, pennsylvania." *Report No. 271*.

Wolman, M. G. and Brush Jr, L. (1961). "Factors controlling the size and shape of stream channels in coarse noncohesive sands." *Report No. 282-G*.

Yalin, M. S. (1976). *Mechanics of sediment transport*. Pergamon press.

Yang, C. T. (1972). "Unit stream power and sediment transport." *Journal of the Hydraulics Division*, 98(10), 1805–1826.

Yang, C. T. (1976). "Minimum unit stream power and fluvial hydraulics." *Journal of the Hydraulics Division*, 102(7), 919–934.

Yang, C. T. and Song, C. (1979). "Theory of minimum rate of energy dissipation." *Journal of the Hydraulics Division*, 105(7), 769–784.

Yang, C. T., Song, C., and Woldenberg, M. J. (1981). "Hydraulic geometry and minimum rate of energy dissipation." *Water Resources Research*, 17(4), 1014–1018.

Yu, G., Knight, D., et al. (1998). "Geometry of self-formed straight threshold channels in uniform material.." *Proceedings of the ICE-Water Maritime and Energy*, 130(1), 31–41.

Yussuff, S., Chauhan, H., Kumar, M., and Srivastava, V. (1994). "Transient canal seepage to sloping aquifer." *Journal of Irrigation and Drainage Engineering*, 120(1), 97–109.

Department of Civil Engineering

Indian Institute of Technology Guwahati

Guwahati 781039, India